Mechanisms of Modulation and Adaptation in Pheromone-Sensitive Trichoid Sensilla of the Hawkmoth *Manduca sexta*

Mechanismen der Modulation und Adaptation in pheromonabhängigen

Trichoidsensillen des Tabakschwärmers *Manduca sexta*

Dissertation

zur

Erlangung des Doktorgrades

der Naturwissenschaften

(Dr. rer. nat.)

dem

Fachbereich Biologie

der Philipps-Universität Marburg

vorgelegt von

Jan Dolzer

aus Kiel

Marburg/Lahn

Februar 2002

To those
who know the difference
between research and science

Gewidmet all denen,
die den Unterschied
zwischen Forschung
und Wissenschaft kennen

Inhaltsverzeichnis   Contents

Chapter 3:

Cyclic guanosine-monophosphate and tetraethylammonium modulate action potentials
of olfactory receptor neurons in trichoid sensilla of the hawkmoth *Manduca sexta* 43

Chapter 4:

XtraCell, a Microsoft Excel add-in for the automated evaluation of
tip recordings from insect sensilla 51

Part II

Chapter 5:
Pharmacological investigation of ion channels in cultured olfactory receptor neurons of the hawkmoth *Manduca sexta* 93

Zusammenfassung

Die meisten nachtaktiven Schmetterlinge finden ihre Sexualpartner mit Hilfe von Lockstoffen, den Pheromonen. Das Weibchen gibt ein Pheromongemisch, dessen Zusammensetzung für die Art charakteristisch ist, aus paarigen Drüsen am Hinterleibsende ab. Das Männchen nimmt den Duftstoff mit spezialisierten Riechsinneshaaren auf seiner Antenne wahr, den Sensilla trichoidea. Auf jeder Antenne befinden sich bis zu mehreren zehntausend dieser hochempfindlichen Sinnesorgane, die sich in der Regel durch ihre aussergewöhnliche Länge und oft auch durch eine charakteristische Anordnung auszeichnen. Durch ihre Vielzahl, ihre leichte Identifizierbarkeit und ihre vorhersagbare Spezifität stellen Pheromonsensillen ein ideales Modellsystem für die Untersuchung von Transduktion und Adaptation in olfaktorischen Rezeptorzellen dar.

Die vorliegende Dissertation befasst sich mit den Mechanismen der Modulation und Adaptation in pheromonabhängigen Sensilla trichoidea beim Tabakschwärmer *Manduca sexta*. Ziel der Arbeit war es, mit elektrophysiologischen Methoden zu untersuchen, wie viele Adaptationsmechanismen in Trichoidsensillen vorliegen und Hinweise zu sammeln, um welche Mechanismen es sich dabei handeln könnte. Dazu wurden zwei verschiedene elektrophysiologische Techniken angewendet, zum einen *Tip Recordings*, eine extrazelluläre Ableittechnik, und zum anderen *Patch Clamp*-Ableitungen, die die Messung von Ionenströmen durch die gesamte Membran einer Zelle oder durch einzelne Kanalporen erlauben. Nach diesen methodischen Gesichtspunkten gliedert sich die Dissertation in zwei Teile.

Teil I

Nach einer kurzen allgemeinen Einleitung werden im ersten Teil der Arbeit, der die Kapitel 1–4 umfasst, Ergebnisse vorgestellt, die in mit der *Tip Recording* Methode gewonnen wurden. Bei dieser extrazellulären Ableitmethode wird die Ableitelektrode über die abgeschnittene Spitze eines Riechsinneshaares gestülpt (Kaissling, 1995). *Tip Recordings* erlauben es, die Aktivität des gesamten Sensillums abzuleiten. Im Gegensatz zu vielen anderen extrazellulären Ableitmethoden haben *Tip Recordings* jedoch den Vorteil, Zugang zu einem klar definierten Satz elektrisch aktiver Zellen zu bieten: zu zwei olfaktorischen Rezeptorneuronen (ORNs), die umgeben sind von drei akzessorischen Zellen (Introduction, Abb. 1; Keil, 1989). Die akzessorischen Zellen erzeugen ein transepitheliales Potential (TEP), dessen Aufgabe gemeinhin in einer Erhöhung der elektromotorischen Kraft gesehen wird, die das Rezeptorpotential treibt.

Kapitel 1

Das TEP ist im Zeitverlauf nicht stabil, sondern zeigt Fluktuationen, die typischerweise nach einigen Stunden periodisch werden und einen charakteristischen Kurvenverlauf haben. Dies war bereits längere Zeit bekannt (Zack, 1979), ist aber in der im ersten Kapitel beschriebenen Studie „Oscillations of the transepithelial potential of moth olfactory sensilla are influenced by octopamine and serotonin" (Dolzer et al., 2001) erstmals genauer untersucht worden. In dieser Studie wurde ausgenutzt, dass das Versuchstier während der Ableitung zwar in einem Halter fixiert ist, aber weitgehend unversehrt bleiben kann. Das bringt zweierlei Vorteile: Zum einen können diese Ableitungen am intakten Tier ungewöhnlich lange gehalten werden (bis zu 100 h). Zum anderen zeigt das Tier noch Verhalten, so dass die Flugaktivität mit Hilfe eines Piezo-Sensors aufgezeichnet werden konnte. Es zeigte sich, dass die Oszillationen des TEP und die Flugaktivität negativ korreliert sind. Während der meist einige Stunden dauernden Phasen, in denen das TEP oszilliert, bleibt das Versuchstier normalerweise

völlig ruhig. Während der Flugaktivitätsphasen, die selten länger als eine Stunde dauern, zeigt das TEP einen nicht-periodischen Zeitverlauf (Kapitel 1, Abb. 1). Weiterhin konnte gezeigt werden, dass sich die Oszillationen durch die Injektion der biogenen Amine Octopamin und Serotonin nahe der Antennenbasis unterschiedlich beeinflussen lassen. Octopamin unterdrückt die Oszillation vollständig, während Serotonin den Kurvenverlauf ändert. Dies hat zu einer neuen Hypothese einer Regulation des TEP geführt, das vermutlich in einem zweistufigen Prozess von einer V-ATPase und einem nachgeschalteten H^+/K^+-Antiport erzeugt wird. Die Oszillationen sind offenbar Regelungsschwankungen dieser beiden Proteine, die durch die biogenen Amine beeinflusst werden können.

Neben den langsamen Schwankungen des TEP lassen sich in *Tip Recordings* von unstimulierten Trichoidsensillen Aktionspotentiale beider ORNs ableiten, die in *Bursts* auftreten, schnellen Abfolgen von, im Mittel, etwas über 3,3 Aktionspotentialen (Kapitel 1, Tab. 3). Da die Unterschiede in der Amplitude der Aktionspotentiale, die von den beiden ORNs generiert werden, geringer sind als bei vielen anderen nachtaktiven Schmetterlingen, und zudem während der *Bursts* die Amplituden der beiden Klassen einander überlagern, galten die Aktionspotentiale bisher bei *M. sexta* als nicht zuverlässig zu unterscheiden (Kaissling et al., 1989; Marion-Poll und Tobin, 1992; Kalinová et al., 2001). Der im Rahmen dieser Arbeit entwickelte Sortier-Algorithmius, der den zeitlichen Kontext mit berücksichtigt, hat es jedoch ermöglicht, die Aktionspotentiale beider ORNs in über 80% der Ableitungen zu unterscheiden und die Spontanaktivität sehr detailliert zu charakterisieren. Ebenso war es erst hierdurch möglich zu zeigen, dass die Spontanaktivität in Abwesenheit von Pheromon nicht von Octopamin beeinflusst wird. Studien an anderen Arten hatten ergeben, dass Octopamin die Hintergrundaktivität in Anwesenheit selbst sehr geringer Pheromondosen erhöht (Pophof, 2000; Grosmaitre et al., 2001).

Kapitel 2

Das zweite Kapitel, „Adaptation in pheromone-sensitive trichoid sensilla of the hawkmoth *Manduca sexta*", befasst sich mit den Antworten der Sensillen auf olfaktorische Stimulation. Pheromonsensillen nachtaktiver Schmetterlinge eignen sich besonders gut zur Untersuchung quantitativer Fragestellungen, da ihre Spezifität schon anhand der Morphologie eindeutig erkennbar ist. Daher muss nicht, wie bei Sensillen, die auf Futter- oder andere Düfte antworten, zunächst der adäquate Reiz gefunden werden. Trichoidsensillen antworten auf Stimulation mit Bombykal, der Hauptkomponente im arteigenen Pheromongemisch, mit einem vergleichsweise langsamen Sensillenpotential, einem reizkorrelierten Absinken des TEP, und überlagerten schnellen Aktionspotentialen (Kapitel 2, Abb. 1). Die Sensillenpotentiale spiegeln vermutlich zu einem großen Teil die Rezeptorpotentiale wider, die im ersten Schritt der chemo-elektrischen Transduktionskaskade im äusseren dendritischen Segment der ORNs entstehen. Die Aktionspotentiale dagegen entstehen, räumlich wie elektrisch weit entfernt, im Soma- oder Axonhügelbereich. Daher wurden diese Einzelkomponenten der Antwort voneinander getrennt und nach mehreren verschiedenen Parametern charakterisiert. Auf diese Weise wurde die Dosisabhängigkeit der Pheromonantwort im nicht-adaptierten Zustand und nach Adaptation durch einen starken Reiz ermittelt und verglichen. Es zeigte sich, dass die Aktionspotentialantwort stärker adaptiert als die Sensillenpotentialantwort. Dies weist auf die Existenz von mindestens zwei Adaptationsmechanismen hin. Das darüber hinaus gefundene schnellere Abklingen der Sensillenpotentiale im adaptierten Zustand führt weiter zu der Annahme, dass noch ein dritter Adaptationsmechanismus eine Rolle spielt, der wahrscheinlich über eine Stabilisierung des Ruhepotentials wirkt.

Diese Studie fügt sich in die bisher veröffentlichten Arbeiten über extrazelluläre Ableitungen am Pheromonsystem von *M. sexta* ein (Kaissling et al., 1989; Marion-Poll und Tobin, 1992; Kalinová et al., 2001).

Während Kaissling et al. und Kalinová et al. sich hauptsächlich mit qualitativen Fragestellungen befassten, hatten die beiden letztgenannten Arbeiten ausschließlich die Aktionspotentialantwort zum Thema. Die vorliegende Studie stellt daher erstmals eine Untersuchung dar, die sich quantitativ mit der Adaptation sowohl der Sensillenpotentiale, als auch der Aktionspotentiale, sowie deren Beziehung zueinander befasst.

Kapitel 3

Dieses Kapitel mit dem Titel „Cyclic guanosine-monophosphate and tetraethylammonium modulate action potentials of olfactory receptor neurons in trichoid sensilla of the hawkmoth *Manduca sexta*" stellt das Bindeglied zwischen den extrazellulär- und den Patch Clamp-Ableitungen dar. Nachdem im ersten Kapitel gezeigt worden ist, dass Substanzen, die an der Antennenbasis injiziert wurden, in die Antenne transportiert werden und auf Ziele in den akzessorischen Zellen wirken, gehen die hier vorgestellten Experimente noch darüber hinaus. Es wird gezeigt, dass 8-Bromo-3',5'-zyklisches Guanosinmonophosphat (8bcGMP), ein membrangängiges cGMP-Analogon, an der Antennenbasis injiziert, die Kurvenform spontaner Aktionspotentiale beeinflusst. Neben einer Erhöhung der Gesamtamplitude der Aktionspotentiale kommt es zu einer Verlängerung der Repolarisationsphase. Dies lässt auf eine Wirkung des zyklischen Nukleotids auf zwei verschiedene Klassen von Ionenkanälen schließen, unspezifische Kationenkanäle und *delayed rectifier*-Kaliumkanäle. Die Veränderung der Aktionspotentialform zeigt bei den beiden Amplitudenklassen einen unterschiedlichen Zeitverlauf. Dies zeigt, dass die Zielstrukturen von 8bcGMP innerhalb der ORNs liegen müssen.

Des Weiteren wurden die Auswirkungen von 8bcGMP und dem Ionenkanalblocker TEA in der Elektrolytlösung der Ableitelektrode auf Pheromonantworten untersucht. Diese Arbeiten werden derzeit unter meiner praktischen Anleitung von Christian Flecke im Rahmen seiner Diplomarbeit durchgeführt. Die ersten Ergebnisse zeigen, dass beide Agenzien innerhalb von drei Stunden in die Sensillen diffundiert sind und auf Ziele innerhalb der ORNs wirken. TEA verändert nicht, wie zu erwarten gewesen wäre, die Sensillenpotentialantwort, sondern verringert offenbar spezifisch die Frequenz der Aktionspotentiale und verlängert deren Latenzzeit. Das Sensillenpotential bleibt dagegen weitgehend unverändert, was den Schluss nahelegt, dass TEA in die Zellen hinein gelangt. Andere mögliche Wirkungswege werden aber ebenfalls zur Diskussion gestellt. Die Wirkung von 8bcGMP ist ähnlich der von TEA: Die Frequenz der Aktionspotentiale nimmt ab, die Latenzzeit nimmt zu und das Sensillenpotential ist nur wenig verändert. Darüber hinaus hat 8bcGMP aber auch in dieser Applikationsform eine Auswirkung auf die Kurvenform der Aktionspotentiale. Damit wird es sehr wahrscheinlich, dass derjenige Adaptationsmechanismus, der – wie in Kapitel 2 gezeigt – die Aktionspotentialantwort stärker adaptiert als die Sensillenpotentialantwort, cGMP-abhängig ist.

Diese jüngsten Experimente zeigen deutlich, dass die *Tip Recording*-Technik ein wichtiges und – nicht zuletzt dank der hier vorgestellten Methoden und Ergebnisse – gut charakterisiertes und effizient handhabbares *in situ*-System zur Ergänzung der *in vitro* gewonnenen Erkenntnisse ist.

Kapitel 4

Elektrophysiologische Ableitungen die bis hin zu mehreren Tagen dauern, wie in Kapitel 1 dargestellt, gleichzeitig aber eine zeitliche Auflösung erfordern, die die Unterscheidung und Charakterisierung von Aktionspotentialen erlauben, sind mit Standardmethoden nicht auswertbar. Darüber hinaus gibt es bis heute keine kommerziell erhältliche Software, die Pheromonantworten nach den in dieser Arbeit verwendeten Kriterien zu charakterisieren in der Lage ist. Daher habe ich im Rahmen meiner Doktorarbeit ein Programm entwickelt, das diese Anforderungen erfüllt. Aus ursprünglich verwendeten Batch-Dateien und einzelnen

Makroprozeduren in verschiedenen Anwendungen ist letztlich ein Programm entstanden, das die effiziente Auswertung der in den Kapiteln 1–3 beschriebenen Versuche überhaupt erst ermöglicht hat. Dieses Programm trägt den Namen XtraCell und ist als Add-In zur Tabellenkalkulation Microsoft Excel konzipiert. Zur Rohauswertung der aufgenommenen Daten aus Stimulationsversuchen ist darüber hinaus das Programm Clampfit aus dem Programmpaket pCLAMP 8 (Axon Instruments, Union City, Kalifornien) notwendig. Die Auswertung der Spontanaktivität kann dagegen prinzipiell auch mit ASCII-Daten aus anderer Quelle durchgeführt werden. Dieses Kapitel dient der Dokumentation von XtraCell und ist daher ähnlich wie ein Programmhandbuch angelegt. Neben der Beschreibung von Systemvoraussetzungen, Installation und grundsätzlicher Bedienung werden die einzelnen Programmfunktionen anhand der Auswertung von Beispieldateien Schritt für Schritt erklärt. Die Bespieldateien wurden dabei so ausgewählt, dass auch potentielle Fehlerquellen behandelt werden, und das Vorgehen in solchen Fällen aufgezeigt werden kann, in denen eine automatische Verarbeitung nicht zuverlässig möglich ist.

XtraCell wird anderen Forschern unter der GNU General Public License unentgeltlich zur Verwendung und Weiterentwicklung zur Verfügung gestellt. Das Programm befindet sich auf der den gedruckten Exemplaren dieser Arbeit beigefügten CD-ROM, wird aber auch im Internet verfügbar sein (www.jan-dolzer.de).

Teil II

Kapitel 5

Biochemische und physiologische Untersuchungen lassen vermuten, dass cGMP eine Rolle bei der Adaptation pheromonsensitiver ORNs spielt (Ziegelberger et al., 1990; Boekhoff et al., 1993; Redkozubov, 2000; Stengl et al., 2001; Kapitel 3 der vorliegenden Arbeit). Daher wurde in *Patch Clamp*-Ableitungen der Einfluss zyklischer Nukleotide auf Ionenkanäle in kultivierten ORNs untersucht. Es wurden zwei unterschiedliche Ansätze verfolgt. In *cell-attached-* und *inside-out*-Ableitungen, in denen die Aktivität einzelner Ionenkanäle untersucht werden kann (Kapitel 5, Abb. 1), wurde eine Vielzahl unterschiedlicher Kanaltypen gefunden. Diese Kanäle wurden nach ihrer Leitfähigkeit in drei Klassen eingeteilt, klein, mittelgroß und groß. Die kleinen Kanäle wurden relativ selten abgeleitet und konnten nicht genauer charakterisiert werden, da sie meist von den beiden größeren Kanaltypen überlagert und damit verdeckt wurden.

Ein Typ der mittelgroßen Kanäle mit einer Leitfähigkeit von 30–70 pS trat meist in mehreren Kopien in jedem *Patch* auf. Diese Kanäle aktivierten häufig ohne Applikation von Pharmaka, vermutlich aufgrund einer erhöhten Ca^{2+}-Konzentration auf der cytoplasmatischen Seite der Membran. Sie wurden häufiger nach der Applikation von 8bcGMP beobachtet als ohne Applikation von Pharmaka. Noch häufiger traten sie jedoch nach Aktivierung der Proteinkinase C durch Phorbolester auf. Ob es sich dabei jedoch um die Aktivierung derselben Kanaltypen auf verschiede Arten handelt, oder um verschiedene Kanaltypen, bleibt vorerst offen. Diese mittelgroßen Kanäle haben eine lineare Strom-Spannungs-Kennlinie mit einem Umkehrpotential um 0 mV, sind also offenbar unspezifische Kationenkanäle. Ein anderer Typ mittelgroßer Ionenkanäle, ein auswärts gleichrichtender Kaliumkanal, der weitaus seltener abgeleitet werden konnte, wurde durch 8bcGMP inaktiviert.

Die großen Kanäle mit einer Leitfähigkeit von bis zu mehreren hundert pS schienen ebenfalls Ca^{2+}-abhängig zu sein. Der Strom durch diese Kanäle verringerte sich praktisch nicht, wenn alle Kationen durch N-Methyl-D-Glucamin ersetzt wurden, ein sehr großes Kation, für das die meisten Kationenkanäle nicht durchgängig sind. Daher ist es wahrscheinlich, dass es sich um Chlorid- oder Anionenkanäle handelt. Gegenüber einer Vielzahl

bekannter Chloridkanalblocker waren sie jedoch unempfindlich. Auch die großen Kanäle wurden nach der Gabe von 8bcGMP und nach Aktivierung der Proteinkinase C häufiger beobachtet. Die mittelgroßen und großen Kanäle aktivierten oft in engem zeitlichem Zusammenhang unmittelbar nacheinander, was auf die Anwesenheit von Transducisomen hinweisen könnte.

In *perforated Patch*-Ableitungen, in denen Ströme durch die Membran der ganzen Zelle gemessen werden, wurden elf Stromkomponenten unterschieden. Einige dieser Ströme waren bereits vorher in ORNs von Nachtschmetterlingen gezeigt worden. Drei Stromtypen werden jedoch im Rahmen dieser Arbeit erstmals beschrieben. Ein auswärts gleichgerichteter Kaliumstrom, der sich durch eine langsame Inaktivierung nach Depolarisation der Zellmembran auszeichnet, wurde signifikant häufiger nach Applikation von 8bcGMP, aber auch etwas häufiger nach Gabe von 8-Bromo-cAMP (8bcAMP) beobachtet. Damit könnte dieser Strom die in Kapitel 3 gezeigte Verlängerung der Repolarisationsphase der Aktionspotentiale verursachen. Ein weiterer Strom, der sich ebenfalls durch seine aussergewöhnlich langsame Kinetik auszeichnet, wurde häufig nach langer, starker Depolarisation abgeleitet, was auf eine Aktivierung durch Ca^{2+} hinweist. Dieser Strom aktivert mit einer Zeitkonstante von mehr als 1.5 s bei Depolarisation und inaktiviert mit einer etwa dreifach kürzeren Zeitkonstante bei Hyperpolarisation. Er wurde signifikant seltener nach Gabe von 8bcAMP abgeleitet, bleibt aber von 8bcGMP offenbar unbeeinflusst. Dieser Strom könnte eine Rolle bei der Stabilisierung des Ruhepotentials spielen und damit der in Kapitel 2 beschriebenen Verkürzung der Abklingphase von Sensillenpotentialen im adaptierten Zustand zu Grunde liegen. Der dritte neu beschriebene Strom ist linear und hat ein Umkehrpotential von 0 mV, ist also ein unspezifischer Kationen- oder Anionenstrom. Er hat eine hohe Leitfähigkeit und ist vermutlich Ca^{2+}-aktiviert. Es ist anzunehmen, dass die in den Einzelkanalableitungen beobachteten großen Kanäle diesen Strom verursachen. Auch sie könnten für eine Stabilisierung des Ruhepotentials verantwortlich sein.

Obwohl die in den *Patch Clamp*-Ableitungen gewonnenen Ergebnisse auf Grund der Vielzahl von Ionenkanälen und -strömen einer gezielteren Untersuchung einzelner Aspekte bedürfen, stellen sie doch einen weiteren Schritt auf dem Weg zum Verständnis der Funktion olfaktorischer Rezeptorneurone dar.

Veröffentlichte Teile der Arbeit

Kapitel 1 („Oscillations of the transepithelial potential of moth olfactory sensilla are influenced by octopamine and serotonin") ist im Sommer 2001 im *Journal of Experimental Biology* veröffentlicht worden (Dolzer et al., 2001). Das Kapitel entspricht in der hier wiedergegebenen Ausführung der Veröffentlichung, wurde aber noch um zwei Anhänge erweitert. Kapitel 2 („Adaptation in pheromone-sensitive trichoid sensilla of the hawkmoth *Manduca sexta*") wurde beim *Journal of Experimental Biology* zur Veröffentlichung eingereicht. Dieses Kapitel entspricht der eingereichten Fassung des Manuskripts. Das Layout orientiert sich demnach, ebenso wie bei den übrigen Kapiteln, an den Maßgaben dieser Zeitschrift. Kurz vor der Fertigstellung dieser Dissertation lag das Gutachten zum Manuskript vor. Die von den Gutachtern geforderten Änderungen machen eine entsprechende Überarbeitung notwendig. Daher wird sich die letztendlich veröffentlichte Version des Manuskripts in einigen Punkten von der hier vorgelegten unterscheiden.

Über diese bereits erschienenen bzw. eingereichten Veröffentlichungen hinaus habe ich im Rahmen meiner Doktorarbeit ein Kapitel mit Übungen (*Tutorials*) zum Handbuch der von uns verwendeten elektrophysiologischen Software pCLAMP verfasst (Axon Instruments, 1999). Da diese Arbeit rein methodischer Natur ist, und auch die Autoren des Handbuchs nicht namentlich genannt sind, ist dieses Kapitel

nicht Teil der vorgelegten Dissertation. Zwei der dort dargelegten Szenarien sind thematisch jedoch eng mit der Auswertung der extrazellulären Ableitungen verwandt, wie sie in Kapitel 4 vorgestellt wird. Ich habe eine der Abbildungen (Kapitel 4, Abb. 22) und einige wenige Textpassagen aus dem Manuskript für das Handbuch übernommen. Eine Genehmigung des Urheberrechtsinhabers, Axon Instruments Inc., liegt vor.

Die übrigen Kapitel sind bislang unveröffentlicht und vorerst nicht zur Veröffentlichung vorgesehen.

Da ich im Laufe der Doktorarbeit mehrere internationale Kontakte geknüpft habe, wird diese Dissertation in englischer Sprache vorgelegt. Dies wurde vom Dekan des Fachbereiches Biologie am 30.11.2001 genehmigt.

Eigene Beiträge zu Teilen der Dissertation, die aus gemeinsamer Forschung entstanden

Laut Promotionsordnung müssen bei den Teilen der Dissertation, die aus gemeinsamer Forschungsarbeit entstanden, „die individuellen Leistungen des Doktoranden deutlich abgrenzbar und bewertbar sein." Dies betrifft die Kapitel 1–3 und 5.

Beitrag zum Kapitel 1 („Oscillations of the transepithelial potential of moth olfactory sensilla are influenced by octopamine and serotonin"):

- Entwicklung und Umsetzung der Methoden zur Injektion der Agenzien, zur Datenaufnahme und Auswertung (vgl. Kapitel 4),
- Durchführung und Auswertung eines Teiles der Ableitungen[1],
- Verfassen der Veröffentlichung in Zusammenarbeit mit HD Dr. M. Stengl.

Beitrag zum Kapitel 2 („Adaptation in pheromone-sensitive trichoid sensilla of the hawkmoth *Manduca sexta*"):

- Aufbau des elektrophysiologischen Messstandes in Regensburg (in Anlehnung an einen Messstand im Max-Planck-Institut für Verhaltensphysiologie in Seewiesen),
- Entwicklung und Umsetzung der Methoden zur computergesteuerten Reizgebung, Datenaufnahme und Auswertung,
- Betreuung des methodischen Teils der Diplomarbeit von Karin Fischer, geb. Bittmann (Bittmann, 1999). Die Experimente, die im Rahmen dieser Arbeit durchgeführt wurden, stellen den größten Teil der Daten dar, die dem Manuskript zugrunde liegen,
- Durchführung und Auswertung eines Teiles der Ableitungen[2],
- Verfassen des Manuskripts zur Veröffentlichung in Zusammenarbeit mit HD Dr. M. Stengl.

Beitrag zum Kapitel 3 („Cyclic guanosine-monophosphate and tetraethylammonium modulate action potentials of olfactory receptor neurons in trichoid sensilla of the hawkmoth *Manduca sexta*"):

- Durchführung und Auswertung eines Teils der Ableitungen zur Injektion von 8bcGMP, die im Rahmen des in Kapitel 1 beschriebenen Projekts stattfanden,
- Entwicklung der Auswertmethode zur Darstellung des Zeitverlaufs der Aktionspotentialform (Kapitel 3, Abb. 1; vgl. Kapitel 4),
- Betreuung des methodischen Teils des Laborpraktikums und der Diplomarbeit von Christian Flecke, in deren Verlauf die übrigen Daten gewonnen wurden.

---

[1] Der Großteil der Ableitungen wurde im Rahmen eines von mir betreuten Praktikums in Zusammenarbeit mit Steffi Krannich durchgeführt. Häufig hat einer der Experimentatoren die Ableitung begonnen und der/die andere mehrere Stunden später die Injektion durchgeführt, während beide in der Zwischenzeit schon Teile der Ableitung ausgewertet haben. Daher ist die Angabe eines prozentualen Anteils selbst durchgeführter Ableitungen nicht möglich.

[2] Neben den Ableitungen, die im Zusammenhang mit ihrer Diplomarbeit zusammen mit Karin Fischer durchgeführt und ausgewertet wurden, gingen noch einige Experimente in das Kapitel ein, die davor oder danach von mir selbst, oder im Rahmen von mir betreuter Kurse von Studenten durchgeführt wurden.

Beitrag zum Kapitel 5 („Pharmacological investigation of ion channels in cultured olfactory receptor neurons of the hawkmoth *Manduca sexta*"):

- Durchführung und Auswertung aller Experimente.

Literaturverzeichnis

Die Zahl der Literaturverweise wurde in dieser Zusammenfassung bewusst möglichst gering gehalten. Ausführlichere Verweise finden sich in den einzelnen Kapiteln.

Axon Instruments (1999). User's Guide to Clampex and Clampfit. *pCLAMP Windows Data Acquisition and Whole Cell Analysis*. Foster City: Axon Instruments Inc.

Bittmann, K. (1999). Spontanaktivität und Adaptation in olfaktorischen Rezeptorneuronen beim Tabakschwärmer *Manduca sexta*. Master Thesis, Universität Regensburg.

Boekhoff, I., Seifert, E., Göggerle, S., Lindemann, M., Krüger, B. W. und Breer, H. (1993). Pheromone-induced second-messenger signaling in insect antennae. *Insect Biochem. Mol. Biol.* **23**(7), 757-762.

Dolzer, J., Krannich, S., Fischer, K. und Stengl, M. (2001). Oscillations of the transepithelial potential of moth olfactory sensilla are influenced by octopamine and serotonin. *J. Exp. Biol.* **204**, 2781-2794.

Grosmaitre, X., Marion-Poll, F. und Renou, M. (2001). Biogenic amines modulate olfactory receptor neurons firing activity in *Mamestra brassicae*. *Chem. Senses* **26**, 653-661.

Kaissling, K.-E. (1995). Single unit and electroantennogram recordings in insect olfactory organs. In *Experimental Cell Biology of Taste and Olfaction* (ed. A. I. Spielman), pp. 361-377. Boca Raton, New York, London, Tokyo: CRC Press.

Kaissling, K.-E., Hildebrand, J. G. und Tumlinson, J. H. (1989). Pheromone receptor cells in the male moth *Manduca sexta*. *Arch. Insect Biochem. Physiol.* **10**, 273-279.

Kalinová, B., Hoskovec, M., Liblikas, I., Unelius, C. R. und Hansson, B. S. (2001). Detection of sex pheromone components in *Manduca sexta* (L.). *Chem. Senses* **26**(9), 1175-1186.

Keil, T. A. (1989). Fine structure of the pheromone-sensitive sensilla on the antenna of the hawkmoth, *Manduca sexta*. *Tissue Cell* **21**(1), 139-151.

Marion-Poll, F. und Tobin, T. R. (1992). Temporal coding of pheromone pulses and trains in *Manduca sexta*. *J. Comp. Physiol. A* **171**, 505-512.

Pophof, B. (2000). Octopamine modulates the sensitivity of silkmoth pheromone receptor neurons. *J. Comp. Physiol. A* **186**, 307-313.

Redkozubov, A. (2000). Guanosine 3',5'-cyclic monophosphate reduces the response of the Moth's olfactory receptor neuron to pheromone. *Chem. Senses* **25**, 381-385.

Stengl, M., Zintl, R., de Vente, J. und Nighorn, A. (2001). Localization of cGMP immunoreactivity and of soluble guanylyl cyclase in antennal sensilla of the hawkmoth *Manduca sexta*. *Cell Tissue Res.* **304**, 409-421.

Zack, C. (1979). Sensory adaptation in the sex pheromone receptor cells of saturniid moths. Ph.D. Thesis, Ludwig-Maximilians-Universität, München.

Ziegelberger, G., van den Berg, M. J., Kaissling, K.-E., Klumpp, S. und Schultz, J. E. (1990). Cyclic GMP levels and guanylate cyclase activity in pheromone-sensitive antennae of the silkmoths *Antheraea polyphemus* and *Bombyx mori*. *J. Neurosci.* **10**(4), 1217-1225.

Introduction

Most nocturnal moths find their mating partners with the help of pheromones released by the females and attracting the males. The males perceive the pheromone blend with a large number of specialized sensory hairs on their antennae, the sensilla trichoidea. In the sphinx moth *Manduca sexta*, each trichoid sensillum contains two olfactory receptor neurons, ensheathed by a common set of accessory cells, the innermost thecogen cell, the trichogen and the tormogen cell (Fig. 1; Keil, 1989; Lee and Strausfeld, 1990). The trichogen and the tormogen cell secrete the receptor lymph or sensillum lymph, which fills the receptor lymph cavity and the lumen of the sensory hair. The receptor lymph contains high concentrations of potassium (up to 200 mmol l^{-1}) and pheromone-binding protein (Kaissling et al., 1985; Vogt and Riddiford, 1986).

In extracellular tip recordings, the tip of the sensory hair is clipped off, and the recording electrode, containing sensillum lymph ringer, is slipped over the open hair (Kaissling, 1995), while the reference electrode is inserted into the haemolymph space. In this way, the electrical activity of the olfactory receptor neurons and the accessory cells are recorded as a composite signal. In contrast to many other extracellular recording techniques, tip recordings thus give access to a clearly defined set of electrically active cells. The first part of this thesis, comprising Chapters 1–4, presents results obtained in tip recordings. Chapter 1 describes the electrical activity of trichoid sensilla in the absence of pheromone. Oscillations of the

transepithelial potential and their negative correlation with flight activity were characterized. The oscillations were influenced by injections of the biogenic amines octopamine and serotonin near the antennal base. In addition, the spontaneous action
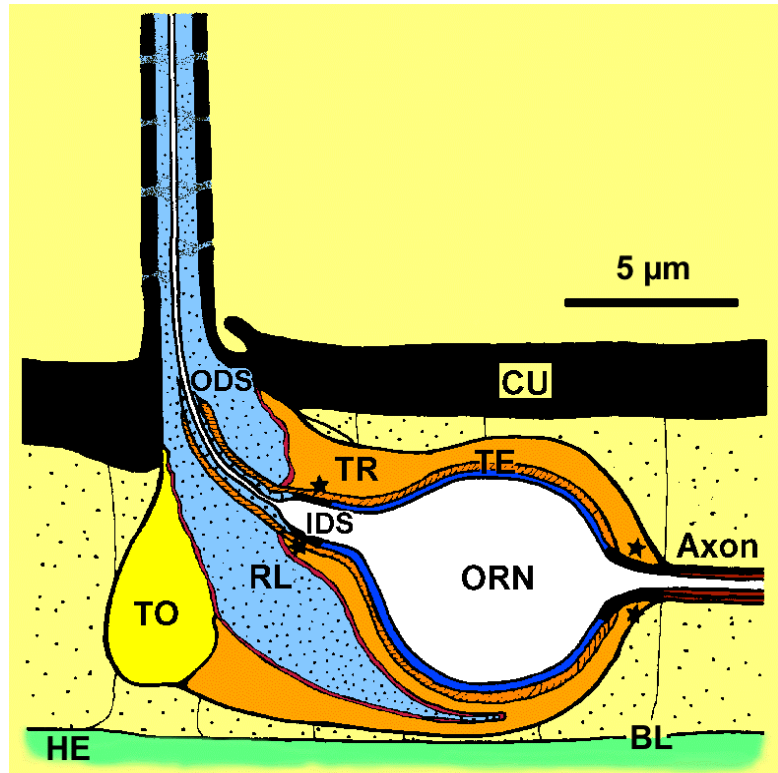
Fig. 1: Schematic drawing of an insect olfactory sensillum. Pheromone-dependent trichoid sensilla of *M. sexta* contain two receptor neurons. ODS: outer dendritic segment, CU: cuticle, TR: trichogen cell, TE: thecogen cell, IDS: inner dendritic segment, TO: tormogen cell, RL: receptor lymph and receptor lymph cavity, ORN: olfactory receptor neuron, HE: haemolymph, BL: basal lamina. The asterisks mark zones of septate junctions at the transition between inner and outer dendritic segment, and at the axon hillock.

potential activity of both ORNs was quantitatively investigated. There is obviously no correlation between the time course of the transepithelial potential and the spontaneous action potential activity. Likewise, the action potential activity was not significantly influenced by amine injection. This chapter was published in the *Journal of Experimental Biology* (Dolzer et al., 2001).

Pheromone receptors are made for the detection of pheromone. So Chapters 2 and 3 deal with the responses of trichoid sensilla to stimulation with

bombykal, the main component in the conspecific pheromone blend (Tumlinson et al., 1989). In response to pheromone, trichoid sensilla generate a negative deflection of the transepithelial potential, the sensillar potential, and a series of action potentials. These responses were quantitatively investigated, and their dose-dependence was determined in two different states of adaptation. While it has long been known that two different adaptation mechanisms act on the generation of sensillar potentials and action potentials, respectively (Zack, 1979), this study suggests the presence of a third mechanism that presumably acts via stabilization of the resting potential.

Biochemical and physiological evidence have suggested the involvement of cyclic GMP in adaptation. Chapter 3 describes the effects of a membrane-permeant cyclic GMP analogue on spontaneous action potentials and on action potentials generated in response to bombykal. The waveform of spontaneous action potentials was altered by cyclic GMP in a way that suggests the action of this messenger on at least two different types of ion channels. In pheromone responses, cyclic GMP selectively reduced the action potential response, but did not influence the sensillar potentials. Furthermore, it reduced the decrease of the action potential amplitude that is observed during pheromone responses, suggesting that it acts on ion channels that contribute to the overall resistance of the receptor neurons, but do not participate in sensillar potential generation. The ion channel blocker tetraethylammonium, which acts on potassium channels and a number of other cation channels, mimicked the action of cyclic GMP on the action potential response and presumably also on the reduction of the action potential amplitude. So the results presented in this chapter provide new insight in the mechanisms of adaptation, but raise a number of questions, especially on the contribution of receptor potentials to sensillar potentials.

Non-standard experiments require non-standard methods. The recordings presented in Chapter 1 were maintained for up to several days. Very slow components, such as the oscillations of the transepithelial potential, and fast components, such as the spontaneous action potentials, were to be monitored continuously and analyzed in an efficient way. Furthermore, no commercially available software is capable of evaluating those parameters by which pheromone responses were characterized in Chapters 2 and 3. Therefore, a program was developed that allows the time-efficient analysis of both, spontaneous activity and responses to adequate stimulation, recorded from insect sensilla. To make use of pre-existing functionality whenever possible, the program is designed to co-operate with commercially available software. Chapter 4 serves for the documentation of the program and explains its use for the analysis of recordings step by step. The developed software may be applicable to recordings of olfactory sensilla in other species, too, and might even be useful in the analysis of recordings from sensilla of other sensory modalities. Therefore, the program is made available to other researchers under the GNU General Public License, is contained on the CD ROM distributed with the print copies of this thesis, and will also be available in the internet (www.jan-dolzer.de).

Chapter 5, which makes up the second part of the thesis, describes patch clamp recordings of cultured olfactory receptor neurons. In both, single-channel recordings and perforated patch whole-cell recordings, a large variety of ion channels and currents was recorded. The single-channel recordings revealed a number of medium-sized ion channels that are activated by an increase in intracellular calcium, by cyclic GMP and by activation of protein kinase C. In addition, a class of large presumptive anion channels is described for the first time, which also appears to be activated by these factors. In the perforated patch recordings,

besides a collection of known currents, three currents or current components were recorded, which are described in insect olfactory receptor neurons for the first time. Two of them are obviously potassium and/or cation currents, which are characterized by their slow kinetics. They are influenced by cyclic GMP and cyclic AMP in different ways. The third newly described current is a large, apparently calcium-activated, nonspecific current that is presumably caused by the large channels found in the single-channel recordings.

While the *in situ* approach of the tip recordings maintains the compartmentalization of the olfactory receptor neurons, but always includes contributions of the accessory cells, the *in vitro* approach of the patch clamp recordings provides more direct access to ion channels of the receptor neurons themselves, but does not allow a statement about their localization in an individual compartment *in situ*. Therefore, both recording techniques were employed in this doctoral thesis to contribute a little share to the understanding of modulation and adaptation in pheromone sensilla of *Manduca sexta*.

References

Dolzer, J., Krannich, S., Fischer, K. and Stengl, M. (2001). Oscillations of the transepithelial potential of moth olfactory sensilla are influenced by octopamine and serotonin. *J. Exp. Biol.* **204**, 2781-2794.

Kaissling, K.-E. (1995). Single unit and electroantennogram recordings in insect olfactory organs. In *Experimental Cell Biology of Taste and Olfaction* (ed. A. I. Spielman), pp. 361-377. Boca Raton, New York, London, Tokyo: CRC Press.

Kaissling, K.-E., Klein, U., de Kramer, J. J., Keil, T. A., Kanaujia, S. and Hemberger, J. (1985). Insect olfactory cells: electrophysiological and biochemical studies. In *Molecular Basis of Nerve Activity* (ed. J. P. Changeux), pp. 173-183. Berlin: de Gruyter.

Keil, T. A. (1989). Fine structure of the pheromone-sensitive sensilla on the antenna of the hawkmoth, *Manduca sexta*. *Tissue Cell* **21**(1), 139-151.

Lee, J. K. and Strausfeld, N. (1990). Structure, distribution and number of surface sensilla and their receptor cells on the olfactory appendage of the male moth *Manduca sexta*. *J. Neurocytol.* **19**, 519-538.

Tumlinson, J. H., Brennan, M. M., Doolittle, R. E., Mitchell, E. R., Brabham, A., Mazomemos, B. E., Baumhover, A. H. and Jackson, D. M. (1989). Identification of a pheromone blend attractive to *Manduca sexta* (L.) males in a wind tunnel. *Arch. Insect Biochem. Physiol.* **10**, 255-271.

Vogt, R. G. and Riddiford, L. M. (1986). Pheromone reception: a kinetic equilibrium. In *Mechanisms in Insect Olfaction* (ed. T. L. Payne), pp. 201-208. Oxford University Press.

Zack, C. (1979). Sensory adaptation in the sex pheromone receptor cells of saturniid moths. Ph.D. Thesis, Ludwig-Maximilians-Universität, München.

Part I

Chapter 1

Chapter 2

Chapter 3

Chapter 4

OSCILLATIONS OF THE TRANSEPITHELIAL POTENTIAL OF MOTH OLFACTORY SENSILLA ARE INFLUENCED BY OCTOPAMINE AND SEROTONIN

JAN DOLZER[1,2], STEFFI KRANNICH[1], KARIN FISCHER[2] AND MONIKA STENGL[1,2,*]

[1]*Biologie, Tierphysiologie, Philipps-Universität Marburg, Karl-von-Frisch-Straße, D-35032 Marburg, Germany* and
[2]*Institut für Zoologie, Universität Regensburg, D-93040 Regensburg, Germany*

*Author for correspondence at address 1 (e-mail: stengl@mailer.uni-marburg.de)

Summary

The biogenic amine octopamine is known to enhance the sensitivity of male moths to their species-specific pheromones in flight-tunnel experiments. This sensitization of pheromone-guided upwind flight is at least partly due to octopamine-dependent increases in the peak nerve impulse frequency of the pheromone response of olfactory receptor neurons. It is not known, however, whether octopamine exerts its effects directly on the electrical properties of the olfactory receptor neurons or indirectly, *via* modulation of the accessory cells of the sensillum.

In extracellular tip recordings of pheromone-dependent trichoid sensilla on the antennae of male *Manduca sexta* moths, we investigated the effects of octopamine and serotonin on the transepithelial potential, which is generated by the activity of V-ATPases in sensillar accessory cells. In addition, the action potential activity of unstimulated olfactory receptor neurons was examined in the presence of biogenic amines. Under constant environmental conditions, the transepithelial potential oscillated regularly with periods of 2–8 min and with a 1–25 mV peak-to-peak amplitude over periods of several hours. These oscillatory intervals were interrupted by periods of relatively stable transepithelial potential, correlated with flight activity by the moth. Octopamine reduced the amplitude of the transepithelial potential oscillation and decreased the resistance of the sensillum preparation in a dose-dependent manner. Serotonin altered the waveform of the transepithelial potential, but did not change the resistance of the preparation. Thus, both amines affect the accessory cells, but have different targets in the regulation of the transepithelial potential. Neither amine significantly influenced the spontaneous action potential activity of the olfactory receptor neurons.

Key words: *Manduca sexta*, pheromone sensillum, tip recording, transepithelial potential, oscillation, action potential, octopamine, serotonin.

Introduction

Octopamine, a biogenic monoamine structurally related to norepinephrine, is an invertebrate-specific neurotransmitter, neuromodulator and neurohormone (Roeder, 1999). It acts as a stress hormone, which is released from neurohaemal organs to cope with energy-demanding situations, such as pheromone-dependent flight in insects. In wind-tunnel experiments with various moth species, octopamine improved pheromone blend discrimination and orientation towards pheromone sources, possibly also *via* effects on antennal olfactory sensilla (Linn, 1997; Linn and Roelofs, 1986; Linn and Roelofs, 1992; Linn et al., 1992; Linn et al., 1996). Octopamine is released into insect antennae *via* secretion onto antennal hearts that circulate haemolymph into the antennae (Pass et al., 1988; H. Agricola, personal communication). In addition, 1–2 octopamine-immunoreactive neurons project into the antennal nerve of the moth *Manduca sexta* (U. Homberg, personal communication). Furthermore, putative receptors for octopamine and/or serotonin have been cloned from the antennae of the moths *Bombyx mori* and *Heliothis virescens* and localized in an unidentified cell type at the base of olfactory sensilla (von Nickisch-Rosenegk et al., 1996), suggesting an effect of octopamine on olfactory sensilla in moth antennae. In accordance with these observations, the peak nerve impulse frequency in response to pheromone was found to be increased specifically by octopamine in the moth *Antheraea polyphemus* (Pophof, 2000). It is still not known, however, whether octopamine exerts its effects directly on the olfactory receptor neurons (ORNs) or indirectly *via* effects on the accessory cells of the olfactory sensillum. The accessory cells generate a transepithelial potential (TEP), which has been assigned an important function in increasing the driving force for the ionic movements underlying the receptor potential, thus improving the sensitivity of the sensillum (Thurm, 1972; Thurm and Wessel, 1979). Slow oscillations in the TEP of moth pheromone sensilla are generated by unknown mechanisms (Zack, 1979), and these have also been found in the Malpighian tubules of the beetle *Onymacris plana* (Nicolson and Isaacson, 1987) and of the mosquito *Aedes aegypti* (Williams and

Beyenbach, 1984; Beyenbach et al., 2000). However, it is not clear whether these TEP oscillations are artefacts or have a functional significance.

In tip recordings of pheromone-dependent sensilla trichoidea, we tested whether the biogenic amines octopamine and serotonin affect the accessory-cell-dependent TEP in *Manduca sexta* antennae or the spontaneous action potential activity of the two pheromone-dependent ORNs found in each sensillum (Kaissling et al., 1989; Keil, 1989). Our experiments revealed no significant effects of the biogenic amines on the spontaneous activity of unstimulated ORNs, but showed that both amines, either directly or indirectly, affect different targets in the accessory cells that generate the TEP.

Materials and methods

Animals and preparation for electrophysiological recordings

Manduca sexta moths (Johannson) (Lepidoptera: Sphingidae) were raised from eggs, and larvae were fed on an artificial diet (modified after Bell and Joachim, 1976). The animals were kept under a long-day photoperiod (L:D 17 h:7 h, lights off at 08:00 h) at 24–27 °C and 40–60 % relative humidity. Male pupae were isolated 1 day before emergence, gently cleaned with 70 % ethanol and allowed to hatch without any contact with pheromone. During their second dark phase, the adults were fixed into a Teflon holder. The head capsule was pierced with a syringe needle approximately 1 mm dorsocaudal to the antennal base. The flagellum of the right antenna was immobilized with dental wax (Boxing wax, Sybron/Kerr, Romulus, Michigan, USA), and the 15–20 most apical annuli were clipped off. A glass electrode filled with haemolymph Ringer (Kaissling, 1995) was inserted into the flagellar lumen and sealed with ECG electrode gel (PPG, Hellige, Freiburg, Germany). The tips of long trichoid sensilla from the apical row on the third to tenth remaining annuli were clipped off using sharpened forceps. The recording electrode, filled with sensillum lymph Ringer (Kaissling, 1995), was slipped over one sensillum. A connection to the amplifier inputs was established with Ag/AgCl wires immersed in the electrolytes. In side-wall recordings, an electrochemically sharpened tungsten wire placed near the sensillar base was used as the recording electrode. Signals were amplified approximately 200-fold in a custom-built amplifier (direct current to 2 kHz, input impedance $10^{12} \Omega$) and passed through a 2 kHz anti-aliasing filter (900C/9L8L, Frequency Devices, Haverhill, Massachusetts, USA). Flight activity of the animals was monitored using a piezo-electric element placed on the thorax. A Digidata 1200 B digitizer (Axon Instruments, Union City, California, USA) and pCLAMP 8 software from the same manufacturer were used to acquire data. The electrophysiological signal and a highpass-filtered equivalent (cut-off frequency 2 or 5 Hz), as well as the piezo signal, were continuously recorded on a strip chart recorder (EasyGraf, Gould, Valley View, Ohio, USA). Sections of the direct-current-coupled recording and the piezo-electric signal were also stored on DAT (DTR-1202, Bio-Logic, Claix, France).

After the recordings, more than 90 % of the moths were in sufficiently good condition to be returned to the flight cage.

Environmental conditions

All recordings were performed at room temperature (18–23 °C). The long-term recordings were performed in constant room light to exclude circadian effects. No part of the electrophysiological apparatus had been in contact with pheromone for at least 15 months. Charcoal-filtered and moistened air was blown continuously over the preparation ($13 \, l \, min^{-1}$).

Drug application

Octopamine and serotonin (Sigma, Deisenhofen, Germany), dissolved in haemolymph Ringer, were injected through the hole in the head capsule with a glass capillary. We injected a minimum of $2 \, \mu l$ of a $0.5 \, mmol \, l^{-1}$ octopamine stock solution and a maximum of $5 \, \mu l$ of a $500 \, mmol \, l^{-1}$ solution, resulting in doses of 1–2500 nmol. The highest dose was of the same order of magnitude as in previous studies by Pophof (Pophof, 2000) and Grosmaitre et al. (Grosmaitre et al., 2001), who injected a maximum dose of $1 \, \mu l$ of a $100 \, \mu g \, \mu l^{-1}$ solution ($527 \, mmol \, l^{-1}$). Because an adult moth contains approximately 1 ml of haemolymph (J. Truman, unpublished observation), the final octopamine concentration in the haemolymph was between $1 \, \mu mol \, l^{-1}$ and $2.5 \, mmol \, l^{-1}$.

In addition, we injected a minimum of $2 \, \mu l$ of a $5 \, mmol \, l^{-1}$ serotonin solution and a maximum of $15 \, \mu l$ of a $50 \, mmol \, l^{-1}$ solution, resulting in a dose of 10–750 nmol and a haemolymph concentration of $10–750 \, \mu mol \, l^{-1}$. In a set of pilot experiments, food dye injected at the same site was transported into the antenna with a delay of <1 to 3–5 min.

Polarity conventions

Voltage polarity is given for the sensillum lymph electrode with reference to the haemolymph electrode. Current flow is defined in terms of the movement of positive charge. The sign of current values was chosen to match the polarity of the corresponding voltage response. Therefore, current is termed positive if it flows out of the sensory hair into the sensillum lymph electrode, and negative if it flows the opposite way (see Redkozubov, 2000).

Data-acquisition protocols

At the beginning of each recording, a series of 5 mV calibration pulses was applied to the haemolymph electrode, which was otherwise grounded. The resistance of the preparation (R_{prep}) was then determined by injecting current pulses of $-100 \, pA$ through the recording electrode (de Kramer, 1985). To improve the signal-to-noise ratio, 10 current steps were subsequently applied, and the voltage responses were averaged. For current injections, the input resistance of the amplifier (R_i) was reduced to $10^9 \, \Omega$. Since the amplification factor changes, if R_i and R_{prep} are in the same range/of the same order of magnitude, an additional calibration step was performed for voltage measurements during current injection.

The correct calibration of the injected currents was regularly verified with a reference resistor connected to the amplifier.

Current step protocols were used to determine the current amplitude required to elicit action potentials electrically. Positive current pulses of 50 ms duration, incrementing by 25 pA, were injected, and the capacitative transients originating from the passive properties of the sensillum in combination with the capacitance neutralization circuit of the amplifier were eliminated by adding the voltage responses to two pre-pulses of half the amplitude and of opposite polarity (P/N leak subtraction). The current that elicited action potentials was determined for large and small action potentials separately using the averaged results of five sequential protocols. To account for spontaneously occurring action potentials, action potentials were only considered to be elicited if they were also present in at least the succeeding two sweeps (i.e. at a higher current amplitude). For the same reason, protocols with more than 36 action potentials in the baseline region (50 ms pre-step and 50 ms post-step for each sweep) were discarded. In these cases, the mean of the remaining protocols was analyzed.

For long-term recordings, the signals were acquired in segments of 10 min, at a sampling rate of 19.6 kHz (Clampex, fixed-length events). Each action potential triggered a sweep of 12.75 ms duration, and the highpass-filtered signal served as a trigger channel only. All analyses were performed using the direct-current-coupled signal. The mean voltage during the initial 2.5 ms was defined as the baseline and used to measure the TEP. Thus, the time course of the TEP was monitored with variable sampling intervals depending on the occurrence of action potentials. The baseline of all action potential sweeps was then adjusted to 0 mV (see Fig. 5A) to identify sweeps that were triggered by artefacts. The peak-to-peak amplitude of each action potential was measured and plotted *versus* the time of its occurrence (see Fig. 5B). In addition, amplitude distribution histograms were created (see Fig. 5C). A combination of these plots was used to determine the threshold for action potential sorting.

Action potential sorting

Action potentials separated by an interspike interval (ISI) of no more than 50 ms were defined as members of bursts. The decreasing amplitude of the action potentials within a burst (see Fig. 4C, Fig. 5B) did not allow a simple threshold-based procedure for action potential sorting. Instead, an MS-Excel macro was used that performed the following steps: if the interspike interval preceding the action potential under consideration was larger than 50 ms, only the peak-to-peak amplitude was used for action potential classification. Any action potential that occurred 50 ms or less after an action potential classified as large was also considered to be large. Since the amplitude only decreased, but never increased, during bursts, all action potentials with an amplitude above threshold were classified as large, even if they occurred within 50 ms of a small action potential. This could cause misclassifications, however, if a single large action potential

were to occur within a burst of small ones, since the subsequent members of the burst would incorrectly be classified as large. The action potential sorting algorithm recorded such cases, and these action potentials were classified manually.

Bursting behaviour

After separating the action potentials into two classes, we determined the interspike intervals (ISIs) for each 10 min data segment. The variables computed to describe the spontaneous action potential activity and the bursting behaviour of the ORNs were (i) the mean action potential frequency, (ii) the percentage of action potentials that were members of bursts, (iii) the mean number of action potentials per burst and (iv) the coefficient of variation (CV) of the ISIs, where CV=s.D./mean. In a sequence of events that occur independently of preceding events, i.e. in a Poisson process, the CV of the intervals between every two successive events is equal to 1 (Rospars et al., 1994). Thus, a CV significantly different from 1 indicates that the action potentials are not randomly distributed.

Resistance and transepithelial potential

At the beginning of each recording, when typically no TEP oscillations were present, the TEP and the resistance of the preparation were measured. The measured TEP value was corrected for the electrode potential (−35.6±1.4 mV; median ± s.E.M.; $N=6$). To investigate the influence of drug injections, the resistance was measured twice within 2–10 min before the injection, twice within a period of 2–10 min after the injection, and once more 10 min later. Since no significant difference in the group of pre-injection measurements and in the group of post-injection measurements was found, each group was averaged to yield the resistances before (R_{before}) and after (R_{after}) drug injection. The normalized resistance R_{after}/R_{before} was then computed.

Results

In extracellular tip recordings from long trichoid sensilla, we investigated the transepithelial potential (TEP), spontaneous action potential activity and the effects of octopamine and serotonin injections on both these variables. So far, no report has been published on the general properties of spontaneously active ORNs (such as action potential distribution, thresholds and amplitude distributions). Thus, we first characterized these general properties before testing for any effects of biogenic amines on these variables. Because action potential patterns are known to determine neuronal gene expression (Brosenitsch and Katz, 2001), we place particular emphasis on the analysis of burst behaviour.

The recordings could be maintained for up to 100 h when no drugs were injected, but were usually terminated earlier. No steady trend in action potential frequency could be detected during the course of long-term recordings (Fig. 1), and the action potentials of both amplitude classes appeared to undergo random fluctuations. If a sensillum appeared to be damaged, as judged from rapid TEP breakdown or the disappearance of one
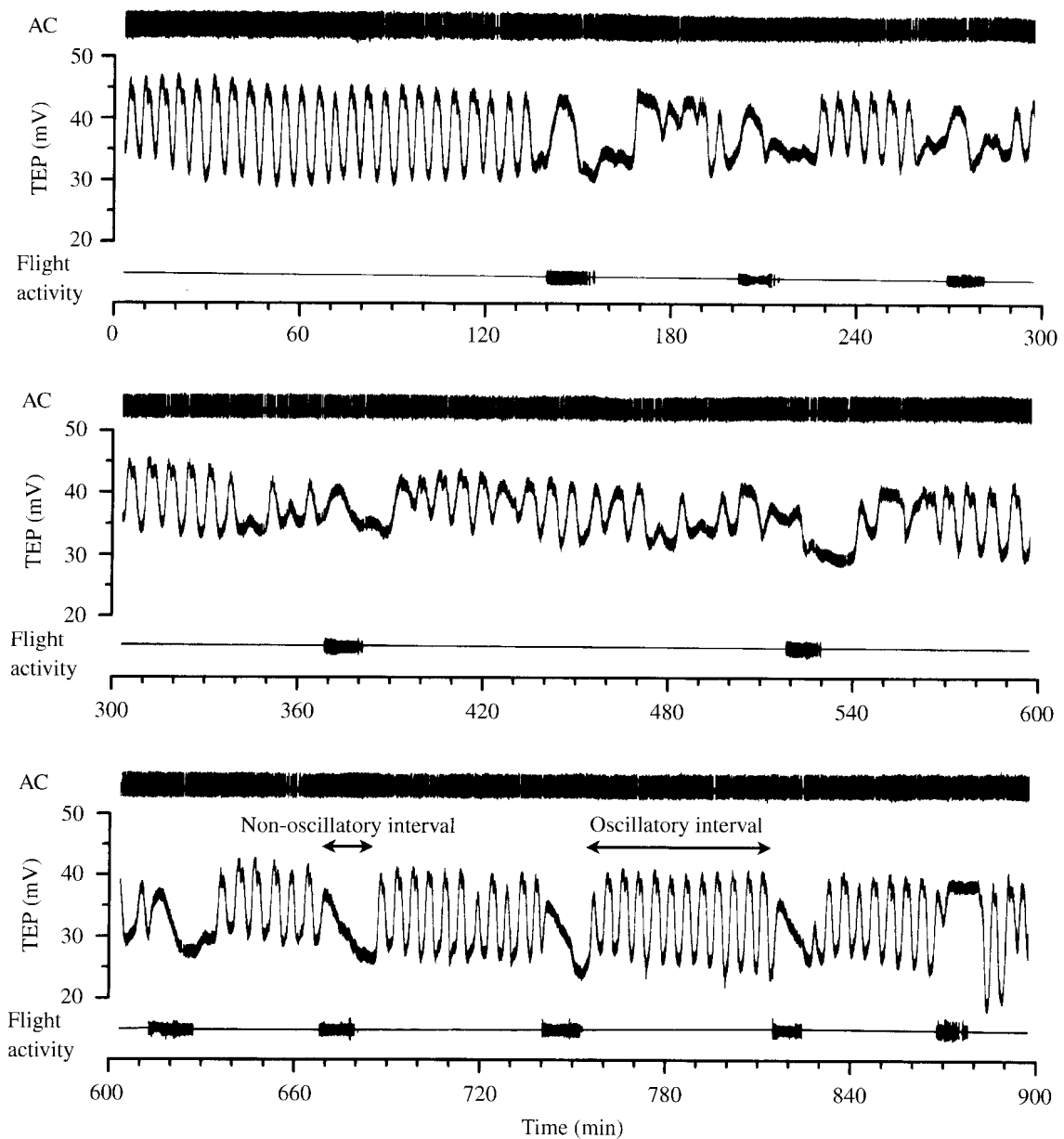
Fig. 1. Fifteen hours of a recording of action potentials and the transepithelial potential (TEP) of a trichoid sensillum with respect to the flight activity of the moth. The recording starts approximately 50 h after the beginning of the tip recording. The highpass-filtered signal (AC) reveals the action potentials superimposed on the slow fluctuations of the TEP, illustrating that there was no trend in the action potential activity. The time course of the TEP exhibited regular oscillations for periods of up to several hours, termed 'oscillatory intervals'. These were interrupted by shorter periods, 'non-oscillatory intervals', during which the TEP fluctuated less regularly or remained constant. Flight activity, recorded by a piezo-electric sensor at the thorax, was restricted to non-oscillatory intervals.

Table 1. *Transepithelial potential (TEP) oscillations and flight activity in long-term recordings*

Number of recordings	TEP oscillations	Oscillatory and non-oscillatory intervals*	Flight activity	
			In the absence of TEP oscillations	In the presence of TEP oscillations
58	57	47	58	6

The table only contains observations from recordings that lasted more than 15 h.
*A sequence of at least two oscillatory intervals interrupted by a non-oscillatory interval.

action potential class, the recording was discarded. In total, 177 sensilla from 138 animals were recorded, but most measurements were only performed on a subset.

Oscillations of the transepithelial potential

In 57 of 58 recordings that lasted more than 15 h (Table 1), the TEP exhibited a periodically oscillating time course with a peak-to-peak amplitude between 1–2 and >25 mV and a period of 2–8 min. The waveform was typically asymmetrical, with a shoulder on the decay phase of the positive peak (Fig. 1, see Fig. 3B), but sinusoidal signals were also observed. The oscillations were occasionally present from the beginning of a recording, but typically started between 2 and 15 h after the recording had been established. In most recordings, the oscillations developed gradually, with slowly increasing amplitude, thus preventing a quantitative analysis of the onset time. During the periods of oscillating TEP, referred to here as oscillatory intervals, the animals typically exhibited no flight activity (Table 1). The oscillatory intervals were interrupted by periods during which the time course of the TEP fluctuated less periodically or remained constant (Fig. 1). These periods are termed non-oscillatory intervals. Flight activity typically was observed only during non-oscillatory intervals, occurring in bursts of approximately 5–15 s duration separated by periods without flight activity of 15 to >100 s.

Oscillatory intervals typically lasted 1–5 h, but their duration was highly variable (up to >20 h). Non-oscillatory intervals, in contrast, had a shorter and more constant duration of approximately 20–50 min.

Fig. 2. (A–D) Recordings from four different animals showing the transepithelial potential (TEP) and flight activity during injections of octopamine. (A) After a delay of 1–2 min, the TEP oscillation was abolished by an injection of 1500 nmol of octopamine. Even after 15 h, the peak-to-peak amplitude had not recovered (after the axis break). During the gaps, current step protocols and resistance measurements (not shown) were performed. (B) While a control injection of haemolymph Ringer only slightly and transiently reduced the amplitude of the TEP oscillations, 150 nmol of octopamine almost completely suppressed it. At 113 min, the animal exhibited flight activity, marking the beginning of a non-oscillatory interval of approximately 2 h (not shown), after which the oscillation reappeared. (C) After an injection of 20 nmol of octopamine, the amplitude of the oscillation was reduced, but the time course of the TEP remained periodic. Over the course of several hours after the injection, the oscillation gradually regained its original amplitude and regularity. (D) The effect of an injection of 2 nmol of octopamine into an oscillation with a complex waveform could not reliably be distinguished from the effects of control injections. Note the two non-oscillatory intervals without TEP oscillations (12–30 min, 112–138 min) during which flight activity was recorded.

Because the spontaneous occurrence and the duration of non-oscillatory intervals were very variable and appeared random, we did not attempt any further analysis. The sequence of oscillatory intervals without flight activity and non-oscillatory intervals associated with flight activity was observed in 47 of the 58 recordings of more than 15 h duration. Flight activity occasionally decreased over the course of long recordings and could be completely absent by the end. Flight activity during oscillatory intervals, however, was only observed in six experiments (Table 1).

The injection of 1–2500 nmol of octopamine into the head capsule suppressed the TEP oscillations after a delay of one to
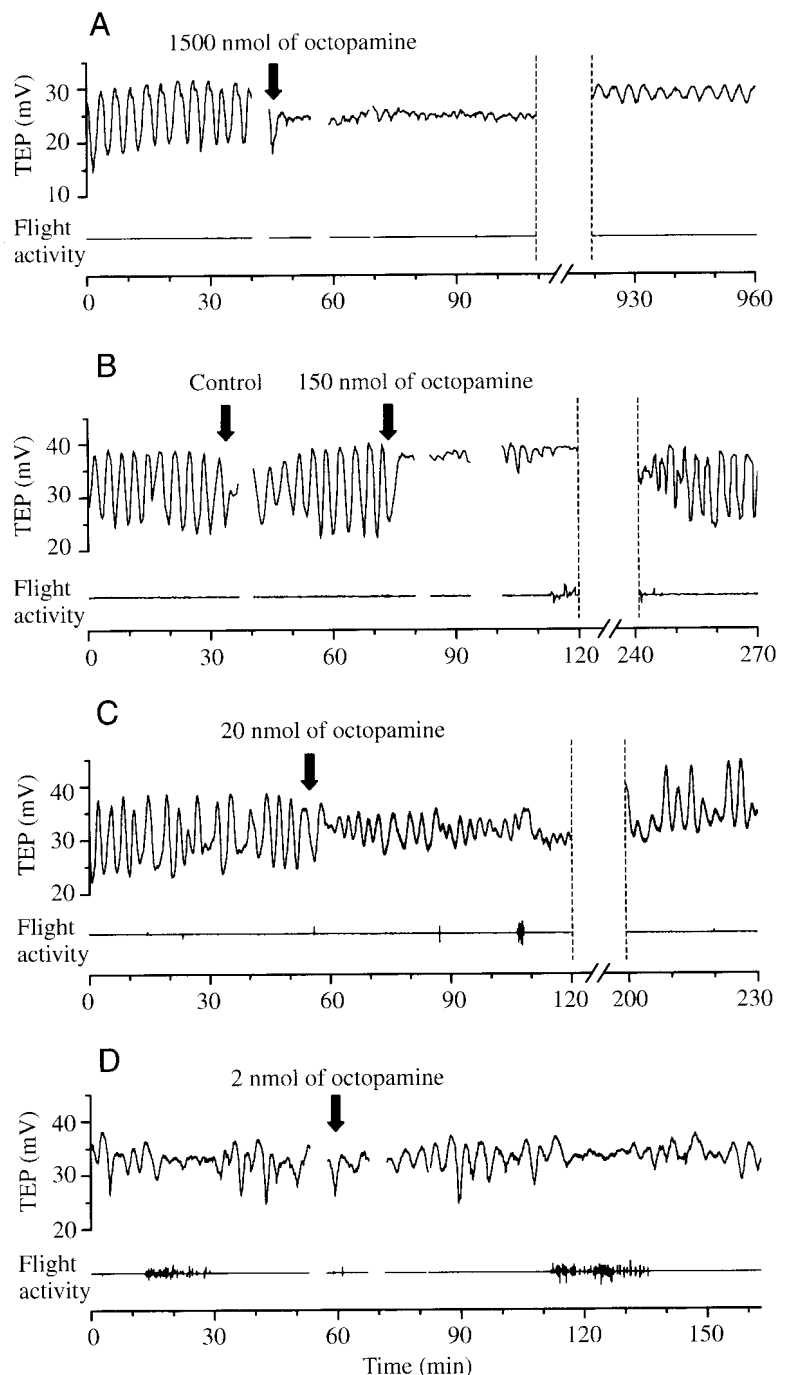
Table 2. *The effects of drug injections during oscillatory intervals*

	Dose (nmol)	N	TEP oscillation suppressed*	No effect‡
Control		21	2	19
Serotonin	10–50	6	5	1
	100–750	9	7	2
Octopamine	1–5	6	4	2
	10–50	9	8	1
	100–500	14	12	2
	1000–2500	9	8	1

TEP, transepithelial potential.

*Complete suppression of the oscillation for ⩾20 min or clear reduction in the oscillation amplitude for ⩾30 min.

‡No suppression or suppression for <20 min and no amplitude reduction or reduction for <30 min.

Table 3. *Spontaneous action potential frequency and burst behaviour*

Variable	Small APs	Large APs
Mean AP frequency (Hz)	0.542±0.129	0.390±0.057
% APs in bursts	45.7±2.1	47.4±2.7
Mean number of APs per burst	3.31±0.12	3.36±0.09
Coefficient of variation	1.95±0.09	1.78±0.06

AP, action potential.

Data from 66 recordings acquired before drug injection were analyzed in 438 segments of 10 min duration. The segments of individual recordings were averaged, and the mean and s.e.m. of these averages were then computed.

several minutes (Fig. 2; Table 2). The TEP stabilized at variable values between the maximum and minimum potential during the previous oscillations. Both the degreee of suppression and the duration of the effect were dose-dependent. At doses above 1000 nmol, the oscillations were completely absent after 89 % of the injections during an oscillatory interval. At these doses, the amplitude of the oscillation did not fully recover for the rest of the recording (Fig. 2A). At lower doses, the suppression was usually incomplete and more transient (Fig. 2B–D). After some control injections with haemolymph Ringer, we observed a transient suppression of the TEP oscillations or a phase shift (Fig. 2B, see Fig. 7A; Table 2) reminiscent of the effect of a low octopamine dose. To account for these effects, for the quantitative analysis (Table 2), we scored the complete absence of oscillations for at least 20 min or a clear reduction in the oscillation amplitude (to two-thirds or less) for at least

30 min as suppression. More transient changes or the absence of any obvious influence were scored as no effect, which applied to 90 % of the control injections during oscillatory intervals.

Serotonin injections (N=15) led to a less pronounced reduction in the oscillation amplitude. The effect of serotonin typically resembled that of a 10-fold lower octopamine dose. However, the waveform of the oscillation was more regular after 13 of 14 serotonin injections that were associated with a suppression of the oscillation that was sufficiently transient to allow an analysis. In addition, after five of these injections, the shoulder after the positive peaks was less prominent than before. After five injections, the shoulder was completely absent, as shown in Fig. 3. A similar change in the oscillation waveform was never observed after octopamine injections. When injected during non-oscillatory intervals (N=10), none of the doses of octopamine or serotonin tested had any detectable effects. Because of their variable duration, it was not possible to analyze whether the non-oscillatory intervals were prolonged by drug injections. In none of the experiments did oscillations occur earlier than 20 min after the injection.
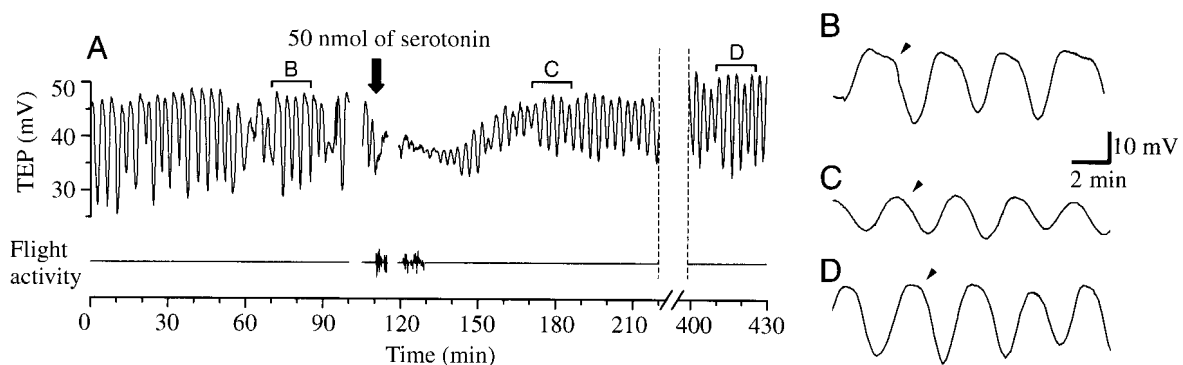
Fig. 3. (A–D) The time course of the transepithelial potential (TEP) during injection of 50 nmol of serotonin. The sections indicated in A are shown on an enlarged time scale in B–D. The TEP oscillation before drug injection was asymmetrical, exhibiting a shoulder (arrowhead) after the positive peak (B). After the injection, the oscillation was transiently suppressed and then gradually recovered to approximately two-thirds of the original peak-to-peak amplitude. After recovery, the oscillation was more regular than before, and the shoulder was absent (C). Five hours after the injection, the peak-to-peak amplitude had fully recovered, but the shoulder was not as prominent as before (D). The animal exhibited flight activity only transiently immediately after the drug injection.

Fig. 4. (A,B) Spontaneous action potentials in the two olfactory receptor neurons (ORNs) in a trichoid sensillum, distinguishable by their amplitudes. The three parts in A are one continuous sequence. The action potentials of neither class were randomly distributed, but (both) exhibited bursting activity. Bursts of large action potentials are marked with filled circles, bursts of small action potentials with open circles. The indicated burst (star) is shown on an enlarged time scale in B. (C) A burst of large action potentials from a different recording, illustrating the reduction in amplitude of the action potentials. (D) Action potential bursts were also recorded with tungsten electrodes placed near the hair base. The three parts of D are one continuous trace, highpass-filtered at 5 Hz.
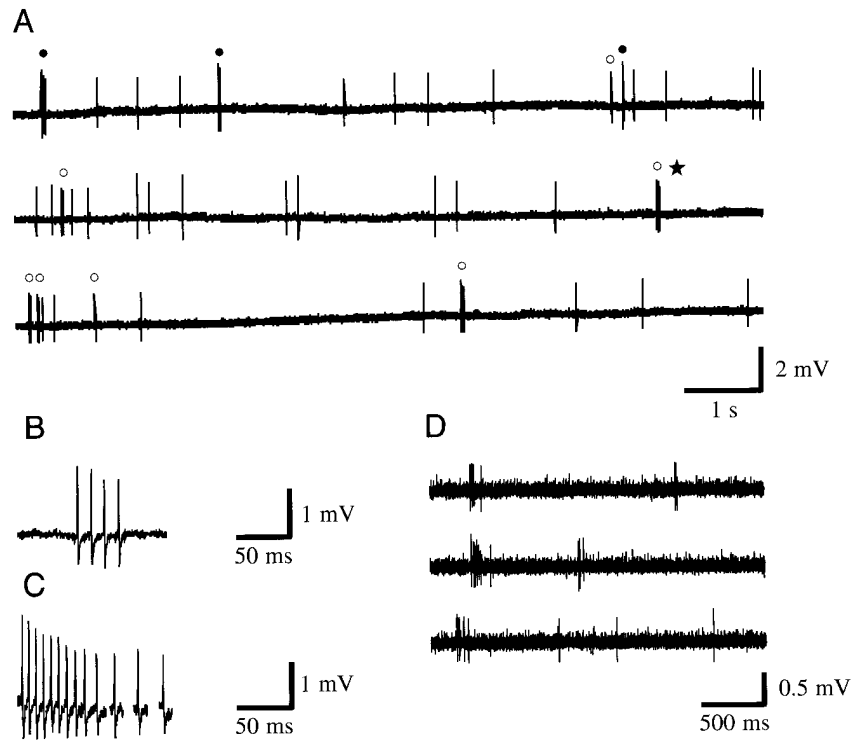
Fig. 5. (A) Action potentials recorded in sweeps of 12.75 ms duration. The initial 2.5 ms of each sweep were defined as baseline and used to measure the transepithelial potential. The baseline was then adjusted to 0 mV. One large (red line) and one small (blue line) action potential are highlighted. The peak-to-peak (p-p) amplitudes of each action potential occurring over a 10 min period were measured and plotted *versus* time (B). The amplitude reduction during bursts then became obvious (arrowheads). The massive bursting activity of the cell firing the small action potentials (solid arrowhead) gives rise to a third peak when the data are presented as an amplitude histogram (C), generating a false third action potential class (arrowhead). Both types of plot were analyzed to determine the threshold for action potential sorting (dashed lines).
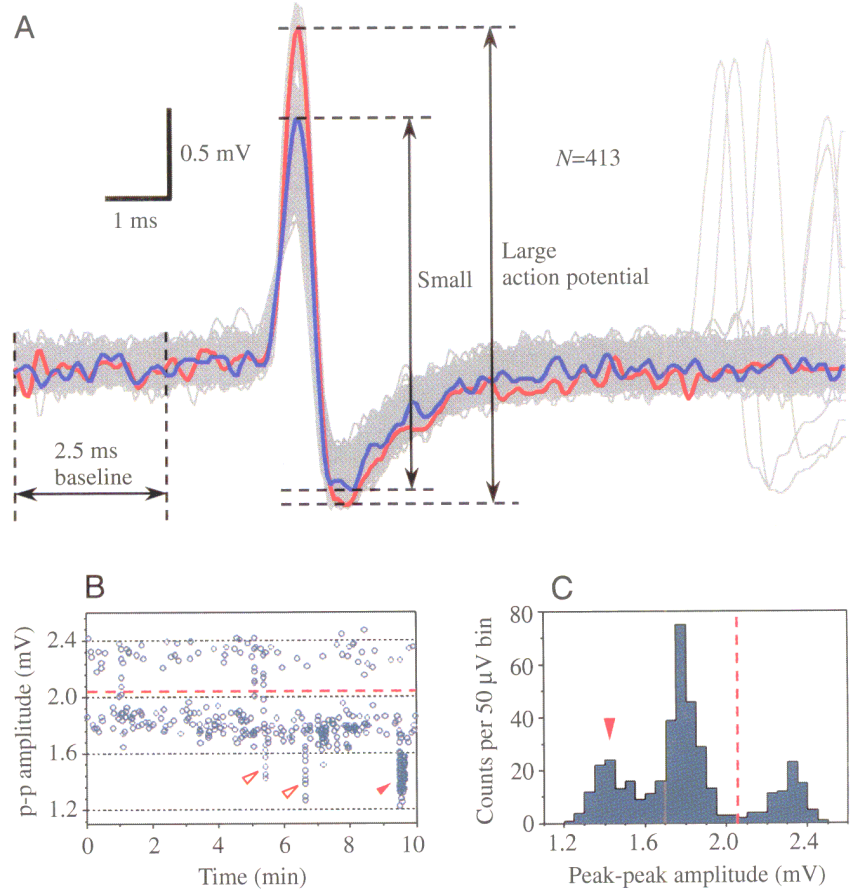
Fig. 6. (A,B) Action potential variables during oscillatory and non-oscillatory intervals of the transepithelial potential (TEP). (A) The upper panel shows the time course of the TEP and flight activity, while the lower panels illustrate the action potential activity of the small and large action potentials (APs), evaluated in bins of 10 s. Periods of elevated action potential activity and quiescent periods occurred independently of the TEP and of flight activity, during oscillatory as well as during non-oscillatory intervals. (B) No correlation between the phase of the TEP oscillations and any evaluated variable of the action potential activity was found. All variables were analyzed in bins of 10 min and plotted on the same time axis as in A. The frequency of the small action potentials was more variable than that of the large ones (Table 3). The percentage of action potentials that were members of bursts fluctuated randomly between <25 and >75 %. Similarly, the mean number of action potentials in each burst and the coefficient of variation (CV) did not exhibit any correlation with the time course of the TEP. The dashed line marks a CV of 1, which would indicate a random distribution of the action potentials.
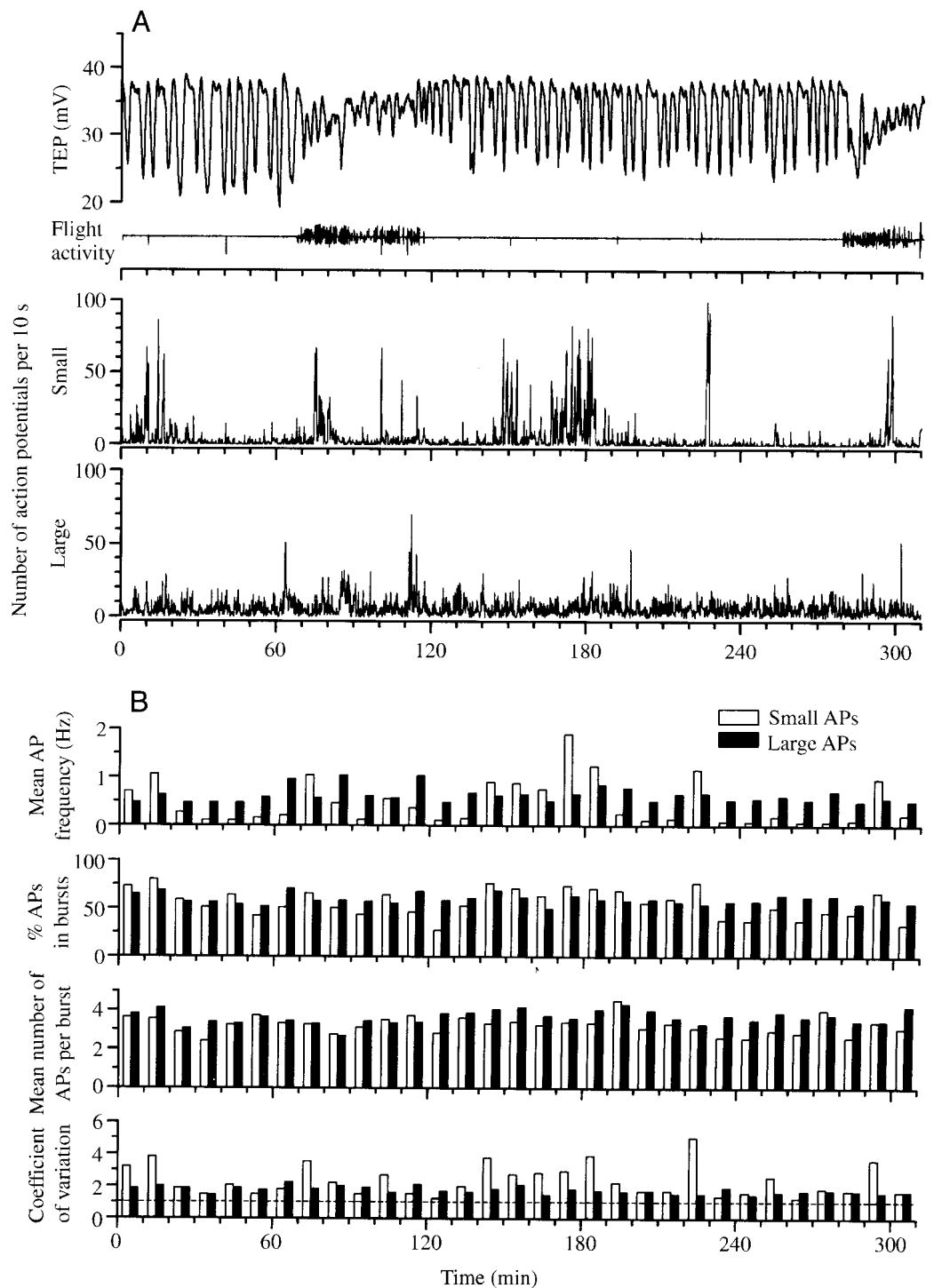
Spontaneous action potentials

The distribution of the spontaneous action potentials was not random (Table 3). On average, 45.7±2.1 % of the small action potentials occurred in bursts made up of 3.31±0.12 action potentials and 47.4±2.7 % of the large action potentials occurred in bursts made up of 3.36±0.09 action potentials (means ± S.E.M.; Fig. 4, Fig. 5; Table 3). The action potential amplitude decreased during bursts, depending on the burst duration. Bursts were also observed in each of five recordings

made using tungsten electrodes (Fig. 4D). Occasionally, a single large action potential occurred within a burst of small ones or both ORNs fired bursts simultaneously. Unless the frequency of both action potential classes was rather high (>2 Hz), these cases were very infrequent (≤1 % of the total action potentials), indicating that bursts were independent in the two ORNs. The coefficient of variation computed for the interspike intervals (ISIs) of both action potential classes was clearly higher than 1 (Table 3). The action potential frequency
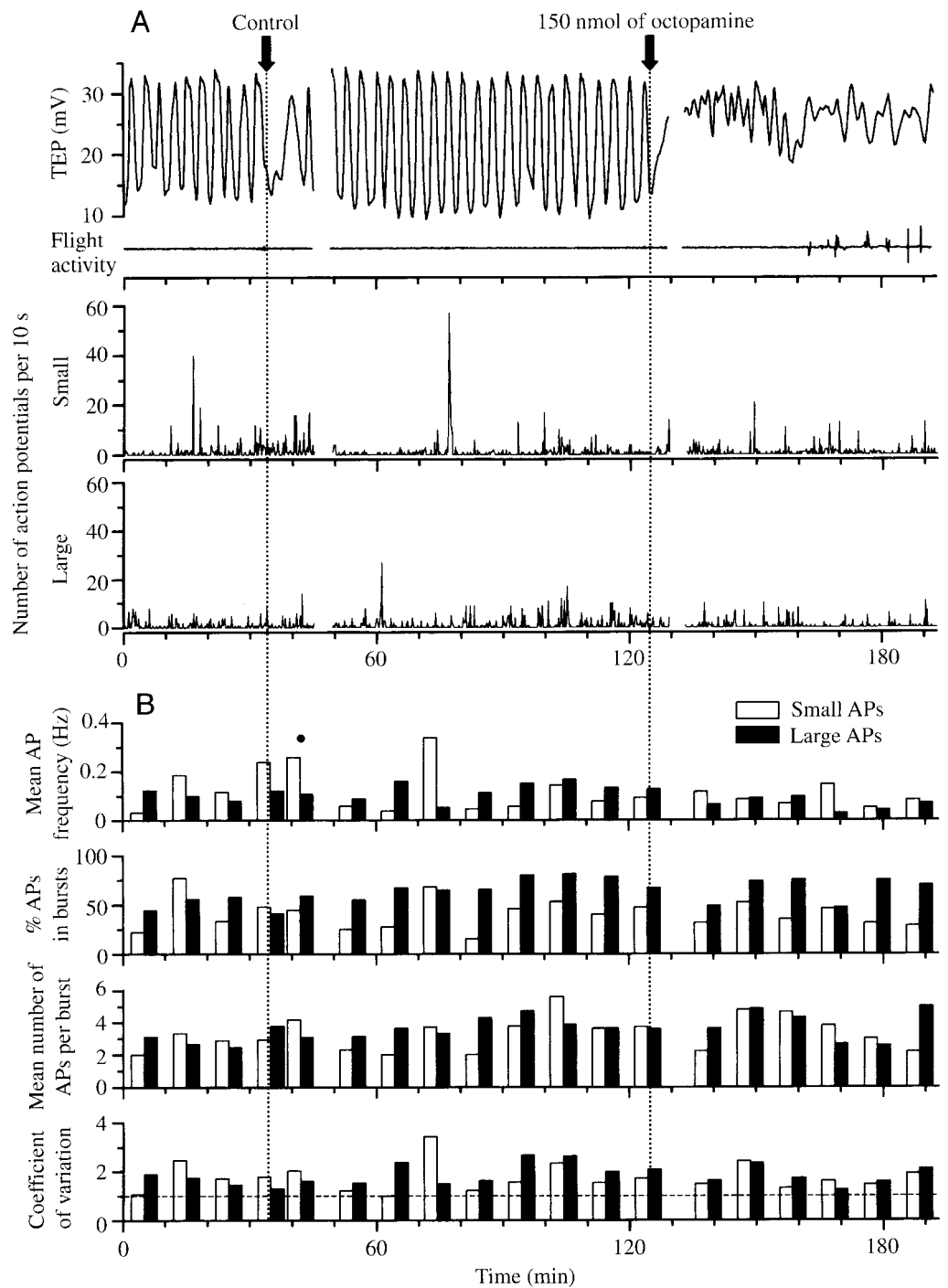
Fig. 7. No variable of the action potential (AP) activity correlated with octopamine-dependent modulation of the transepithelial potential (TEP). (A) Haemolymph Ringer (control) injection only slightly reduced and phase-shifted the TEP oscillation for less than 20 min, while injection of 150 nmol of octopamine caused a long-term depression of TEP oscillations. Flight activity marked the beginning of a non-oscillatory interval. The frequency of both action potential classes was unaffected by control or octopamine injections. (B) None of the evaluated variables of the action potential activity was affected by the injections. The first bin after the control injection (filled circle) is only 5.2 min long.

of both ORNs was highly variable between preparations and even between different sensilla of the same animal. In the complete absence of pheromone, the highest measured frequencies were 6.7 Hz for the small and 5.8 Hz for the large action potentials when averaged over 10 min. Both ORNs, however, also had transient periods when less than one action potential occurred in 10 min. The mean action potential frequencies evaluated for 438 data segments without drug injection from 66 recordings were 0.542±0.129 Hz (small action potential) and 0.390±0.057 Hz (large action potentials) (means

± S.E.M.). The frequency of each action potential class changed during the recordings, with periods of increased activity and quiescent periods in apparently random sequence (Fig. 6). However, when examined over the duration of a recording, the more active ORNs were consistently more active, while the more silent ones maintained a low average activity.

Neither with subjective judgement nor with cross-correlation tests on three sample recordings (not shown) did we find any significant correlation between the time course of the TEP oscillation and the action potential frequency.

A
Small APs

B
Large APs

Fig. 8. (A,B) Neither of the two action potential (AP) classes was significantly influenced by amine injections. The frequencies of small and large action potentials were evaluated for segments 10 min in duration within 30 min before (v_{before}) and after (v_{after}) drug injections, and the normalized frequency v_{after}/v_{before} was computed. For comparison, data segments of 10 min, separated by 40–50 min, but without any injection, were analyzed the same way. One-way 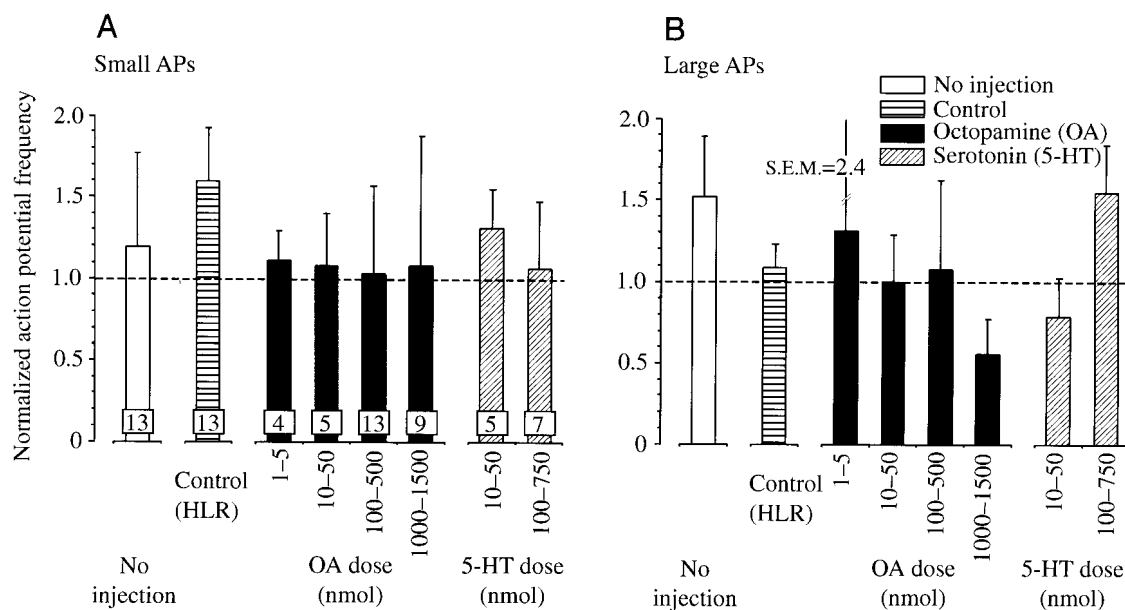analysis of variance (ANOVA) did not reveal significant differences between any dose of the injected drugs, the control (injected with haemolymph Ringer) and the non-injected state. Values are medians + S.E.M. Values of N given in A also apply to B. 5-HT, serotonin; OA, octopamine; HLR, haemolymph Ringer.

Furthermore, there was no detectable difference between oscillatory and non-oscillatory intervals with respect to the action potential frequency or any of the variables evaluated that describe the burst behaviour (Fig. 6). Consequently, injections of octopamine or serotonin did not significantly influence the action potential activity either (Fig. 7, Fig. 8).

Electrically elicited action potentials

During the application of current step pulses (Fig. 9), large action potentials were elicited by a significantly smaller step

amplitude (208.3±7.3 pA) than small ones (243.7±8.0 pA; means ± S.E.M., N=123, P<0.01, Student's t-test). No significant changes were found after the injection of any dose of the tested drugs or of haemolymph Ringer (not shown).

Resistance and transepithelial potential

At the beginning of each recording, when TEP oscillations were not usually present, the resistance of the preparation and the TEP were measured. The mean resistance of 159 sensilla was 68.3±2.3 MΩ (mean ± S.E.M.). Octopamine injections

Fig. 9. Significantly more current was necessary to elicit small action potentials than large action potentials. (A) Action potentials elicited by a series of 50 ms current steps, increasing by +25 pA from bottom to top. Passive electrical responses were compensated by adding the responses of two pre-pulses of opposite polarity and half the amplitude to each sweep. The large action potentials (filled arrowheads) required a current of 175 pA, while the small action potentials (open arrowheads) were first elicited by a 225 pA step. The action potentials marked with open circles were considered to be spontaneous, since either no action potential was present in the next sweep or the action potential occurred outside the current step. (B) The small action potentials required significantly more current
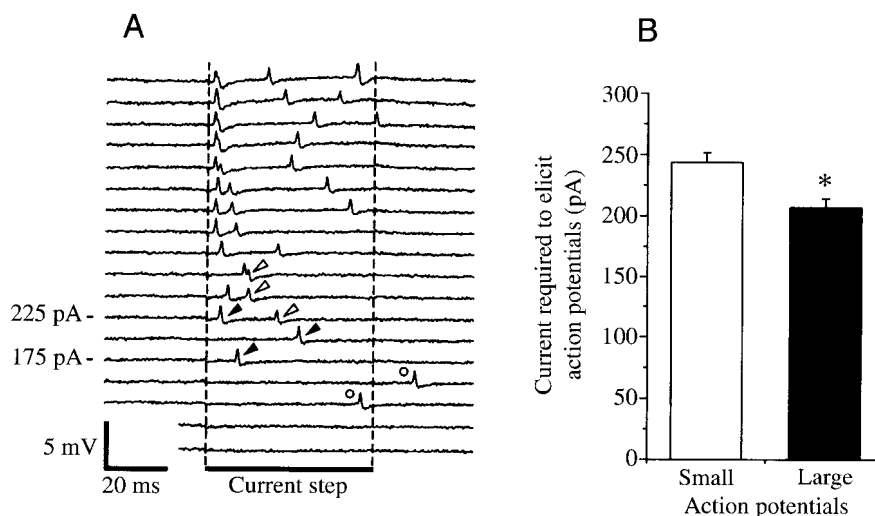
(244 pA) than the large ones (208 pA). Values are means + S.E.M., N=123 sets of five step protocols without drug injection. The asterisk indicates a significant difference from the control (P<0.01, Student's t-test). For both classes of action potential, no significant changes were detected after the injection of any dose of octopamine or serotonin (not shown).

reduced the resistance of the preparation by up to 20% in a dose-dependent manner (Fig. 10). Serotonin, in contrast, did not significantly alter the resistance.

The TEP, as measured at the beginning of the recordings, was +33.8±0.8 mV (mean ± s.e.m.; N=177) irrespective of whether or not a drift or oscillation was present at the time of the measurement. During non-oscillatory intervals, the TEP fluctuated around variable values between the maximum and minimum potential in preceding and subsequent oscillatory intervals (Fig. 1). Similarly, after amine-dependent suppression of the oscillations, no consistent change in the absolute value of the TEP was found. Instead, the TEP stabilized around variable potentials between the upper and lower bounds of the previous oscillations, apparently
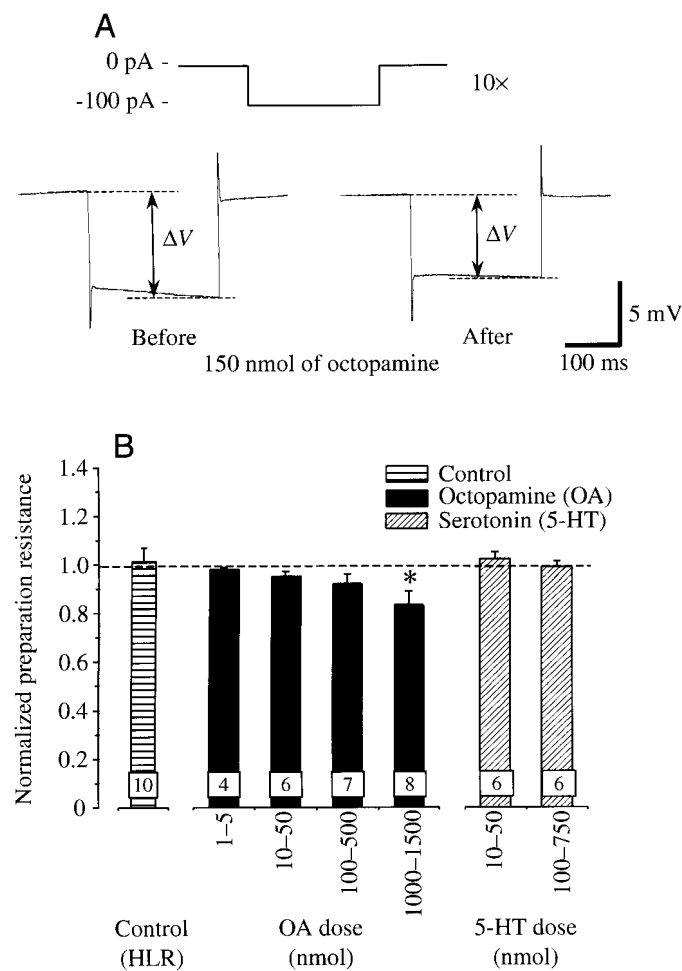

Fig. 10. Octopamine reduced the resistance of the preparation in a dose-dependent manner. (A) For resistance measurements, 10 subsequent pulses of negative current were applied. When compared with the averaged voltage response (ΔV) before drug injection (left), an injection of 150 nmol of octopamine decreased the response (right). (B) The normalized resistance R_{after}/R_{before} was computed. While control injections of haemolymph Ringer (HLR) did not alter the resistance of the preparation, octopamine (OA) reduced it in a dose-dependent manner. Serotonin (5-HT), however, had no effect. Values are means + s.e.m. The asterisk indicates a significant difference from the control ($P<0.02$, Student's t-test).

dependent on the value of the TEP at the moment that drug action occurred (Fig. 2A–C, Fig. 3A, Fig. 7A).

Discussion

Using extracellular tip recordings from pheromone-sensitive sensilla, we investigated whether the biogenic amines octopamine and serotonin affect the kinetics of the transepithelial potential (TEP) and the occurrence of action potentials in the absence of adequate stimuli. We wanted to know whether the octopamine-dependent increase in the peak nerve impulse frequency in response to pheromone (Pophof, 2000; Grosmaitre et al., 2001) is mediated by accessory cells that generate the TEP of long trichoid sensilla. In addition, we wanted to test whether octopamine exerts its effects *via* modulation of the spontaneous action potentials in ORNs. For the first time, we were able to distinguish the two ORNs in one sensillum and to record for several days from the same intact olfactory sensillum before and after amine injection. Thus, we could analyze slow temporal changes in the kinetics of the TEP and the properties of the action potential. While the biogenic amines did not influence spontaneous action potentials, we found that both amines affected the kinetics of the TEP, presumably acting on different targets.

Amine-dependent effects on the transepithelial potential

Interestingly, we found that octopamine suppressed the oscillations of the TEP in a dose-dependent manner, while serotonin changed the waveform of the oscillation. In accordance with our findings, octopamine did not alter the mean value of the TEP in trichoid sensilla of *Antheraea polyphemus* (Pophof, 2000). In contrast to studies in moths, Küppers and Thurm (Küppers and Thurm, 1975) found an increase in the amplitude of the TEP in whole antennae of the cockroach *Blaptica dubia* after the application of serotonin. In both these studies, the recordings lasted only a few minutes, so slow TEP oscillations were not observed. Octopamine-dependent suppression of TEP oscillations in *M. sexta* could stabilize the TEP at variable values, suggesting that an additional mechanism determines the mean value of the TEP.

Zack (Zack, 1979) concluded from her studies that accessory cells generate the TEP in insect sensilla. It is generally assumed that the TEP is generated by active K^+ transport through the apical membranes of the tormogen/trichogen cells into the sensillum lymph cavity (Thurm, 1972; Thurm, 1974). The high K^+ concentration of approximately 200 mmol l^{-1} in the sensillum lymph causes a potential difference of up to 50 mV between the sensillum lymph and the haemolymph. This potential difference is assumed to add to the transmembrane potential of the outer dendrites. The localization of the *M. sexta* midgut V-ATPase in accessory cells of antennal moth sensilla (Klein, 1992; Klein and Zimmermann, 1991) suggests the presence of the same two-step mechanism for generation of the TEP in the antennal epithelium, as has been described for the midgut and for a number of other epithelia in insects (for

reviews, see Wieczorek, 1992; Wieczorek et al., 2000). Therefore, it is likely that the slow TEP oscillations reflect feedback-coupled regulatory mechanisms both in H^+ transport by the V-ATPase and in the subsequent K^+/H^+ antiport. Because serotonin rather selectively suppressed the shoulder of the TEP waveform, it is assumed that two distinct, but coupled, mechanisms are involved in the generation of the TEP. Octopamine injection, in contrast, reduced the amplitude of the oscillation, suggesting that the octopamine-sensitive mechanism is the initial process, acting on the V-ATPase. The serotonin-sensitive process, however, is delayed, and might therefore reflect a mechanism modulating K^+/H^+ antiport. We will test this hypothesis in future experiments by targeting the V-ATPase and K^+/H^+ antiport. TEP oscillations also occur in pheromone sensilla of the moth A. polyphemus (Zack, 1979) and in Malpighian tubules of mosquitoes (Beyenbach et al., 2000), which also contain V-ATPases (Wieczorek et al., 2000). The question of whether the oscillations have any biological significance, however, or are just a by-product of feedback-regulated processes, remains to be determined in pheromone-stimulated sensilla. Interestingly, Zack (Zack, 1979) mentioned that TEP oscillations measured in different sensilla are not necessarily in phase with each other. Possibly, a stable phase relationship between TEP oscillations in different sensilla on the antenna could affect the temporal resolution of pheromone responses. This hypothesis needs to be examined in pheromone stimulation experiments.

It is not clear how octopamine reaches the accessory cells and what the effective drug concentration at the sensilla is. The maximal dose used in these experiments was within the range reported to influence pheromone responses in other moths (Pophof, 2000; Grosmaitre et al., 2001). We then reduced the dose by three orders of magnitude until we reached a concentration that ceased to be effective. An octopamine concentration of between 2 and 17 nmol l^{-1} has been reported in the haemolymph of M. sexta (Lehman, 1990). However, it is not known whether active transport can cause octopamine to accumulate in specific tissues, such as the antenna. In addition, it is not known how much octopamine is released by the 1–2 octopaminergic neurons that project into the antenna (U. Homberg, personal communication). Thus, effective doses are difficult to determine. But the findings of amine-dependent effects on the TEP in M. sexta reported here and on pheromone responses in other moths (Pophof, 2000; Grosmaitre et al., 2001) indicate that the doses of haemolymph-carried octopamine employed have a functional significance in the antenna. This assumption is further supported by the localization of a neuronal type 3 octopamine receptor, which inhibits cyclic AMP synthesis, at the base of olfactory sensilla on the antennae of the moths Bombyx mori and Heliothis virescens (von Nickisch-Rosenegk et al., 1996). In addition, the weak and transient octopamine-like effects observed after several of the control injections (Fig. 2B, Fig. 7A) suggest that the TEP oscillations are equally affected by endogenous octopamine. The manipulations during an injection aroused the animals and occasionally caused flight activity (Fig. 3). Flight

activity is known to be elicited and maintained by octopamine (Kinnamon et al., 1984; Orchard et al., 1993). Thus, we assume that, during some control injections, a stress-dependent increase in endogenous octopamine levels caused the observed transient suppression of the TEP oscillations together with the initiation of flight activity.

Action potentials

The absence of effects of octopamine and serotonin on action potential activity in the absence of adequate stimuli indicates that these amines alone do not directly influence the action potential generator. It appears that a synergistic factor is required to increase the background activity after octopamine injections in the presence of low pheromone doses (Pophof, 2000; Grosmaitre et al., 2001). It has yet to be tested whether rises in intracellular Ca^{2+} concentration or increases in cyclic GMP or cyclic AMP levels mimic the presence of a low pheromone dose for these octopamine effects. In addition, no correlation between the time course of the TEP and any aspect of the spontaneous action potential activity of the ORNs was found, despite the fact that the TEP adds to the driving force for the generator potential (Thurm, 1972). Thus, the ionic conductivity of the plasma membrane in the outer dendritic segment, the location of the chemo-electrical transduction machinery, is obviously very low in the absence of adequate stimuli. If this were not the case, changes in the driving force up to 20 mV, such as were present during oscillatory intervals, would very likely be reflected in the action potential frequency. This assumption is further supported by the fact that no ion channel openings occurred in unstimulated pheromone-dependent ORNs either in situ or in vitro (Zufall and Hatt, 1991; Stengl et al., 1992).

Action potentials were elicited by the injection of positive, but not negative, current (see de Kramer, 1985; de Kramer et al., 1984). Positive currents hyperpolarize the outer dendritic segments of the ORNs, but depolarize membranes that are situated basal to the zones of septate junctions located at the transitional region between the inner and outer dendritic segment (Keil, 1989). Together with the polarity of the recorded action potentials (positive phase first), this further confirms the hypothesis that the action potential generator is located in the soma or axon hillock region. Action potentials with the opposite polarity, as would be expected for dendritic action potentials, were never observed. Unexpectedly large currents of more than 200 pA were necessary to elicit action potentials. In current-clamp recordings of vertebrate (Lynch and Barry, 1989; Iida and Kashiwayanagi, 1999; Ma et al., 1999), lobster (Schmiedel-Jakob et al., 1989) and cultured insect (M. Stengl, unpublished observations; I. Jakob, personal communication) ORNs, currents as small as 1–10 pA were sufficient to elicit action potentials. Thus, it appears likely that most of the injected current does not flow through the ORNs, but through a shunt pathway, i.e. through the accessory cells and the surrounding epithelium. Since the measurement of preparation resistance is also based on current injections, the measured resistance is presumably governed by the resistance

of the shunt pathway. This was also assumed by Zack (Zack, 1979) in *A. polyphemus*. The reduction in the resistance of the preparation found after octopamine injection therefore further supports the hypothesis that the accessory cells are targets for the biogenic amines. It has yet to be resolved whether and how this decrease in the resistance of accessory cells can influence TEP oscillations. Zack (Zack, 1979) also showed that the preparation resistance oscillates. These resistance oscillations, however, cannot be directly responsible for the TEP oscillations because the two types of oscillation differed in their kinetics and showed a stable phase difference. If resistance oscillations are also present in *M. sexta*, the actual changes in the preparation resistance after octopamine injection might be even larger than observed.

Physiological implications

What is the physiological relevance for a biogenic-amine-controlled olfactory sensillum? Because biogenic amines can act as hormones, they could adjust the general sensitivity (or state of adaptation) of various targets, at the periphery as well as centrally, at the same time. Such a sensitivity adjustment could possibly be triggered by a biologically relevant signal, such as sex pheromones. The octopamine-dependent increase in the action potential activity of ORNs only in the presence of a low pheromone dose (*Antheraea polyphemus*, Pophof, 2000; *Mamestra brassicae*, Grosmaitre et al., 2001) is consistent with this hypothesis of a sensitivity adjustment in response to a relevant stimulus. In addition, an amine-dependent sensitivity adjustment could be governed by the circadian clock of a nocturnal moth because increased sensitivity to pheromone is strongly dependent on photoperiod cues (Linn, 1997; Linn and Roelofs, 1986; Linn and Roelofs, 1992; Linn et al., 1992; Linn et al., 1996). It is known that octopamine levels in the haemolymph show a circadian rhythm and are high at night, during the activity phase of the moths (Lehman, 1990), when the females release pheromone (Itagaki and Conner, 1988). In our experiments, we tried to keep endogenous octopamine levels constant by disturbing the circadian rhythm of endogenous octopamine release using constant light application (which stops the circadian clock). Thus, we do not know whether the TEP oscillations show a circadian rhythm in undisturbed moths. In future experiments, we will test whether there is a circadian rhythm in the pheromone response of *M. sexta*, whether it is dependent on the presence of octopamine and whether it correlates with circadian changes in the kinetics or the amplitude of the TEP.

References

Bell, R. A. and Joachim, F. A. (1976). Techniques for rearing laboratory colonies of tobacco hornworms and pink bollworms. *Ann. Ent. Soc. Am.* **69**, 365–373.

Beyenbach, K. W., Aneshansley, D. J., Pannabecker, T. L., Masia, R., Gray, D. and Yu, M.-J. (2000). Oscillations of voltage and resistance in Malpighian tubules of *Aedes aegypti*. *J. Insect Physiol.* **46**, 321–333.

Brosenitsch, T. A. and Katz, D. M. (2001). Physiological patterns of electrical stimulation can induce neuronal gene expression by activating N-type calcium channels. *J. Neurosci.* **21**, 2571–2579.

de Kramer, J. J. (1985). The electrical circuitry of an olfactory sensillum in *Antheraea polyphemus*. *J. Neurosci.* **5**, 2484–2493.

de Kramer, J. J., Kaissling, K.-E. and Keil, T. A. (1984). Passive electrical properties of insect olfactory sensilla may produce the biphasic shape of spikes. *Chem. Senses* **8**, 289–295.

Grosmaitre, X., Marion-Poll, F. and Renou, M. (2001). Biogenic amines modulate olfactory receptor neurons firing activity in *Mamestra brassicae*. *Chem. Senses* (in press).

Iida, A. and Kashiwayanagi, M. (1999). Responses of *Xenopus laevis* water nose to water-soluble and volatile odorants. *J. Gen. Physiol.* **114**, 85–92.

Itagaki, H. and Conner, W. E. (1988). Calling behavior of *Manduca sexta* (L.) (Lepidoptera: Sphingidae) with notes on the morphology of the female sex pheromone gland. *Ann. Ent. Soc. Am.* **81**, 798–807.

Kaissling, K.-E. (1995). Single unit and electroantennogram recordings in insect olfactory organs. In *Experimental Cell Biology of Taste and Olfaction* (ed. A. I. Spielman and J. G. Brand), pp. 361–377. Boca Raton, New York: CRC Press.

Kaissling, K.-E., Hildebrand, J. G. and Tumlinson, J. H. (1989). Pheromone receptor cells in the male moth *Manduca sexta*. *Arch. Insect Biochem. Physiol.* **10**, 273–279.

Keil, T. A. (1989). Fine structure of the pheromone-sensitive sensilla on the antenna of the hawkmoth, *Manduca sexta*. *Tissue & Cell* **21**, 139–151.

Kinnamon, S. C., Klaassen, L. W., Kammer, A. E. and Claassen, D. (1984). Octopamine and chlordimeform enhance sensory responsiveness and production of the flight motor pattern in developing and adult moths. *J. Neurobiol.* **15**, 283–293.

Klein, U. (1992). The insect V-ATPase, a plasma membrane proton pump energizing secondary active transport: immunological evidence for the occurrence of a V-ATPase in insect ion-transporting epithelia. *J. Exp. Biol.* **172**, 345–354.

Klein, U. and Zimmermann, B. (1991). The vacuolar-type ATPase from insect plasma membrane: immunocytochemical localization in insect sensilla. *Cell Tissue Res.* **266**, 265–273.

Küppers, J. and Thurm, U. (1975). Humorale Steuerung eines Ionentransportes an epithelialen Rezeptoren von Insekten. *Verh. Dt. Zool. Ges.* **67**, 46–50.

Lehman, H. K. (1990). Circadian control of *Manduca sexta* flight. *Soc. Neurosci. Abstr.* **16**, 1334.

Linn, C. E. (1997). Neuroendocrine factors in the photoperiodic control of male moth responsiveness to sex pheromone. In *Insect Pheromone Research. New Directions* (ed. R. T. Cardé and A. K. Minks), pp. 194–209. New York: Chapman & Hall.

Linn, C. E., Campbell, M. G., Poole, K. R., Wu, W.-Q. and Roelofs, W. L. (1996). Effects of photoperiod on the circadian timing of pheromone response in male *Trichoplusia ni*. *J. Insect Physiol.* **42**, 881–891.

Linn, C. E., Campbell, M. G. and Roelofs, W. L. (1992). Photoperiod cues and the modulatory action of octopamine and 5-hydroxytryptamine on locomotor and pheromone response in male gypsy moths, *Lymantria dispar*. *Arch. Insect Biochem. Physiol.* **20**, 265–284.

Linn, C. E. and Roelofs, W. L. (1986). Modulatory effects of octopamine and serotonin on male sensitivity and periodicity of response to sex pheromone in the cabbage looper moth *Trichoplusia ni*. *Arch. Insect Biochem. Physiol.* **3**, 161–172.

Linn, C. E. and Roelofs, W. L. (1992). Role of photoperiodic cues in regulating the modulatory action of octopamine on pheromone-response threshold in the cabbage looper moth. *Arch. Insect Biochem. Physiol.* **20**, 285–302.

Lynch, J. W. and Barry, P. H. (1989). Action potentials initiated by single

channels opening in a small neuron (rat olfactory receptor). *Biophys. J.* **55**, 755–768.

Ma, M., Chen, W. R. and Shepherd, G. M. (1999). Electrophysiological characterization of rat and mouse olfactory receptor neurons from an intact epithelial preparation. *J. Neurosci. Meth.* **92**, 31–40.

Nicolson, S. W. and Isaacson, L. C. (1987). Transepithelial and intracellular potentials in isolated Malpighian tubules of tenebrionid beetle. *Am. J. Physiol.* **252**, 645–653.

Orchard, I., Ramirez, J.-M. and Lange, A. B. (1993). A multifunctional role of octopamine in locust flight. *Annu. Rev. Ent.* **38**, 227–249.

Pass, G., Sperk, G., Agricola, H., Baumann, E. and Penzlin, H. (1988). Octopamine in a neurohaemal area within the antennal heart of the American cockroach. *J. Exp. Biol.* **135**, 495–498.

Pophof, B. (2000). Octopamine modulates the sensitivity of silkmoth pheromone receptor neurons. *J. Comp. Physiol. A* **186**, 307–313.

Redkozubov, A. (2000). Guanosine 3′,5′-cyclic monophosphate reduces the response of the moth's olfactory receptor neuron to pheromone. *Chem. Senses* **25**, 381–385.

Roeder, T. (1999). Octopamine in invertebrates. *Prog. Neurobiol.* **59**, 533–561.

Rospars, J.-P., Lánský, P., Vaillant, J., Duchamp-Viret, P. and Duchamp, A. (1994). Spontaneous activity of first- and second-order neurons in the frog olfactory system. *Brain Res.* **662**, 31–44.

Schmiedel-Jakob, I., Anderson, P. A. and Ache, B. W. (1989). Whole cell recording from lobster olfactory receptor cells: responses to current and odor stimulation. *J. Neurophysiol.* **61**, 994–1000.

Stengl, M., Zufall, F., Hatt, H. and Hildebrand, J. G. (1992). Olfactory receptor neurons from antennae of developing male *Manduca sexta* respond to components of the species-specific sex pheromone *in vitro*. *J. Neurosci.* **12**, 2523–2531.

Thurm, U. (1972). The generation of receptor potentials in epithelial receptors. In *Olfaction and Taste IV* (ed. D. Schneider), pp. 95–101. Stuttgart: Wissenschaftliche Verlagsgesellschaft.

Thurm, U. (1974). Mechanisms of electrical membrane responses in sensory receptors, illustrated by mechanoreceptors. In *Biochemistry of Sensory Functions* (ed. L. Jaenicke), pp. 367–390. Berlin, Heidelberg, New York: Springer.

Thurm, U. and Wessel, G. (1979). Metabolism-dependent transepithelial potential differences at epidermal receptors of arthropods. I. Comparative data. *J. Comp. Physiol. A* **134**, 119–130.

von Nickisch-Rosenegk, E., Krieger, J., Kubick, S., Laage, R., Strobel, J., Strotmann, J. and Breer, H. (1996). Cloning of biogenic amine receptors from moths (*Bombyx mori* and *Heliothis virescens*). *Insect Biochem. Mol. Biol.* **26**, 817–827.

Wieczorek, H. (1992). The insect V-ATPase, a plasma membrane proton pump energizing secondary active transport: molecular analysis of electrogenic potassium transport in the tobacco hornworm midgut. *J. Exp. Biol.* **172**, 335–343.

Wieczorek, H., Grüber, G., Harvey, W. R., Huss, M., Merzendorfer, H. and Zeiske, W. (2000). Structure and regulation of insect plasma membrane H+ V-ATPase. *J. Exp. Biol.* **203**, 127–135.

Williams, J. C., Jr and Beyenbach, K. W. (1984). Differential effects of secretagogues on the electrophysiology of the Malpighian tubules of the yellow fever mosquito. *J. Comp. Physiol. B* **154**, 301–309.

Zack, C. (1979). Sensory adaptation in the sex pheromone receptor cells of saturniid moths. PhD dissertation, Ludwig-Maximilians-Universität, München.

Zufall, F. and Hatt, H. (1991). Dual activation of a sex pheromone-dependent ion channel from insect olfactory dendrites by protein kinase C activators and cyclic GMP. *Proc. Natl. Acad. Sci. USA* **88**, 8520–8524.

Appendix

I Compensation of capacitive transients during current injection

To facilitate understanding of the method passive voltage responses were compensated in Fig. 9A, the P/N leak subtraction method and its effects are illustrated in Fig. 11. This compensation method is common in the patch clamp technique, but has to our knowledge not been applied to other recording techniques. This figure was included in the original manuscript, but omitted on request of one of the referees.
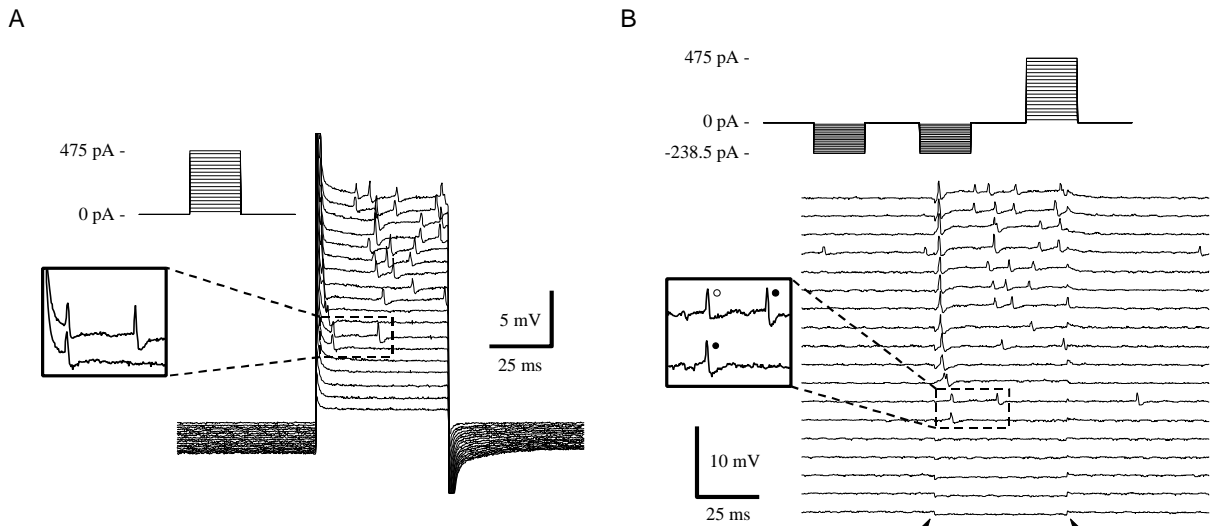

Fig. 11. (A - B) A new method for a corrected voltage response to current step protocols allows the analysis of the minimal current necessary to elicit action potentials in both ORNs. The current step duration is 50 ms. Positive current (i.e. current flowing out of the sensory hair, into the recording electrode) elicited action potentials. (A) Large capacitive transients (truncated for clarity) prevented the reliable classification of action potentials occurring early after the on-step (insert). (B) For each current step, two pre-pulses of opposite polarity and half the amplitude of the main pulse were applied. The responses to pre- and main pulses were added (P/N leak subtraction), and the resulting traces – which would be superimposed – were offset by 2.5 mV. Thus, all passive electrical responses cancelled each other, except for small residuals (arrowheads). This method allowed the reliable distinction and classification of the first action potentials (insert) also at higher currents. The open circle marks a small action potential, the filled circles mark large ones.

II A simple model of the oscillation waveform

The typical shoulder in the waveform of the TEP oscillations (Figs. 1, 2A, 3B, 6A, 7A) was simulated with a simple mathematical model, the addition of two sine waves (Fig. 12). When a sine wave of wavelength 1 and amplitude 1 (Fig. 12A) and a sine wave of half the amplitude and wavelength and with a phase advance of $\pi/3$ (Fig. 12A) are added, the resulting function (Fig. 12C) closely resembles the typical waveform of the TEP oscillations.

This further supports our hypothesis of feedback-coupled regulatory mechanisms underlying the oscillations. Thus, the smaller sine wave (Fig. 12B) reflects the lagging process, that is serotonin-sensitive. If serotonin is injected into an oscillation with a shoulder (Fig. 3B/12C), this component is abolished, and the remaining waveform is a simple sine wave (Fig. 3C/12A). The larger sine wave reflects the leading, octopamine-sensitive process. If the leading component is abolished, the oscillations are entirely absent (Fig. 2).

Furthermore, even complex waveforms, as in Fig. 2D, can be achieved with this model if phase coupling is removed (not shown).
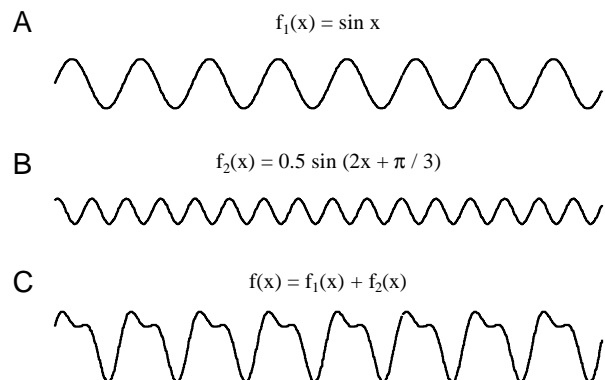

Fig. 12. (A - C) A simple model simulates the typical waveform of TEP oscillations. Adding two sine functions with a fixed relation of amplitude and wavelength and a phase advance (A,B) results in a function with the characteristic shoulder after the positive peaks.

Adaptation in pheromone-sensitive trichoid sensilla of the hawkmoth *Manduca sexta*

Jan Dolzer[1,2], Karin Fischer[2], and Monika Stengl[1,2,*]

[1]Biologie, Tierphysiologie, Philipps-Universität Marburg, D-35032 Marburg, Germany

[2]Institut für Zoologie, Universität Regensburg, D-93040 Regensburg, Germany

*Corresponding author at address 1 (email: stengl@mailer.uni-marburg.de)

Summary

In extracellular tip recordings from long trichoid sensilla of male *Manduca sexta* moths, we quantified responses to bombykal, the main component of the conspecific pheromone blend, in different states of adaptation. Properties of the slow, amplitude-modulated sensillar potentials were compared to the frequency and latency of the fast, frequency-modulated, propagated action potentials. Evidence is presented for the existence of at least three different mechanisms of adaptation, which affect distinct steps of the transduction cascade. One mechanism alters properties of the sensillar potential, which reflects the first step in the chemo-electrical transduction cascade. In the adapted state, the dose-response curves of the sensillar potential amplitude, as well as the initial slope of its rising phase are shifted to higher stimulus concentrations by 1 log unit. The shift in the dose-response curve of the action potential response is larger than for the sensillar potential response, suggesting that an additional adaptation mechanism acts at the level of action potential generation. Furthermore, the faster decline of the sensillar potentials in the adapted state suggests that the resting potential of the olfactory receptor neurons is stabilized in the adapted state.

Introduction

Adaptation, the adjustment of sensitivity in response to previous strong stimulation, enlarges the dynamic range of olfactory receptor neurons (ORNs), prevents damage by overstimulation and provides an early step in the processing of sensory information. While the transduction cascade of pheromone-sensitive ORNs in the sphinx moth *Manduca sexta* has been thoroughly investigated in vitro (Stengl et al., 1992; Stengl, 1993; Stengl, 1994), little is known about olfactory adaptation and the mechanisms involved. In a qualitative study, Kaissling et al. (Kaissling et al., 1989) investigated the specificity of the two ORNs in each trichoid sensillum of *M. sexta*. In each tested sensillum, as was shown by selective adaptation, one of the ORNs responded to bombykal, the main component in the conspecific pheromone blend (Starratt et al., 1979; Tumlinson et al., 1989). Temporal coding and aspects of adaptation of the action potential response were investigated by Marion-Poll and Tobin (Marion-Poll and Tobin, 1992). Their study focused on the modulation of action potential responses generated in the second step of the chemo-electrical transduction, the transformation of the amplitude-modulated receptor potentials into frequency-modulated action potentials. The aim of the current study, however, is the quantitative description of sensillar potential responses, which are assumed to mainly reflect the receptor potentials originating from the primary process in the transduction cascade, and their relation to action potential responses generated in the second transduction step.

In vertebrate olfaction, three stages of adaptation are distinguished by their effects and the underlying mechanisms: short-term adaptation, desensitization, and long-lasting adaptation (Zufall and Leinders-Zufall, 2000). While short term adaptation occurs after short stimuli and declines within several seconds, desensitization is the reduction of the odorant response during maintained stimulation. Long-lasting adaptation, in contrast, is also triggered by short, but strong stimulation, and lasts many minutes. Long-lasting adaptation may superimpose the two other forms of adaptation. In the current study we examined, whether different mechanisms of adaptation, distinguishable by their time course, their targets, or their persistence, are also present in pheromone-sensitive sensilla of the sphinx moth *M. sexta*. Regarding the time course, we focused on the investigation of short-term adaptation and desensitization. The possible targets of adaptation mechanisms in insect ORNs are elements of the chemo-electrical transduction machinery in the outer dendritic segment and elements in the action potential generator, located in the soma or axon hillock region (de Kramer, 1985). In tip recordings, both these targets can easily be distinguished by their electrical activity. While the slow, negative sensillar potential mainly reflects the receptor potential originating from the outer dendrite, the fast

action potentials have the opposite polarity (the depolarizing phase recorded first is positive) and are therefore generated in an electrically – and presumably also morphologically – remote compartment of the ORNs (Zack, 1979; Kaissling and Thorson, 1980; de Kramer, 1985; Kodadová and Kaissling, 1996; Dolzer et al., 2001). With our analysis of the adaptation of parameters that characterize the sensillar potential and the action potential response, we wanted to determine, whether there are different mechanisms of adaptation, and at which levels of the transduction cascade they occur. Our study suggests the presence of at least three functionally distinct mechanisms of adaptation.

Materials and methods

Animals and preparation for electrophysiological recordings

Manduca sexta moths (Johannson) (Lepidoptera: Sphingidae) were raised from eggs, feeding on an artificial diet (modified after Bell and Joachim, 1976). The animals were kept under a long-day photoperiod (L:D 17:7 h, lights off at 8:00 am) at 24–27°C and 40–60% relative humidity. Male pupae were isolated one day before emergence, gently cleaned with 70% EtOH, and allowed to hatch without contact to pheromone. During their second dark phase, the adults were fixed in a teflon holder. The flagellum of the right antenna was immobilized with dental wax (Boxing wax, Sybron / Kerr, Romulus, Michigan), and the 15–20 most apical annuli were clipped off. A glass electrode filled with haemolymph Ringer (Kaissling, 1995) was inserted into the flagellar lumen and sealed with ECG electrode gel (PPG, Hellige, Freiburg, Germany). The tips of long trichoid sensilla from the apical row on the 2nd to 10th remaining annulus were clipped off using sharpened forceps. The recording electrode, filled with sensillum lymph Ringer (Kaissling, 1995), was slipped over one sensillum. To minimize contributions of the electroantennogram, we recorded from an annulus close to the tip of the haemolymph electrode. The connection to the amplifier inputs was established with Ag/AgCl wires immersed in the electrolytes. Signals were amplified about 200-fold in a custom-built amplifier (0 Hz–2 kHz, input impedance 10^{12} Ω), and passed through a 2 kHz anti-aliasing filter (900C/9L8L, Frequency Devices, Haverhill, Massachusetts). Flight activity of the animals was monitored using a piezo-electric element (PI Ceramic, Lederhose, Germany) placed at the thorax. For data acquisition, a Digidata 1200 B digitizer (Axon Instruments, Union City, California) and pCLAMP software (versions 6–8) from the same manufacturer were used. The electrophysiological

signal and a highpass-filtered equivalent (cut-off frequency 2 or 5 Hz), as well as the piezo signal were continuously recorded on a strip chart recorder (WindoGraf or EasyGraf, Gould, Valley View, Ohio). Sections of the recordings were additionally stored on FM tape (Store 4 D, RACAL, Bergisch Gladbach, Germany) or DAT (DTR-1202, Bio-Logic, Claix, France). Voltage polarity is given with the sensillum lymph electrode in reference to the haemolymph electrode. After the recordings, more than 90% of the moths were in sufficiently good condition to be returned to the flight cage.

Pheromone stimulation

All recordings were performed at room temperature (18–23°C). Charcoal-filtered and moistened air was permanently blown over the preparation through a glass cartridge (13 l/min). The air stream could be redirected through cartridges containing a piece of filter paper (about 1 cm^2) loaded with synthetic bombykal (E,Z-10,12-hexadecadienal, BAL) generously provided by T. Christensen (Tucson, Arizona). The cartridges were placed with the outlet in a distance of 4.5–6 cm from the recording site. The air stream was switched between the cartridges using solenoid valves (JFMH-5-PK and MFH-5-1/8, FESTO, Esslingen, Germany) controlled by the computer. Air stream velocity was monitored with a thermistor (BC32L1, Fenwal, Framingham, Massachusetts) placed near the recording site and connected to a custom-built anemometer. Limited by the specified switching time of the solenoids (15 ms), and verified by the anemometer recording, the shortest applicable stimulus duration was about 50 ms. Doses between 10^{-6} and 100 µg BAL dissolved in n-hexane (Merck, Frankfurt, Germany) were applied to the filter papers (10 or 100 µl per paper), and the solvent was allowed to evaporate. Stimulus intensity is always given in terms of the BAL dose applied to the filter paper. A suction tube of 10 cm diameter was placed below the animal to rapidly remove the pheromone after the stimulations and to avoid uncontrolled stimulation by bombykal leaking out of the stimulus cartridges, which were brought in place about 5–30 s prior to stimulation. Between the recording sessions, the cartridges were stored at -80°C in individual glass scintillation vials. Control cartridges loaded with hexane alone were prepared and treated the same way. When stored together with the vials containing the bombykal cartridges, the control cartridges elicited weak responses after several recording sessions, indicating a cross contamination that is likely to have occurred for the lower stimulus doses, too. A set of stimulus cartridges was used for 5–20 recording sessions, the control cartridges were replaced more frequently.
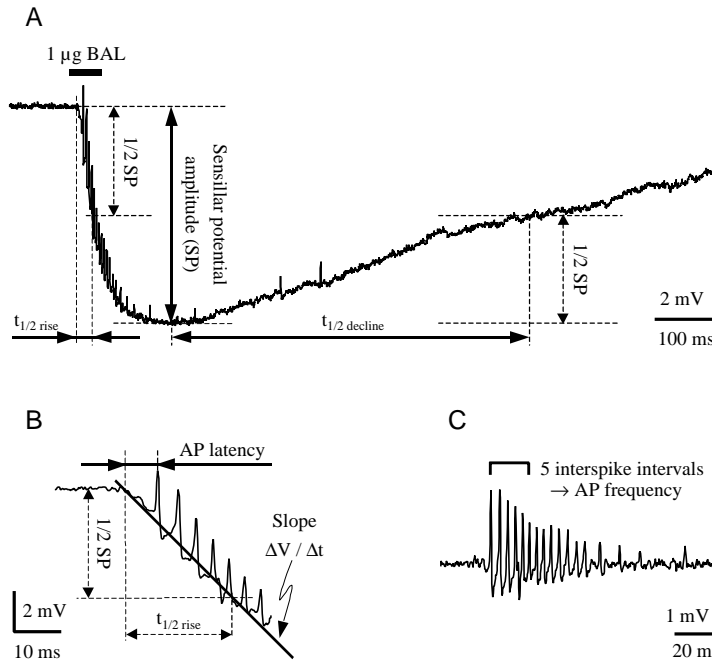
Fig. 1: The pheromone response is characterized by 6 parameters. (A) An unfiltered response to a 50 ms stimulus of 1 μg bombykal (BAL). Action potentials are superimposed on the negative deflection of the transepithelial potential, the sensillar potential. The maximal sensillar potential amplitude (SP) is measured between the baseline before the response and the negative peak during the response. The half-time of the rising phase ($t_{1/2\ rise}$) is determined between the onset of the sensillar potential and the time the potential has reached 50% of SP. The half-time of the decline phase ($t_{1/2\ decline}$) is measured between the end of the response, which at short stimulus duration coincides with the negative peak, and the time the potential has decayed to 50% SP. For the analysis of all parameters describing the sensillar potential, the responses are lowpass-filtered at 50 or 70 Hz (see Fig. 6). (B) The initial phase of the response at an enlarged time scale. The initial slope is determined by dividing 0.5*SP by $t_{1/2\ rise}$. The AP latency is measured between the onset of the sensillar potential and the peak of the first action potential. (C) For the analysis of action potentials, the lowpass-filtered response is subtracted from the original trace, yielding a straight baseline. The initial action potential frequency (AP frequency) is computed from the first five interspike intervals.

Acquisition protocols and data analysis

In the beginning of each recording, a series of 5 mV calibration pulses was applied to the haemolymph electrode, which was otherwise grounded. The pheromone responses were recorded in sweeps of 3 s duration at sampling frequencies of 5 and 1.67 kHz (Clampex, Episodic Stimulation Mode with a Gear Shift after 1000 ms). The solenoids were controlled by a digital output signal switched high 20 ms after the sweep start. The stimulus air stream, as monitored by the anemometer, arrived at the recording site about 50 ms after the trigger signal.

The recordings were evaluated using macros in Clampfit 6, Microsoft Excel (versions 7 and 8), and Automate 4 (Unisyn Software, Los Angeles, California). For the analysis of the sensillar potential, the responses were lowpass-filtered at a cutoff frequency of 50 or 70 Hz (Clampfit, Gaussian filter). The evaluated parameters of the sensillar potential, as illustrated in Fig. 1A,B were: 1. the overall amplitude (SP amplitude), 2. the initial slope between the onset of the DC response and the half-maximal SP amplitude (slope), 3. the half-time of the rising phase ($t_{1/2\ rise}$), and 4. the half-time of the declining phase ($t_{1/2\ decline}$). The half-times of the rising and declining phases were analyzed to compare our results with studies on *Antheraea sp.* (Zack, 1979; Kaissling et al., 1987; Kodadová, 1993; Kodadová and Kaissling, 1996).

For the analysis of the action potentials (Fig. 1C), the lowpass-filtered trace was subtracted from the original response. This pseudo-highpass filtering procedure, in contrast to actual highpass filters, does not distort the shape of the action potentials, and therefore allows the analysis of their amplitude and waveform. The action potential response was characterized by: 1. the peak frequency computed from the first five interspike intervals (AP frequency; Fig. 1C) and 2. the latency between the beginning of the DC response and the first action potential (AP latency; Fig. 1B). When action potentials of both amplitude classes were observed during the response, they were analyzed separately. For the quantitative analysis, the response parameters were normalized to the highest response during each recording. The highest response was defined as the largest value of those parameters that were positively correlated to the stimulus intensity, and as the smallest values of $t_{1/2\ rise}$ and the AP latency, which were negatively correlated to the stimulus intensity. Thus, the normalized responses were computed from

$$Response_{norm} = Response / Response_{max}$$
and
$$Response_{norm} = Response_{min} / Response,$$
respectively.

Stimulation protocols

In total, 1462 stimulations (all doses including controls) were applied to 70 sensilla of 42 animals. Since the experiments were done with a whole-animal preparation, no rundown of the responses was observed, even during recordings of more than 3 h with repetitive stimulation.

Unadapted responses were obtained by applying 50 ms stimuli of increasing bombykal dose, separated by 60 s (dose ramp). Control stimuli with only hexane on the filter paper were applied before each dose ramp. In some recordings, additional control stimuli were applied. Adapted responses were achieved by conditioning the sensilla with 10 µg stimuli of 250 ms duration, applied 20 s before the test stimuli of 50 ms duration (Fig. 2). To ensure identical conditions, each test stimulus was preceded by its own conditioning stimulus. The sensilla were allowed to recover for at least 10 min between every two stimulus pairs to avoid accumulative adaptation. This interval between the stimulus pairs was chosen, since pilot experiments had suggested the complete recovery from adaptation by a stimulus as used in the adaptation protocol after about 5 min (Dolzer, 1996).

For the investigation of desensitization, stimuli of 1000 ms duration were applied. The action potential response characteristics were analyzed with peri-stimulus-time histograms.

Results

In extracellular tip recordings from long trichoid sensilla we investigated the electrical responses to stimulation with bombykal (BAL). The responses of, in total, 70 sensilla of 42 animals to BAL doses between 10^{-6} and 100 µg BAL were characterized and compared in different states of adaptation. Most experiments were only performed on a subset of the sensilla.

Pheromone responses

In response to pheromone stimulation, the transepithelial potential exhibited a negative deflection, the sensillar potential (SP), which was superimposed by action potentials (Figs. 3, 5, 6). Action potentials of two amplitude classes also occurred spontaneously between the stimulations (Dolzer et al., 2001). The action potentials, whether spontaneous or in a pheromone response, were
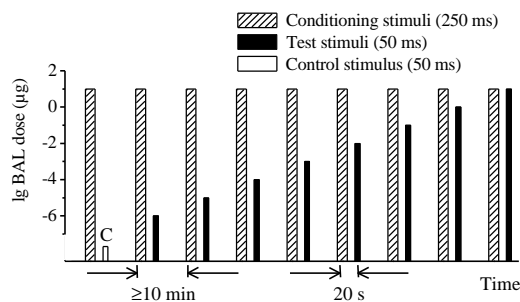

Fig. 2: The adaptation protocol. A conditioning stimulus of 10 µg bombykal (BAL) and 250 ms duration was applied 20 s before each test stimulus of 50 ms duration. Test stimuli of various BAL doses (filled columns) or the control (C; open column) were applied in increasing order. To avoid accumulative adaptation, stimulus pairs were separated by at least 10 min. The time axis is not drawn to scale.

always recorded with their positive phase first. There was a large variability in both the sensillar potential and action potential responses between individual sensilla (Table 1). Sixty-nine of the 70 sensilla tested responded to bombykal. The only non-responding sensillum had no spontaneous activity, indicating that it was damaged.

In 18 of 22 animals analyzed, bombykal stimulation did not elicit flight activity. In 3 cases the animals exhibited continuous flight activity. Only in 1 animal, flight activity occurred immediately after strong stimulation, whereas the animal was silent before. Oscillations of the transepithelial potential (Dolzer et al., 2001) were observed in the recordings from 16 sensilla. In no case did bombykal stimulation suppress or detectably influence the oscillations.

Specificity of the ORNs

Unless the stimulus dose exceeded 10 µg, only action potentials of the large amplitude class were observed during the responses. When small action potentials occurred at these dosages, they could not be distinguished from spontaneously occurring action potentials by their frequency or reduction of the amplitude. At doses of 10 µg BAL, however, the small action potentials occurred at a frequency that could not be considered sponta-neous in 22 of 68 stimuli of 50 ms duration (Fig. 3, Table 2). In the presence of action potentials of the

Table 1. Variability of unadapted responses to strong stimulation.

		Mean	Median	S.D.	S.E.M.	Min	Max
DC	SP amplitude (mV)	10.10	10.07	3.45	0.53	3.92	17.02
	initial slope ($\mu V\ ms^{-1}$)	157	164	78	12	50	412
	$t_{1/2\ rise}$ (ms)	34	35	9	1	13	58
	$t_{1/2\ decline}$ (ms)	897	788	344	53	435	1847
AC	AP frequency (Hz)	278	296	81	12	99	423
	AP latency (ms)	33	27	15	2	5	72

N = 73 responses of 43 sensilla. Bombykal dose: 10 µg, stimulus duration: 50 ms.
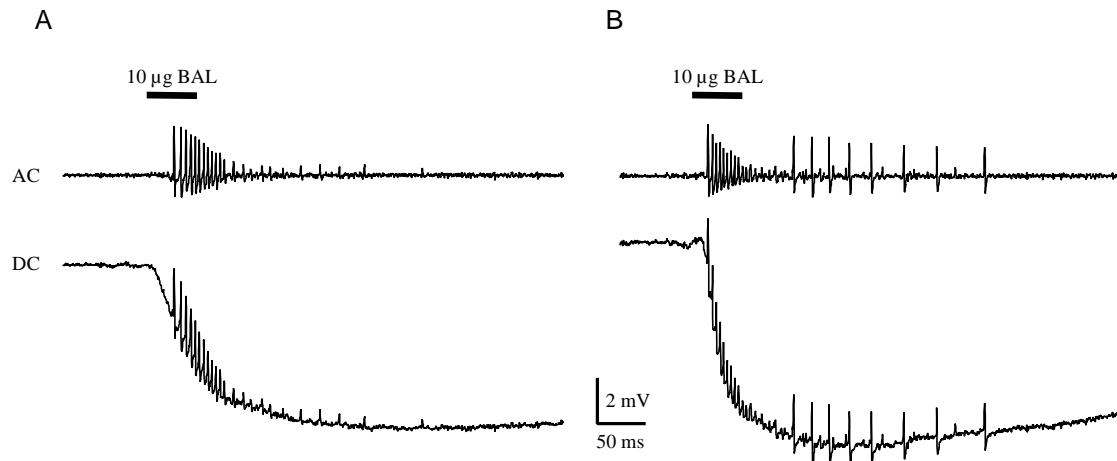DC, variables of the sensillar potential (SP); AC, variables of the action potentials (AP).

Fig. 3: Cross-excitation of the non-bombykal cell occurred after a subset of the 10 µg BAL stimuli of 50 ms duration (see Table 2). While in (A) bombykal stimuli elicited only large action potentials of one class, in (B) also small action potentials were elicited at a lower frequency and after a longer latency. Whenever cross-excitation of the non-bombykal cell was observed, the amplitude of the late, slow action potentials was smaller than that of the early, fast action potentials. Responses of small action potentials were not elicited at BAL doses below 10 µg. AC: Pseudo-highpass-filtered traces, obtained by subtracting lowpass-filtered responses (70 Hz Gaussian filter) from the original signals (DC).

Table 2. Cross-excitation of the non-bombykal cell.

Bombykal dose (µg)	1		10	
Duration (ms)	50	250	50	250
N responses	108	14	68	69
With non-BAL APs	0	0	22	29
Only BAL APs	108	14	46	40

BAL, bombykal; APs, action potentials.

Table 3. Frequency and latency of large and small action potentials in responses with cross-excitation.

Action potentials	Large		Small
Frequency (Hz)	319 ± 10	$- ** -$	105 ± 10 [a]
AP latency (ms)	23 ± 2	$- ** -$	79 ± 5

Data are means $\pm$ S.E.M; bombykal dose 10 µg; stimulus duration 50 ms; N = 22, except [a], where N = 18: in 4 responses the AP frequency over 5 interspike intervals could not be determined, since less than 6 small action potentials occurred. **, $p < 0.01$ (Student's t-test).
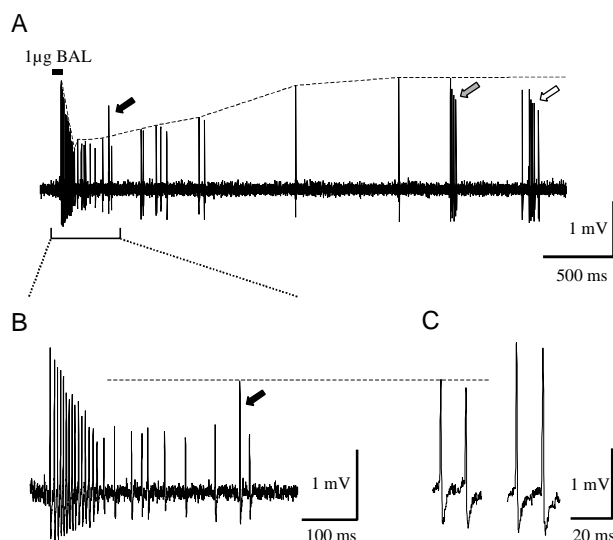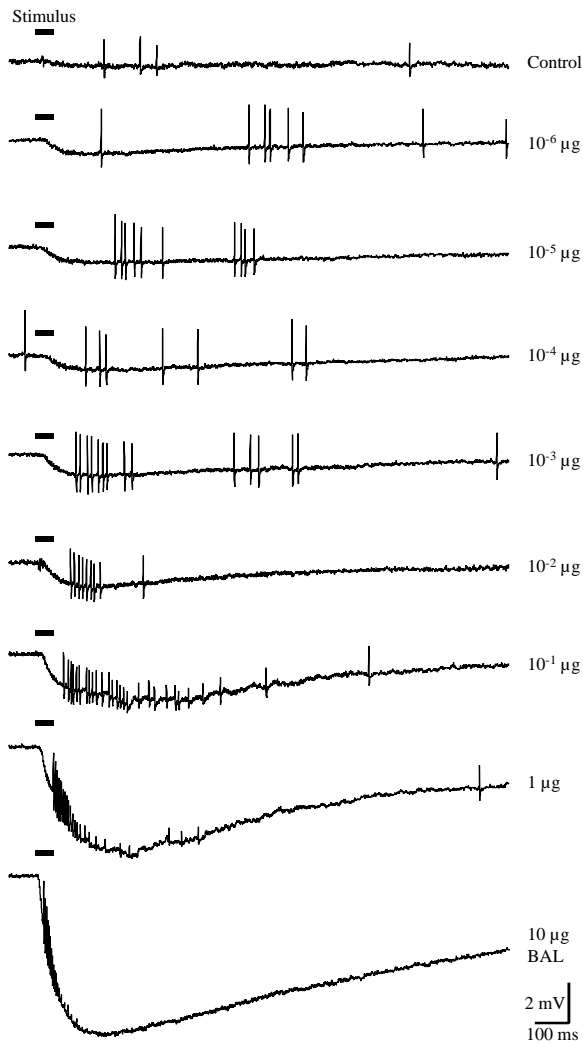

Fig. 4: At doses below 10 µg BAL, only action potentials of the large class were affected by the stimulus-correlated amplitude reduction. (A) Response to a 50 ms stimulus of 1 µg BAL, pseudo-highpass-filtered as in Fig. 3. The amplitudes of the large action potentials were reduced after strong bombykal stimuli and regained their original amplitude in the course of several seconds (dashed envelope). Occasionally, spontaneous small action potentials occurred during (filled arrow) or after the response (open arrow). The reduction of the amplitude during bursts of large (shaded arrow) and small action potentials (open arrow) has been reported previously (Dolzer et al., 2001). (B) Enlarged view of the marked section in A. (C) Two small and two large spontaneous action potentials recorded before the stimulation, plotted at the same amplitude scaling as in B. The small action potential during the response was of the same amplitude as the small spontaneous action potentials.

non-bombykal cell, the SP amplitude was significantly larger (10.85 ± 0.64 mV) than in responses with only one action potential class (8.75 ± 0.50 mV; means ± S.E.M.; p < 0.01, Student's t-test). The AP frequency of the small action potentials was significantly lower and the AP latency was significantly longer than for the large action potentials (Table 3).

In response to strong bombykal stimuli, the amplitude of successive action potentials decreased (Figs. 1C, 3–6), indicating a reduction in the resistance of the adequately stimulated ORN. When

Stimulus

Control

10^{-6} µg

10^{-5} µg

10^{-4} µg

10^{-3} µg

10^{-2} µg

10^{-1} µg

1 µg

10 µg
BAL

2 mV
100 ms

Fig. 5: Pheromone responses are dose-dependent. Stimulation with a solvent-loaded filter paper (Control) did not elicit a measurable sensillar potential. The action potentials of the small class occurred at random. Stimulations with increasing doses of bombykal elicited sensillar potentials of increasing amplitude, together with large action potentials at increasing frequency. At stimulus loads of 10^{-2} µg and up, the reduction of the action potential amplitude during the response became obvious. The stimulus duration was 50 ms, stimuli were applied in increasing order, separated by intervals of 60 s. BAL, bombykal.

each recording. The sensillar potential (SP) amplitude, the initial slope of the SP and the half-time of the decay phase ($t_{1/2 \text{ decline}}$) as well as the action potential response were dose-dependent (Figs. 5 and 7). The threshold was between 10^{-3} and 10^{-2} µg BAL for all these variables. The half-time of the rising phase ($t_{1/2 \text{ rise}}$) exhibited no dose dependence (Fig. 7C).

Short-term adaptation

When the sensilla were adapted by a strong conditioning stimulus (10 µg, 250 ms duration) 20 s prior to the test stimulus, the SP amplitude, the initial slope, and the action potential frequency were reduced (Fig. 6A). In addition, the decay of the sensillar potential was accelerated (Fig. 6B), as characterized by a shorter $t_{1/2 \text{ decline}}$ (Fig. 7D). The dose-response curves of the SP amplitude and the initial slope were shifted to higher stimulus intensities by about 1 log unit (Fig. 7A,B). The half-time of the rising phase, which was virtually dose-independent, was also not significantly altered by the adapting stimulus (Fig. 7C). The dose-response curve of the AP frequency was shifted by 2 log units, and the shift of the dose-response curve of the latency between the onset of the SP and the first action potential was even larger (Fig. 7E,F). For none of the variables, there was an obvious

cross-excitation occurred during a response to 10 µg BAL, the amplitude reduction of the small action potentials was less prominent than of the large ones (Fig. 3B). At lower doses, the amplitude and frequency of small action potentials occurring during the response was the same as during spontaneous activity (Fig. 4).

Dose dependence

The responses varied considerably between individual sensilla (Table 1). Therefore, for the quantitative analysis the response parameters were normalized to the highest response observed during
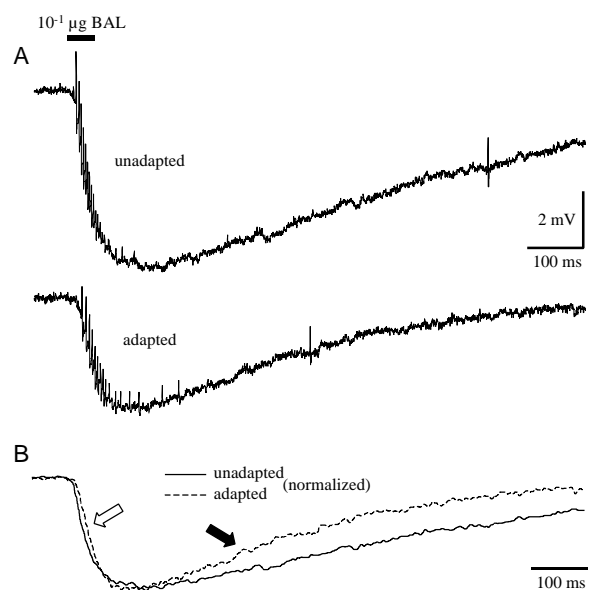
Fig. 6: A strong conditioning stimulus caused adaptation of the sensillar potential- and the action potential response. (A) Compared to a response without a preceding strong stimulus (upper trace) the sensillar potential amplitude and the action potential frequency were reduced (lower trace) after an adapting stimulus. (B) After lowpass-filtering and normalizing both responses to the same maximal amplitude, the faster decline (filled arrow) of the sensillar potential in the adapted state (dashed line) became obvious. The kinetics of the rising phase (open arrow) were almost unaffected. Stimulus duration was 50 ms. BAL, bombykal.

10^{-1} µg BAL

A

unadapted

adapted

2 mV

100 ms

B

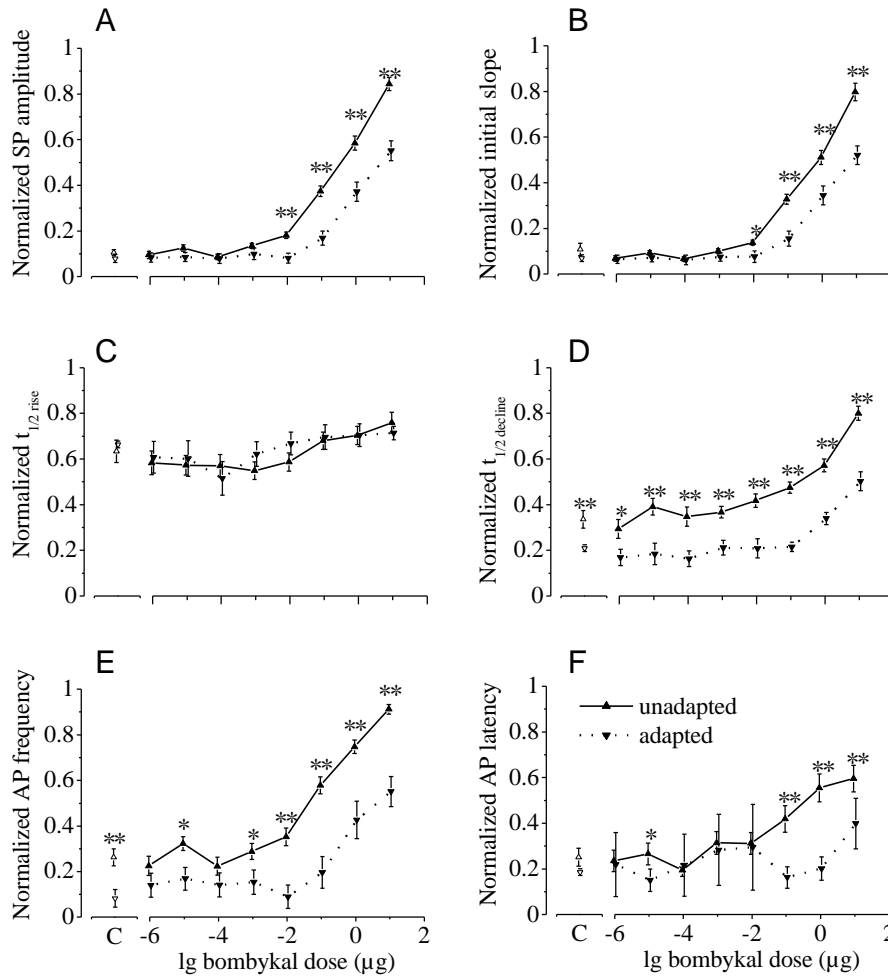unadapted
adapted
(normalized)

100 ms

Fig. 7: Adaptation shifted the dose-response curves to higher stimulus intensities. While the sensillar potential (SP) amplitude (A) and the initial slope (B) increased over the baseline at doses $\geq 10^{-2}$ µg bombykal, $t_{1/2\ rise}$ (C) showed only a very weak dose dependence. The decline of the SP (D) was relatively slow, even at low doses. After adapting stimuli (dotted lines), the dose-response curves of those parameters that describe the initial phase of the SP were shifted to the right by about 1 log unit (A,B). The decline, in addition to a right-shift by more than 1 log unit was accelerated even in the baseline region of the dose-response curve (D). The action potential frequency and the AP latency were shifted by more than 1 log unit (E,F).

C: Control. Data represent means ± S.E.M. The stimulus duration was 50 ms. N = 31 (A–D unadapted), 24 (E,F unadapted), 10 (A–F adapted). Data were normalized to the highest response during each recording. Asterisks indicate significant differences between the adapted and non-adapted state (* $p < 0.05$, ** $p \leq 0.01$; Student's t-test).

difference in the slopes of the adapted and the unadapted dose-response curves.

Desensitization

With stimulations of 1000 ms duration in the absence of a preceding adapting stimulus (N = 129), the action potential response was phasic-tonic at all doses between 10^{-6} µg and 100 µg BAL (Fig. 8). The phasic component was more prominent with increasing pheromone dose. After the phasic peak, the action potential frequency declined to a tonic plateau with a time constant of about 150 ms.

Discussion

In extracellular tip recordings of long trichoid sensilla we investigated the electrical responses to stimulation with bombykal (BAL), the main component in the conspecific pheromone blend. While previous studies on pheromone sensilla in *M. sexta* focused on the specificity of the olfactory receptor neurons (ORNs) (Kaissling et al., 1989) and on temporal coding in the action potential response (Marion-Poll and Tobin, 1992), we characterized and compared the dose dependence of the sensillar

potential- and the action potential response in different states of adaptation. We found in response to short pheromone stimuli that a previous strong pheromone stimulus reduced the amplitude of the sensillar potential, slowed its rise and accelerated the decline. In addition, the initial action potential frequency was reduced even further than the parameters of the sensillar potential. Thus, at least three different mechanisms of adaptation occur: one that decreases the amplitude and the speed of the sensillar potential rising phase, one that accelerates the repolarization phase, and one that further decreases the action potential response. Whether these three adaptation mechanisms act at different time scales, as has been shown in vertebrate olfaction (reviewed in Zufall and Leinders-Zufall, 2000), remains elusive.

Adaptation of the rising phase and the amplitude of the sensillar potential

In our study, the rising phase of the sensillar potentials was characterized using two different parameters, the initial slope and $t_{1/2\ rise}$. The initial slope, whether determined by a straight line fit (not shown) or computed from $t_{1/2\ rise}$ and half the SP amplitude, exhibited a clear dose dependence (Fig.

7B). In contrast to studies with pheromone sensilla of *Antheraea polyphemus* and *A. pernyi* (Zack, 1979; Kaissling et al., 1987; Kodadová, 1993; Kodadová and Kaissling, 1996; Pophof, 1998) and benzoic acid-sensitive sensilla of *Bombyx mori* (Kodadová, 1993), in our experiments $t_{1/2\ rise}$ showed virtually no dose-dependence and was not influenced by adaptation (Fig. 7C). The major difference in the regimens of stimulation between our study and the studies mentioned above is the stimulus duration (50 ms *vs.* 2 or 5 s). Thus, we suspect that the longer stimulus duration, which resulted in a larger pheromone amount totally applied, produced long-lasting adaptation, which is reflected by a change in the kinetics of the rising SP phase. This assumption is supported by previous recordings in *M. sexta* at stimulus durations of 1000 ms. These recordings showed a dose-dependence of $t_{1/2\ rise}$ and a reduction (of the normalized response, corresponding to a prolongation of $t_{1/2\ rise}$) after adapting pheromone stimuli (Dolzer, 1996), as was also found in *A. polyphemus* (Zack, 1979; Kaissling et al., 1987).

Assuming that the sensillar potential predominantly reflects the receptor potential of the adequately stimulated ORN, the waveform of the sensillar potential is probably governed by the complex processes of the chemo-electrical transduction cascade (review: Stengl et al., 1998). Therefore, it is insufficient to characterize the rising phase of the sensillar potential by one time constant or by linear regression. Only the first portion of the rising phase could reasonably be approximated by a linear parameter as in the current study. Attempts to fit the entire rising phase with higher-order exponential functions, however, led to poor results, especially at lower pheromone doses (not shown). To determine, whether individual portions of the sensillar potential can be assigned to individual steps of the transduction cascade, we currently further refine fitting methods by using a segmental approach.
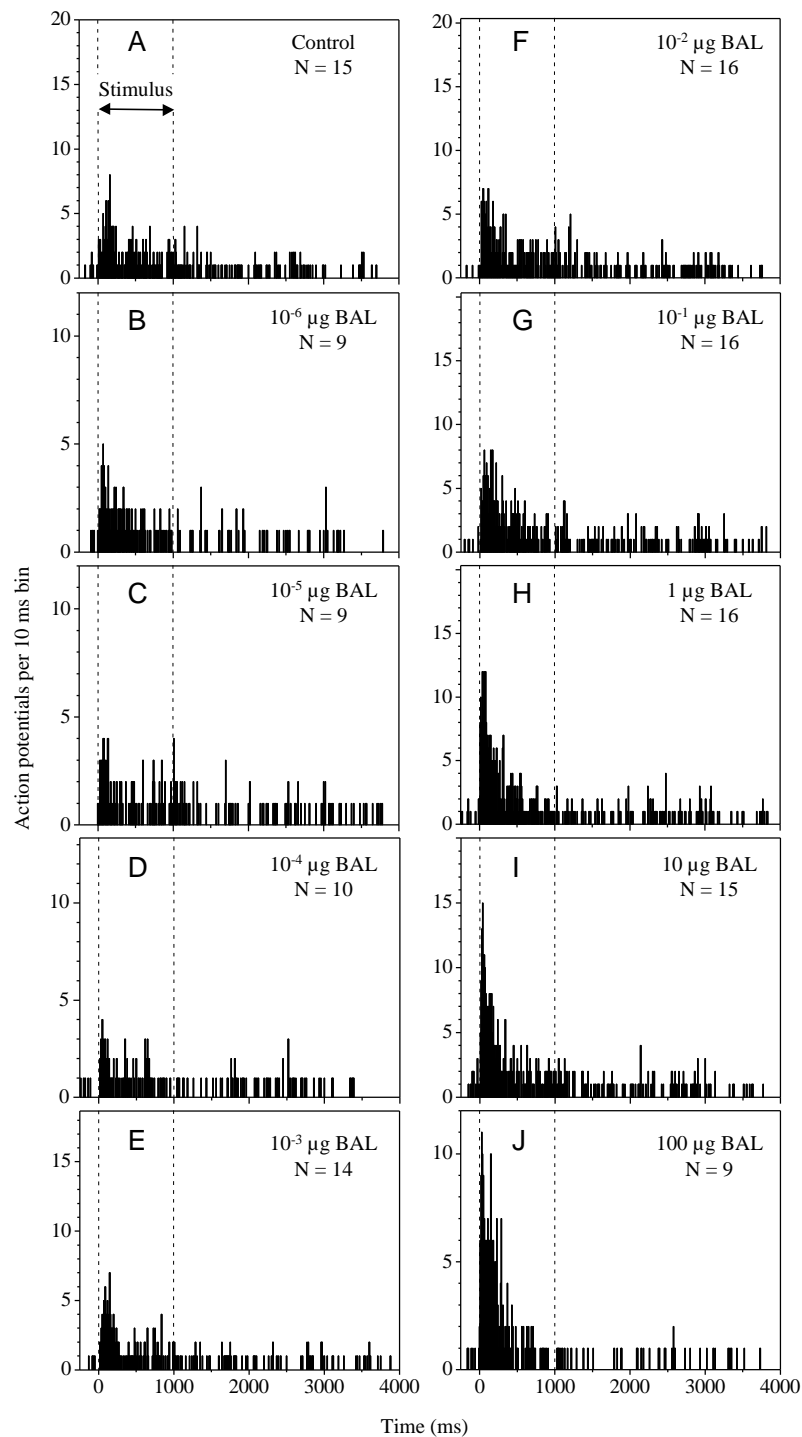
Fig. 8: (A–J) Desensitization of pheromone responses during long pheromone stimuli. The action potential response to long bombykal stimuli became more phasic with increasing stimulus intensity. Peri-stimulus-time-histograms (PSTHs) at a bin width of 10 ms were created for action potentials elicited by 1000 ms stimuli of bombykal, indicated by the dashed lines. While at all stimulus intensities phasic-tonic responses occurred, the phasic component was more prominent at high intensities. This indicates the presence of desensitization. Since the sample sizes (N) differed for the individual doses, all Y axes were scaled to $4/3 * N$. The considerable responses elicited by control stimulations with solvent-loaded filter papers (A) are discussed in the text.

From patch clamp studies on cultured ORNs of *M. sexta* we know that after application of a very low dose of BAL first inositol-1,4,5-trisphosphate (IP_3)-dependent Ca^{2+} channels open, causing a very transient rise of intracellular Ca^{2+} concentrations

(Stengl, 1994). This rapid rise of intracellular Ca^{2+} concentrations then opens Ca^{2+}-dependent cation channels, which may determine the speed of the rising phase and the amplitude of the sensillar potential (Stengl, 1993, Stengl, 1994; Stengl et al., 1992; Stengl et al., 1998). Because both channel types are permeable to Ca^{2+} and because both are closed in a Ca^{2+}-dependent manner, it is very likely that intracellular Ca^{2+} rises are involved in short-term adaptation.

Adaptation of the declining phase of the sensillar potential

The faster decline of the sensillar potentials in the adapted state (Figs. 6B, 7D) suggests the presence of an additional adaptation mechanism, acting via stabilization of the resting potential. Biochemical and physiological evidence suggests the involvement of cyclic GMP (Ziegelberger et al., 1990; Boekhoff et al., 1993; Stengl et al., 2001) and Ca^{2+} rises (Stengl, 1993; Stengl, 1994; Dolzer et al., 1999) in adaptation. Large chloride- or non-specific cation channels, that are probably Ca^{2+}- and/or cGMP-dependent (Dolzer and Stengl, 1998), might be responsible for this stabilization of the resting potential. We are currently testing this hypothesis.

Adaptation of the action potential response

In accordance with the study by Kaissling et al. (Kaissling et al., 1987), we found that the dose-response relation of the action potential response underwent a larger shift to higher stimulus intensities than the relations of the SP amplitude and the initial slope (Fig. 7A,B,E,F). This suggests the presence of at least one additional mechanism of adaptation, acting on the transformation of receptor potentials into action potentials. This transformation process takes place in the soma or axon hillock region, morphologically remote from the origin of the receptor potentials, which favors a functionally distinct adaptation mechanism. We will test, whether cyclic GMP (Zufall et al., 1991; Zufall and Hatt, 1991; Stengl et al., 1992; Stengl et al., 2001) or the phosphorylation of ion channels (Zufall and Hatt, 1991; Stengl, 1993) are involved in the adaptation of the action potential response. The phasic-tonic action potential response observed with long stimulations (Fig. 8), indicating the presence of desensitization (Zufall and Leinders-Zufall, 2000), together with the delayed time course of the cGMP rise (Boekhoff et al., 1993) favors a Ca^{2+}- and/or phosphorylation-dependent mechanism over cGMP. Because after long pheromone stimuli intracellular Ca^{2+} rises closed IP_3-dependent Ca^{2+} channels and Ca^{2+}-dependent cation channels, but opened protein kinase C-dependent cation channels, it is likely that these Ca^{2+}-dependent mechanisms underlie desensitization. Very likely, after long, strong pheromone stimuli the population of the more

slowly activating protein kinase C-dependent cation channels, which are less Ca^{2+}-permeable and which are not blocked by Ca^{2+}, dominate the late phase of the sensillar potential and underlie the tonic depolarization of ORNs.

Dose dependence

Kaissling et al. (Kaissling et al., 1987) found a change in the slope of the dose-response curves of the SP amplitude, $t_{1/2\ rise}$, and the action potential frequency after adapting stimulation. Responses to weak stimuli were further reduced than responses to strong stimuli, leading to a steeper slope of the dose-response relation in the adapted state. In M. sexta, however, the dose-response curves were only shifted to higher stimulus intensities, but not obviously altered in their slope. Our study aimed to investigate stimuli in a physiological range. Thus, we did not routinely exceed a stimulus dose of 10 µg and did not statistically analyze, whether there is a change in the slope. In the study by Kaissling et al., applied pheromone doses were corrected for a nonlinearity in the ratio of the pheromone dose loaded onto the filter paper and its release, as found by studies on radioactively labeled pheromone (Kaissling, 1995). Because no radioactively labeled bombykal is available to date, we do not know whether the same nonlinearity exists for bombykal. Nevertheless, we assume that the differences in the results are rather due to differences in the stimulus protocols used to adapt the sensilla. Kaissling et al. used the strongest stimulus of a protocol that resembles our dose ramp as the only adapting stimulus for a sequence of test stimuli that were applied in increasing order successively. Thus, the time interval between the adapting stimulus and the test stimulus was longer for the test stimuli of higher dose, giving the sensillum more time to recover. In the current study, however, the intervals were kept constant (Fig. 2).

Specificity of the olfactory receptor neurons

As described previously (Dolzer et al., 2001), but in contrast to other studies in M. sexta (Kaissling et al., 1989; Marion-Poll and Tobin, 1992), two classes of action potentials, which most likely can be assigned to the two ORNs in each sensillum (Keil, 1989), could be distinguished by their amplitude in most of the recordings. Our experiments showed that in M. sexta, like in other moth species investigated, the ORN that fires the action potentials with the larger amplitude responds to the main component of the conspecific pheromone blend (Bombyx mori: Kaissling et al., 1978; Antheraea polyphemus and A. pernyi: Zack, 1979; Mamestra suasa: Lucas and Renou, 1989; Mamestra brassicae: Grosmaitre et al., 2001). Only at very high pheromone doses, the cell with the smaller action potential amplitude was excited in addition. Such cross-excitation was also described in Antheraea polyphemus by Kodadová

and Kaissling (Kodadová, 1993; Kodadová and Kaissling, 1996).

Behavioral aspects

In wind tunnel assays, Tumlinson et al. (Tumlinson et al., 1989) found that both, bombykal and (E,E,Z)-10,12,14-hexadecatrienal, are required to elicit a sequence of anemotaxis and mating behavior. They did not test for activation however. Our results suggest that bombykal alone is not sufficient to activate the animals. Neither did bombykal stimulation elicit flight activity, nor did it suppress oscillations of the transepithelial potential, as would have to be expected, if activation is assumed to be correlated with octopamine release (Roeder, 1999; Dolzer et al., 2001). Although the experiments were performed during the activity phase of the nocturnal moths (reared in an inversed culture), we cannot exclude influences of the preparation procedure or the unnatural situation during the recordings. Thus, this finding needs to be confirmed in experiments with freely behaving moths.

Cross-contamination of the pheromone cartridges

The baselines of the dose-response curves are relatively high (Fig. 6). Even stimuli with control cartridges loaded with the solvent alone could elicit considerable responses (Fig. 8A) after several recording sessions. Although special care was taken with the handling of the pheromone cartridges, the comparison between responses to a fresh set of stimulus cartridges and one that had been used for 20 recording sessions clearly showed that cross-contamination of the cartridges with low pheromone doses and the control cartridges had occurred (data not shown). These effects are presumably enhanced by molecules of the highly hydrophobic pheromone component adhering to parts of the electrophysiological setup. These contaminations influence the baseline of the dose-response curves, as well as the peri-stimulus-time histograms at low pheromone doses, but they do not affect the main conclusions of our study.

Acknowledgements

References

Bell, R. A. and Joachim, F. A. (1976). Techniques for rearing laboratory colonies of tobacco hornworms and pink bollworms. *Ann. Entomol. Soc. Am.* **96**, 365-373.

Boekhoff, I., Seifert, E., Göggerle, S., Lindemann, M., Krüger, B. W. and Breer, H. (1993). Pheromone-induced second-messenger signaling in insect antennae. *Insect Biochem. Mol. Biol.* **23**(7), 757-762.

de Kramer, J. J. (1985). The electrical circuitry of an olfactory sensillum in *Antheraea polyphemus. J. Neurosci.* **5**(9), 2484-2493.

Dolzer, J. (1996). Mechanismen der Adaptation bei olfaktorischen Sensillen des Schwärmers *Manduca sexta*. Master Thesis, Universität Regensburg.

Dolzer, J. and Stengl, M. (1998). Pharmacological investigation of ion channels in cultured olfactory receptor neurons of the hawkmoth *Manduca sexta. Göttingen Neurobiology Report 1998* (Vol. II), 380.

Dolzer, J., Bittmann, K. and Stengl, M. (1999). Olfactory adaptation in *Manduca sexta. ESITO* **VI**, 54.

Dolzer, J., Krannich, S., Fischer, K. and Stengl, M. (2001). Oscillations of the transepithelial potential of moth olfactory sensilla are influenced by octopamine and serotonin. *J. Exp. Biol.* **204**, 2781-2794.

Grosmaitre, X., Marion-Poll, F. and Renou, M. (2001). Biogenic amines modulate olfactory receptor neurons firing activity in *Mamestra brassicae. Chem. Senses* **26**, 653-661.

Kaissling, K.-E., Kasang, G., Bestmann, H. J., Stransky, W. and Vostrowsky, O. (1978). A new pheromone of the silkworm moth *Bombyx mori*. Sensory pathway and behavioral effect. *Naturwissenschaften* **65**, 382-384.

Kaissling, K.-E. and Thorson, J. (1980). Insect olfactory sensilla: structural, chemical and electrical aspects of the functional organization. In *Receptors for Neurotransmitters, Hormones and Pheromones in Insects* (ed. D. B. Satelle, L. M. Hall and J. G. Hildebrand), pp. 261-282. Amsterdam: Elsevier / North-Holland.

Kaissling, K.-E., Zack-Strausfeld, C. and Rumbo, E. R. (1987). Adaptation processes in insect olfactory receptors. Mechanisms and behavioral significance. *Ann. N. Y. Acad. Sci.* **510**, 104-112.

Kaissling, K.-E., Hildebrand, J. G. and Tumlinson, J. H. (1989). Pheromone receptor cells in the male moth *Manduca sexta. Arch. Insect Biochem. Physiol.* **10**, 273-279.

Kaissling, K.-E. (1995). Single unit and electroantennogram recordings in insect olfactory organs. In *Experimental Cell Biology of Taste and Olfaction* (ed. A. I. Spielman), pp. 361-377. Boca Raton, New York, London, Tokyo: CRC Press.

Keil, T. A. (1989). Fine structure of the pheromone-sensitive sensilla on the antenna of the hawkmoth, *Manduca sexta. Tissue Cell* **21**(1), 139-151.

Kodadová, B. (1993). Effects of temperature on the electrophysiological response of moth olfactory sensilla. Ph.D. Thesis, Max-Planck-Institut für Verhaltensphysiologie, Seewiesen.

Kodadová, B. and Kaissling, K.-E. (1996). Effects of temperature on silkmoth olfactory responses to pheromone can be simulated by modulation of resting cell membrane resistances. *J. Comp. Physiol. A* **179**, 15-27.

Lucas, P. and Renou, M. (1989). Responses to pheromone compounds in *Mamestra suasa* (Lepidoptera: Noctuidae) olfactory neurones. *J. Insect Physiol.* **35**(11), 837-845.

Marion-Poll, F. and Tobin, T. R. (1992). Temporal coding of pheromone pulses and trains in *Manduca sexta*. *J. Comp. Physiol. A* **171**, 505-512.

Pophof, B. (1998). Inhibitors of sensillar esterase reversibly block the responses of moth pheromone receptor cells. *J. Comp. Physiol. A* **183**, 153-164.

Roeder, T. (1999). Octopamine in invertebrates. *Prog. Neurobiol.* **59**, 533-561.

Starratt, A. N., Dahm, K. H., Allen, N., Hildebrand, J. G., Payne, T. L. and Röller, H. (1979). Bombykal, a sex pheromone of the sphinx moth *Manduca sexta*. *Z. Naturforsch.* **34**, 9-12.

Stengl, M., Zufall, F., Hatt, H. and Hildebrand, J. G. (1992). Olfactory receptor neurons from antennae of developing male *Manduca sexta* respond to components of the species-specific sex pheromone *in vitro*. *J. Neurosci.* **12**(7), 2523-2531.

Stengl, M. (1993). Intracellular-messenger-mediated cation channels in cultured olfactory receptor neurons. *J. Exp. Biol.* **178**, 125-147.

Stengl, M. (1994). Inositol-trisphosphate-dependent calcium currents precede cation currents in insect olfactory receptor neurons in vitro. *J. Comp. Physiol. A* **174**, 187-194.

Stengl, M., Ziegelberger, G., Boekhoff, I. and Krieger, J. (1998). Perireceptor events and transduction mechanisms in insect olfaction. In *Insect Olfaction* (ed. B. S. Hansson), pp. 49-66. Berlin, New York, Heidelberg: Springer.

Stengl, M., Zintl, R., de Vente, J. and Nighorn, A. (2001). Localization of cGMP immunoreactivity and of soluble guanylyl cyclase in antennal sensilla of the hawkmoth *Manduca sexta*. *Cell Tissue Res.* **304**, 409-421.

Tumlinson, J. H., Brennan, M. M., Doolittle, R. E., Mitchell, E. R., Brabham, A., Mazomemos, B. E., Baumhover, A. H. and Jackson, D. M. (1989). Identification of a pheromone blend attractive to *Manduca sexta* (L.) males in a wind tunnel. *Arch. Insect Biochem. Physiol.* **10**, 255-271.

Zack, C. (1979). Sensory adaptation in the sex pheromone receptor cells of saturniid moths. Ph.D. Thesis, Ludwig-Maximilians-Universität, München.

Ziegelberger, G., van den Berg, M. J., Kaissling, K.-E., Klumpp, S. and Schultz, J. E. (1990). Cyclic GMP levels and guanylate cyclase activity in pheromone-sensitive antennae of the silkmoths *Antheraea polyphemus* and *Bombyx mori*. *J. Neurosci.* **10**(4), 1217-1225.

Zufall, F. and Hatt, H. (1991). Dual activation of a sex pheromone-dependent ion channel from insect olfactory dendrites by protein kinase C activators and cyclic GMP. *Proc. Natl. Acad. Sci. U. S. A.* **88**, 8520-8524.

Zufall, F., Stengl, M., Franke, C., Hildebrand, J. G. and Hatt, H. (1991). Ionic currents of cultured olfactory receptor neurons from antennae of male *Manduca sexta*. *J. Neurosci.* **11**(4), 956-965.

Zufall, F. and Leinders-Zufall, T. (2000). The cellular and molecular basis of odor adaptation. *Chem. Senses* **25**, 473-481.

Cyclic guanosine-monophosphate and tetraethylammonium modulate action potentials of olfactory receptor neurons in trichoid sensilla of the hawkmoth *Manduca sexta*

Jan Dolzer*, Christian Flecke, Steffi Krannich and Monika Stengl

Biologie, Tierphysiologie, Philipps-Universität Marburg, D-35032 Marburg, Germany

* Corresponding author: olfaction@jan-dolzer.de

Summary

Olfactory receptor neurons (ORNs) in pheromone-dependent sensilla trichoidea of male *Manduca sexta* moths fire action potentials spontaneously and in response to adequate stimulation. In extracellular tip recordings, slow sensillar potentials superimposed by action potentials are recorded in response to pheromone. The amplitude of action potentials elicited during a pheromone response decreases rapidly and recovers in the course of several seconds. We investigate the influence of 8-bromo cyclic GMP (8bcGMP) injected into the head capsule on spontaneous action potentials. In addition, the properties of the pheromone-dependent sensillar potential and the action potential responses are investigated with 8bcGMP and tetraethylammonium (TEA), a K^+ and cation channel blocker, included in the recording electrode.

First results indicate that 8bcGMP injected into the head capsule alters the waveform of spontaneous action potentials of both ORNs independently, suggesting an effect on ion channels within the ORNs. Two aspects of the waveform, the peak-to-peak amplitude and the repolarizing phase, were affected independently, hinting influences on nonspecific cation- or anion channels and on delayed rectifier potassium channels. Both, 8bcGMP and TEA, reduced the frequency of the action potential response to pheromone and prolonged its latency, while the sensillar potential remained unaffected. The reduction of the action potential amplitude during the response was decreased by 8bcGMP, and possibly also by TEA.

Introduction

There is increasing evidence for the involvement of cGMP in adaptation and/or regulatory processes in moth pheromone sensilla (Ziegelberger et al., 1990; Boekhoff et al., 1993; Stengl, 1993; Redkozubov, 2000; Stengl et al., 2001; Chapter 5). Extracellular tip recordings from pheromone-dependent trichoid sensilla have, furthermore, revealed a shift of the dose-response curves to higher stimulus intensities in the adapted state. The shift is larger for the action potential- than for the sensillar potential response, suggesting the presence of more than one adaptation mechanism (Zack, 1979; Chapter 2). One adaptation mechanism acts on the first step in olfactory transduction, the generation of receptor potentials, which is assumed to occur in the outer dendritic segment of the olfactory receptor neurons (ORNs) (Kaissling and Thorson, 1980; Stengl et al., 1998). The second adaptation mechanism obviously acts on the second step in the transduction cascade, the transformation of amplitude-modulated receptor potentials into frequency-modulated action potentials. The action potential generator is located in a morphologically and electrically remote compartment of the ORNs, presumably in the soma- or axon hillock region, as

indicated by the polarity of action potentials and the currents that are necessary to elicit them (Kaissling and Thorson, 1980; de Kramer et al., 1984; de Kramer, 1985; Chapter 1 (Dolzer et al., 2001); Chapter 2). To determine, whether cGMP is involved in any of these adaptation mechanisms, we investigated spontaneous action potentials and pheromone responses of the hawkmoth *Manduca sexta* in the presence of the membrane-permeant cGMP analogue 8-bromo cGMP (8bcGMP) applied in two different ways.

Biogenic amines injected into the head capsule near the base of the antenna influenced oscillations of the transepithelial potential of trichoid sensilla (Chapter 1 (Dolzer et al., 2001)). This indicates that the agents were transported into the antenna after injection. We tested the influence of 8bcGMP injected in the same way on spontaneous action potentials of the trichoid sensilla. This application mode is further referred to as hemolymph injection.

Drug application to pheromone sensilla during tip recordings by perfusion with water-soluble agents was first suggested by Kaissling et al. (Kaissling et al., 1991). The application of dibutyryl cGMP in this way suppressed both the sensillar potential and the

action potential response in the moth *Bombyx mori* (Redkozubov, 2000). To test, whether this application mode is also applicable to trichoid sensilla of *M. sexta*, we first included the ion channel blocker tetraethylammonium (TEA) in the sensillum lymph ringer of the recording electrode. Since the experiments indicated that the sensillum was, in fact, perfused, we applied 8bcGMP in the same way. Long-term recordings from intact animals revealed no damage of the sensilla when continued for up to several days (Chapter 1 (Dolzer et al., 2001)). So we allowed the sensillum lymph ringer to passively perfuse the sensillum lymph cavity and did not apply any pressure and suction, as suggested by Kaissling et al. (Kaissling et al., 1991). This application method is further referred to as sensillum lymph perfusion.

First results revealed unexpected effects of sensillum lymph perfusion with TEA. The effects of 8bcGMP applied by hemolymph injection and sensillum lymph perfusion firmly support the role of cGMP in adaptation. Furthermore, cGMP appears to be involved in the adaptation mechanism that acts on the action potential generator.

Materials and Methods

See Chapters 1 and 2 for details in materials and methods. Only the differences are described here. The ringers used for sensillum lymph perfusion and the respective controls were prepared with N-(2-hydroxyethyl)-piperazine-N'-(2-ethane sulfonic acid) (HEPES; all chemicals from Sigma, Deisenhofen, Germany) instead of the phosphate buffer used previously (Table 1). The pH was adjusted to 6.5, osmolality was adjusted to 475 mosmol l^{-1} with D-glucose.

Hemolymph injection

All methods, including drug injection and data acquisition and analysis, were identical to those in Chapter 1. After action potential sorting, the action potential waveform was determined by separately averaging all small and large action potentials acquired during 10 min. Thus, the number of action potentials that contributed to the average waveform depended on the action potential activity.

Sensillum lymph perfusion

All methods, including stimulus application, were identical to those described in Chapter 2. For data acquisition version 8 of pCLAMP was employed, in contrast. Thus, no Gear Shift was necessary, and the

Table 1: Composition of the ringers used in the sensillum lymph perfusion experiments

	NaCl	KCl	CaCl$_2$	MgCl$_2$	TEA-Cl	8bcGMP	HEPES
SLR	25	172	1	3			10
SLR/TEA	25	172	1	3	20		10
SLR/8bcGMP	25	172	1	3		10	10

All concentrations are given in mmol l^{-1}. SLR: sensillum lymph ringer, TEA-Cl: tetraethyl ammonium chloride, 8bcGMP: 8-bromo-cGMP, HEPES: N-(2-hydroxyethyl)-piperazine-N'-(2-ethane sulfonic acid)

data files were acquired at a continuous sampling rate of 20 kHz with a pre-trigger- portion of 200 ms and a post-trigger portion of 5 s. The spontaneous activity between the stimuli was recorded as described in Chapter 1. Stimuli of 1 µg bombykal (BAL) and 50 ms duration were applied every 5 min during about 3 h. The response parameters discussed here, except for the time constant, are explained in Chapter 2. In addition to the parameters described there, the second portion of the rising phase of the sensillar potential was fitted with a first-order exponential function (Chapter 4, Fig. 20). Only the time constant of the fit function was used for further analysis.

Results

Spontaneous action potentials

Changes in the waveform of both action potential classes were observed after 6 of 8 hemolymph injections of 30–500 nmol 8bcGMP. In one recording (Fig. 1) the time course of the action potential waveform could be monitored almost continuously for 6 hours after the injection. In the other recordings, either the action potential activity ceased completely after a shorter period, or the activity was lower, leading to a noisier average waveform. Even if not analyzed in the same detail as shown in Fig. 1, the changes in the action potential waveform were unambiguously seen on the paper strip charts and on the archive prints (cf. Chapter 4, Fig. 8) in all 6 recordings. The waveforms of both action potential classes were influenced independently, suggesting that the 8bcGMP effect took place within the individual ORNs. After injection of 8bcGMP, two aspects of the waveform were altered: The peak-to-peak amplitude increased, and the negative phase was prolonged. These effects reverted in the further course and reappeared later, suggesting the presence of feedback-coupled mechanisms that were triggered by 8bcGMP injection. A consistent change in the frequency or burst behavior of the action potentials was not observed.
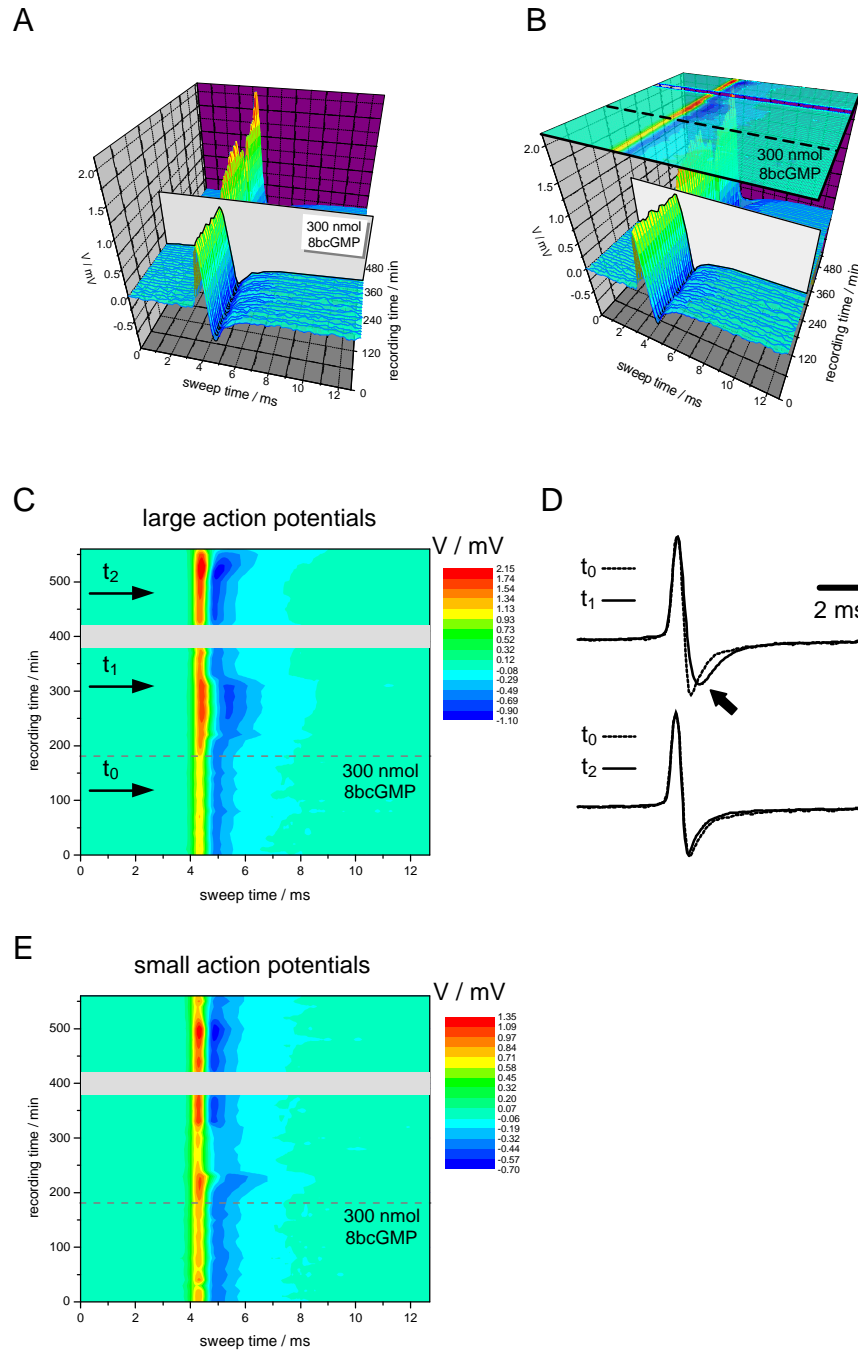
Fig. 1: The shape of both action potential classes was influenced by the injection of 8-bromo cyclic GMP (8bcGMP). (A) The waveform of large APs was averaged for intervals of 10 min and plotted versus the time of the recording. After the injection of 8bcGMP at t = 182 min (transparent wall) both, positive and negative, phases of the APs increased, indicating an increase in the resistance of the ORN. (B) The voltage levels were color-coded and projected into a plane, as shown in C. (C) While before the injection amplitude and time course of the APs remained relatively constant, 8bcGMP increased the peak-to-peak amplitude and prolonged the negative phase of the APs. (D) Average action potential waveforms at the times indicated in C, normalized to the same positive peak amplitude to visualize changes in the time course. When compared to the waveform before the injection (t_0, dotted line), the negative phase was prolonged and slightly reduced in amplitude 140 min after the injection (t_1, solid line). In the further course, the negative phase was shortened again, and 300 min after the injection the time course of the averaged and normalized waveform (t_2, solid line) was identical to the pre-injection waveform (t_0, dotted line). (E) Changes in the waveform of the small action potentials also showed increases of the peak-to-peak amplitude and a prolongation of the negative phase, but at a different time course: The prolongation of the negative phase reversed after 50 min, while with the large action potentials this occured after 150 min. The peak-to-peak amplitude was transiently reduced back to the pre-injection level between 70 and 120 min after the injection, while the large action potentials reached their highest peak-to-peak amplitude at the same time.

During the gap in the data (gray areas in C and E), small and large APs could not be distinguished.

Pheromone responses

In 6 control experiments with only sensillum lymph ringer in the recording electrode, no decrease of any parameter of the sensillar potential- or action potential response was observed during 3 h of repetitive stimulation (Fig. 2). Every 5 min, a stimulus of 1 µg bombykal and 50 ms duration was applied. During 160 min of sensillum lymph perfusion with 10 mmol l^{-1} 8bcGMP, the action potential frequency continuously decreased, while the latency between the onset of the sensillar potential and the first action potential increased (Figs. 3, 4). The parameters that describe the sensillar potential, however, remained virtually constant. Furthermore, the reduction of the action potential amplitude during the response (cf. Chapter 2, Fig. 4) continuously decreased, until it was virtually absent (Fig. 3B). These effects were consistently observed in each of 5 recordings. In one experiment, AP frequency and AP latency had recovered to the initial level 14 h later, suggesting a decay of 8bcGMP. The SP response remained constant all the time.

The effects of sensillum lymph perfusion with 20 mmol l^{-1} TEA closely resembled those of 8bcGMP: While the sensillar potential response remained unaltered, the action potential frequency was reduced and the latency was prolonged in 2 of 3 experiments (Figs. 5, 6). In the remaining experiment, these effects were less clear, but the same in tendency. Whether TEA causes the same change in the reduction of the action potential amplitude as observed after 8bcGMP application, remains to be quantified (Fig. 5).

Discussion

In tip recordings from pheromone-sensitive trichoid sensilla of the hawkmoth *Manduca sexta*, 8bcGMP injected into the head capsule altered the waveform of spontaneous action potentials (APs). Furthermore, when included in the recording electrode, 8bcGMP reduced the frequency of the APs and prolonged their latency in response to pheromone stimulation. The sensillar potential (SP) remained unaffected, in contrast. The effect of TEA closely resembled the effect of 8bcGMP, suggesting that both agents act on the same targets. The effects of 8bcGMP and TEA on the amplitude reduction of the APs, requires a more careful examination and quantification. Nevertheless, the effects were consistently different from the controls, and were therefore included, also considering their importance for the understanding of the results presented in Chapters 2 and 5.

For the first time, we have been able to isolate one of the adaptation mechanisms present in pheromone-dependent moth sensilla (Zack, 1979; Chapter 2). Both, 8bcGMP and TEA, mimic the adaptation of the AP response while leaving the SP response unaffected. This finding proves *i)* the presence of more than one adaptation mechanism, and *ii)* the assumption that cGMP is involved in olfactory adaptation in moths, as proposed by a number of authors (Ziegelberger et al., 1990; Boekhoff et al., 1993; Stengl, 1993; Stengl et al., 2001; Chapter 5). However, our findings raise a number of new questions. Especially surprising is the similarity of the effects caused by 8bcGMP and
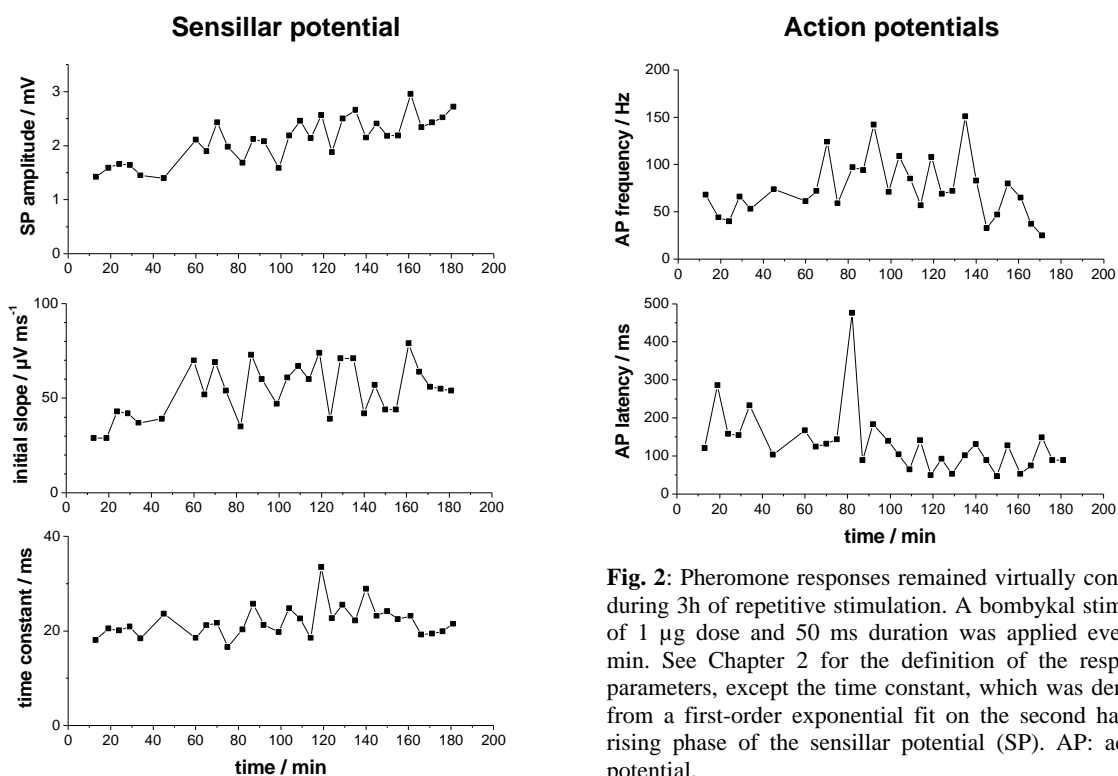
Sensillar potential

Action potentials

Fig. 2: Pheromone responses remained virtually constant during 3h of repetitive stimulation. A bombykal stimulus of 1 µg dose and 50 ms duration was applied every 5 min. See Chapter 2 for the definition of the response parameters, except the time constant, which was derived from a first-order exponential fit on the second half of rising phase of the sensillar potential (SP). AP: action potential.

TEA. The expectation was that TEA acts on ion channels in the outer dendritic segment, causing a reduction of the sensillar potential. Two types of cation channels, Ca^{2+}-activated and protein kinase C (PKC)-activated cation channels, which are both sensitive to TEA (Stengl, 1993), are involved in the primary process in olfactory transduction, the generation of receptor potentials (Stengl et al., 1998). On this background, TEA was used to determine, whether substances, which are included in the recording pipette, passively diffuse into the sensillum at all – which is evidently the case. The observed lack of TEA effects on the SP response apparently contradicts the assumption of an involvement of TEA-sensitive channels in receptor potential generation, at least in response to short stimuli, as used in the current study. On the other hand, assuming that both the TEA-sensitive cation channels are involved in receptor potential generation, one must either postulate the activation of other channels that compensate for the TEA block, or raise the question to what extent the SP, which is recorded from the entire sensillum, reflects the receptor potential, as generated by the ORN. Each of these possible explanations for the absence of TEA effects on the SP is in contradiction to generally accepted concepts. Therefore, a lot of challenging experiments remain to be done until the electrical circuitry of a trichoid sensillum is fully understood.

Another newly arising question is how TEA, which is not membrane-permeant, exerts its effect on the action potential generator. Direct access of sensillum lymph-carried substances to the action
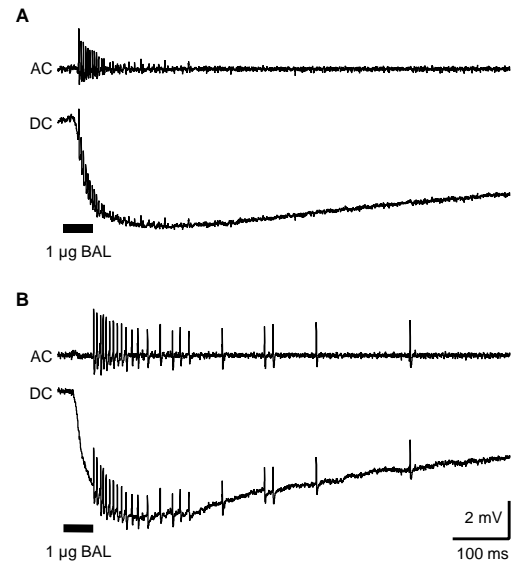

Fig. 3: Sensillum lymph perfusion with 10 mmol l^{-1} 8bcGMP reduced the action potential (AP) response, but left the sensillar potential (SP) response unaltered. (A) At the beginning of the recording, the AP frequency in response to bombykal (BAL) stimulation was 245 Hz, the delay between the onset of the SP and the first AP was 10 ms. (B) After 158 min, the SP was unaltered, but the AP frequency was reduced to 147 Hz, and the first AP occurred 37 ms after SP onset. The stimulus-correlated reduction of the AP amplitude, which was very prominent in A, almost disappeared. Scaling is identical in A and B. AC: Pseudo-highpass-filtered response obtained by subtraction of the lowpass-filtered signal from the unfiltered response (DC).
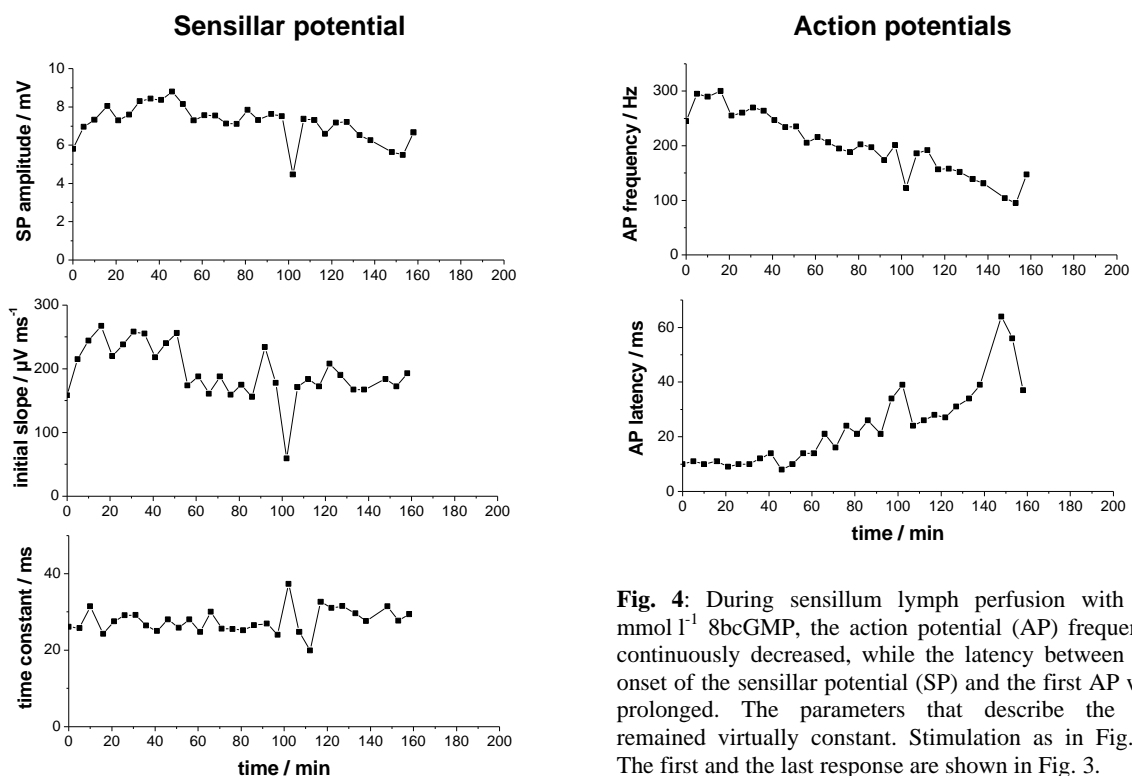

Fig. 4: During sensillum lymph perfusion with 10 mmol l^{-1} 8bcGMP, the action potential (AP) frequency continuously decreased, while the latency between the onset of the sensillar potential (SP) and the first AP was prolonged. The parameters that describe the SP remained virtually constant. Stimulation as in Fig. 2. The first and the last response are shown in Fig. 3.

potential generator can virtually be excluded. All action potentials and -currents recorded from olfactory sensilla using the tip recording technique were reported to have a positive initial phase (Den Otter, 1977; Zack, 1979; Kaissling and Thorson, 1980; de Kramer et al., 1984; Redkozubov, 1995; Kodadová and Kaissling, 1996; Chapter 1 (Dolzer et al., 2001) and numerous other references), indicating that there is no Galvanic connection between the sensillum lymph space and the action potential generator. This is further supported by the polarity of current steps that elicited action potentials electrically. Only in response to positive currents (i.e., currents out of the sensillum, into the recording electrode, which would hyperpolarize all membranes in direct access to the sensillum lymph) action potentials were elicited (de Kramer et al., 1984; Chapter 1). Therefore, direct diffusion of TEA to the action potential generator does not appear possible.

Large ion channels that were insensitive to the replacement of all cations by the large cation N-methyl-D-glucamine (NMDG) were observed in patch clamp recordings (Chapter 5). Their ionic selectivity is unclear, but it does not appear likely that – if they were constantly permeable to cations, such as TEA – they are located in the membrane of the outer dendrite, since this would lead to steady depolarization of the ORNs. It is possible, however, that they only open in response to stimulation, allowing a sufficiently high concentration of TEA to enter. This hypothesis can easily be tested by applying a reference stimulus in the very beginning of the recording and then allowing TEA to perfuse the sensillum for 3 h without stimulation. When the
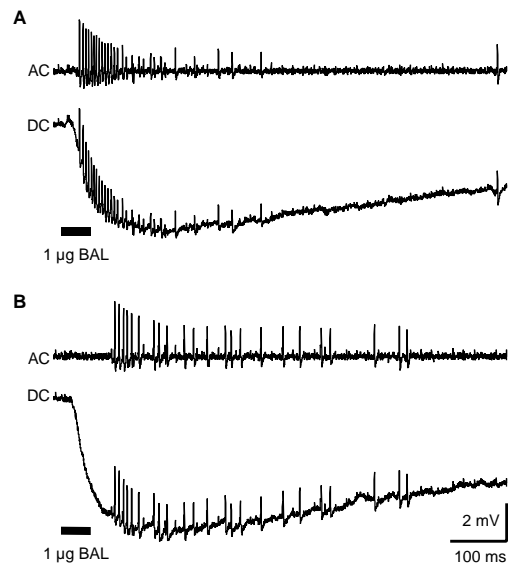

Fig. 5: The effect of sensillum lymph perfusion with 20 mmol l^{-1} TEA resembled the effect of 8bcGMP. (A) The response to BAL recorded at the beginning of the recording was smaller than the response shown in Fig. 3A. This is due to the variability between individual sensilla that is normally observed. (B) After 171 min the AP frequency was reduced and the latency prolonged. The SP response was virtually identical to that in A, however. AC: Pseudo-highpass-filtered response obtained by subtraction of the lowpass-filtered signal from the unfiltered response (DC).
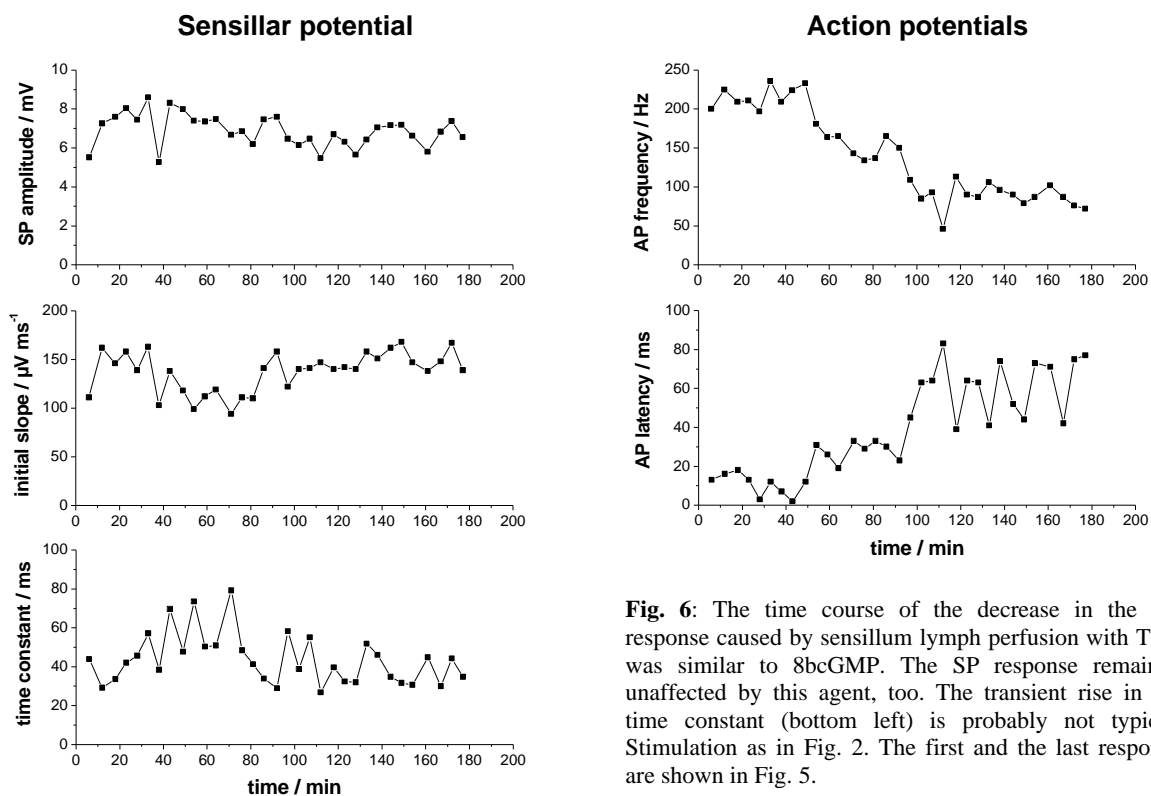

Fig. 6: The time course of the decrease in the AP response caused by sensillum lymph perfusion with TEA was similar to 8bcGMP. The SP response remained unaffected by this agent, too. The transient rise in the time constant (bottom left) is probably not typical. Stimulation as in Fig. 2. The first and the last response are shown in Fig. 5.

response to a stimulus applied after this period is compared to the reference, it should become obvious, whether or not TEA passes through ion channels that are activated stimulus-dependently.

It is very likely that the same circuitry that is responsible for the antidromatic propagation of action potentials to the recording electrode (de Kramer, 1985) also conducts the depolarization during a receptor potential to the AP generator. This circuitry appears to be influenced by 8bcGMP, as the increased AP amplitude (or the reduction of their decrease) observed in both the hemolymph injection- and sensillum lymph perfusion experiments suggests. According to Ohm's Law, a larger AP amplitude recorded from the sensillum lymph would indicate a higher resistance between the AP generator and the sensillum lymph cavity – provided the actual AP amplitude remains constant. A higher symmetrical resistance, i.e. the inactivation of nonspecific ion channels, however, would also increase the potential difference that is propagated to the AP generator during a receptor potential, thus causing an increase of the AP response instead of the observed decrease. Therefore, if the reduction of the AP response is caused by inactivation of ion channels by 8bcGMP and TEA, these channels must be rectifiers, inward or outward, depending on their localization within in the ORNs.

The reduction of the AP frequency alone could be explained by a change in the gating of delayed rectifier K^+ channels, as suggested by a prolonged negative phase of spontaneous APs (Fig. 1). Whether there is a similar change in the waveform of the background APs recorded between the stimuli, remains to be analyzed. The prolonged activation of delayed rectifiers cannot account for the prolonged latency of the first AP in pheromone responses, however. Opening of delayed rectifiers requires depolarization, such as during an action potential. Therefore, if only the openings of these channels were prolonged, the first AP should occur at the same time as in the controls, and only the frequency of successive APs should be reduced.

Our findings are in contradiction to the findings of Redkozubov (Redkozubov, 2000), who described a dibutyryl cGMP-dependent reduction of both the SP and the AP response in *Bombyx mori*. This may be due to the fact that we recorded voltage without any current clamp circuitry, while Redkozubov recorded currents in transepithelial voltage-clamp conditions. Our experiments suggest that the reduction of the AP amplitude that is observed during responses (Figs. 3A, 5A) is not caused by the opening of ion channels whose currents contribute to the SP. Otherwise, as long as the SP remains constant, the APs recorded in the presence of 8bcGMP or TEA would have to be reduced in their amplitude as far as in the absence of these agents. Since this is not the case, the reduction of the transepithelial resistance during a response, as described by Zack (Zack, 1979), is probably due to a

reduction of the shunt resistance over the accessory cells, not a reduction of the resistance of the ORNs. The amplitude of currents necessary to elicit APs (about 250 pA; Chapter 1) suggests that most of the current injected in tip recordings does not flow through the ORNs, but through this shunt pathway. This, in turn, means that the transepithelial resistance predominantly reflects the resistance of the shunt pathway. This might lead to the differences of the cGMP effects observed between voltage recordings and current recordings under voltage-clamp conditions. Two other explanations are also possible. Firstly, the cGMP derivative used in both studies was different, and Redkozubov applied a 100fold lower dose than we did. To exclude effects of substitute groups and dose, we will also test dibutyryl cGMP and try a reduced dose of both derivatives. The other explanation is that there are differences between pheromone sensilla in *B. mori* and *M. sexta* with respect to the role of cGMP.

In conclusion, the experiments presented here have added knowledge to the understanding of adaptation processes in insect pheromone sensilla, but also given rise to a number of new questions and hypotheses, some of which are easy to test. Furthermore, they have shown that tip recordings are a powerful *in situ* approach for the completion of knowledge obtained with *in vitro* experiments, such as patch clamp recordings.

Acknowledgements

References

Boekhoff, I., Seifert, E., Göggerle, S., Lindemann, M., Krüger, B. W. and Breer, H. (1993). Pheromone-induced second-messenger signaling in insect antennae. *Insect Biochem. Mol. Biol.* **23**(7), 757-762.

de Kramer, J. J. (1985). The electrical circuitry of an olfactory sensillum in *Antheraea polyphemus*. *J. Neurosci.* **5**(9), 2484-2493.

de Kramer, J. J., Kaissling, K.-E. and Keil, T. A. (1984). Passive electrical properties of insect olfactory sensilla may produce the biphasic shape of spikes. *Chem. Senses* **8**, 289-295.

Den Otter, C. J. (1977). Single sensillum responses in the male moth *Adoxophyes orana* (F.v.R.) to female sex pheromone components and their geometrical isomers. *J. Comp. Physiol.* **121**, 205-221.

Dolzer, J., Krannich, S., Fischer, K. and Stengl, M. (2001). Oscillations of the transepithelial potential of moth olfactory sensilla are influenced by octopamine and serotonin. *J. Exp. Biol.* **204**, 2781-2794.

Kaissling, K.-E. and Thorson, J. (1980). Insect olfactory sensilla: structural, chemical and electrical aspects of the functional organization. In *Receptors for Neurotransmitters, Hormones and Pheromones in Insects* (ed. D. B.

Satelle, L. M. Hall and J. G. Hildebrand), pp. 261-282. Amsterdam: Elsevier / North-Holland.

Kaissling, K.-E., Keil, T. A. and Williams, J. L. D. (1991). Pheromone stimulation in perfused sensory hairs of the moth *Antheraea polyphemus. J. Insect Physiol.* **37**(1), 71-78.

Kodadová, B. and Kaissling, K.-E. (1996). Effects of temperature on silkmoth olfactory responses to pheromone can be simulated by modulation of resting cell membrane resistances. *J. Comp. Physiol. A* **179**, 15-27.

Redkozubov, A. (1995). High electrical resistance of the bombykol cell in an olfactory sensillum of *Bombxy mori*: voltage- and current-clamp analysis. *J. Insect Physiol.* **41**(6), 451-455.

Redkozubov, A. (2000). Guanosine 3',5'-cyclic monophosphate reduces the response of the Moth's olfactory receptor neuron to pheromone. *Chem. Senses* **25**, 381-385.

Stengl, M. (1993). Intracellular-messenger-mediated cation channels in cultured olfactory receptor neurons. *J. Exp. Biol.* **178**, 125-147.

Stengl, M., Ziegelberger, G., Boekhoff, I. and Krieger, J. (1998). Perireceptor events and transduction mechanisms in insect olfaction. In *Insect Olfaction* (ed. B. S. Hansson), pp. 49-66. Berlin, New York, Heidelberg: Springer.

Stengl, M., Zintl, R., de Vente, J. and Nighorn, A. (2001). Localization of cGMP immunoreactivity and of soluble guanylyl cyclase in antennal sensilla of the hawkmoth *Manduca sexta. Cell Tissue Res.* **304**, 409-421.

Zack, C. (1979). Sensory adaptation in the sex pheromone receptor cells of saturniid moths. Ph.D. Thesis, Ludwig-Maximilians-Universität, München.

Ziegelberger, G., van den Berg, M. J., Kaissling, K.-E., Klumpp, S. and Schultz, J. E. (1990). Cyclic GMP levels and guanylate cyclase activity in pheromone-sensitive antennae of the silkmoths *Antheraea polyphemus* and *Bombyx mori. J. Neurosci.* **10**(4), 1217-1225.

XtraCell, a Microsoft Excel add-in for the automated evaluation of tip recordings from insect sensilla

Jan Dolzer[1,2]

[1]Biologie, Tierphysiologie, Philipps-Universität Marburg, D-35032 Marburg, Germany*

[2]Institut für Zoologie, Universität Regensburg, D-93040 Regensburg, Germany

*Current address; Correspondence to: xtracell@jan-dolzer.de

Summary

A Windows software for the evaluation of extracellular tip recordings of insect sensilla is introduced. The software, called XtraCell, aids in the analysis of both, spontaneous activity including fluctuations of the transepithelial potential and flight activity, and responses to adequate stimulation. XtraCell is capable of sorting the spontaneous action potentials into two classes of different amplitudes, even in the presence of bursts that are correlated with amplitude reductions and make the amplitudes of both classes overlap. The distributions of spontaneous action potentials and bursts are statistically analyzed. Sensillar potentials and action potentials in response to stimulation are separated and characterized by several parameters. XtraCell was developed for the analysis of recordings from pheromone sensilla in the hawkmoth *Manduca sexta*, but may also be applicable to recordings from other olfactory sensilla, or even sensilla of other sensory modalities.

The software is designed as an add-in for Microsoft Excel and designated to co-operate with pCLAMP by Axon Instruments. Due to the flexibility of pCLAMP regarding input formats, data files acquired with other programs might also be analyzed. The module for the evaluation of spontaneous action potential activity is potentially open enough to operate with ASCII data from any source.

1 Introduction

In contrast to extracellular recordings in most other systems, tip recordings of insect sensilla give access to a clearly defined, limited set of electrically active cells. In pheromone-sensitive trichoid sensilla of the sphinx moth *Manduca sexta*, two olfactory receptor neurons (ORNs), tuned to different components of the pheromone blend, are ensheathed by a common set of three accessory cells (Kaissling et al., 1989; Keil, 1989; Kalinová et al., 2001). The ORNs fire spontaneous action potentials (APs), distinguishable by their amplitude and superimposed on fluctuations of the transepithelial potential (TEP), which is generated by the accessory cells. Bursts of APs are frequently observed and are associated with a reduction of the AP amplitude (Kalinová et al., 2001; Chapter 1, Fig. 5). In response to pheromone stimulation, the sensilla generate a sensillar potential (SP) and a train of action potentials (APs) (Kaissling et al., 1989; Marion-Poll and Tobin, 1992; Chapter 2). Thus, in both, spontaneous activity and responses to adequate stimulation, there are fast and slow components that originate from different compartments of the cells or sensillum and are recorded as a compound signal.

The characterization of the physiology of pheromone sensilla requires the separation of individual components of this compound signal. A software for this purpose must therefore fulfill the following criteria: 1. It must be capable of separating APs from slow fluctuations of the baseline. 2. The APs must be sorted according to their amplitude, even in the presence of AP bursts during which the amplitudes overlap. 3. The spontaneous AP activity must be analyzed according to parameters such as frequency, distribution, and frequency and composition of bursts. 4. The time course of the TEP and additional recorded parameters, such as the flight activity, must be put out on a long-term time scale. 5. Sensillar potentials in response to adequate stimulation must be characterized in amplitude and time course. 6. Action potentials in response to stimulation must be analyzed in their temporal sequence and amplitude.

These requirements are fulfilled by **XtraCell**, an add-in to the spreadsheet program Microsoft Excel. The concept of XtraCell involves the use of the analysis of the raw data files using Clampfit 8 (part of pCLAMP, Axon Instruments, Union City, California). In part, the program completely controls the analysis in Clampfit. XtraCell is the synthesis of its two predecessors that served for the analysis of spontaneous activity and pheromone responses, respectively. This is reflected by the menu structure with the first two items **SpontAct** and **ReSponse**. Both these modules originate from macro procedures and batch files that were formerly executed sequentially and saved their respective results in separate files of various formats, depending on the analysis steps they performed. With time, XtraCell has become more and more comfortable to operate and is today an integrated solution that can be distributed as a small number of files included in a ZIP archive. Nevertheless,

being non-commercial software and undergoing steady development, there is still room for improvement, and a couple of desirable features have not been implemented yet.

The division into the two major modules, SpontAct and ReSponse, is also used for the step-by-step guide (section 5) that treats the analysis of tip recording data and shows up potential pitfalls using a set of sample data files that are distributed together with the program. The appendices (Section 9) list known bugs and limitations, define the expected structure of input data and give a more detailed description of the output on the **Error** sheet and of the **Program Options**. In addition, this section provides some information for programmers, who want to develop XtraCell further, and the meaning of a few common error messages.

XtraCell is distributed under the GNU General Public License (GPL).
See www.gnu.org/copyleft/gpl.html for more details.

2 System requirements and compatibility

XtraCell was developed and extensively tested with Microsoft Office 97 running under Windows NT and 2000. A number of tests was also performed under Windows 98. However, I cannot provide any guarantee for the performance under Windows 98 or any future operating systems. You should therefore verify the correctness of the results, if you run XtraCell under other than the specified conditions. More probable than incorrect results, however, appear program errors that prevent the software from running properly.

2.1 Hardware

The hardware resources should not be critical, except for performance speed. Every system that runs Microsoft Office 97 and up, or pCLAMP 8 and up should be able to run XtraCell. Slow computers (<400 MHz) might have problems with those procedures that send simulated keyboard input to Clampfit (ReSponse).

2.2 Software

- Microsoft Excel 97 or later, including VBA, is required as host application for XtraCell.
- Windows Scripting Host is necessary for the evaluation of response data. This tool can be downloaded free of charge from the Microsoft web site. Try the web addresses www.microsoft.com/downloads or ../scripting.
- Clampfit 8 is required for the evaluation of the data files. Since Clampfit 8 does not feature any macro function, the procedures that employ this application work with simulated keyboard shortcuts. Should Axon Instruments change the accelerator keys for the required features, these procedures will not work anymore. A pre-release version of Clampfit 9 available at the time this dissertation is submitted did not respond correctly. So it is not very likely that Clampfit versions later than 8 will immediately work. However, the code includes comments for each command, so that the adoption should be easily done.

  A number of Clampfit 8 versions had bugs in **Analyze / Statistics**. Some early 8.0 versions only analyzed the first sweep and duplicated these results for all sweeps. All Clampfit versions between 8.0.3.169 and 8.2.0.224 do not correctly handle overlapping sweeps after adjusting the baseline. So if you experience any problems that appear to be caused by Clampfit, download the latest pCLAMP version (**Help / Web Info on Updates**). More information is found in Appendix I.1.

  XtraCell changes some (uncritical) registry settings for Clampfit, such as window size and position, trace selection, and filter settings (see Appendix VI for more details). Should the pCLAMP registry structure be altered, these settings must also be corrected for proper function.

- The use of FinePrint (www.fineprint.com) is recommended. FinePrint is a printer driver that is capable of collecting several print jobs and printing them on one page. In contrast to FinePrint, the multi-page-per-page function featured by many generic printer drivers can typically only collate the pages of one print job.

3 Setup

XtraCell currently does not have a dedicated installer. It is distributed as a ZIP archive. Unpack the archive, retaining the folder structure when prompted. XtraCell is designed as a Microsoft Excel add-in. So it is sufficient to copy the three files **XtraCell.xla**, **XtraCell.hlp** and **XtraCell.cnt** contained in the **..\Program** folder to any location. The program can either be run by executing the XLA file, or it can be implemented into MS Excel

using the Add-In Manager. In this case, the program file must be located in the MS Office Add-In folder. The help files must be located in the same folder as the program file.

The folder **SampleData** contains data files and sample analysis results. Copy the data files and the subfolders to an empty folder. When first started, XtraCell prompts for your working path. Specify this folder there. You can find samples for files that are created as output files in the folder **EvalSamples**, which has a structure identical to the folder **Eval**.

The files **SpontAct.pro** and **Stim50ms.pro**, which are located in the folder **Params**, are similar to the Clampex protocol files the sample data files were acquired with. Acquisition in Clampex is described in sufficient detail in the Clampex 8 manual (Axon Instruments, 1999) and is therefore not treated here.

4 Running XtraCell for the first time

4.1 Operating system and Excel version

When XtraCell is started for the first time, it determines which operating system and MS Office version you run. If you do not receive a warning, you run a combination, under which the program was tested. If you run a combination which has not been tested, XtraCell issues a warning, together with a prognosis on the probability that it will work.

4.2 The decimal separator must be a decimal point for the analysis of pCLAMP data

pCLAMP ignores the Windows Control Panel settings for the decimal separator and puts out all results and measurements with a decimal point. Excel, however, cannot correctly handle this kind of data, if you specified a comma in your **Control Panel / International** settings. Therefore, XtraCell checks for this setting on startup and issues a warning, if the decimal separator is not a decimal point.

You can choose to have XtraCell automatically adjust the settings for you. Both, the decimal separator for numbers and for currency, are set to a decimal point. The thousand separators are set to space characters. Note that these settings affect your entire system. For the new settings to apply, Excel must be restarted, since it reads the **Windows Control Panel** settings at startup only. XtraCell, being an Excel add-in, can automatically quit, but not restart its host application. So you have to restart manually.

Alternatively, you can choose not to start XtraCell and change the settings yourself.

If you do not work with data from a pCLAMP analysis and do not want to change your Control Panel settings, you can disable the check. You can later enable it in the in the **Program Options**.

Note: The message may also mean that you specified a decimal point, but also have a point as thousand separator. This also may confuse Excel – not only in the analysis of physiological data.

4.3 Program options

When run for the first time, XtraCell automatically opens the **Program Options** dialog. You only need to verify the entries on the **Paths** tab at this time. See Appendix IV for more details.

While XtraCell is loaded, the Excel menu contains an additional item named **XtraCell**. This menu item should typically be placed after the built-in **Tools** menu. Not all of XtraCell's menu items are available from diagram sheets.

Fig. 1: The **Program Options** dialog opens the first time XtraCell is run. Only the entries on the Paths tab must be made, if the defaults are not applicable.
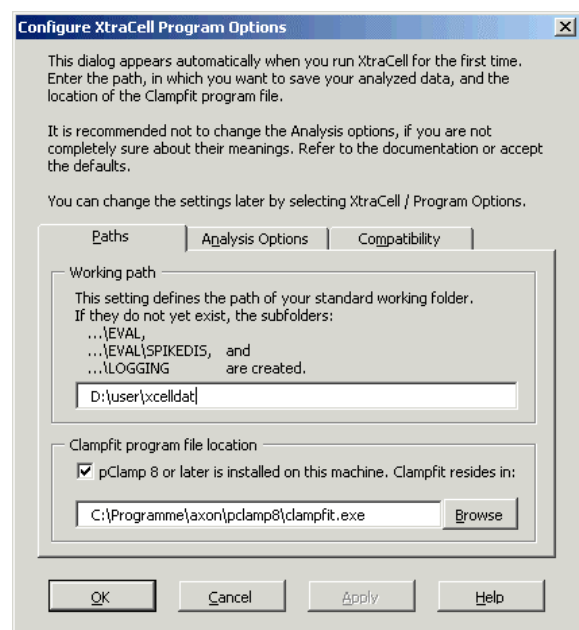
5 Step-by-Step Guide

Although most Clampfit commands are explicitly described in this section, some basic knowledge of handling the program and operating the **Analysis** windows is required to perform the step-by-step guide. Refer to the pCLAMP User's Guide (Axon Instruments, 1999, also available online at www.axon.com), if you are unsure about anything. It may be useful to read, or rather perform, the Clampfit tutorials in chapter 8 of the manual. In two of the scenarios, I described analysis procedures closely related to the procedures introduced here, but with more emphasis on the operation of Clampfit.

5.1 Analysis of the spontaneous activity

5.1.1 Introduction

Pheromone-sensitive trichoid sensilla are spontaneously active (Marion-Poll and Tobin, 1992; Kalinová et al., 2001; Dolzer et al., 2001 (Chapter 1)). In the hawkmoth *Manduca sexta*, two classes of action potentials (APs)[1] can be discerned by their amplitude. The transepithelial potential (TEP), on which the action potentials are superimposed, exhibits slow fluctuations, whose waveform is correlated with the flight activity of the animals. In this section, we are going to analyze spontaneous action potentials, the time course of the TEP, and the flight activity, as monitored by a piezo sensor. These parameters were recorded to a data file of 10 min duration.

5.1.2 The analysis of spontaneous activity using a fixed threshold for action potential sorting

Start Excel and/or open XtraCell. Then start Clampfit and open the sample data file **SpontAct.abf** you find in your **Working Folder**. You might have to **Auto Scale** the signals to obtain an appearance as in Fig. 2. The highpass-filtered signal **AC** was used as the trigger channel to record one sweep for each action potential. **DC augment** is basically the same signal, but without any highpass filtering. The **Piezo** signal reflects the flight
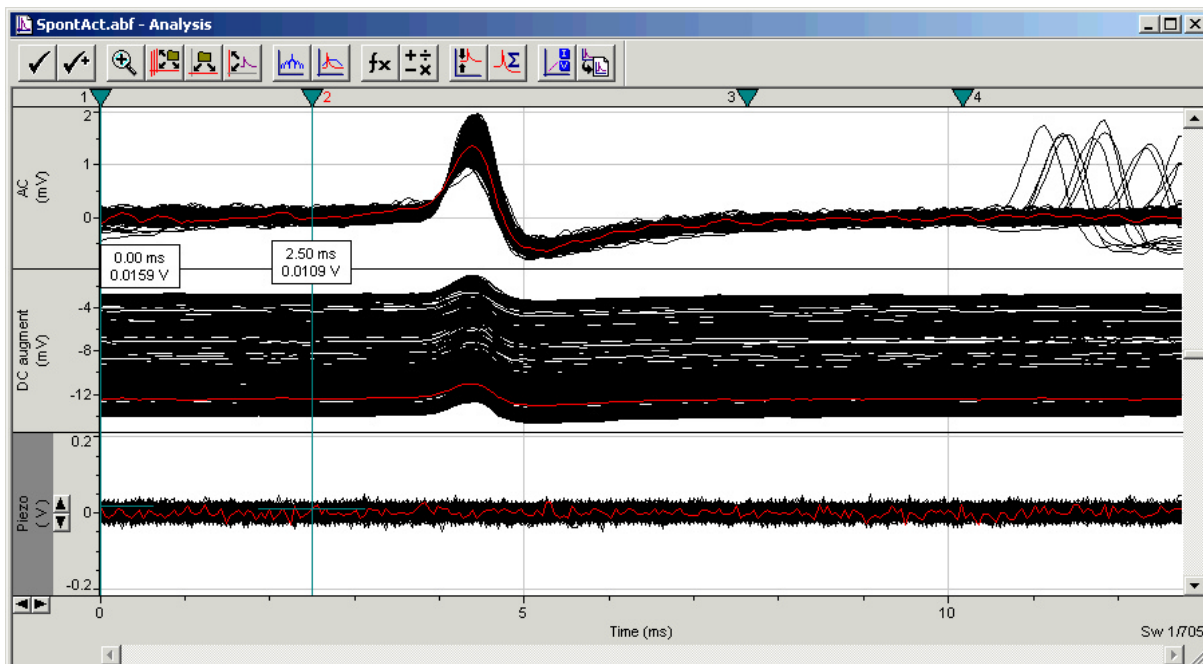

Fig. 2: The sample data file **SpontAct.abf** after rescaling the Y axes. Action potentials are recorded in the signals **AC** (highpass-filtered) and **DC augment**. The **Piezo** signal shows that the animal did not exhibit any flight activity.

activity of the experimental animal. During the 10 min this file was recorded, the animal remained completely silent, however. Maximize Signal **DC augment**, right-click on the X axis and select **Continuous Display** to make the oscillations of the transepithelial potential (TEP) visible (Fig. 3). See Chapter 1 for more details on

---

[1] The terms **action potential** and **spike** are often used as synonyms in electrophysiology. In this chapter, the term action potential (or its abbreviation AP) is used to describe a physiological process within a cell. The term spike more abstractly refers to the waveform in the recorded signal.
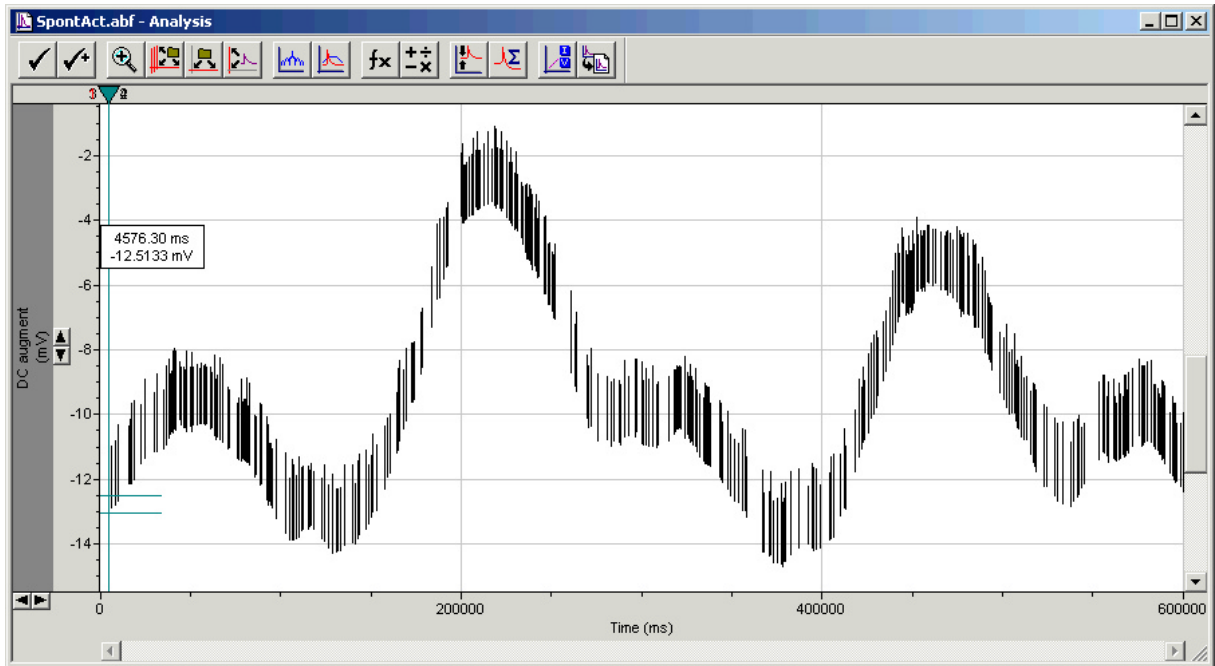
Fig. 3: In continuous display, the DC signal reflects the time course of the transepithelial potential.

these oscillations. **Select File / Page Setup** and set **Printed Windows / Number per page** to **1**. Go to the **Layout** tab and set the **Orientation** to **Landscape**. Now print the file. It is recommended to use FinePrint, a printer driver that is capable of collecting several print jobs and printing them on one page. We will create 4 prints for every data file, which are most conveniently viewed on a single page.

After printing, set the **Display** back to **Sweeps**. Set cursor 1 to the beginning of the sweeps (0 ms) and cursor 2 to 2.5 ms, so they include the baseline region. Double-clicking on the cursors allows you to specify their position numerically. **Tile** the **Signals**, make sure **DC augment** is the active signal, and select **Analyze / Statistics**. Specify a **Positive Peak polarity**, set the **Region to search** to **Cursors 1..2**, the **Trace Selection** to **Active signal, All visible traces**, and select the **Destination Option Replace results in sheet**. Upon OK, Clampfit puts the statistics of the baseline region out to the **Results** window. The only interesting parameter of
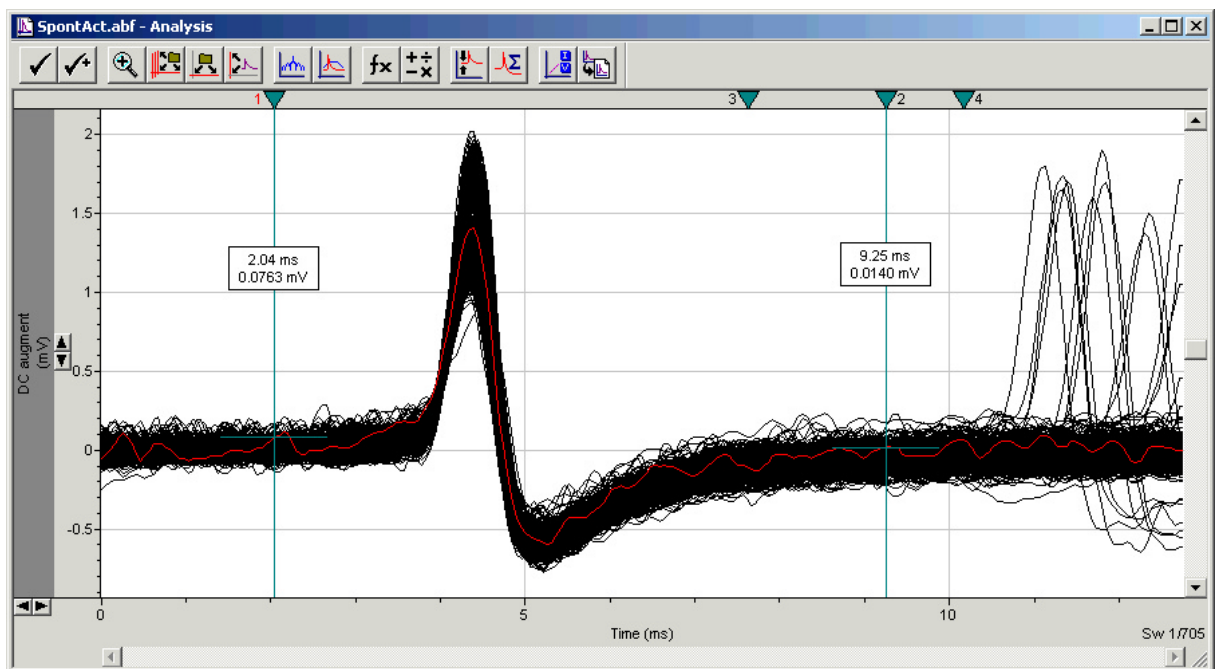

Fig. 4: After adjusting the baseline, the spikes in the signal **DC augment** are superimposed. The cursors delimit the region to analyze for the spike statistics.

the baseline region is the **Mean**, which reflects the time course of the TEP. So select this column in the **Results** window by clicking on its header and copy it to the clipboard. Change to Excel and create a new workbook, if not already present. Activate **Sheet2,** paste the clipboard contents into cell **A1** and return to Clampfit. Activate the **Piezo** signal and perform **Analyze / Statistics** with the same settings as before to determine the statistics of this signal. Copy the **Mean** column to cell **B1** in the Excel worksheet and enter "Piezo" into cell **B1**.

To remove the baseline offset from the APs, return to Clampfit, Maximize signal **DC augment** and select **Analyze / Adjust / Baseline**. Select the **Method Subtract mean of Cursor 1..2**. The **Trace Selection** should still be **Active signal, All visible traces**. Auto scale the signal after baseline adjustment is complete (Fig. 4) and print the window.

Set cursors 1 and 2 so that they include the action potentials that triggered the sweeps, but exclude the subsequent action potentials at the end of the sweeps (Fig. 4). If you do not see the subsequent action potentials, refer to Appendix I. Perform **Analyze / Statistics** once more, again with all settings as before. Activate the **Results** window, select the column **Anti-Peak (ms)** and go to **Edit / Insert / Columns**. To compute the peak-to-peak amplitudes in the newly created column, select **Analyze / Column Arithmetic** and apply the expression **cK = cH-cJ** to the **Full column**. Rename column **K** to "Peak-Peak" and save the **Results** window as **SpontAct.rlt**. With the **Peak-Peak** column selected, click the **Y+** button, select the column **Trace Start** and Click **X**. These
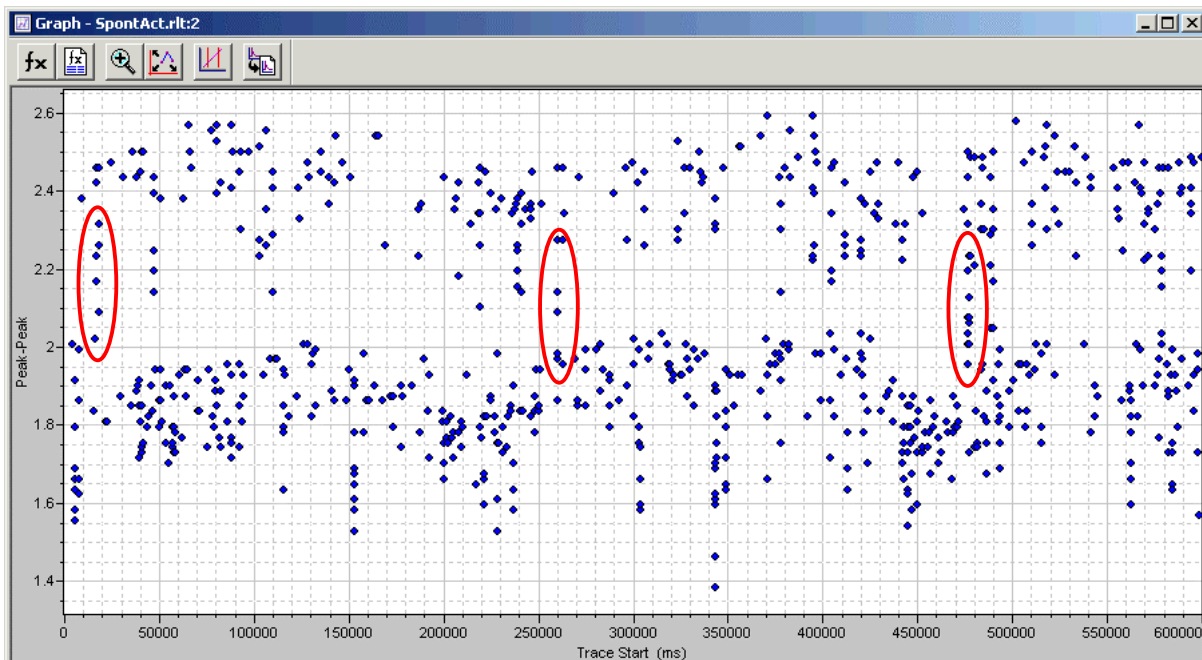

Fig. 5: Scatter plot of the action potential amplitudes over time. Two classes of amplitudes can be distinguished. During bursts, however, the amplitudes of large action potentials are reduced so far that they reach into the amplitude band of the small action potentials (marked by ellipses).

commands define the specified columns as the sources for a plot that you now can create by selecting **Analyze / Create Graph**. Unless a different Graph Window is open, the default template is a **Line** graph. Customize the graph by double-clicking on it: select **Scatter** and, on the **General** tab, disable **Major** and **Minor title** and **Legend** to end up in an appearance similar to Fig. 5. Select **File / Page Setup**, set the **Aspect Ratio** to **Fit to page** and the orientation (**Layout** tab) to **Landscape** and print the graph. If you experience any printing problems, refer to Appendix I.

In our example, two bands of amplitudes are evident. The lower band ranges from 1.33 mV to about 2.05 mV, the upper band reaches up to 2.6 mV. So the threshold for spike sorting should be 2.1 mV. However, at least at the three places highlighted in the figure, the amplitude of the large action potentials is reduced so far during a burst, as indicated by a sequence of data points with decreasing amplitude, that it crosses the threshold. So the temporal context must be taken into account for spike sorting. Were the spikes sorted with a simple threshold-based algorithm, all those large APs within a burst that cross the threshold would incorrectly be classified as small ones.

A more classical way to determine the threshold for spike sorting is a frequency distribution histogram. It is recommended to consider both, the scatter plot and the histogram, to determine the threshold. With the **Peak-Peak** column selected, go to **Analyze / Basic Statistics.** Of the **Statistics Options** that are available in this function, only the **Number per category** is relevant for this type of analysis. Select **Perform Breakdown**
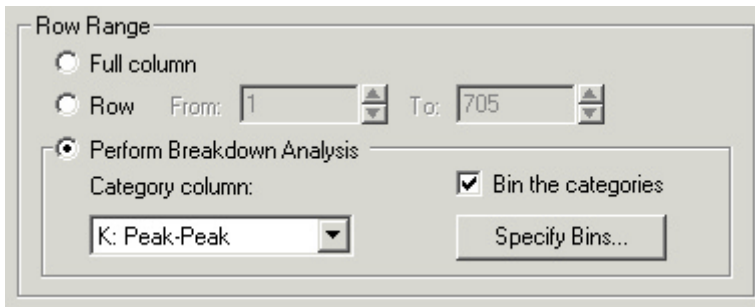
Fig. 6: Settings for the **Basic Statistics** of the peak-to-peak amplitude.

Analysis, highlight **Peak-Peak** in the **Category column** drop-down, check **Bin the categories**, and press **Specify Bins**. A dialog comes up, allowing to specify bins of user-defined or fixed size. To cover the entire range of the occurring peak-to-peak amplitudes, select **Fixed bin size** and specify 30 bins with the **Initial Value** 1.3 mV and a **Width** of 0.05 mV.

Clampfit puts the statistics out on the **Basic Stats** sheet in the **Results** window. Select the **Bin center** column first and press the **X** toolbutton to make it the X-column, which is reported in the column header. Then select the **#/Cat-Peak-Peak** column and press the **Y+** button.

Now **Create** another **Graph**, set the **Plot Type** to **Histogram** and the **Line Thickness** to **5**. On the **Y-Axis** tab, enter 0 in the **Bottom limit** field. After **OK**, the plot should look similar to the histogram in Fig. 6. Like the scatter plot, the histogram reveals a minimum in the amplitude frequency between its two peaks in the bin that ranges from 2.05 to 2.10 mV. Make sure that **Fit to page** and **Landscape** orientation in the **Page Setup** apply to this Graph window, too[2], and print the graph. The histogram is our fourth print. If you experience any printing problems, refer to Appendix I.
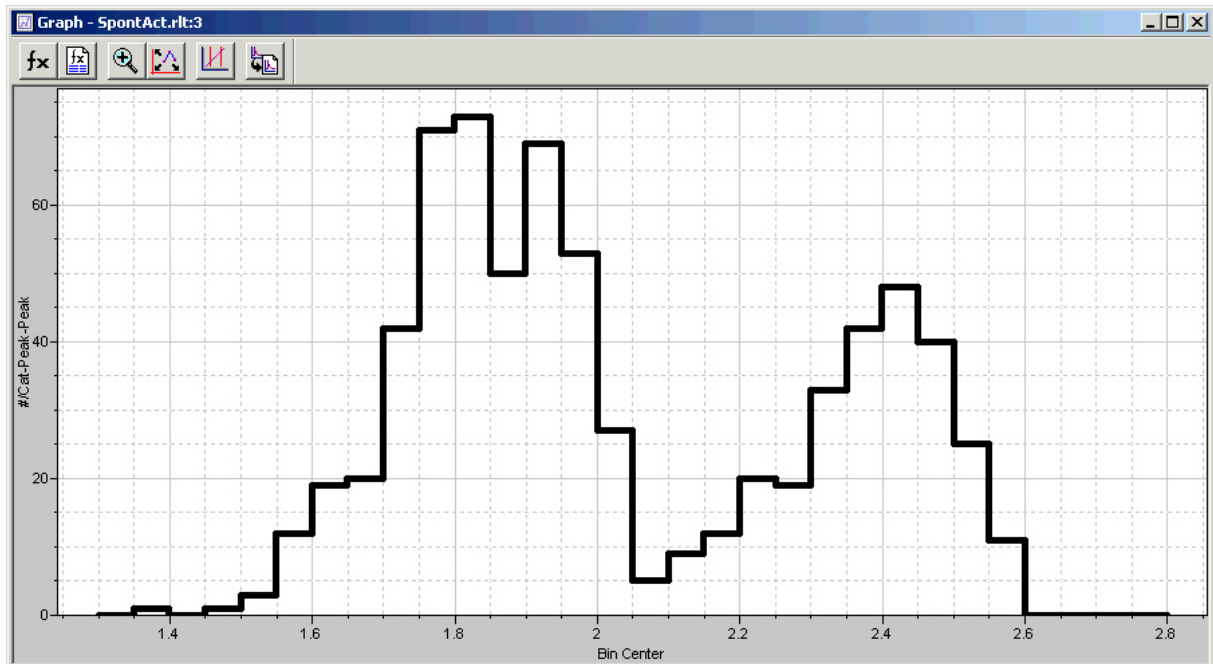

Fig. 7: Like the scatter plot (Fig. 5), the frequency distribution of the action potential amplitudes suggests a sorting threshold of 2.1 mV.

If you use FinePrint, activate this application now. Go to the **Jobs** tab and drag the first job to the last position. If **Ordering** on the **Layout** tab is set to **Across**, the prints are arranged in a way that allows to compare the time course of AP amplitude fluctuations and the TEP (Fig. 8). Even if the time axes of the two plots are not perfectly aligned, this is an efficient way to create a print for archiving.

After printing, return to Clampfit, save the results once more, activate the **Statistics** sheet, **Edit / Select All** and copy the selection to the clipboard. Paste the clipboard contents into cell **A1** on **Sheet1** of the Excel workbook that was previously created, and select **XtraCell / SpontAct / Integrate DC Measurements**. This procedure first checks, whether the number of rows is identical in **Sheet1** and the first two columns on **Sheet2**. If not, it issues a warning. Then both columns on **Sheet2** are moved to columns **L** and **M** on the first worksheet. These two columns originally contained the **Mean** and the **Standard Deviation** between the cursors, two parameters that do not provide useful information about pulse-type signals like our APs. Finally, all but the first sheet are deleted. Therefore: **Do not place any important data on other worksheets!**

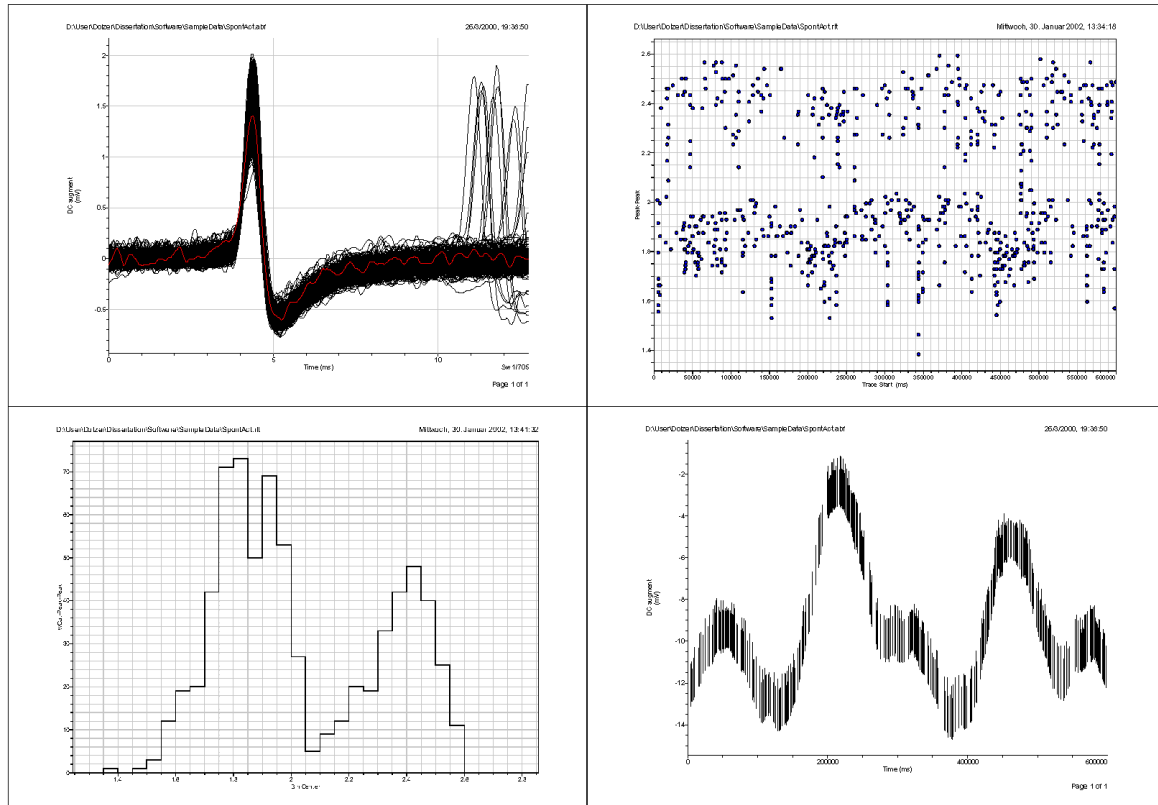[2] In some Clampfit versions this setting was set back.

Fig. 8: For archiving purposes, it is most convenient to print individual analysis steps of each file together on a single page. This page was created using FinePrint, as described in the text. If the first print, the **DC augment** signal in **Continuos Display**, is moved to the last place in the Fine Print **Jobs** list, it appears on bottom right in the print. This is a simple way to determine, whether there is a correlation between AP amplitude fluctuations and the TEP. The outline of the histogram (bottom left) does not have a constant line width due to compatibility limitations between Clampfit and FinePrint. When the **Line Thickness** is set to 5, it is possible to work with, however.

Then the same procedure starts, as if you select **XtraCell / SpontAct / Spike Times from / Clampfit 8 Results**. XtraCell first checks for the following:

The Signal name in column **B** must be similar to '**DC**',
The header of column **K** must be similar to '**peak-peak**'.

If this is not the case, you are prompted to confirm that you are actually going to analyze the data set you intended. The contents of these cells are not crucial for correct results, however. XtraCell rearranges a few columns (which has historical reasons), and adds together the **Trace Start** time and the **Peak** time to yield the **Spike Time**, which is put out in column **A**. Then the program computes the interspike intervals (ISIs) in column **H**.

Finally the workbook is saved as **[DataFileName].xls**. The data file name is taken from cell **B2**, the extension (.abf) is removed. After the ISIs are computed, XtraCell tells you, how many spikes were found, and prompts you whether to continue. If you select **Yes**, XtraCell calculates the statistics of the burst behavior and computes the inter-event intervals. When prompted whether to proceed with Spike Sorting, click **Quit and Save** for now to review what has been computed so far.

5.1.2.1 Burst Statistics

The burst statistics are put out in a table on the sheet named '**# Spikes**' (Fig. 9). The first column contains the number of spikes in each burst. The next three columns hold the frequency at which the bursts occurred in the data set. In column **B** only bursts with an ISI up to 25 ms are considered, while in column **C** ISIs between 25 ms and the **Burst Criterion** are considered. You can adjust the setting for the **Burst Criterion** in the **Program Options**. The burst statistics between the **Minimal ISI**, as defined in the **Program Options**, and the **Burst Criterion** are put out in column **D**. Columns **E** and **F** contain the absolute number of spikes in each burst category and their percentage of the total spikes, respectively.

	A	B	C	D	E	F
1	# Spikes	1.5..25 ms	25..50 ms	Sum	# Spikes	% of Total
2	per Burst	(40..667 Hz)	(20..40 Hz)			
3	1			347	347	49.2
4	2	34	19	53	106	15.0
5	3	17	5	22	66	9.4
6	4	14	5	19	76	10.8
7	5	3	1	4	20	2.8
8	6	6	2	8	48	6.8
9	7	2		2	14	2.0
10	8	1		1	8	1.1
11	9		1	1	9	1.3
12	10					
13	11	1		1	11	1.6
14	Bursts	78	33	111		
15	BurstSpikes	259	99	358	358	50.8
16	Events			458		
17	TotalSpikes			705	705	100.0
18			Avg. # Spikes			
19	Overall Freq. / Hz	per Burst	per Event			% BurstEvents
20	1.17508542		3.22522523	1.53930131		24.2
21						
22			Mean ISI	ISI SD	ISI CV	
23			845.707741	1247.54314	1.47514688	
24						
25			Mean IEI	IEI SD	IEI CV	
26			1302.79702	1355.00445	1.04007334	

Fig. 9: The burst statistics are put out on the sheet **# Spikes**. The structure of the table is explained in the text. The number of rows in the table is automatically adapted to the burst with the highest number of members.
Freq.: frequency, Avg.: average, ISI: interspike interval, SD: standard deviation, CV: coefficient of variation, IEI: inter-event interval.

Below the burst with the largest number of members, the number of bursts is computed. Again, there are the three ISI categories, Minimal ISI - 25 ms, 25 ms - Burst Criterion, and Minimal ISI - Burst Criterion (**Sum**). In the next row, the numbers of burst spikes are recorded in both the time windows. The total number of burst spikes is put out twice: Once the number of spikes XtraCell has determined while processing the data set, and as a formula summing up the entries in the **# Spikes** column. This double output originally served to monitor the reliability of the algorithms. Should there be discrepancies, the text is formatted in red, indicating that there is something wrong with the data set. The discrepancy should disappear after re-analyzing the data set.

The Total number of spikes, again determined in two different ways, is put out in the last row of the table. The total percentage should equal 100, of course.

Below the table, the general statistics of the data set are computed: The Overall Frequency, from the beginning of the file (t = 0) to the last spike, the average number of Spikes per **Burst** and per **Event**, and the percentage of the events that are bursts (**% BurstEvents**). An **Event** is defined as either a single non-burst spike or a burst. This definition bases on the assumption that spontaneous action potentials in insect sensilla might be caused by brief – maybe elementary – depolarizations of the receptor neurons. Depending on the duration of the depolarization, they might cause a single spike or a burst (Kaissling, 1994). Finally, this sheet contains the Means, standard deviations (SD) and coefficients of variation (CV) of interspike (ISI) and inter-event intervals (IEI). In a sequence, in which each event is independent of preceding events – i.e., in a Poisson process – the coefficient of variation (CV = SD / mean) equals 1 (Rospars et al., 1994). Therefore, a CV considerably higher than 1 indicates that the events are not random. The IEI statistics are a reference to the **IEI** sheet (see below).

Burst List

The sheet **BurstList** contains a list of all occurring bursts and the inter-burst intervals (IBI). The IBIs are computed between bursts of at least 2, 3, 4 and 5 spikes in individual columns, respectively.

Inter-Event Intervals (IEI)

The event statistics are put out on the sheet named **IEI**. The first two columns contain the times of the **Event Start** and **Event End**, which are identical if the respective event is a single spike. The column **NumSpikes** holds the number of spikes in the respective events, while the **Start-to-Start**- and **End-to-Start** inter-event intervals are put out in the next two columns. Only the **Start-to-Start** IEIs are used to determine the **Mean** IEI, the standard deviation (**SD**) and the coefficient of variation (**CV**).

After computing the Burst Statistics for the total spikes, XtraCell prompted whether to continue with spike sorting. If neither the scatter plot, nor the amplitude distribution histogram revealed two classes of action potentials, select **Quit** or **Save and Quit** and continue with **XtraCell / SpontAct / Summary**. If the plots indicate that the spikes can be sorted, you will typically select **Continue**, however. We interrupted the analysis to review the results. So select **XtraCell / SortSpikes**.

5.1.2.2 Sorting spikes

XtraCell sorts action potentials according to their **peak-to-peak amplitude** as long as the preceding interspike interval (ISI) exceeds the **Burst Criterion**. If the subsequent spike occurs within the **Burst Criterion**, it is classified as being of the same type, irrespectively of its amplitude. This accounts for the amplitude reduction during bursts.

Threshold

The threshold between small and large spikes can be entered numerically or selected with the spinner. This value is used throughout the processed file.

Floating Threshold

If the scatter plot indicates that the threshold does not remain constant throughout the analyzed file, select **Floating Threshold**. This feature is explained in detail in Section 5.1.3.

Restricted Amplitude Reduction

If this option is checked, the spike sorting algorithm only allows an amplitude reduction by the specified percentage of the amplitude of the preceding spike. If a spike occurs within the **Burst Criterion** after a large spike of e.g. 2 mV, it is considered large while this option is unchecked, no matter how high its amplitude. If the **Amplitude Reduction** feature is being applied at the default setting of **25%**, however, only spikes with an amplitude of at least 1.5 mV are classified as large, otherwise they are

Fig. 10: The **Spike Sorting** dialog.

recorded as small ones. This feature has proven to enhance the performance of the sorting algorithm, when the difference between the amplitudes of the two spike classes is rather large, i.e., if the amplitudes do hardly or not at all overlap.

Duration of the Data File

Here you can specify the duration, during which the spontaneous activity was recorded to the file that is currently processed. This setting only affects the X axis scaling of the **Sorting Results**- or **Floating Threshold** plots, respectively. There is no impact on the performance of the sorting algorithm.

5.1.2.3 Sorting Results

XtraCell distributes the action potentials onto two sheets named **SmallSpikes** and **LargeSpikes**. The sorting progress is displayed in the status bar at the bottom edge of the Excel application window. When sorting is complete, a graph sheet named **Sorting Results** is created to visualize the results (Fig. 11). The spikes classified as large and small are plotted in different colors to allow judging the quality of sorting. In addition, possible sorting errors (see below) are marked with circles.
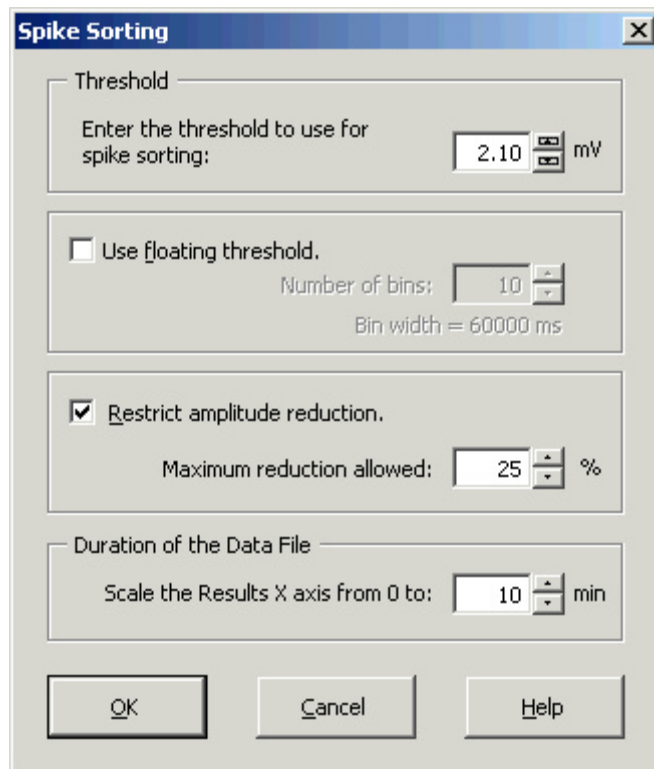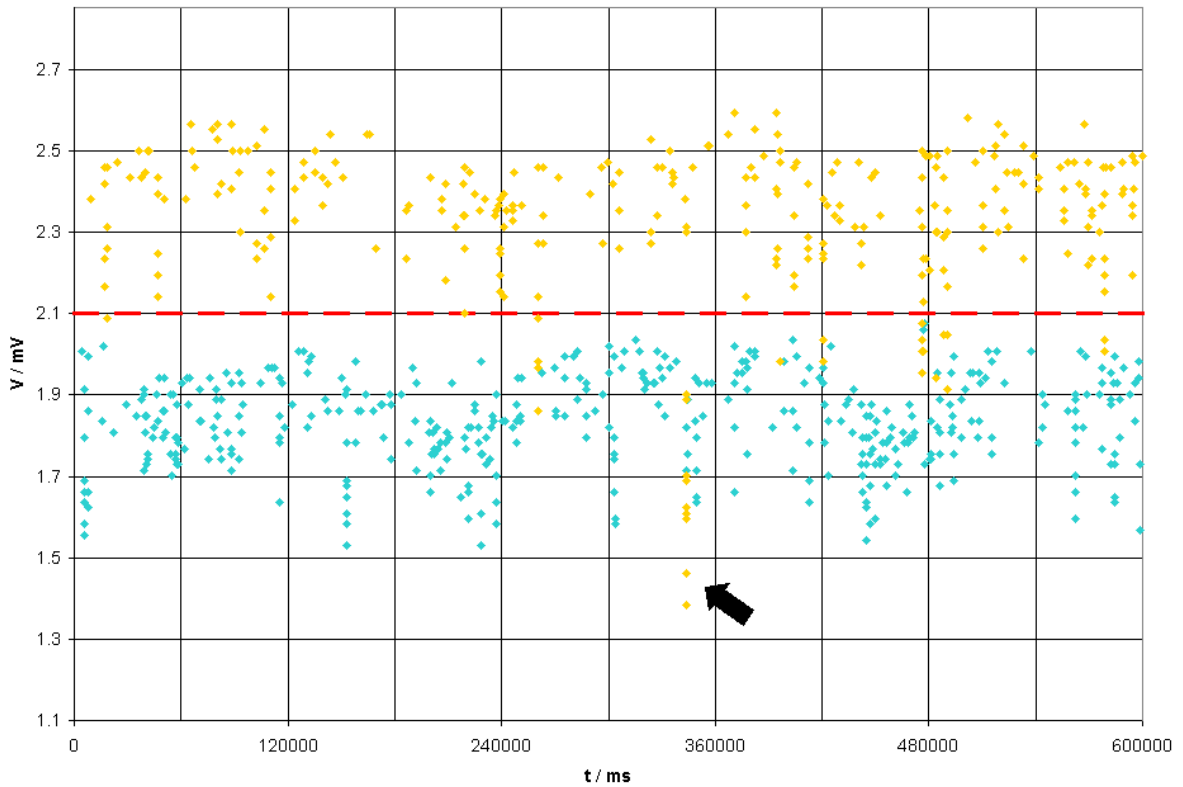
Fig. 11: The Sorting Results are visualized in an Excel diagram. The action potentials classified as large and small are plotted in different colors. The dashed line indicates the sorting threshold. The arrow denotes a sequence of spikes that were potentially misclassified and should be reviewed in the data file (Fig. 12).

5.1.2.4 Sorting Errors

Two kinds of potential sorting errors are recorded on the **Error Sheet** and visualized on the **Sorting Results**- or **Floating Threshold** plots, respectively:

Interspike intervals shorter than the **Minimal ISI** specified in the **Program Options**. If the ISI is too short, sorting based on the amplitude is not applicable anymore. These events should be reviewed in the original data file.

A large spike between two small ones. If a single large spike occurs within a burst of small ones, the large spike is correctly recognized, but all subsequent small spikes might be misclassified as large (Fig. 16). The same is true, if bursts of both spike types coincide. The row number of the first potentially misclassified spike is put out on the **Error Sheet**. Refer to Appendix III for more details on the **Error Sheet**.

One of the bursts assigned to the large action potentials is reduced conspicuously far in amplitude (Fig. 11). In cases like this, it is necessary to review the original data file to properly classify the spikes. So click **Save and Quit**. Determine the time this burst occurred by holding the mouse cursor over one of the data points in the **Sorting Results** plot. After a short delay, Excel reports the coordinates of the data point (cf. Fig. 15). Activate Clampfit, right-click on the time axis, select **Continuous Display**, and zoom the region around 343500 ms (Fig. 12). One might argue, whether this sequence of action potentials is a burst of large spikes, or rather three large spikes followed by a burst of small ones. Typically, the amplitude reduction during a burst is relatively continuous (Chapter 1, Fig. 4C). In the questionable sequence, there is a step in the enveloping curve of the positive peaks, however. This favors the interpretation that, by coincidence, a burst of small spikes occurred within the **Burst Criterion** (50 ms) after the three large spikes.

The amplitude reduction during bursts is not very prominent in the sample file. Convince yourself of this fact by viewing a few other bursts in **Continuous Display**. Therefore, reducing the allowed percentage in the
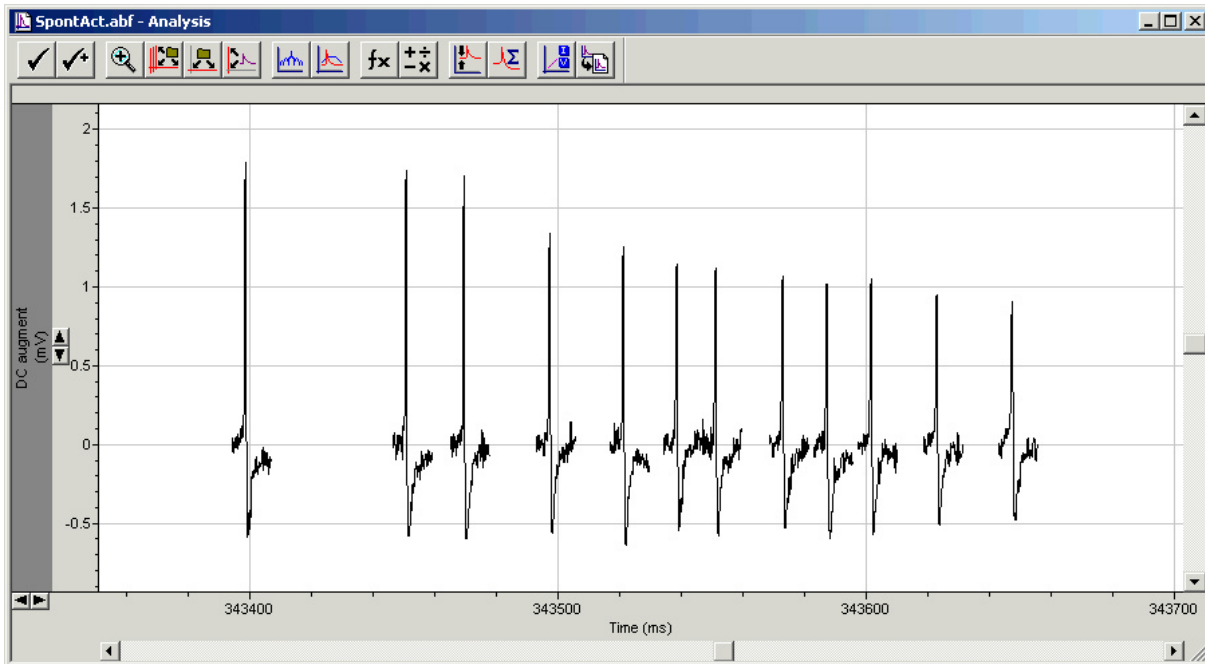

Fig. 12: Three large action potentials followed by a burst of small ones. Depending on the setting of the **Restricted Amplitude Reduction**, this sequence may lead to a misclassification of the small action potentials.

Restricted Amplitude Reduction avoids this misclassification. Activate one of the spreadsheets and select **XtraCell / SpontAct / Sort Spikes** (this menu item is disabled when selected from a diagram sheet). XtraCell recognizes that the spikes have already been sorted and issues a warning that all sheets concerned with small and large spikes are deleted before re-sorting. **Note**: This action cannot be undone. Once deleted, all changes you did on these sheets manually are lost. In the **Spike Sorting** dialog, set the **Maximum reduction allowed** to 15%. Now the small spikes are correctly classified.

   Note: In *M. sexta*, the degree of the amplitude reduction varies from one recording to the other. The default value of **25%** is a reasonable compromise to start with, which only occasionally requires adjustment. The sample file was chosen to demonstrate what to do in one of these rare cases.

   If you quitted after sorting, activate one of the sheets **SmallSpikes** or **LargeSpikes** and select **XtraCell / SpontAct / Spike Times from / Other List** to perform the same analysis that has been done for the total spikes on each of the spike classes. To make sure no empty row is left in the spike list, you are taken to what is interpreted as the last spike in the list and prompted to confirm the correct selection (see Appendix II.1.1.3 for more details). If you selected **Continue** after sorting, however, the analysis proceeds with the correct parameters automatically. XtraCell prompts whether to continue after each spike class. In the end, a **Summary** sheet is created, on which the most important parameters are summarized (Fig. 13).

5.1.3 The Summary sheet

   On the **Summary** sheet, XtraCell puts out the statistics of the analyzed data file. The total numbers of Spikes, Bursts, and Events are recorded in the first three rows (Fig. 13). The **Threshold** row is only relevant, when the spikes were sorted. If the evaluation was done without any interruption, XtraCell automatically enters the correct **Threshold** value. However, if the evaluation was interrupted after sorting, e.g. to check for possible errors, XtraCell prompts for the threshold that was used for sorting. Unless you sorted another list with a different threshold, the default value is the threshold you used. The **Threshold** prompt also has a **Floating Threshold** checkbox, which will be explained in the next section. Quite similarly, when an existing **Summary** sheet is to be replaced, XtraCell takes the threshold from this source, if possible. Only if the existing **Summary** sheet does not have a **Threshold** entry, you are prompted to specify it.

	A	B	C	D
1	spontact	Sum	Small	Large
2	# Spikes	705	429	276
3	# Bursts	111	61	48
4	# Events	458	300	168
5	Threshold / mV	2.10		
6	Overall Freq / Hz	1.175	0.717	0.460
7	% in Bursts	50.8	44.3	56.5
8	% Bursts/Events	24.2	20.3	28.6
9	Avg. #Spikes/Burst	3.23	3.11	3.25
10	Avg. #Spikes/Event	1.54	1.43	1.64
11	Avg. ISI / ms	846	1387	2147
12	ISI SD / ms	1248	2016	3432
13	ISI CV	1.48	1.45	1.60
14	Avg. IEI / ms	1303	1985	3536
15	IEI SD / ms	1355	2163	3818
16	IEI CV	1.04	1.09	1.08
17	Burst Criterion / ms	50	50	50

The sixth row contains the Overall Frequency, computed from t = 0 to the time when the last spike occurred. Rows 7 and 8 hold the percentage of the spikes that were members of bursts and the percentage of the events that were bursts, respectively. The average numbers of spikes in each burst and each event are put out in the subsequent two rows. The Rows 11–13 contain the mean interspike interval (ISI), the standard deviation of the ISIs, and the coefficient of variation, followed by the same parameters computed for the inter-event intervals (IEIs). In the last row, the burst criterion used for the evaluation is recorded. When the spikes were sorted, each of the parameters is computed for the total spikes and both spike classes and put out in separate columns.

Fig. 13: In the **Summary** sheet, the analyses of the total, the small and the large spikes are presented in three columns. If the spikes could not be sorted, the columns **Small** and **Large** are absent.

When neither the scatter plot, nor the histogram you created in Clampfit reveal two amplitude classes, the action potentials cannot be sorted. In this case, quit the analysis when prompted whether to continue with spike sorting and select **XtraCell / SpontAct / Summary**. If the spikes were not sorted, the **Summary** sheet only contains the column for the total spikes.

Note that all result cells but the threshold and the burst criterion contain formulas referring to other sheets. So if you want to consolidate the **Summary** sheets of several data files in a different Excel workbook, make sure you paste the **Contents / Values** only to avoid external links. The XtraCell code contains a procedure that is capable of consolidating **Summary** sheets of different files in one Excel workbook. This procedure is currently not fully implemented, however.

5.1.4 Floating Threshold

In some recordings, the scatter plot indicates that the threshold does not remain constant throughout a data file. This does not allow the use of a constant threshold, but requires that the threshold varies over time. The second data file, which we are going to analyze in this part of the step-by-step guide, demands the use of this feature. In addition, the file provides a few more pitfalls that cannot reliably be processed automatically and must be corrected manually.

Open the sample file **SpontAct2.abf**. In this file, the animal exhibited some flight activity, as can be seen by the non-zero **Piezo** trace. One sweep, #419, was quite obviously triggered by an artifact. Select this sweep by clicking on it and hide it by hitting the <Del> key. Exclude the sweep from the analysis by doing the rest of the analysis on the **Visible Traces** only. Due to a bug in Clampfit 8, the results files (*.rlt) grow enormously large, if new Results simply overwrite existing ones. Therefore, with the Results window active, select **Edit / Clear All Sheets** before proceeding. You could alternatively select **File / New / Results**, but this would destroy the Graph windows, which we still need.

Now repeat the analysis steps described in the previous section. **Important Note**: If the APs at the end of the sweeps (cf. Fig. 4) disappear after baseline adjustment, please read Appendix I. The most convenient positions to place the cursors after baseline adjustment are 3.7 and 7.7 ms this time. In this way, they include only those action potentials that triggered the sweeps, except for the second AP in sweeps #186 and #381, respectively. We will encounter them again later. After you have computed the peak-to-peak amplitudes, activate the scatter plot you created during the analysis of the first data file. The plot is updated to the new results and already suggests that sorting with a fixed threshold might not be applicable on this file. The fluctuating amplitudes are presumably due to slow oscillations of the resistance of insect sensilla (Zack, 1979), which are sometimes reflected by the amplitudes of the action potentials. If you compare the amplitude fluctuations to the time course of the TEP, as can be seen on the print of the DC signal in **Continuous Display**, you will find that TEP and action potential amplitudes are negatively correlated. this is also the case in the first data file, even if less prominent (Fig. 8).

The histogram, in contrast to the scatter plot, is not updated, since we only changed the values on the **Statistics** sheet. So perform **Analyze / Basic Stats** again, with 36 bins starting at 1.0 mV this time, save the Results and send the print jobs you collected in FinePrint to the printer.
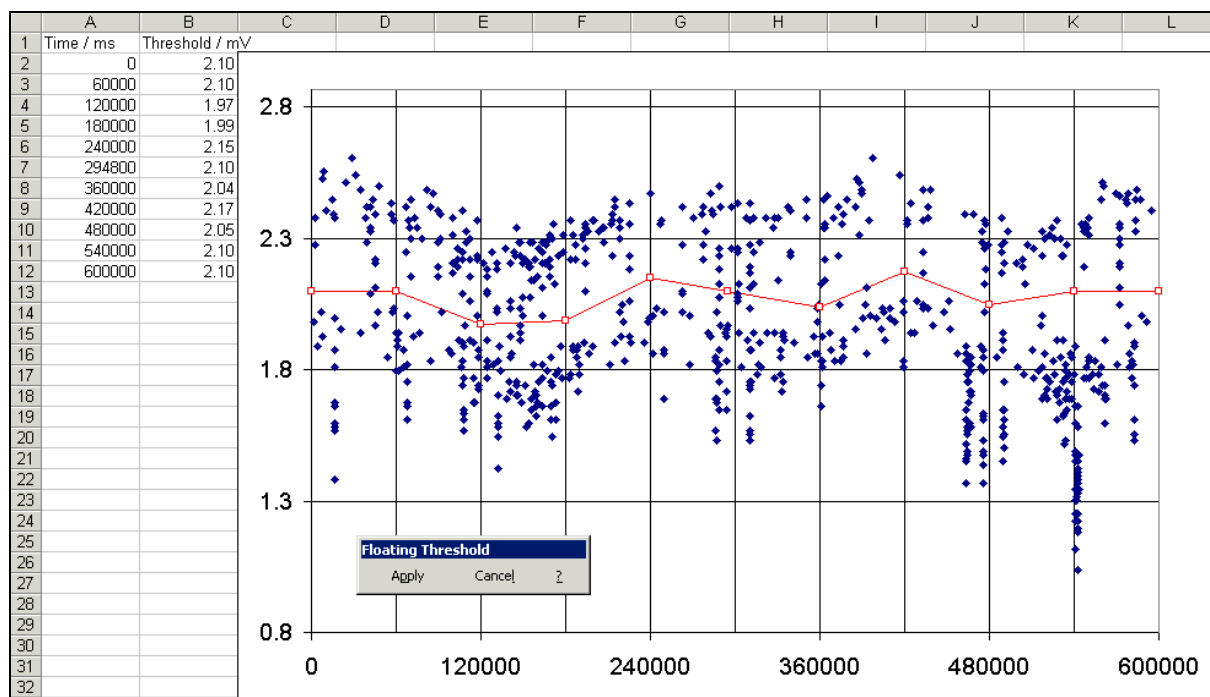

Fig. 14: When the Floating Threshold feature is enabled, XtraCell creates a scatter plot that allows defining the time course of the threshold either graphically or numerically.

After selecting **XtraCell / SpontAct / Integrate DC Measurements**, a new sheet named **Errors** is created and the program issues a warning. Refer to Appendix III for the possible errors recorded on this sheet. The entry on the **Error** sheet points to row 188 on the **SpikeTimes** sheet. The **Trace** column entry in this row indicates that the error is in sweep #187, the sweep after one of those with a second AP in the analyzed region. XtraCell validates the interspike intervals (ISIs) between every two successive spikes and alerts the user whenever an ISI is shorter than the **Minimal ISI** specified in the **Program Options**. Here, this means that both olfactory receptor neurons fired APs almost simultaneously. So we will have to deal with that after spike sorting. Since the warning was issued after the columns have been re-arranged, continue the analysis with the command **XtraCell / SpontAct / Spike Times from / Other List**. Select **Continue** when prompted whether to proceed with spike sorting. In the **Spike Sorting** dialog, activate **Floating Threshold** this time. XtraCell creates a scatter plot similar to the one in Clampfit, but including a colored line plot as the threshold marker.

You can specify the floating threshold by dragging the threshold line to shape. Unfortunately, Excel is a little tricky in this respect[3]. Click on any of the points on the threshold line. This selects the entire line plot. Then click on the point you want to move a second time (**do not double-click!**). In this way, the individual data point is selected. Now you can drag it in X- or Y-direction, but only one direction at a time. Alternatively, you can enter the desired values numerically in columns **A** and **B** on the worksheet.

If there are too many or too few dragging points, click Cancel on the **Floating Threshold** toolbar. Then select **Sort Spikes** again and adjust the **Number of bins** setting accordingly. If the threshold line matches your ideas, click **Apply**.

XtraCell sorts the spikes and, like with a fixed threshold visualizes the results by giving the individual classes different colors (Fig. 15). If analysis errors occurred, spikes recorded on the **Error Sheet** are marked with circles. In the example, it is the action potential in sweep #187 again. So select **Save and Quit** when prompted whether to continue.

Activate the **Error Sheet** to find that the questionable action potential is recorded in row 111 on the sheet **LargeSpikes**. In this row, the sweep number is found in the **Trace** column again, in case you want to review the original data in Clampfit. If you do so, you will find that only one pair of double spikes is recognized. The second action potential in sweep #381 occurred so early in the repolarizing phase of the previous AP that the voltage did not fall under the trigger threshold level of 0.52 mV (select **File / Properties** to obtain information

---

[3] This description applies to Excel 95 and 97. Later versions might behave somewhat different.
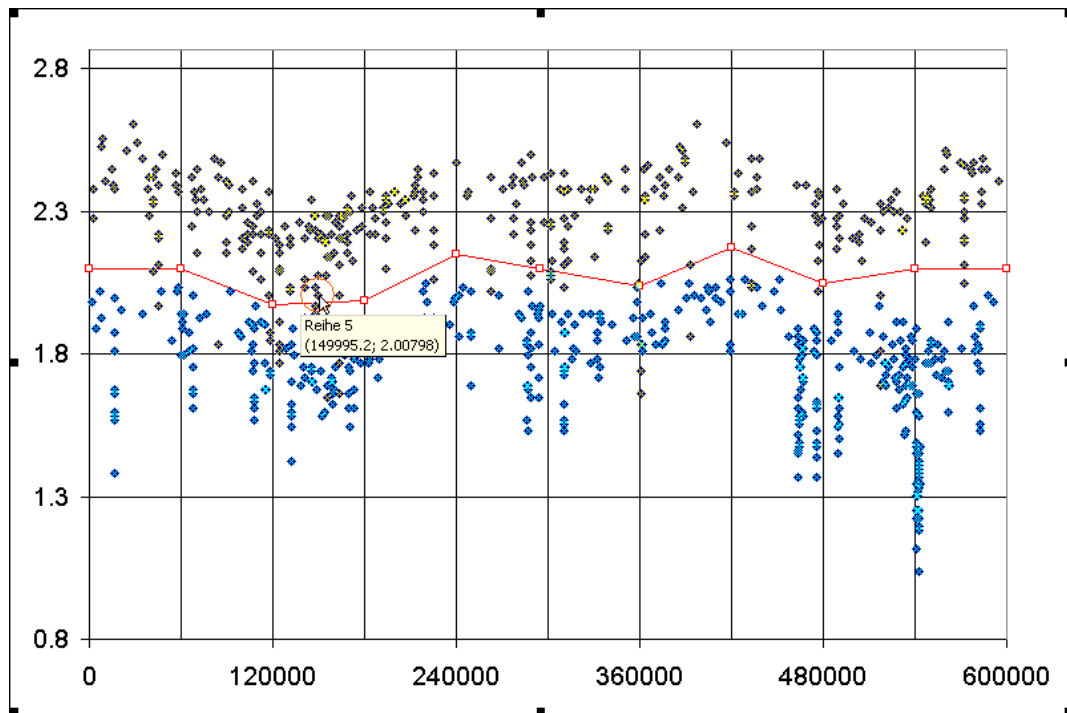
Fig. 15: After sorting with a floating threshold, the two amplitude classes are marked with colors, too. Potential sorting errors are highlighted with red circles. Upon holding the mouse cursor over the potentially erroneous data point, Excel reports its coordinates, allowing to look it up in the list.

about the trigger threshold from a data file). Therefore, the successive action potential did not trigger its own sweep and is lost for the analysis. In a file with more than 700 action potentials a single action potential can be neglected.

If there are less action potentials, you may want to include a spike like this, however. To do this, look for the row the action potential is recorded to on the sheets **SmallSpikes** and **LargeSpikes**. The sweep was triggered by the first action potential, which is a small one according to its positive phase. On the repolarizing phase, the cell that produces the large action potentials fired, in this way generating a large negative phase. Since spike sorting considers the peak-to-peak amplitude, the spike was consequently classified as large. So you find it on the sheet **LargeSpikes**, in row 217[4]. Select the entire row by clicking on its header and copy it to the clipboard. Go to the sheet **SmallSpikes**, look up the row with the next sweep after 381 (row 167), right-click on the column header and select **Insert Copied Cells**. Now you have to correct a few parameters. The time the action potential occurred is correct, since it corresponds to the absolute maximum in the analyzed region. The peak-to-peak amplitude of the small AP cannot be determined. But a small action potential should not have an amplitude so far above the threshold. Therefore, enter a subthreshold value (e.g. 2.0 mV) into the **Peak-Peak** column. Now note that the amplitude was corrected manually. A good place for this note are the columns **File Name** or **Region**, since they are not used for any other analysis. Take a look at the **ISI** column in row 168 to find that the formula in this cell still refers to row 166. To correct this, select a row well above the inserted one and drag the formula down to at least row 168 with the **AutoFill** handle. Now all formulas should be correct.

Return to the sheet **LargeSpikes.** The amplitude of the large action potential cannot be determined any more precisely either, but is above threshold and therefore does not need any correction. The **Time** needs to be corrected, however. So measure the peak time of the successive AP in Clampfit by placing one of the cursors on the peak. The reading is 5.05 ms, so enter this value into row 167 in the **Peak (ms)** column. The spike time in the first column and the interspike interval are updated automatically. Note your correction in one of the unused columns again. However, now there is an inconsistency in the Excel workbook, since the addition of the numbers of small and large action potentials is different from the number of spikes recorded on the **SpikesTimes** sheet. To remove this inconsistency, duplicate the respective row on the **SpikesTimes** sheet and change the amplitude of the small and the time of the large action potential. To remove the inconsistencies on the other sheets, delete the sheets **# Spikes**, **BurstList** and **IEI** and compute the statistics again (**XtraCell / SpontAct / Spike Times from / Other List**). Of course, you get another warning about an ISI that is too short in row 383. If there is more than one spike to insert manually, it may be more efficient to delete all sheets but **SpikeTimes**, insert the additional spikes only there, and do the sorting again.

---

[4] **Note**: The row numbers given here and below only apply if you specified the threshold exactly as in Fig. 14 (refer to the numerical values on the left). If you used other values, the row numbers may be slightly different.

After sorting, still the incorrectly classified action potential in sweep #187 remains to correct. Sweep #186 was triggered by a small action potential. The positive phase of the action potential that triggered sweep #187 coincided with the declining negative phase of the previous action potential, leading to a large peak-to-peak amplitude that is identical in both sweeps. Consequently, both action potentials were classified as large. So go to row 110 on the sheet **LargeSpikes** (the one that contains the small action potential), select the entire row and cut it to the clipboard. Activate the sheet **SmallSpikes**, look up the sweep after #186 (row 79), right-click on the row header and select **Insert Cut Cells**. Correct the ISIs and the amplitude as before and return to the sheet **LargeSpikes**. Delete the empty row and update the formula in the ISI column accordingly. Delete the **Error** sheet, activate the sheet **FloatingThreshold** and delete the Error marker by selecting it and hitting the <Del> key. Since the total number of action potentials remains unaltered, no inconsistency is introduced this time. So activate on of the sheets **SmallSpikes** or **LargeSpikes** and continue with **XtraCell / SpontAct / Spike Times from / Other List**.

5.1.5 Time course of transepithelial potential and flight activity

To obtain the long-term time course of TEP and flight activity, concatenate the **Mean** and **Piezo** columns from the **SpikeTimes** sheets of several data files acquired successively. The **Time** columns must be corrected for the time that passed since the start of the first data file. You can retrieve the start time of a data file through **File / Properties** in Clampfit. Alternatively, use Clampfit to create a **Data File** index, in which all relevant parameters, including the start times are listed. Note that the long-term time course obtained in this way consists of data points that are not separated by a fixed "sampling interval", but depend on the occurrence of action potentials. If the AP frequency was very low in a recording, this method might insufficiently describe the time course. In these cases, paper strip charts may aid in the reconstruction. Depending on the amplifier used for the recordings, the amplitude of the **DC augment** signal must be corrected for an offset determined during the experiment to yield the TEP. In the sample files, the offset was -34 mV. These last steps of the analysis can be done in any spreadsheet program.

5.1.6 Limitations of the Spike Sorting algorithm

Figure 16 shows two examples for situations that require manual spike classification. One or more large spikes in a burst of small ones are correctly classified as large. However, the sub-threshold spikes that follow after the large one cannot be correctly detected as being small ones. Only if the amplitude difference is rather large, as shown in the figure, applying the **Restricted Amplitude Reduction** feature for sorting (see above) prevents the sorting algorithm from considering the small spikes as large ones with a reduced amplitude during a burst.

These situations are recognized by XtraCell and the first potentially misclassified spike is recorded on the **Error** sheet. They require manual correction. Fortunately, this does not occur frequently in all systems investigated so far.
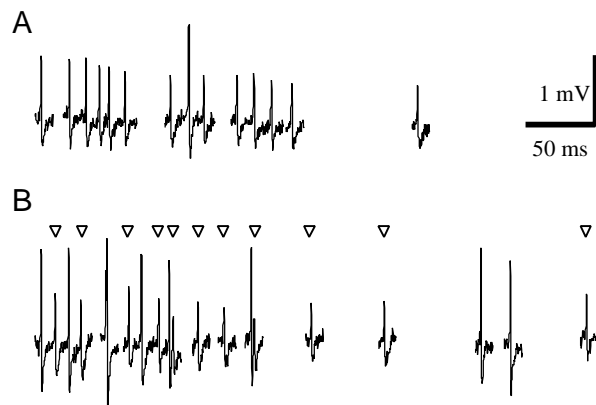

Fig. 16: Limitations of the sorting algorithm. (A) A single large spike within a burst of small ones leads to misclassification of the small spikes after the large one. (B) Both ORNs fired a burst simultaneously. The small spikes (triangles) would be classified as large. Applying the **Restricted Amplitude Reduction** at its default setting of 25% leads to correct results in both examples shown. If the difference in the amplitudes is significantly smaller, this algorithm fails to sort the spikes automatically, however.

5.2 The analysis of pheromone responses

In response to adequate stimulations, insect sensilla produce sensillar potentials, relatively slow, negative deflections of the TEP, and faster action potentials superimposed on them in tip recordings (Thurm, 1972; Kaissling and Thorson, 1980; chapter 2). While the sensillar potentials are generated in the outer dendrite of the olfactory receptor neurons, the action potentials originate from the soma- or axon hillock region, as judged by their opposite polarity. The much slower time course of the sensillar potential (SP), when compared to the action potentials (APs), makes it possible to separate these contributions of different cell compartments to the multi-component signal of a sensillar response from each other.

In this second part of the step-by-step guide, we will evaluate responses of *M. sexta* trichoid sensilla to bombykal, the main component of the conspecific pheromone blend. In the end, all measurements of one recording will be summarized on one Excel sheet named **Overview**. Besides the measurements that characterize the response, this sheet will also contain the stimulus parameters and the history, i.e., information about the preceding stimulus, of every stimulus applied (see 5.2.4.4).

The measurements that describe a sensillar response include those parameters introduced in chapter 2 (Fig. 1), but comprise a few more that, in part, were included later, or were found to be less useful to characterize the response. In analogy to the terminology used in electronics, those parameters that describe the SP are further summarized as **DC response** (DC = direct current, in a sense of a slow component). The parameters that characterize the APs are referred to as **AC response** (AC = alternating current, fast component).

5.2.1 Parameters of the DC response

- **SP**: the maximal SP amplitude, measured between the baseline before the response and the negative peak during the response.
- **$t_{1/2\ rise}$**: the half-time of the rising phase, measured between the onset of the sensillar potential and the time the potential has reached 50% of SP.
- **initial slope**: $0.5 \cdot SP / t_{1/2\ rise}$.
- **fit tau**: the time constant of a first-order exponential fit on the second half of the SP rise.
- **$t_{1/2\ decline}$**: The half-time of the decline phase, measured between the end of the response, which at short stimulus duration coincides with the negative peak, and the time the potential has decayed to 50% SP.
- **DC trigger latency**: the time between the trigger signal that controlled the stimulus and the onset of the SP.

5.2.2 Parameters of the AC response

The peak AP frequency is measured in four ways:
- **1ISI**: the frequency computed by the first interspike interval (ISI).
- **5ISI**: the frequency computed by the first 5 interspike intervals.
- **10ISI**: the frequency computed by the first 10 interspike intervals.
- **RD***: the frequency computed over the first 200 ms or over the stimulus duration, if it exceeded 200 ms.

The other AC parameters are:
- **# Spikes**: the number of action potentials during 1 s after the onset of the SP.
- **response type**: a numerical value between 0 and 1 that characterizes the phasicicity of a response[5].
- **DC onset latency**: the time between the onset of the SP and the peak of the first AP.
- **AC trigger latency**: the time between the trigger signal that controlled the stimulus and the peak of the first AP[6].

The AC response is determined for both AP classes separately, whenever APs of two amplitude classes are present in a data file and can be distinguished.

5.2.3 Encoding stimulus parameters in the data file names

Data file names should contain as much information about the file as possible. While Clampex suggests the recording date as the file name prefix, followed by an incrementing index, XtraCell follows a different strategy. Recordings of the spontaneous activity can be processed, regardless of the file name. The evaluation of

---

[5] The phasicicity is computed from the number of APs during the first half of the stimulus duration (RD) after the onset of the DC response in relation to the number of APs during the entire RD. Instead of the actual stimulus duration, RD was set to 200 ms, when the stimulus was shorter. Therefore, the closer to 1.0 the result of the quotient **$\#APs_{0.5 \cdot RD}$ / $\#APs_{RD}$** is, the more phasic is the response. This algorithm still needs some improvement, however.

[6] Only the DC onset latency is dealt with in Chapter 2.

responses to adequate stimulation, however, extracts the stimulus parameters from the file name, and therefore requires a stereotypic name structure. Since response- and spontaneous activity data files are recorded in rapid succession, it is not feasible to set the data file names during the recordings. In addition, Clampex uses 3 digits as an incrementing index. To maintain compatibility to the DOS-based analysis programs shipped with pCLAMP 8, however, an 8.3 nomenclature shall be retained, leaving only two digits for the index. So the response data files must be renamed after the recordings. In the next section, the data file naming conventions as used by XtraCell are defined. After that, the steps required to rename the files are described in detail.

5.2.3.1 Data file naming conventions

After renaming, the data file names must have the structure **AABCCD00.ext**, where:

AA   = **Animal ID**, a two-character alphabetical identifier for the experimental animal,

B   = **Sensillum ID**, a one-digit numerical identifier for the sensillum,

CC   = **Stimulus dose**, a two-character identifier for the decadic logarithm of the stimulus dose. Since the characters '+' and '-' may lead to complications when used in file names (e.g. in Clampfit / **Analyze / Arithmetic**), they are replaced by '**p**' and '**m**', respectively. Thus, '**m6**' means a dose of 10^{-6} µg, '**p2**' encodes a stimulus of $10^2 = 100$ µg. A stimulus of $10^0 = 1$ µg is encoded by '**00**'. Due to the limit of two characters, the dose is restricted to the range between 10^{-9} and 10^9 µg.
Control stimulations are given the ID '**ko**', while '**th**' indicates a thermistor measurement. Recordings of the spontaneous activity between the stimuli are encoded by '**sp**', and finally '**tr**' marks data files that are trashed, i.e., excluded from the evaluation for any reason.

D   = **Stimulus duration**, a one-digit identifier encoding the stimulus duration on a pseudo-logarithmic scale (1, 2, 5, 10, 20, ...). The code ranges from '**a**' = 1 ms to '**m**' = 10,000 ms.

00   = **File index**, the last two digits of the original pCLAMP file index.

.ext   = **Data file extension**, 'abf' or 'dat' as in the original file.

5.2.3.2 Renaming the data files

To save the user from entering the stimulus parameters of every single data file, they are encoded in the file name, and decoded during the evaluation. During data acquisition, Clampex automatically assigns a three-digit incrementing index to each data file, prefixed by a user-defined file name 'body'. Since altering the file name prefix between two stimuli applied in rapid succession may not be feasible, and since the encoding of all relevant parameters requires six instead of five digits, it is necessary to rename the files. Refer to the previous section for details on the structure of data file names.

I suggest to record the files with the prefix '**AABXX**', where '**AA**' is a two-character identifier for the animal ('aa' through 'zz'), and '**B**' is a one-digit identifier for the sensillum (0 or 1 through 9). '**XX**' may be any temporary ID, since it is removed by the renaming procedure.

For example, after the recording from the first sensillum of animal **IB**, the files in our data folder are:

ib1xx003.abf
ib1xx004.abf
ib1xx005.abf
ib1xx006.abf
ib1xx007.abf

where the files 003, 005, and 007 are stimulations and the files 004 and 006 contain the spontaneous activity in between. These files are among the sample files distributed with XtraCell.

If you select **XtraCell / ReSponse / Rename Data Files**, you are prompted to specify the files you want to rename. You should rename only the data files from one sensillum at a time. For this example, specify all 5 files. XtraCell creates an Excel sheet with the original file names in the first column. In addition, the header

information is read from the data files, and those files acquired in Fixed-Length Event-Detection mode are assumed to contain spontaneous activity ('**sp**' in the dose column). The gray fields are write-protected.

Enter the dose and duration for the three stimulus files, e.g. **ko, 1**, and **1** in the **Dose** column and three times **50** in the **Duration** column. These are the parameters the sample data files were actually recorded with. You may enter any other values, too, since these parameters are not stored anywhere in the data files. Refer to the previous section for the supported range of the doses and durations. A wide range of expressions is interpreted as control: **ko, co, ctrl, control** or **0**. The only valid identifier within data file names is **ko**, however.

Now click **Evaluate Identifiers** on the floating toolbar to see the names the files would be given. Note: this is a preview only, no file is renamed yet. If you used the actual parameters, the file names should then be:

    ib1kof03.abf
    ib1sp004.abf
    ib100f05.abf
    ib1sp006.abf
    ib100f07.abf

Only if you now click **Rename Data Files**, the files are renamed after a safety prompt. The old and new file names are written to the log file **ren_ib1.log** in your [Working Path]\Logging folder.

If you record the same sequence of stimuli and spontaneous activity more frequently, you can work with templates. Select **XtraCell / ReSponse / Rename Data Files** and specify the same set of data files as in the previous paragraph. You can re-use the files, even if they are already renamed.

Then select **Import Template**. Template files have the same structure as the log files, so you may specify one of your log files as template. Adjust the parameters as desired and **Evaluate** the **Identifiers** or **Rename** the **Data Files**.

Alternatively, you can alter the stimulus parameters and save the new parameter set by pressing **Save As Template**. For safety reasons, after saving a template, you have to **Close** and restart the procedure, if you want to rename a set of data files.

5.2.4 Analysis

Since Clampfit 8 does not have a macro functionality, the analysis of the data files is controlled by simulated keyboard input sent from XtraCell to Clampfit (refer to Appendix VI for more details). Therefore, make sure not to activate any other application window while the analysis is in progress. Otherwise, the probability that keys are sent wrong is unfortunately very high.

Before you proceed, it may be useful if you open one of the files **ib100f05.abf** or **ib100f07.abf** into Clampfit and make yourself familiar with their structure. The first signal, **AC**, is a highpass-filtered signal again, and is not used for the analysis. Signal **DC** is the unfiltered response. The **Piezo** signal reflects the flight activity, which is only present in **ib100f07.abf**, however. The signal named Thermistor shows only digitizer noise in the sample files. The thermistor normally serves to monitor the stimulus arrival. In some recordings, however, it introduced noise into the physiological signal. If this was the case, as in the sample files, the stimulus arrival was measured with a control cartridge at the beginning and/or end of a recording session only. This requires, however, that the stimulus delivery system is sufficiently standardized and has proven its stability.

Close the data files and exit Clampfit before proceeding.

5.2.4.1 Creating a new Overview

Now that the stimulus parameters are encoded in the data file names, we can start with the analysis. We will end up in a list that summarizes the measurements of individual data files from one recording, the **Overview** sheet. The original measurements are recorded on separate sheets that are created after the **Overview** sheet. Each response sheet is given the name of the respective data file, and the cells in the **Overview** sheet refer to them using formulas. Therefore, if you copy an **Overview** sheet into another Excel workbook, make sure to paste **Contents / Values** to avoid external links. The Excel workbook is saved as **AAB_ovw.xls**, where **AA** is the animal ID and **B** the sensillum ID. These are extracted from the first data file in the list. XtraCell does not verify that only data files from one sensillum or animal are contained in the workbook.

Select **XtraCell / ReSponse / New Overview** and specify the sample files that were previously renamed. Make sure you do not include the files containing the spontaneous activity. If you do, XtraCell cannot evaluate the stimulus parameters encoded in the file name and gives you the option to either enter the parameters manually or skip the file. If you choose to skip the file, the row in which it was recorded is deleted. You should

only choose to enter the stimulus parameters manually, if you are absolutely sure the file is a valid stimulus response file. XtraCell currently does not validate the file structure, except for whether it is an Axon Binary Format (ABF) file. So it is very likely that Clampfit will not correctly interpret the simulated keyboard input, if the file is not a response file that matches the expected file structure (see above).

XtraCell launches Clampfit and opens the first data file. The first of the sample data files is the response to a control stimulation, in which no measurable sensillar potential and no action potentials occurred. The spike-like signals at about 3.2 s are action potentials of a neighboring sensillum, as we will see with the next data file. Since there is no measurable response[7], click **Skip** whenever the **ReSponse Progress** dialog under the Clampfit application window appears. If no dialog is visible and the Clampfit window exceeds the bottom edge of your screen, activate Excel, hit <Esc> and select **XtraCell / Program Options**. Go to the **Compatibility** tab, activate **Display Resolution / Manual** and select a lower resolution. In this case, close the overview file and start again by creating a **New Overview**.

5.2.4.2 Analysis of the DC response
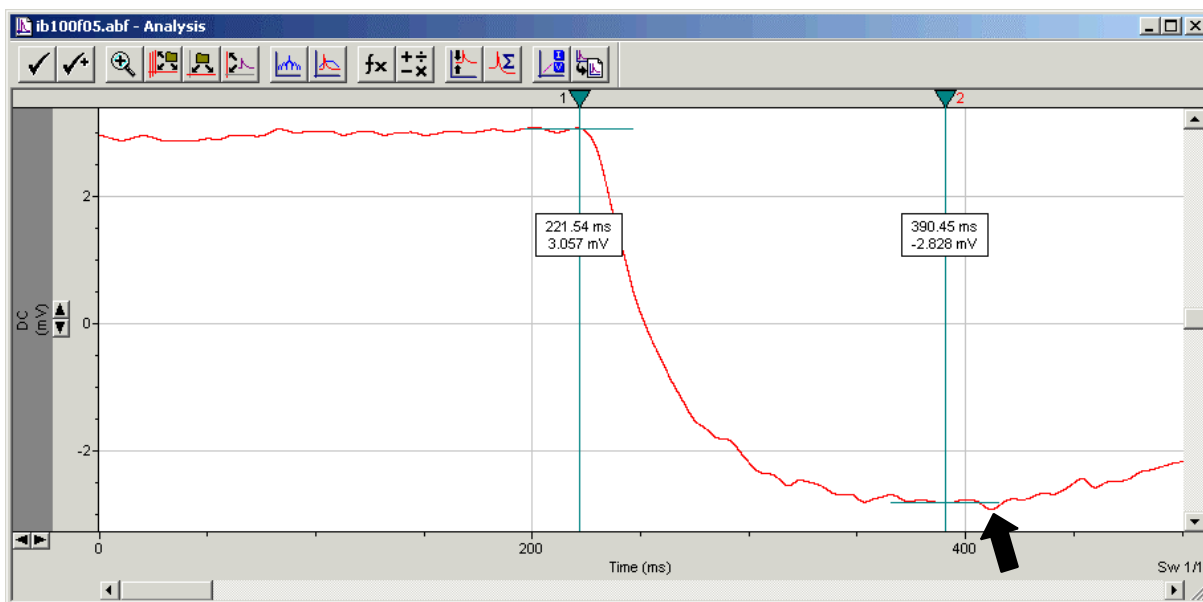
Fig. 17: Cursors 1 and 2 are set to the onset and the (negative) peak of the lowpass-filtered sensillar potential. Rapid fluctuations of the potential, as marked by the arrow, are residuals of action potentials not completely eliminated by the lowpass filter. These residuals should not be considered in the analysis.

The next data file, **ib100f05.abf**, contains a response that can be evaluated. The signal **DC** is maximized and lowpass-filtered at 50 Hz to remove the action potentials. Then the first 500 ms are zoomed and you are prompted to place cursors 1 and 2 at the beginning of the response and the negative peak, respectively (Fig. 17). The residual of an action potential, marked by the arrow in Fig. 17, is not the negative peak, although it is the most negative sample in the file. You should smoothen the signal by eye a little more than the filter did to determine the correct cursor position. Residuals like this could be eliminated by using a lower filter cut-off frequency than the 50 Hz used by default. This, however, would also affect the waveform of the SP, especially in its relatively fast initial phase. So we have to rely on our visual system. But it normally performs rather good at filtering.

When you have done so, click **Done** in the **ReSponse Progress** dialog. XtraCell prompts you to place cursor 1 to half the SP amplitude and puts out the voltage the cursor must read then. Move the cursors with the mouse or the <Left> or <Right> cursor keys. Hold down <Shift> while pressing the cursor key to move the cursor by 10 pixels. <Ctrl>+<Cursor Key> moves the cursor sample by sample. There is no sample with a voltage reading of

---

[7] In a strict sense, there **is** a measurable response, and once you are familiar with the analysis, you should evaluate it. But this is not a good file to start with. I wanted to include a control stimulation, however, and there was no data set with the control applied after two response data files that would have been equally convenient for demonstration purposes as the ones included.
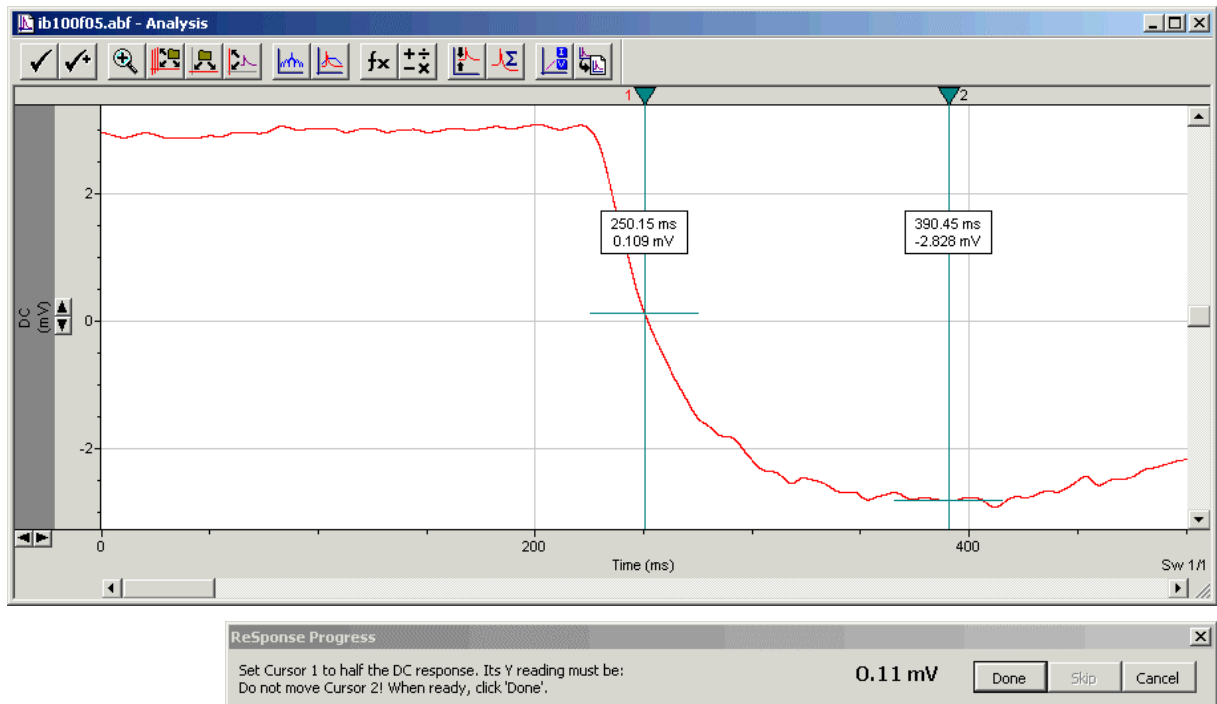
Fig. 18: Cursor 1 is set as closely as possible to the position given in the **ReSponse Progress** dialog.

exactly 0.11 mV[8]. So choose the one that is closer to this value from the neighboring samples at 0.109 and 0.113 mV, respectively. Do not move cursor 2! When cursor 1 is set (Fig. 18), click **Done**.

XtraCell fits a first-order exponential function over the second half of the initial phase of the sensillar potential, which is enclosed by the cursor pair now (Fig. 19). Since fitting may take some time on slow computers, you are prompted to confirm that the fit is complete before the analysis proceeds.

To measure the half time of the decline phase, set Cursor 1 to half the SP amplitude in the decline (Fig. 20). Do not move Cursor 2, if there is no plateau in the sensillar potential. At short stimulus durations, as the 50 ms in the sample files, the sensillar potential typically exhibits only one minimum. Thus, the minimum and the onset of
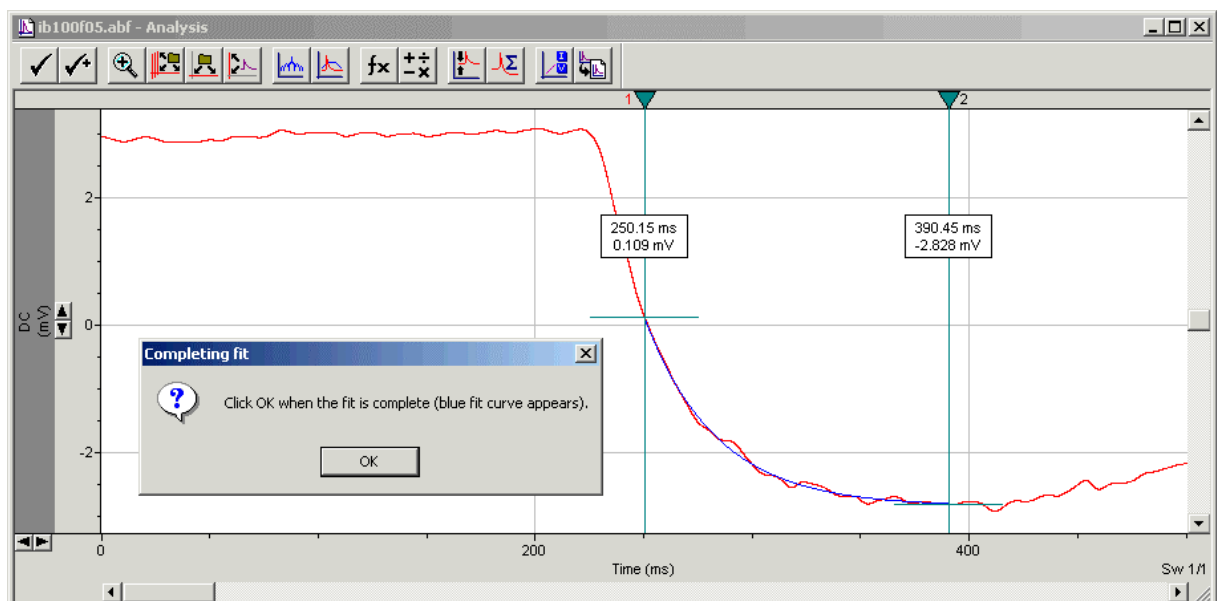
Fig. 19: After fitting the second half of the rising phase, XtraCell waits for a confirmation.

---

[8] The values may be slightly different, if you did not place the cursors exactly as in Fig. 17.
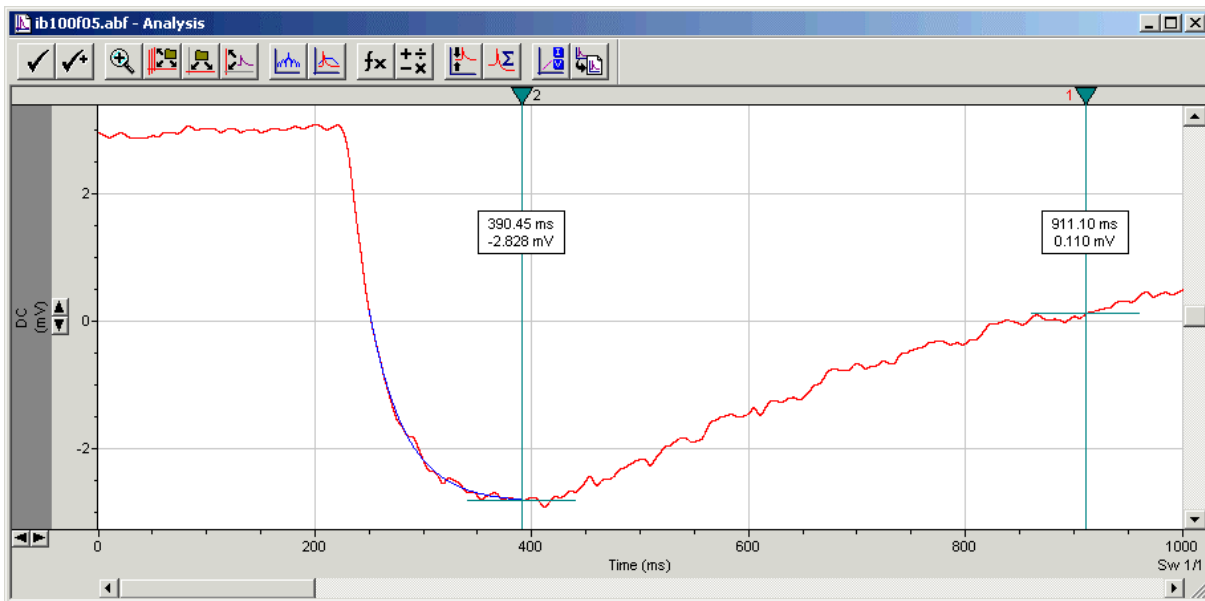
Fig. 20: Measuring the half time of the declining phase ($t_{1/2decline}$).

the decline coincide. At stimulus duration of more than about 200 ms the SP typically has a plateau. If this is the case, place cursor 2 at the end of the plateau.

Finally, set cursor 1 to the end of the sensillar potential. The transepithelial potential typically does not completely return to the value before the response (Fig. 21). So the end of the response is defined as the time, after which the potential remains stable. It is not unusual, however, if this point cannot be determined. So this parameter is currently not used for any further analysis.
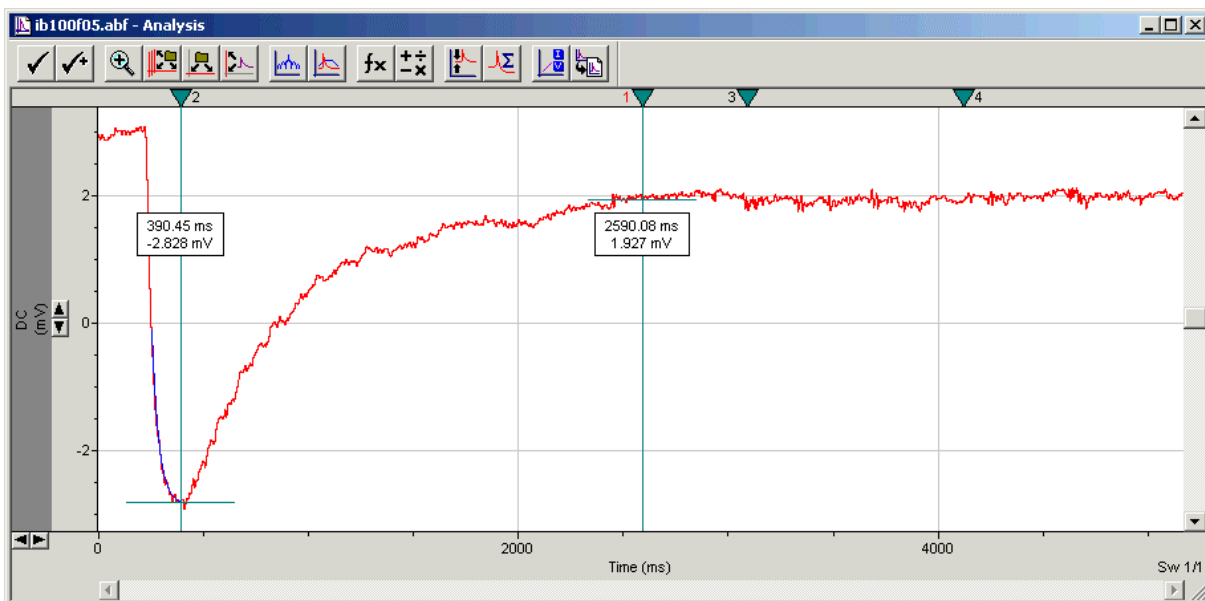
Fig. 21: The end of the response cannot be determined that clearly in all data files.

5.2.4.3 Analysis of the AC response

After the DC response has been analyzed, XtraCell proceeds to the evaluation of the action potentials (AC response). Two parameters, the time of the occurrence and the peak amplitude of each action potential are measured. Since there are two classes of action potentials, they are counted separately, if they can be distinguished. A common way of revealing action potentials superimposed on a more slowly fluctuating baseline are highpass filters. However, all highpass filters, whether analog devices or digital implementations, have the disadvantage of distorting the waveform of the fast signals they allow to pass. Depending on the filter algorithm and cutoff frequency, highpass filters applied to pheromone responses may either exhibit a residual from the steep portion of the sensillar potential or introduce ringing in response to fast changes in the signal, such as the steep portion of the sensillar potential. In any case, they overemphasize the repolarizing phase of the action potentials. Fig. 22 illustrates and compares the impact of the two highpass filter algorithms Clampfit 8 provides at different cutoff frequencies on a pheromone response of *M. sexta*. It is recommended to read the respective
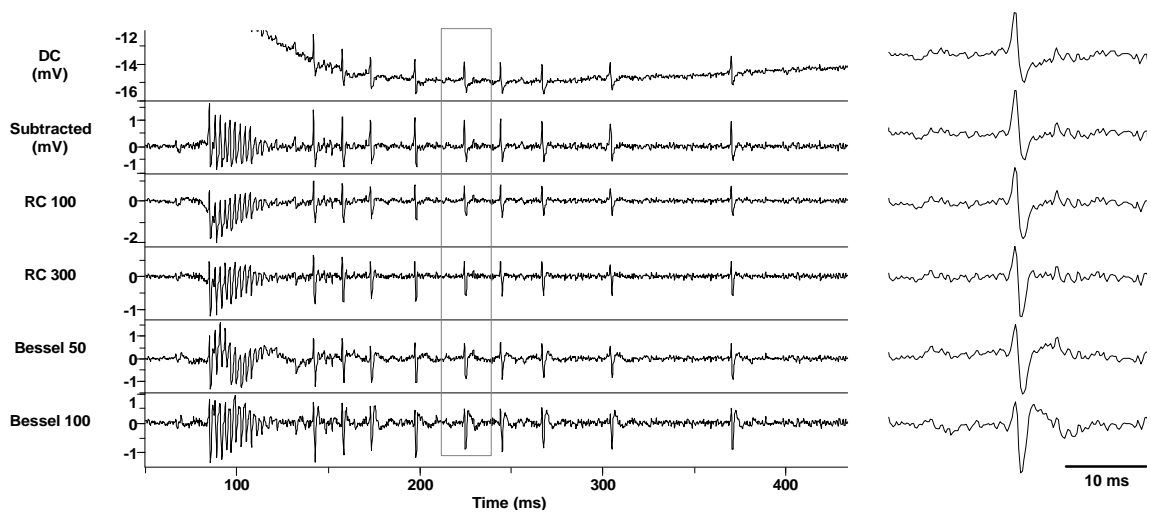

Fig. 22: Highpass filtering severely affects the waveform of action potentials (APs). A pheromone response of *Manduca sexta* (DC) was highpass-filtered at a cutoff frequency of 100 Hz with the **Single-Pole RC** filter implementation in Clampfit 8 (RC 100). There is a considerable residual from the steep portion of the sensillar potential (SP). At a cutoff frequency of 300 Hz, the RC filter mostly eliminates the steep portion of the SP, but overemphasizes the repolarizing phase of the APs (RC 300). The right panel shows the AP indicated on the left at an enlarged scale. The 8-pole Bessel filter introduces ringing in response to the steep portion of the SP at a cutoff frequency of 50 Hz (Bessel 50). At 100 Hz, there is no ringing, but the waveform of the APs is extremely distorted (Bessel 100). When the lowpass-filtered response was subtracted from the original, however, the SP was completely eliminated, and the waveform of the APs remained intact (Subtracted). Reproduced with kind permission of Axon Instruments Inc.

tutorial in the Clampfit 8 manual for a more detailed description of filtering in Clampfit (Axon Instruments, 1999, chapters 8 & 10). The disadvantages of highpass filtering can be avoided by subtracting the lowpass-filtered signal from the original. In addition to a perfect removal of the sensillar potential, this algorithm leaves the waveform of the action potentials virtually unaffected (Fig. 22 Subtracted). Therefore, XtraCell uses this algorithm that I termed pseudo-highpass filtering (Chapter 2).

The lowpass-filtered signal is already present in the file we are analyzing. We used it for the evaluation of the DC response. XtraCell duplicated the original signal before applying the filter, so the original is also available. The subtraction is performed using the **Math** signal, which is not identical to a physical input signal, but results from a mathematical expression performed on one or two of the input signals. XtraCell enables the **Math** signal and displays it together with the original response. The other signals are hidden from display (Fig. 23).

The two classes of action potentials can be distinguished by their amplitude in the **Math** signal. The large APs have a positive phase of about 2.2 mV, while the small APs remain below 2 mV or exceed this value only slightly. One may argue, whether the burst starting at 3.1 s (question mark in Fig. 23) is a burst of large or small APs. In case of doubts, it may be useful to consult the recordings of the spontaneous activity before the response (ib1sp004.abf). Since the burst occurs long after the end of the response, however, a misclassification should not have any severe impact on the results in this case. When small action potentials occur earlier during the response, they are typically easy to recognize (Chapter 2, Fig. 4).
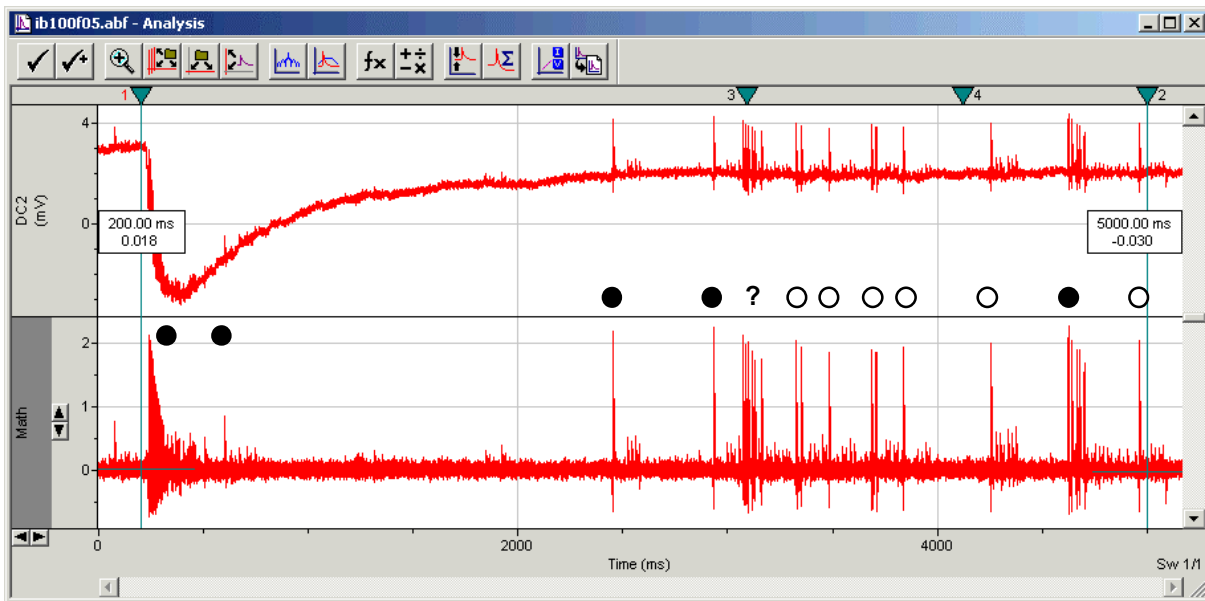
Fig. 23: After pseudo-highpass filtering, XtraCell arranges the original and the pseudo-highpass-filtered signal in the analysis window. The time axis is set to full scale to give an overview of the presence of small APs. In this figure, large APs and bursts of them are marked with filled dots, while small APs are indicated by open dots. The burst denoted by the question mark cannot unambiguously be classified. The APs occurring at a high frequency in the beginning of the response are associated with a reduction of their amplitude.

    The counting of the action potentials is done in two rounds. First, we count all large APs (i.e., those fired by the cell responding to bombykal (BAL). XtraCell does not proceed before you click **Done** or **Skip** in the **ReSponse Progress** dialog. For counting spikes, you need to change the scaling of the X axis, but it is not recommended to change the scaling of the Y axis, unless the first overview (Fig. 23) has shown that no small APs are present in the entire file.
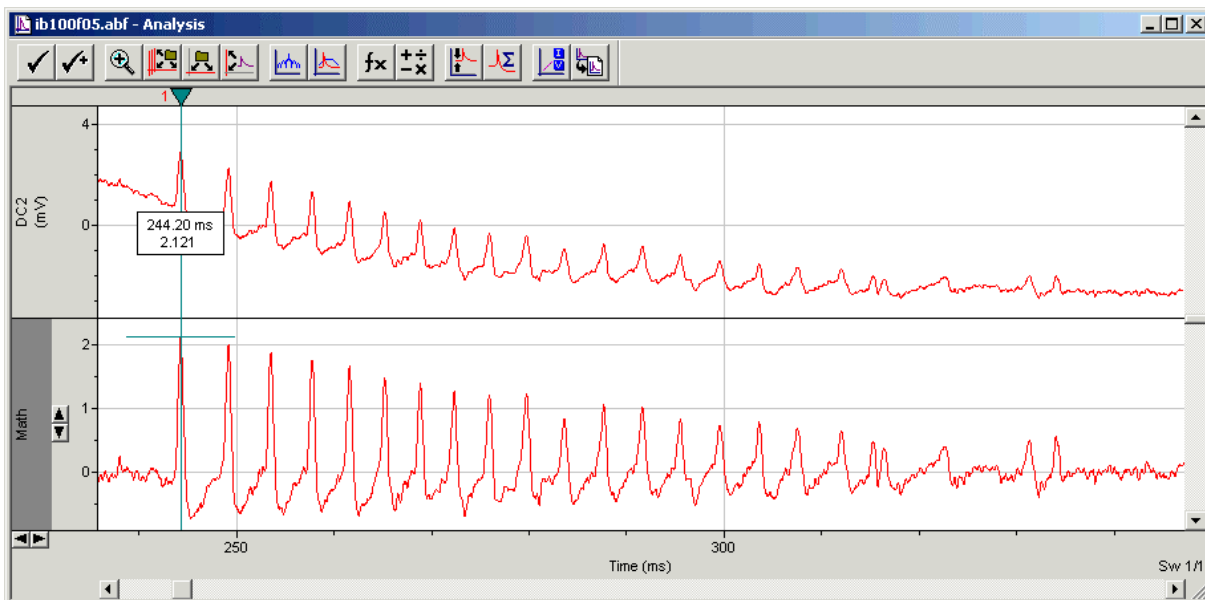
Fig. 24: The initial portion of the response at an enlarged time scale.

    Zoom the initial portion of the response (Fig. 24), place cursor 1 on the peak of the each AP using the mouse or the cursor keys, and hit <F9>. This command appends the readings of all cursors to the **Cursors** sheet in the **Results** window. If you use the mouse for placing the cursor, release the mouse button before pressing <F9>. Else the readings not are not recorded. Only the readings of cursor 1 are further used by XtraCell. Therefore, make sure not to unintentionally use one of the other cursors. Likewise, if you happen to click into signal DC2 while moving the cursor, this signal is activated. Then the voltage reading of signal DC2 is written to the results, and the analysis of the action potential amplitudes is impossible. So activate signal **Math** in this case, before
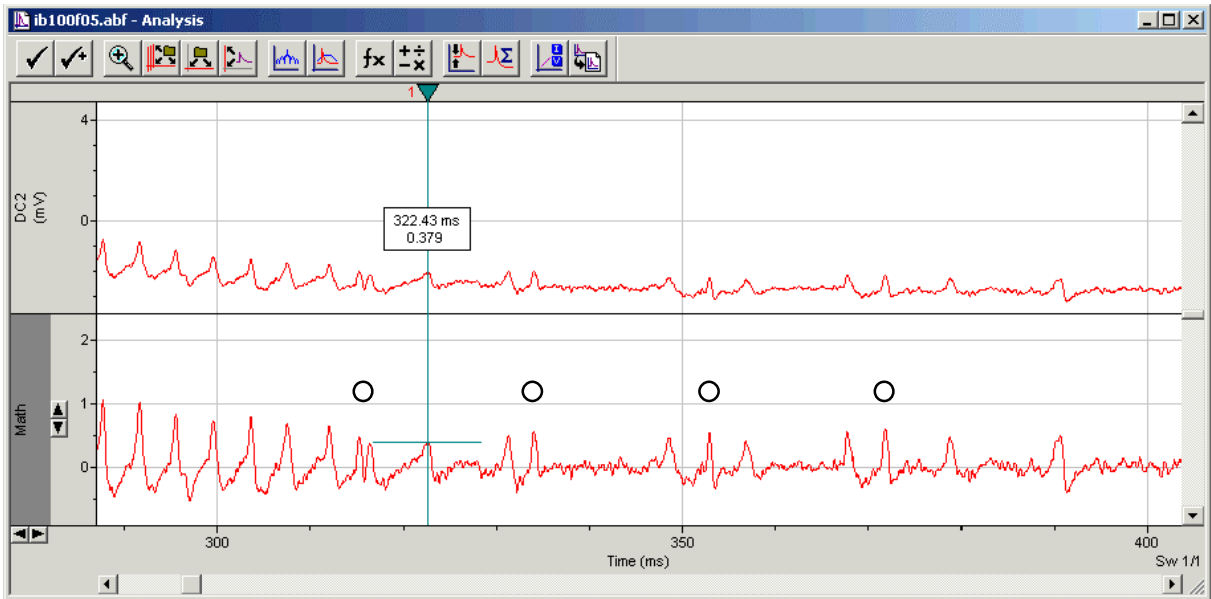
Fig. 25: In the recording APs from a neighboring sensillum were picked up. In the end of the early response, the amplitude of the APs originating from the sensillum under the electrode were reduced so far that they cannot be distinguished from those of the neighboring sensillum by amplitude. The waveform of the picked up APs (open dots), is shorter than that of the original APs, as can be verified when they are compared with those that occurred after the response (Fig. 26). It cannot reliably be determined, which of the double spikes marked by the first dot originates from which sensillum. It is very likely, however, that one of them was produced by the sensillum under the electrode.

writing the next action potential to the results. If you are unsure, whether you have already processed an AP, rather append it a second time. XtraCell validates the interspike intervals after each AP class is finished and prompts you what to do, whenever an ISI is shorter than the **Minimal ISI** specified in the **Program Options**. Likewise, it does not matter, if you did not write the APs in the correct order. They are sorted by time before further processing.

As you approach the end of the early, high-frequency response, two different kinds of small APs are present (Fig. 25). As mentioned previously, action potentials of a neighboring sensillum were picked up in this recording. This occasionally occurs, but it remains unclear, whether the signals conducted through the basal regions of the sensilla or capacitively couple in from a sensillum that touches the outside of the recording electrode. The fact that these APs are hardly affected by the stimulus correlated amplitude reduction favors the transmission via the basal region, where the sensilla are situated in close proximity to each other. This has been shown to be the case in *Antheraea polyphemus* (de Kramer, 1985).
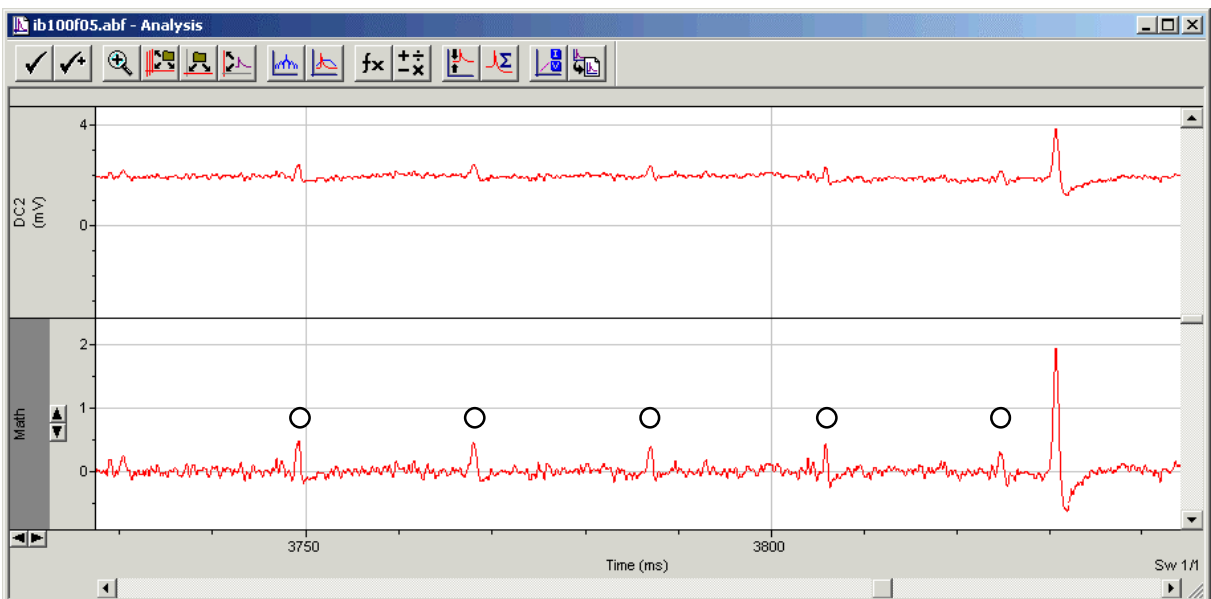

Fig. 26: Late after the response, the APs of the neighboring sensillum can clearly be discerned by their amplitude. Their shorter half width serves as template for the identification of the APs during the response (Fig. 25).

If you compare the waveform of the APs in Fig. 25 to those that occur after the response (Fig. 26), it is evident that the APs of the neighboring sensillum are much shorter. Therefore, only the ones with a longer half width, unmarked in Fig. 25, are part of the AC response in our sensillum. After you have counted all large APs, click **Done** and continue with the small ones.

When the small APs are analyzed, too, XtraCell saves the changes to the analyzed data file as **ib100f05_eval.abf**, exits Clampfit and proceeds to the next response.

5.2.4.4 Structure of the Overview sheet

When all files are processed, activate the **Overview** sheet. The first four columns contain **General** parameters. The time each file was recorded, the file name and the animal- and sensillum ID. The date the recording started is should already be in cell **A3**, but you still have to enter the start time into cell **A5**. Typically this is the time when the initial calibration file was recorded. For the sample files, it was 14:40:23.

The next block is labeled **History**. In this block, parameters of the last stimulus and applied drugs are recorded. The parameters of the last stimulus, i.e. inter-stimulus interval, duration, absolute dose and the dose relative to that of the current stimulus, allow applying a filter to the table. Applying the criteria used for Chapter 2, all responses obtained **20 s** after a stimulus of dose **1** and **250 ms** duration would be adapted. When drugs were injected into the hemolymph, enter the injection time in **K2**. When agents were included in the recording electrode, the "injection" time is identical to the beginning of the recording, so copy this value. Finally write the drug and the dose into columns **I** and **J** and save the changes.

The next block holds the parameters of the current stimulus. The total number of stimulations is put out in **P5**. Control stimuli do not count. We used two different types of solenoid valves, a monostable and bistable one. The distance between the outlet of the stimulus cartridge and the preparation should have remained constant for the entire recording. A pre-potential or pre-response was occasionally observed, when pheromone leaked out of the stimulus cartridge while it was installed. This cannot be detected in the stimulus files, so the paper charts must be analyzed. I suggest the following categories: 1 = slight TEP deflection, no APs; 2 = increased AP frequency; 3 = clearly response-like. Leave the cells empty, when no pre-potential occurred.

The rest of the blocks contain the response measurements as explained in Sections 5.2.1 and 5.2.2. The AC response is put out separately for the bombykal spikes, for non-bombykal spikes and for both together. In row **5**, XtraCell puts out, how many of the responses were evaluable, i.e., had a measurable SP or APs of the respective class.

5.2.4.5 Appending data files to an existing Overview

You do not need to evaluate all data files from the same recording in one session. If you want to append additional data files to an existing Overview, select **XtraCell / ReSponse / Append to Overview**. This requires that the open workbook is an **Overview** file and the active sheet has this name.
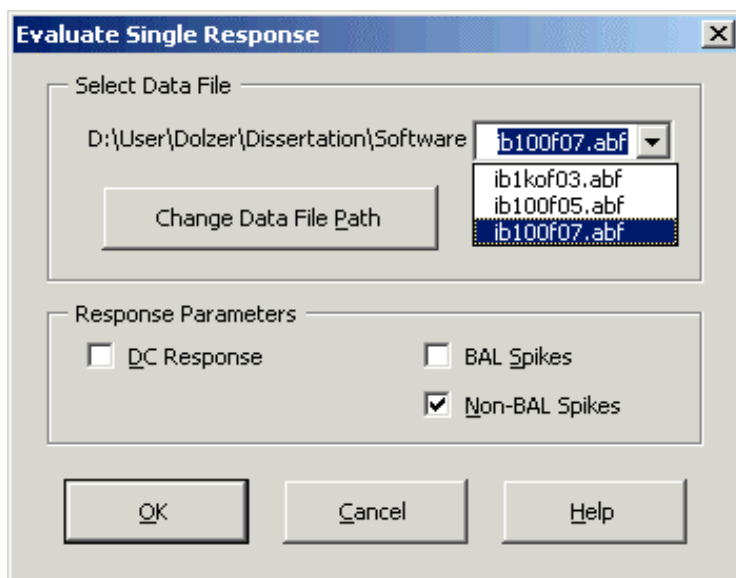
5.2.4.6 Re-evaluating an individual data file

Should you later realize that you misclassified spikes or want to process a particular data file for other reasons again, select **XtraCell / ReSponse / Re-evaluate Single File**. You are prompted to specify one of the files contained in the active Overview, and you may choose to re-evaluate either of the DC response and each of the two spike classes. The Excel sheet with the original results is renamed to **[DataFileName].old** and remains in the workbook, unless you decide to delete it when prompted in the end.

6 Conclusion

XtraCell has proven to be a well-suited tool for the analysis of extracellular tip recordings of pheromone sensilla of *M. sexta*. The studies described in Chapters 1–3 would not have been possible without use of an automated analysis software. In recordings of spontaneous action potentials, the analysis of a segment of 10 min duration took several hours when the action potentials were counted manually. Using the approach described here, a 10 min recording with few or no artifacts can typically be analyzed in about 2 min, depending on the action potential frequency and the performance of the computer employed. It should be noted that the sample data files distributed with XtraCell were chosen to contain several potential pitfalls. The scope of this chapter is to document and to introduce the use of the program, including the description of those situations that require manual correction. Typically, given the recordings are of sufficiently good quality, situations like the ones described occur infrequently, and XtraCell performs well at characterizing the spontaneous action potential activity. Otherwise it would not have been possible to do the study described in Chapter 1, which involved the gap-free analysis of recordings of many hours in duration.

With help of the spike sorting algorithm in XtraCell, which takes the temporal context into account, it has been possible to reliably distinguish the action potentials, that were previously considered to have a too small difference in amplitude (Kaissling et al., 1989). In the recordings from 100 of 121 sensilla analyzed to date, the action potentials could be distinguished during the entire recording or at least for several 10 min segments. The spontaneous activity in recordings from pheromone sensilla of another moth, *Mamestra brassicae*, was also analyzed using XtraCell (J. Dolzer, unpublished observation; referred to in Grosmaitre et al., 2001). In this species, the difference in the amplitudes of the two action potential classes is much larger, however, so overlapping amplitudes have not been observed. The frequency of action potential bursts is also much lower in *M. brassicae*.

A further increase in the efficiency of the analysis of the spontaneous activity has been obtained by using AutoMate 4 (Unisyn Software, Los Angeles, California) for the analysis steps in Clampfit. This macro program, like the ReSponse module, simulates keyboard input. Since it was used before ReSponse was finished, and since a future version of XtraCell will most likely include this functionality, the use of AutoMate is not described here.

XtraCell has also exhibited a good performance in the analysis of pheromone responses. The results presented in Chapter 2 were obtained with a predecessor of the module ReSponse, which based on an analysis with Clampfit 6. The control of a DOS-based program like Clampfit 6 is completely different from the Windows-based Clampfit 8. So the procedures were completely re-written, but many of the algorithms used now still base on the early versions. The recordings presented in Chapter 3 were analyzed using the ReSponse module in its current implementation. Clampfit 9 will feature highly sophisticated event detection algorithms that will further facilitate the analysis of action potentials in response to adequate stimulation.

It is hard to define a time when software can be called "ready" with good conscience. Even with commercial software, this does not appear to be possible, as reflected by the release of service packs, updates, or whatever bugfixes are euphemistically called. In its current form, XtraCell should run without errors, and the results it puts out are correct – or at least do not differ from those determined manually in many test analyses. Nevertheless, there are some items, especially in the online help, where the program appears incomplete. I hope this can be apologized in non-commercial software.

7 Acknowledgements

8 References

Axon Instruments (1999). User's Guide to Clampex and Clampfit. *pCLAMP Windows Data Acquisition and Whole Cell Analysis.* Foster City: Axon Instruments Inc.

de Kramer, J. J. (1985). The electrical circuitry of an olfactory sensillum in *Antheraea polyphemus. J. Neurosci.* **5**(9), 2484-2493.

Dolzer, J., Krannich, S., Fischer, K. and Stengl, M. (2001). Oscillations of the transepithelial potential of moth olfactory sensilla are influenced by octopamine and serotonin. *J. Exp. Biol.* **204**, 2781-2794.

Grosmaitre, X., Marion-Poll, F. and Renou, M. (2001). Biogenic amines modulate olfactory receptor neurons firing activity in *Mamestra brassicae. Chem. Senses* **26**, 653-661.

Kaissling, K.-E. (1994). Elementary receptor potentials in insect olfactory cells. In *Olfaction and Taste XI* (ed. K. Kurihara), pp. 812-815. Tokyo: Springer.

Kaissling, K.-E. and Thorson, J. (1980). Insect olfactory sensilla: structural, chemical and electrical aspects of the functional organization. In *Receptors for Neurotransmitters, Hormones and Pheromones in Insects* (ed. D. B. Satelle, L. M. Hall and J. G. Hildebrand), pp. 261-282. Amsterdam: Elsevier / North-Holland.

Kaissling, K.-E., Hildebrand, J. G. and Tumlinson, J. H. (1989). Pheromone receptor cells in the male moth *Manduca sexta . Arch. Insect Biochem. Physiol.* **10**, 273-279.

Kalinová, B., Hoskovec, M., Liblikas, I., Unelius, C. R. and Hansson, B. S. (2001). Detection of sex pheromone components in *Manduca sexta* (L.). *Chem. Senses* **26**(9), 1175-1186.

Keil, T. A. (1989). Fine structure of the pheromone-sensitive sensilla on the antenna of the hawkmoth, *Manduca sexta. Tissue Cell* **21**(1), 139-151.

Marion-Poll, F. and Tobin, T. R. (1992). Temporal coding of pheromone pulses and trains in *Manduca sexta. J. Comp. Physiol. A* **171**, 505-512.

Rospars, J. P., Lánský, P., Vaillant, J., Duchamp-Viret, P. and Duchamp, A. (1994). Spontaneous activity of first- and second-order neurons in the frog olfactory system. *Brain Res.* **662**, 31-44.

Thurm, U. (1972). The generation of receptor potentials in epithelial receptors. In *Olfaction and Taste IV* (ed. D. Schneider), pp. 95-101. Stuttgart: Wissenschaftliche Verlagsgesellschaft.

Zack, C. (1979). Sensory adaptation in the sex pheromone receptor cells of saturniid moths. Ph.D. Thesis, Ludwig-Maximilians-Universität, München.

9 Appendix

I Known bugs and limitations

I.1 Clampfit versions between 8.0.3.169 and 8.2.0.224, the most recent version available by the time this thesis is submitted, do not correctly handle overlapping sweeps after adjusting the baseline. The end of a sweep that is overlapped by the subsequent sweep is truncated, and the **Statistics** put out for a region that spans the truncated section are incorrect. You can recognize this behavior during the analysis of spontaneous activity: When action potentials present at the end of some sweeps (Fig. 4) disappear after baseline adjustment, you have a version that cannot be used. Workaround: Download the latest pCLAMP version (**Help / Web Info on Updates**) and see if it has been fixed. If not, try to get version 8.0.3.128, one that definitely works.

I.2 On some systems, Clampfit crashed when printing **Graph** windows to FinePrint. I have not been able to figure out, which parameters determine, whether or not printing works, nor could Axon Instruments reproduce this behavior. Even the most recent Clampfit version is affected. In many times of trying, I have not found any reliable workaround. Printing with FinePrint appears to be impossible in this case.

I.3 Since only two digits are available for the incrementing index in the response file names – as long as an 8.3 file naming shall be maintained – there is a problem if you do overnight recordings that produce more than 100 data files. Depending on how you decide to name your files, they might be incorrectly sorted on the **Overview** sheet. XtraCell sorts the files according to their file indices. If a file recorded on the second day has the lowest index, it is the first one in the list, and the recording start **date**, that is read from the header of the first file and written to cell **A3**, is incorrect. Workaround: Start with analyzing the files below the 100th only and **Append** the others later.

I.4 When re-evaluating a single data file (**XtraCell / ReSponse / Re-evaluate Single File**) XtraCell occasionally issues a corrupt data file header, although the file is OK. I have not found a way to reliably reproduce this bug and, therefore, not been able to fix it. Workaround: Select **Append to Overview** and specify any response data file. Skip all parameters and delete the row the file is recorded to, and the respective worksheet. After that, XtraCell re-evaluated the desired files each time I tried.

II The expected structure of input data

A relatively simple program like XtraCell cannot cope with any possible error in the structure of the input data. Therefore, the input data must be of a specific structure. This section describes the structure of the input data XtraCell expects. The structure of the data files in ABF format are rather uncritical for the analysis of the spontaneous activity, since this type of analysis starts with ASCII data on one or two Excel sheets. The evaluation of pheromone responses, however, involves Clampfit and therefore critically depends on data files of a defined format.

II.1 Spontaneous Activity

The analysis of the spontaneous activity, as described in the step-by-step guide (Section 5), starts out with data files acquired in **Fixed-Length Event Detection** mode. In this mode, each trigger threshold crossing triggers the acquisition of a sweep of predefined duration. If the trigger threshold is crossed a second time, while the previous sweep is not yet finished, a new sweep is acquired. Thus, there is a certain degree of **Overlap**, i.e., the same section of the signal is recorded twice (see the Clampex online help for more details). Ideally, each action potential triggers its own sweep in this way.

In recordings from pheromone sensilla in *M. sexta*, a sweep duration of 12.75 ms has proven convenient. Three input signals are recorded. The recording from the sensillum is applied to two input connectors at the digitizer and acquired twice. One of these signals (**AC**) is highpass-filtered and serves as the trigger channel. The other equivalent of the signal is not highpass-filtered. It is named **DC augment** in the sample files, since the built-in PGA (programmable gain amplifier) in the digitizer (Axon Instruments Digidata 1200) was set to a gain of 2 for better use of the dynamic range. As pointed out in Section 5.2.4.3, all analyses of the transepithelial potential and the action potential waveform should be done on the DC signal only (Fig. 22). The third signal is the signal from a piezo sensor, which recorded the flight activity of the animal at a very high sensitivity. Piezo crystals are highpass filters themselves, so this signal is only analyzed of whether it is zero or non-zero. At a bandwidth of DC–2 kHz, the sampling rate was 19.6 kHz. Data files of this type can be acquired with the Clampex protocol file **SpontAct.pro** you find in the **Params** folder of **XtraCell.zip**.

The ASCII results that are obtained from this type of data files, as described in the step-by-step guide have a stereotypic arrangement anyway. To keep XtraCell flexible for the analysis of measurements from different recordings, the expected structure of the input data is described here. Item II.1.1 defines the structure after an analysis as described above, while item II.1.2 does not include the TEP and the piezo measurements. Item II.1.3 finally defines the minimum requirements that make an array of action potential times and -amplitudes analyzable with XtraCell.

II.1.1 Input data that come from an analysis with Clampfit: Evaluating the action potentials, the DC offset (reflecting the transepithelial potential), and the signal from a piezo sensor.

Basing on data acquisition with Clampex 7 or higher and analysis with Clampfit 8 or higher, you should start out with an Excel worksheet containing the statistics for all sweeps triggered by action potentials. If you want to analyze the DC offset, the Statistics must be on the first worksheet in the Excel workbook. Copy the Mean of the Baseline measurement into column **A** of the second worksheet, the Piezo measurement in column **B**, and give column **B** the header 'Piezo'.

If you followed the analysis procedure as described in Section 5.1, you end up in an Excel workbook with the following structure:

Sheet 1
    Signal name in column **B**,
    Trace Start times in column **D**,
    Trace number in column **E** (optional),
    Peak time in column **I**,
    p-p amplitude in column **K**,
    Mean in column **L**,
    Std Dev in column **M**,
    Data File Name in cell **B2**.
    Half Width in column **X** (optional[9]).

---

[9] XtraCell expects the Half Width of the action potentials in this column and records an error, when they are larger than the **Maximal Spike Duration specified** in the **Program Options**. Therefore, there is no problem, when this column is all empty. Non-numeric or too large numeric values cause error records, however.

Sheet 2
   Mean in column **A**,
   Piezo in column **B**.

The other columns are currently not used for any further analysis.

If your data have this structure, Start with **XtraCell / SpontAct / Integrate DC Measurements**.

II.1.2   Input data that come from an analysis with Clampfit: Evaluating only the action potentials.

If your data come from an analysis with Clampfit, but you do not want to analyze the DC offset, you can start out with the Clampfit Statistics on any Excel worksheet. XtraCell only edits the current worksheet in this mode. The data must basically have the same structure as described for **sheet 1** under item II.1.1. Since no DC offset and piezo signal overwrite the values in columns **L** and **M**, it does not matter what is recorded there.

If you select **XtraCell / SpontAct / Spike Times from / Clampfit 8 Results**, XtraCell checks for the following:

   The Signal name in column **B** must be similar to '**DC**',
   The header of column **K** must be similar to '**peak-peak**'.

XtraCell rearranges a few columns (which has historical reasons), and adds the Trace Start time and the Peak time to yield the Spike time, which is put out in column **A**. Then the program computes the interspike intervals in column **H**. Finally the workbook is saved as [DataFileName].xls. The data file name is taken from cell **B2**, the extension (.abf) is removed.

II.1.3   Processing data that do not come from an analysis with Clampfit.

If you want to process data that do not come from an analysis following the proposed procedure in Clampfit 8, you can start out with your data on any Excel worksheet. XtraCell only edits the current worksheet in this mode. The data must have the following structure:

   The current worksheet must be named '**SpikeTimes**',
   The first row must contain headers. If your data do not include any headers, do not just insert an empty row,
      but enter anything into each of the listed columns:
   The times of action potentials must be in column **A**,
   The (peak-to-peak) amplitudes must be in column **D**,
   The indices of the action potentials or sweeps should be in column **E** (optional),
   The interspike-intervals must be in column **H** (see below),
   Column **X** must either be empty or contain numeric values smaller than the Maximal Spike Duration specified
      in the **Program Options**.

Note: The interspike intervals in column **H** must contain the interval **preceding** the action potential recorded in the same row. That means, column **H** must contain values from row 2 to the last row. See the file SAMPLE.XLS for a spreadsheet that works.

   Now select **XtraCell / SpontAct / Spike Times from / Other List**.

XtraCell does not perform any consistency check. So if your data have a different structure, runtime errors may occur. Even if not, the results will not very likely be correct.

II.1.4 The number of spikes in the list

If you start analyzing the burst behavior and inter-event intervals from a list of spikes as generated by the **Spike Sorting** procedure, or from data that do not come from a Clampfit analysis, XtraCell needs to know, how many spikes are contained in the list. It is assumed that the spikes are recorded in a continuous block on a worksheet and that no data are found below the last row of this block. To make sure this assumption is correct,

XtraCell displays the last row of the topmost block and prompts for the number of spikes before starting the analysis.

You can exclude the last rows in the list from the analysis by specifying a smaller number of spikes. However, empty rows cannot be processed. So you cannot specify a number larger than proposed.

II.2 Pheromone responses

In contrast to the analysis of spontaneous activity, which can be started with ASCII data, the module **ReSponse** involves Clampfit and expects a clearly defined structure of the data files. Since Clampfit is controlled with simulated keyboard input (see above), XtraCell cannot receive any feedback from Clampfit. Therefore, if the data files do not have the expected structure, XtraCell sends keys to Clampfit, which target the wrong input signal or dialog, and most likely do not elicit the desired action. This continues, until the user stops the procedure or the data that are read from the Clampfit Results sheets fail to pass one of the plausibility checks XtraCell performs for this very reason.

Pheromone response data files are by default expected to have 4 input signals with the **DC** signal being the second one, as in the supplied sample data files. The other three input signals are currently not analyzed by XtraCell. These are the highpass-filtered signal (**AC50**), the Piezo signal that reflects the flight activity, and the thermistor signal that monitors the arrival of the stimulus airstream. In some recordings, the thermistor caused artifacts when placed near the recording site. In these experiments, the stimulus airstream was only measured "offline" after the recording. This was the case with the sample files enclosed, so the thermistor signal is only a straight line there.

The presence of a defined number of input signals is necessary, since in Clampfit there is no way of addressing a signal by name. The only way of selecting a particular signal is moving up or down signal by signal. If your data files have a different structure regarding the input signals, you can adjust the structure expected by XtraCell in the **Program Options**.

Response files were recorded in **Episodic Stimulation** mode using the enclosed Clampex protocol file **Stim50ms.pro**. It is recommended to use this protocol as a basis. The data were acquired at a sampling rate of 20 kHz with the largest sweep duration supported by Clampex 8 (100k samples, corresponding to 5161.2 ms). The stimulus was triggered by a digital output signal set high 100 ms after the **Wave Start**. The time interval before stimulus onset, together with the distance between stimulus cartridge and preparation, determines the time that is assumed as onset of the sensillar potential to compute the latency of the first action potential when the DC response is not evaluable. Like the input signals, you can define a different pre-trigger time in the **Program Options**.

The stimulus duration is determined by the duration of the digital high signal. The other digital outputs were used for marker signals on the tape and strip chart recorder or remained unused. The analog outputs were unused.

III The Error sheet

There is a number of potential data errors that may be present in the input data or occur during the analysis. Whenever such an event occurs, XtraCell creates a sheet named **Errors** and records what might be wrong, and where it can be looked up. Different types of possible errors are recorded in different columns:

missing files

This column lists files that were not found during the evaluation of response data.

no DC response

When a response contains action potentials, but no measurable sensillar potential, the latency between the onset of the sensillar potential and the first action potential cannot be computed. In this case, the user is given the option to use an assumed onset time instead.

sheet

The entry in this column specifies, on which sheet the errors recorded in the subsequent columns can be found.

ISI < MinISI

The entry in this column indicates that the interspike interval preceding the action potential in the respective row was shorter than the minimal ISI specified in the **Program Options**.

AP too long

This entry indicates the row of an action potential, whose duration is longer than the allowed maximal spike duration, as defined in the **Program Options**.

sorting error

If a single large spike occurs within a burst of small ones, the large spike is correctly recognized, but all subsequent small spikes might be misclassified as large. The same is true, if bursts of both spike types coincide (Fig. 16). The row number of the first potentially misclassified spike after the large one is recorded in this column.

next available row

It is recommended to delete the **Error** sheet after all potential errors have been reviewed and corrected, if necessary. In case errors occur in different analysis steps in one file, XtraCell needs to know, in which row to record the next error. To make sure no previous entry is overwritten, the row to record the next error to is stored in this field. **Do not edit this entry!**

If an **Error** sheet is present, when you create a **Summary**, XtraCell prompts, whether you reviewed all potential errors. It is not recommended to leave obsolete **Error** sheets in a file.

IV Configuring the program and analysis options

The **Program Options** dialog automatically opens, when XtraCell is launched for the first time. Later you can change the settings through **XtraCell / Program Options**.

Paths

The entries on this tab are obligatory.

Working path defines the path of your standard working directory. This is where input files are expected, and output files are saved. The subfolders **...\EVAL**, **...\EVAL\SPIKEDIS**, and **...\LOGGING** are created, if they do not yet exist.

The default setting is the **current folder**.

Clampfit program file location specifies, whether pCLAMP is installed on your computer, and where the Clampfit program file is found. This information is required for launching Clampfit during the evaluation of response data. By default, this information is read from the Windows registry. However, under Windows 2000, the pCLAMP Application Path is not registered. Therefore, the default installation location **C:\Axon\pCLAMP8** and the folder **[ProgramFiles]\Axon\pCLAMP8** are assumed. If Clampfit is not found in these locations, you are prompted to look for the program yourself.

SpontAct Options

On this tab you can set a few parameters that may influence the performance of SpontAct, but can also have severe impact on the quality of your analysis. The default settings have been extensively tested and proven reasonable for pheromone sensilla of *Manduca sexta*. I do not recommend to change these values, unless you have good reason to do so.

Burst criterion: Spikes that occur within the Burst Criterion after the preceding spike are considered as members of bursts. So this parameter mainly affects the performance of **Spike Sorting**. If the preceding Spike was large, the spike under consideration is also classified as large, even if its amplitude is below the threshold. The default setting is **50 ms**.

Minimal interspike interval (ISI): The smallest time interval allowed between two spikes. Too short intervals seriously affect the waveform of the subsequent spike, and along with it all measurements. Therefore, XtraCell detects ISIs below the Minimal ISI and records them on the **Error Sheet**. The default setting is **1.5 ms**.

Maximal spike duration: The Half Width of the action potentials may not be longer than specified in this parameter. Originally this feature was implemented to cope with a bug in the software used for the raw evaluation. Now it is just one more feature to make sure you are not analyzing artifacts. The default setting is **1.5 ms**.

If you erroneously changed any of the analysis settings, you can return to them with the **Restore Default Values** button.

ReSponse Options

The settings on this tab determine the structure of data files containing responses to adequate stimulation. Besides the electrophysiological signal, these data files may contain other signals, such as a highpass-filtered signal, a stimulus monitor, or a signal the movement of the animal is recorded to. The presence of a defined number of input signals is necessary, since in Clampfit there is no way of addressing a signal by name. The only way of selecting a particular signal is moving up or down signal by signal. Therefore, XtraCell needs to know, how many signals are present, and which one is the signal to analyze.
In addition, you can set the lowpass filter cutoff frequency used for the analysis.

Number of input signals: This entry defines, how many input signals (1–16) your data files contain. The default value is **4**, as in the supplied sample data files.

Index of DC signal: Determines the signal that is analyzed. It is not necessary that the signal is named DC. The default setting is **2**.

Pre-trigger time: The time after the start of the file, when the control signal that triggers the stimulus is switched on. Note that Clampex adds a pre-episode time in Episodic Stimulation acquisition mode. You can determine this time by opening one of your response data files and selecting **View / Stimulus Waveform Display**. This setting is used to compute the arbitrary response start in a recording, in which action potentials are present, but the DC response is too small to be measured. This arbitrary value is computed by adding 50 ms to the **Pre-trigger time**. If this time is different in your setup, determine the average start of your responses and enter this value less 50 ms. The default **Pre-trigger time** is **180 ms**.

Clampfit lowpass filter cutoff frequency: The filter setting used to obtain the lowpass-filtered signal used for the analysis of the DC response, and the pseudo-highpass-filtered signal for the analysis of the action potentials. For pheromone responses of Manduca sexta, cutoff frequencies between 40 and about 70 Hz have proven useful. The default setting is 50 Hz.

If you erroneously changed any of the analysis settings, you can return to them with the **Restore Default Values** button.

Compatibility

Decimal separator: pCLAMP ignores the Windows Control Panel settings for the decimal separator and puts out all results and measurements with a decimal point. Therefore, the analysis of this kind of data with Excel requires that the decimal separator is a point, not a comma. See Section 4.2 for more details. XtraCell by default checks your Control Panel settings on startup. If you do not work with pCLAMP data, unselect this option to disable the check.

Display resolution: The size of the Clampfit application window and the position of the form that controls the progress during the analysis in Clampfit depend on the display resolution. Typically, this parameter should automatically be determined. The supported resolutions are 800 x 600, 1024 x 768, 1152 x 864, 1280 x 1024, and 1600 x 1200 pixels.

Should you experience problems with the position of the Clampfit window or the progress form, you can manually set another resolution. Selecting a lower resolution than you actually work with should not make any trouble. Specifying a too high resolution, however, will make the form appear below the bottom edge of you screen. In such a case, activate Excel and hit the <Escape> key.

Clampfit start duration: Some features need to launch Clampfit. The time the application requires to start can vary significantly, depending on the speed of your computer and a few other parameters. To make sure no keys get sent to cyber-nirvana, XtraCell waits for a certain period and a number of process steps. If this time is too short or too long on your system, you can adjust the waiting time on a pseudo-logarithmic scale between 1 and 10. The default setting of **5** worked on several tested systems with a CPU speed between 500 and 1000 MHz. Do not change the setting by more than one step at a time. If changing the waiting time does not help, check **Manual timing**. XtraCell then prompts each time it attempts to start or exit Clampfit and does not continue before you respond to the prompt.

This section is only available, if pCLAMP is installed on your system, as specified on the **Paths** tab (see above).

V XtraCell Registry settings

XtraCell saves all settings in the path `HKEY_CURRENT_USER\Software\VB and VBA Program Settings` in the **Windows Registry**. When run for the first time, the key

```
HKCU\Software\VB and VBA Program Settings\XtraCell\..
```

is created. Most sub-keys are created during runtime. These are the sub-keys and their default values (if applicable):

```
..\Analysis Options\..
  ..\Burst Criterion = 50
  ..\Minimal ISI = 15
  ..\Maximal Spike Duration = 15
  ..\Number of Input Signals = 4
  ..\DC Signal Index = 2
  ..\Pre-Trigger Time = 18
  ..\Lowpass Filter Frequency = 50

..\Paths\..
  ..\Program Path = [Path]
  ..\Working Path = [Path]
  ..\Data Path = [Path]
  ..\Log Path = [Path]
  ..\Clampfit Path = [Path]

..\Program Options\..
  ..\Ignore Decimal Separator = 0
  ..\Manual Clampfit Start = 0
  ..\Clampfit Start Duration = 5
  ..\Manual Display Resolution = 0
  ..\Display Resolution = "1152 x 864"
  ..\XtraCell has Run = 0
  ..\pCLAMP is Installed = 1

..\Recent Settings\..
  ..\Re-evaluate DC = 0
  ..\Re-evaluate Main Spikes = 0
  ..\Re-evaluate Secondary Spikes = 0
  ..\Threshold = 150
  ..\Floating Threshold = 0
  ..\Floating Threshold Bins = 10
  ..\Amplitude Reduction = 1
  ..\Amplitude Reduction Percentage = 25
  ..\Data File Duration = 10
  ..\Short Clampfit Start = 0
```

VI Clampfit must be exited before the analysis can continue

Clampfit 8 does not feature any macros. Therefore, XtraCell controls the application by simulated keyboard input (**SendKeys** function). Unfortunately, this is not the most reliable way to control an application. After every key, the procedure has to wait until the target application has completed the command, otherwise the next keys might be sent to the wrong window or dialog. Since the time (or actually number of process steps) the target application requires to perform a requested command may vary considerably – depending on system speed, active background processes, and other factors – reliable operation demands a conservative dimensioning of the time to wait. This, in turn, severely impacts the performance of the controlling procedure itself.

Therefore, to improve the reliability and performance, not all settings are controlled by simulated keyboard inputs in each program loop. Rather, settings that remain constant in each loop are written to the **Windows Registry**. Many registry settings, in turn, are typically read at program start and written at program exit. Therefore, the only way of forcing Clampfit to use the desired settings is exiting, writing the settings to the registry, and then restarting Clampfit.

The registry settings XtraCell alters are uncritical in terms of system- or program stability. See below for more details.

Furthermore, Clampfit child windows can only be addressed by number, not by name. Exiting Clampfit has proven much more reliable for addressing individual windows than closing the window with the analyzed file.

Note: XtraCell cannot recognize, when Clampfit prompts for unsaved changes. Therefore, you might have to exit Clampfit manually. XtraCell either continues automatically after Clampfit is exited, or you have to confirm a prompt.

In Summary, controlling Clampfit with the **SendKeys** method is far from being ideal, but is currently the only feasible way. Clampfit will not feature macros before version 10. So this way has to be considered a compromise that gives room for improvement, but has worked on a number of different computers in tests.

VI.1 Clampfit registry settings altered by XtraCell

The Clampfit registry settings XtraCell changes should be uncritical in terms of system- or program stability. If you are concerned about that, you should export the settings of the path `HKEY_CURRENT_USER\Software\Axon\Clampfit\` before running XtraCell.

These settings are altered:

```
HKCU\Software\Axon\Clampfit\..
```

Main Frame Position

```
..\MainFrame\..
  ..\wp.flags = 0
  ..\wp.showCmd = 1
  ..\wp.top = 10
  ..\wp.left = 15
  ..\wp.bottom = <variable>
  ..\wp.right = <variable>
```

The keys wp.flags and wp.showCmd appear to be required to run Clampfit as a window. The values for wp.bottom and wp.right depend on the display resolution, as defined in the **Program Options**.

Open Data Options

```
..\FileSettings\..
  ..\XAxisFlags = 1
  ..\YAxisFlags = <number of input signals>
  ..\AutoScale = 10000
  ..\EpiFlags = 1
  ..\ChanFlags = 1
  ..\OpenFlags = 1
  ..\EpiUserString = 1
  ..\SameDisplay = 0
```

Filter Settings

```
..\AnalysisFilter\..
  ..\Region = 0
  ..\Signal = 2
  ..\Trace = 0

..\LowpassFilter\..
  ..\eFilterFamily = 4
  ..\eFilterType = 0
  ..\fCornerFreq = 50
  ..\bIsSelected = 1
```

Fit Settings

```
..\FitDlgOption\..
  ..\Method = 1
  ..\Region = 0
  ..\Signal = 2
  ..\Trace = 0

..\FittingOptions\..
  ..\eSearchMethod = 3
  ..\eFunctionType = 13
  ..\eWeightingType = 0
  ..\eMinimMethod = 0
  ..\bFreeAndRefit = 0
  ..\bAutoZeroShift = 1
  ..\bCompareModels = 0
  ..\bFreeAndRefit = 0
  ..\uDlgFitOrder = 1
  ..\uFitOrder = 1
  ..\bAutoAdjustOnFailure = 1
  ..\bDlgUseChebyFilter = 1
  ..\uFirstFitIndex = 0
  ..\bApplySignRestrictions = 0
  ..\bAutoDefaultOptions = 1
  ..\bForceAutoSeed = 1
```

Save As Settings and Options

```
..\FileSaveAsDialog_CAnalysisDocTemplate\..
  ..\Extension = ".abf"
  ..\FileType = "Axon Binary File (floating point) (*.abf)"

..\SaveOptions\..
  ..\SaveFlags = 0
  ..\DataFlags = 3
  ..\DontShow = 1
  ..\ReductionMethod = 0
  ..\ReductionFactor = 1
  ..\StartAtZero = 0
  ..\AllVisibleTraces = 0
```

VII Error Messages

The existence of the sheet '[SheetName]' indicates that the spikes were already sorted

If you select the Spike Sorting command in a file, in which sheets that are concerned with small or large spikes exist, it is assumed that the spikes have already been sorted. Should you want to re-sort the spikes (e.g. to try a different threshold), all sheets that are concerned with small or large spikes, must be deleted first. These are the sheets named:

- SmallSpikes
- # S Spikes
- S BurstList
- S IEI

- LargeSpikes
- # L Spikes
- L BurstList
- L IEI

- Sorting Results, or
- Floating Threshold

Floating Threshold sheet exists

The existence of a sheet named **FloatingThreshold** usually indicates that the spikes were sorted using a Floating Threshold. When a fixed threshold is specified, although there is a **FloatingThreshold** sheet, XtraCell issues a warning.

If you click **No**, the fixed threshold you specified will be recorded on the Summary sheet. However, to maintain the consistency of the file, you should rename the **FloatingThreshold** sheet, if you chose the **Floating Threshold** option, but sorting was actually done with a fixed threshold (i.e., without changing the preset threshold line).

If you used a Floating Threshold for spike sorting, you should click **Yes**, or manually enter **floating** into the **Threshold** field on the **Summary** sheet, depending on the kind of evaluation you actually did.

Floating Threshold sheet does not exist

The existence of a sheet named **FloatingThreshold** indicates that the spikes were sorted using a **Floating Threshold**. If you checked the respective check box, XtraCell verifies the existence of this sheet and issues a warning when it is missing.

If you click **No**, XtraCell creates a **Summary** sheet anyway and records **floating** into the **Threshold** field. But if you, in fact, used a **Floating Threshold** for **Spike Sorting**, this message indicates that there is something wrong. The integrity of the evaluation, as well as its documentation, require that this sheet exists in the file. Unfortunately, there is no way of reconstructing a **Floating Threshold**. So you will have to delete all sheets from **SmallSpikes** to the end and do the sorting again.

If you did not use a Floating Threshold, click **Yes** to specify the fixed threshold you used.

Too few sheets to create a Summary

Before the **Summary** sheet can be created, the woorkbook must contain **EACH** of these sheets:

SpikeTimes
 # Spikes
BurstList
IEI

If the spikes were sorted, as is indicated by the presence of either of the sheets **SmallSpikes** or **LargeSpikes**, there must additionally be **EACH** of the following sheets:

SmallSpikes
 # S Spikes
S BurstList
S IEI

LargeSpikes
 # L Spikes
L BurstList
L IEI

If any of these sheets is missing - even if it contains nothing but the header row - XtraCell cannot create a **Summary** sheet.

Validation Error

Many procedures, such as **Spike Sorting**, require parameters within a certain range. You can specify these values by using the spinner controls, or you can enter them into the text fields using the keyboard. In the latter case, if a value exceeds the allowable range or is non-numeric, XtraCell issues a **Validation Error**, giving you the upper and lower limit of the respective parameter.

Note: This message may also mean that you used a comma (**,**) as decimal separator, while a decimal point is specified in your control panel settings (as recommended), or vice versa.

Unexpected Error

This error message means that a runtime error has occurred that cannot be handled by the program code. Although I carefully tested and debugged XtraCell, it is impossible to cope with all possible error sources in non-commercial software. That does not even appear to be possible in commercial software.

The most probable reason for an unexpected error is an unexpected data structure. Carefully make sure, your data match the **Expected Structure of Input Data** (Appendix II). Then verify that the system you run matches the **System Requirements** (Section 2). Then try to find a colleague who can do programming in Visual Basic 6. If that doesn't help either, try a rain dance around your computer. Then try the rain dance together with colleagues.

Only if there is **no other way**, contact me at xtracell@jan-dolzer.de. I cannot promise to reply the same day, nor can I warrant any support (it is free software, isn't it?). If I find the time, I will look into it. To do so, I need to reproduce your problem. So if it occurs with a particular data file only, I will need this file. In any case, please provide the information given in the error message, your Windows- and Office/Excel version and as much additional information as you can. And again, please contact me only, if you absolutely cannot solve the problem yourself. Thank you very much.

Part II

Patch Clamp Recordings

Chapter 5

Pharmacological investigation of ion channels in cultured olfactory receptor neurons of the hawkmoth *Manduca sexta*

Jan Dolzer[1,2,*] and Monika Stengl[1,2]

[1] Biologie, Tierphysiologie, Philipps-Universität Marburg, D-35032 Marburg, Germany

[2] Institut für Zoologie, Universität Regensburg, D-93040 Regensburg, Germany

* Corresponding author: olfaction@jan-dolzer.de

Summary

Biochemical and physiological evidence have suggested the involvement of cyclic guanosine-3',5'-monophosphate (cGMP) in adaptation of pheromone-sensitive olfactory receptor neurons of moths. To determine, whether cGMP acts on ion channels, we investigated single-channel and whole-cell currents in cultured ORNs of the sphinx moth *Manduca sexta* in cell-attached, inside-out and perforated patch clamp recordings. Both, single-channel and perforated patch recordings, revealed a large variety of ion channels and currents that, in part, appeared to be activated by rises in the cytoplasmic Ca^{2+} concentration. Two classes of nonspecific cation- or anion channels were apparently activated by the membrane-permeant cGMP analogue 8-bromo cGMP (8bcGMP), but also by protein kinase C activation via the application of phorbol ester. One of these channel classes with a single-unit conductance between 30 and 70 pS exhibited fluctuating inward currents, while the outward currents were more stable. The other channel class with a conductance above 70 pS is apparently a chloride- or anion channel and was not sensitive to a variety of blockers. Both channels classes were present in multiple copies per patch and were frequently activated in close temporal correlation, suggesting the presence of transducisomes.

In perforated patch recordings, a number of currents were recorded that had been described in moth ORNs before. For some of these currents, knowledge about their dependence of cyclic nucleotides has been added. Three currents were newly discovered, which have not been recorded in moth ORNs so far. A slowly inactivating delayed rectifier K^+ current, termed I_{Ki}, was activated by 8bcGMP and, to a weaker extent, by 8-bromo cAMP (8bcAMP). It shares properties with some *Shaker* channels, but also has similarities to *ether-á-go-go* (EAG) channels. Another current, which very slowly activated after depolarization and slowly inactivated after hyperpolarization, was observed less frequently after application of 8bcAMP, but not 8bcGMP. The slow time course of this current, which we termed I_{LL}, is also reminiscent of EAG-related currents. The third current is a nonspecific, large-conductance current that appeared to be irreversibly activated by a rise of intracellular Ca^{2+}.

Introduction

Adaptation, the adjustment of sensitivity in response to adequate stimulation, enlarges the dynamic range of an olfactory receptor cell without loss of resolution, and provides the first stage of processing sensory information. At least two second messengers, calcium and cyclic GMP (cGMP), play important roles for the various forms of olfactory adaptation in moths. Calcium concentration changes appear to influence processes of short-term adaptation in insect olfactory receptor neurons (ORNs). Calcium appears to exert its effect directly, as well as via protein kinase C (PKC) activation (Stengl, 1993). A delayed increase of cGMP levels (Ziegelberger et al., 1990; Stengl et al., 2001) has been suspected to be involved in long-term adaptation, presumably via activation of a G-kinase (Boekhoff et al., 1993). The reduction of the response to pheromone after cGMP application that was observed in *Bombyx mori* (Redkozubov, 2000) and *Manduca sexta* (Chapter 3) further support the assumption that this messenger plays a role in olfactory adaptation. In addition, Chapter 3 presents evidence for the influence of cGMP on two types of ion channels, nonspecific cation- or anion channels and delayed rectifier K^+ channels.

The investigation of adaptation in pheromone-sensitive trichoid sensilla of male *Manduca sexta* moths suggested the presence of three adaptation mechanisms (chapter 2). One mechanism influences properties of the early phase of the sensillar potential, suggesting an influence on an early step in the transduction cascade. A second adaptation mechanism additionally reduces the action potential response, presumably acting on the voltage-gated

ion channels that are involved in action potential generation. It appears more likely that this adaptation mechanism influences the delayed rectifier potassium than the voltage-gated sodium channels (Hille, 2001). A third adaptation mechanism accelerates the declining phase of the sensillar potentials, presumably via stabilization of the resting potential of the ORNs.

To find out, which of these adaptation mechanisms is cGMP-dependent, we investigated the influence of membrane-permeant derivatives of the cyclic nucleotides cGMP and cAMP on ion channels and currents in single-channel- and perforated patch clamp recordings of cultured ORNs. Due to the large variability of ion channel types among individual ORNs and the high density of most of the channel types, it was not possible to discern statistically significant effects of cGMP in single-channel recordings. Some of the whole-cell currents recorded in the perforated patch experiments, however, were significantly influenced by cGMP and / or cAMP.

Materials and Methods

Solutions

Unless indicated otherwise, all chemicals and biochemicals were obtained from Sigma (Deisenhofen, Germany), all cell culture media from Gibco (Karlsruhe, Germany). Solutions for cell culture were prepared with autoclaved water and filtered for sterilization. The salts for the electrophysiological salines were obtained from Merck (Frankfurt/M, Germany).

Cell culture

- **ConA/polyL**: Concanavalin A / poly-D-lysine coating solution
  165 µg ml^{-1} concanavalin A
  15 µg ml^{-1} poly-D-lysine

- **HBSS/PS**: Hank's Balanced Salt Solution with Penicillin/Streptomycin
  15% 10xHBSS
  1.5% Pen/Strep (5000 units ml^{-1} penicillin G sodium / 5000 mg ml^{-1} streptomycin sulfate)
  370 µmol l^{-1} 1-Phenyl-3-(2-thiazolyl)-2-thiourea

- **CLNM**: Cell Line Nutritive Medium
  90% Grace's Insect Medium
  10% FBS
  3 g l^{-1} TC Yeastolate
  3 g l^{-1} lactalbumin

- **2:1** cell culture medium
  67% L-15 5% FBS:
    95% Leibovitz's medium (L-15)
    5% Fetal Bovine Serum (FBS)
    12 g l^{-1} mannitol
  33% conditioned medium:
    Supernatant fraction from a *Manduca sexta* cell line (Eide et al., 1975; MRRL-CH1 cells, generously provided by D. Lynn; see Stengl and Hildebrand, 1990) grown in CLNM for 2–4 weeks.

Electrophysiology

All solutions were adjusted to pH 7.1–7.2. The osmolality was adjusted with mannitol to 370–390 mosmol l^{-1} for bath solutions and to 330–350 mosmol l^{-1} for pipette solutions, respectively.

Table 1: Bath solutions.

	NaCl	KCl	CaCl$_2$	BAPTA	TEA-Cl	NiCl$_2$	ZnCl$_2$	NMDG	HEPES	D-glucose	TTX
sTTX	156	4	6						10	5	10^{-8} M
sTTX/TEA	136	4	6		20				10	5	10^{-8} M
sTTX/1Zn	154	4	6				1		10	5	10^{-8} M
sTTX/10Zn	136	4	6				10		10	5	10^{-8} M
sTTX/Ni	156	4				6			10	5	10^{-8} M
sTTX/TEA/Ni	136	4			20	6			10	5	10^{-8} M
sTTX/-7Ca	156	4	0.5	1					10	5	10^{-8} M
sTTX/NMDG			6					160	10	5	10^{-8} M
sTTX/NMDG/-7CA			0.5	1				160	10	5	10^{-8} M

All concentrations, except TTX are given in mmol l^{-1}.
BAPTA: 1,2-bis-(2-aminophenoxy)-ethane-N,N,N',N'-tetraacetate
TEA-Cl: tetraethylammonium chloride
NMDG: N-methyl-D-glucamine
HEPES: N-(2-hydroxyethyl)-piperazine-N'-(2-ethane sulfonic acid)
TTX: tetrodotoxin

Table 2: Pipette solutions.

	CsCl	KCl	NaCl	CaCl$_2$	BAPTA	TEA-Cl	ZnCl$_2$	HEPES	CsAc	CaAc$_2$
Cs	160			0.5	1			10		
Cs/TEA	140			0.5	1	20		10		
Cs/10Zn	140			0.5	1		10	10		
Cs/Ca	148			6				10		
Cs/Ac					1			10	160	0.5
K		160		0.5	1			10		
K/Ca		148		6				10		
K/Na		155	5	0.5	1			10		

All concentrations are given in mmol l^{-1}.
BAPTA: 1,2-bis-(2-aminophenoxy)-ethane-N,N,N',N'-tetraacetate
TEA-Cl: tetraethylammonium chloride
HEPES: N-(2-hydroxyethyl)-piperazine-N'-(2-ethane sulfonic acid)
Ac: acetate

Bath solutions with reduced chloride concentration were obtained by mixing with solutions produced using the respective acetate- (sTTX/Ac, sTTX/TEA/Ac, sTTX/Ni/Ac) and D-gluconate salts (sTTX/Glc). These are referred to as sTTX/Ac/10% (meaning 90% sTTX/Ac + 10% sTTX), or sTTX/Glc/20% and analogously. Likewise, solutions with reduced Ca^{2+} were obtained by mixing sTTX and sTTX/-7Ca.

In analogy to the bath solutions, pipette solutions with reduced chloride concentration were produced by mixing Cs and Cs/Ac, and are referred to as Cs/Ac/10%, etc. The Cs$^+$ solutions were only used in the single-channel recordings, while all perforated patch clamp recordings were done using K$^+$ solutions. For perforated patch clamp recordings, 0.6 mg amphotericin B were dissolved in 10 µl dimethylsulfoxide (DMSO) and added to 2.5 ml pipette solution, yielding a final concentration of 260 µmol l^{-1} amphotericin B and 0.4% DMSO.

Cell culture

Cell cultures were prepared according to Stengl and Hildebrand (Stengl and Hildebrand, 1990). Briefly, male pupae were staged using external markers. For each dispersion, two animals were anesthetized by cooling on ice, and the antennae were dissected in HBSS/PS. Antennal tubes were washed 4 times in HBSS/PS and incubated in HBSS/PS + 7 mmol l^{-1} ethylenglycol-bis-(b-amino-ethylether)-N,N,N',N'-tetra-acetic acid (EGTA) at 37 °C for 5 min. The tissue was digested with papain (1 mg ml^{-1} in HBSS/PS) in two batches for 5 and 10 min at 37°C, respectively. The digestion was stopped by adding L-15 supplemented with 10% FBS, cells were centrifuged at 800–1000 rpm for 5–8 min, and the pellet was resuspended in HBSS/PS. The cells were plated out in glass-bottom culture dishes, coated with ConA/polyL and allowed to settle for 15–30 min before adding 1 ml of 2:1 cell culture medium. The medium was replaced completely within 24 h after the dispersion. Every 4–7 days, part of the medium was replaced subsequently. The cell cultures were used for electrophysiology for up to 4 weeks.

Electrophysiology

For the patch clamp recordings, the culture medium was removed, the cultures were washed with about 1 ml of sTTX, and the dish was placed in the recording setup with about the same volume of sTTX. The culture dishes were continuously perfused with saline at a low flow rate, using a gravity feed perfusion system equipped with 6 reservoirs and a Teflon rotary valve (Rheodyne, Rohnert Park, California). The cells were viewed with an inverted microscope (Axiovert 35 or 135, Zeiss, Göttingen, Germany) equipped with phase contrast optics and an additional heat filter (KG-1, Zeiss). Exposure of the cells to light was kept as low as possible by using low light intensity and placing a piece of black cardboard in the beam whenever no optical control was necessary. Olfactory receptor neurons were identified by their round or only slightly spindle-shaped soma of 5–10 µm diameter. Each recorded cell was documented photographically. Drugs were applied either by switching the perfusion to a different reservoir, by puff application with a PicoSpritzer (General Valve, Fairfield, New Jersey), or by adding the agent into the bath with a pipetteman. The change of solutions was monitored by about 0.1% food dye (McCormick, Baltimore, Maryland) added to the bath solutions. The patch clamp headstage and the drug application pipette were mounted on electronic micromanipulators (Luigs & Neumann, Ratingen, Germany) attached to aluminum profiles (X-95, Newport, Irvine, California).

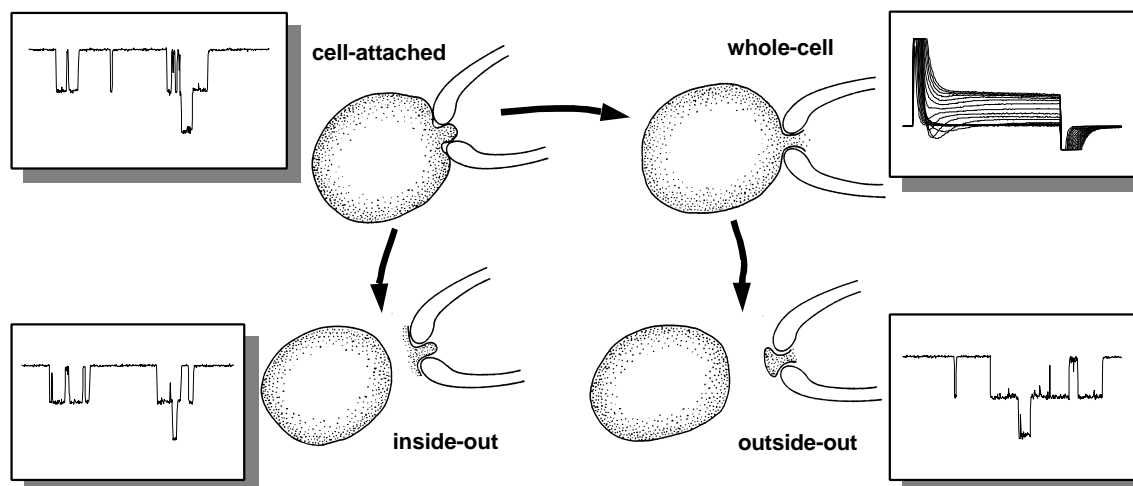Cell-attached- and inside-out patch clamp recordings were performed according to standard

Fig. 1: A brief overview of the patch clamp configurations. After a glass electrode (=pipette) smoothened by fire-polishing is sealed to the membrane of a cell, single-channel currents can be recorded in this so-called cell-attached (=on-cell) configuration. The pipette voltage cannot deliberately control the membrane potential of the patch, since the resting potential of the cell adds to the clamp voltage. To determine the membrane potential, the resting potential of the cell must be determined in current clamp mode or, indirectly, by the reversal potential (=zero-current potential) of known ion channels. By retracting the pipette, the membrane patch is excised. The configuration is now called inside-out, because the inside (=cytoplasmic face) of the patch faces the outside solution in the bath. In inside-out configuration, only the pipette voltage controls the membrane potential. Agents acting on the cytoplasmic face can be applied, and the ionic conditions that the inside of the patch faces can be altered by changing the bath solution.

When, in cell-attached configuration, the membrane patch under the recording pipette is destroyed by applying gentle suction or a short, large voltage pulse, currents through the membrane of the entire cell are measured. In these whole-cell currents, no single channels can be resolved (insert). The membrane potential is entirely under the control of the pipette voltage. The inside of the cell membrane faces the solution in the pipette, while the bath solution, to which the outside is exposed, can be exchanged. The cell is rapidly perfused with the pipette solution in this configuration, so that macromolecules or messengers in the cytoplasm are washed out. Perforated patches, as performed in this study, avoid this disadvantage by not destroying the membrane patch, but inserting pore formers that only allow ions or small molecules to pass. In this way, the electrical access to the cell is similar to the whole-cell configuration, but no cytoplasmic factors are washed out. Finally, an outside-out patch is obtained by withdrawing the recording pipette from the whole-cell configuration. The lipophilic membrane rapidly closes again in the aqueous surroundings to form a small patch. Like in the whole-cell configuration, the outside of the membrane faces the bath, but due to the smaller membrane area, single-channel currents are recorded in the outside-out configuration.

In cell-attached and inside-out configurations, currents flowing into the recording pipette are currents from the **inside** to the **outside** of the membrane. In whole-cell and outside-out configurations, in contrast, currents flowing into the pipette are currents form the **outside** to the **inside** of the membrane. Therefore, depending on the configurations, the signs of the recorded currents and the applied pipette potentials must be inverted. According to the cell-oriented convention commonly used, in all figures presented in this study, **positive** currents are **outward**, while all **negative** currents are **inward**. Positive membrane potentials are **positive** on the **inside** of the membrane with respect to the outside, and vice versa. The figure was adapted from Hille, 2001.

procedures (Hamill et al., 1981). See Fig. 1 for a brief overview. In perforated patch recordings, the electrodes were tip-filled with pipette solution and back-filled with pipette solution containing amphotericin B. Signals were amplified with an Axopatch 1D amplifier (Axon Instruments, Union City, California), passed through the built-in anti-aliasing filter at a cutoff frequency of 2 kHz, digitized in a Digidata 1200 B digitizer (Axon Instruments) at a sampling rate of 10 or 20 kHz, and stored and analyzed using pCLAMP software (versions 6–8, Axon Instruments). In addition, the signals were continuously recorded on a strip chart recorder (EasyGraf, Gould, Valley View, Ohio) and stored on DAT (DTR-1202, Bio-Logic, Claix, France). When signals were digitized offline from the tape, they were either passed through the amplifier or through an external anti-aliasing filter (900C/9L8L, Frequency Devices, Haverhill, Massachusetts) and digitized at different sampling rates, depending on the filter setting.

In perforated patch recordings, the membrane capacitance, the access (=serial) resistance, the membrane resistance, the time constant of the decay of the capacitive currents in response to a voltage pulse, and the holding current were monitored after seal formation with the Membrane Test feature in Clampex 8. The experiment was started, when the

membrane capacitance and the access resistance did not change anymore. The time course of the Membrane Test parameters was saved to disk. In the further course of the recordings, short Membrane Tests were run to monitor changes in the conditions. Of these tests, only the momentary values were recorded. Since the membrane parameters, as computed by Clampex, were extremely sensitive to the settings of the pipette capacitance neutralization circuitry of the amplifier, only the time course or relative changes, not the absolute values were considered. Likewise, the whole-cell capacitance neutralization controls of the amplifier easily tended to overcompensating the capacitive currents, presumably because of the small size of the ORNs. So this circuitry was set to all-zero and left untouched during the experiments.

Data Analysis

Single-channel recordings

In single-channel recordings, single-unit currents were determined from amplitude histograms created with Fetchan 6 (pCLAMP). When the data had to be lowpass-filtered to improve the signal-to-noise ratio, either the analog 8-pole Bessel filter of the amplifier was used for signal conditioning during off-line digitization from the DAT tape, or the data were conditioned with the digital Gaussian filters implemented in Fetchan 6 or Clampfit 8. The cutoff frequencies were typically between 200 Hz and 1 kHz, but in rare cases cutoff frequencies as low as 50 Hz were also used. The amplitude histograms were fitted with Gaussian functions (2nd to 6th order) in pStat 6 with manual seeding of the initial values. The number of terms was determined manually, often by the comparison of different models. Model comparison, implemented in pStat was not used. Although the measures that describe the "Goodness of Fit", as put out by the software, were recorded, the quality of the fits was almost exclusively judged by eye.

The current-voltage (I-V) relations were determined by one of two methods, depending on the experiment. When a single or few copies of only one channel type were active for a longer period, the holding potential was stepped to different values, and the single-unit currents were determined for each potential. Since typically many copies of one channel type, or different channels were open or exhibited transitions, voltage step protocols with a step duration of 100 ms were applied. To exclude effects of electrical (in)activation, two types of step protocols were applied successively. First the holding potential was stepped from negative (typically -120 mV in inside-out recordings) to positive (100 mV) potential in 20 mV increments. Then the potential was stepped from 0 mV to increasing absolute potential values to negative and positive direction in alternating order (0 mV, -20 mV, +20 mV, -40 mV, +40 mV, etc.). The I-V relations determined in this way were only used for

further analysis, if i) the steady-state current before and after a step protocol was identical, and ii) there was evidence for the contribution of single-unit currents to the steady-state current (such as transitions before or after the step protocols). This was the case in only 3 of 682 voltage step protocols (Fig. 7). In most other cases, unitary currents that contributed to the current before or after step protocols could not be determined.

In many experiments drift of the microscope table or the manipulators led to unintended patch excision. Therefore, cell-attached recordings were distinguished from inside-out- or vesicle recordings by patch excision during or at the end of the recording, whenever possible. Nevertheless, we assume that the intracellular Ca^{2+} concentration was raised by mechanical intrusion in most of the cell-attached recordings.

Perforated patch clamp recordings

In perforated patch clamp recordings, whole-cell I-V relations were determined by the application of five successive voltage step protocols and averaging the current response. The occasional activation of currents during one of the protocols was recognized on the strip chart. In these cases, the current response was re-digitized offline from the DAT tape, and only the step protocols before or after the activation were averaged for analysis.

The presence or absence of a current type was scored from -1 to +2 for each step protocol. The clear absence of a current was scored as -1, while the unambiguous presence was scored as +1. Currents that could not be scored present or absent (because they were defined as drug-activated or would have been obscured by a large current) were scored as 0. A score of +2 was assigned to currents that were very large or predominant in the I-V relation. Frequency indices for each current type were computed by averaging the scores.

All time constants were determined by fitting a first-order exponential function to the data (Clampfit; Exponential Standard; Chebychev fitting algorithm).

Results

Polarity conventions

All voltages and currents are given in a cell-oriented way, according to common conventions. Thus, a positive voltage means that the cytoplasmic face of the membrane is positive with respect to the outside, while a negative voltage describes the opposite polarity. All positive currents are outward currents, negative currents are inward. To obey these conventions, the polarity of cell-attached- and inside-out recordings was inverted accordingly.

Single-channel recordings

In cell-attached and inside-out patch clamp recordings (Fig. 1) we investigated the influence of
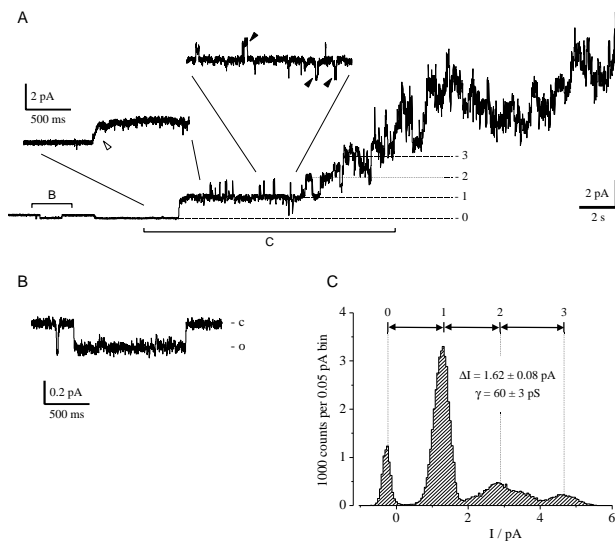
Fig. 2: Medium-sized ion channels activated spontaneously without drug application. In the recording shown, phorbol esters (TPA) were added to the bath about 1h before. (A) In an inside-out recording several copies of a channel of about 60 pS single-unit conductance activated in rapid succession at a membrane potential of +27 mV. The initial opening of the first channel copy took almost 100 ms, suggesting several substates that could not be resolved, or vesicle formation (open arrowhead in the insert). Successive openings of the second channel copy, as well as closings to the zero-level (filled arrowheads) had sharp transitions, however, excluding vesicle formation. Scaling is identical in both inserts. (B) Before the activation of the medium-sized channels a small channel with very long dwell times was active. This channel conducted inward currents at the positive membrane potential, suggesting a calcium channel. c: closed state, o: open state. (C) Amplitude histogram of the section indicated in A. The numbers above the peaks correspond to the current levels indicated in A. After the activation of the third channel copy, distinct current levels could not be detected anymore. Data were lowpass-filtered at 1 kHz.

the membrane-permeant cGMP analogue 8-bromo cGMP (8bcGMP) on cation channels in cultured ORNs of *M. sexta*. Voltage-gated Na^+ and K^+ channels were blocked with tetrodotoxin (TTX) in the extracellular saline and Cs^+ in the pipette solution. In a total of 116 recordings, we regularly observed three classes of ion channels, small, medium-sized, and large.

In the majority of the recordings, the patches were excised during the experiments. Due to mechanical drift, it is very likely that about 98% of the cell-attached recordings were performed under inside-out conditions, i.e., elevated intracellular Ca^{2+}. Therefore, for the analysis of drug effects, these configurations were pooled. For the calculation of single-channel conductances, only those cell-attached recordings were used, in which there was evidence for the resting potential of the cell, such as the apparent reversal potential of nonspecific channels.

Small channels

Small channels of 2–20 pS single-unit conductance were observed in 17 out of 116 recordings. When the absence of other active channels allowed the analysis of their kinetics (n=3), the small channels displayed dwell times of many seconds, as shown in Fig. 2B. In this inside-out recording they conducted inward currents at a membrane potential of +27 mV, suggesting a Ca^{2+} channel. Being obscured by larger channels in most recordings, a founded analysis of the I-V relation and behavior of the small channels was not possible, however.

Medium-sized channels

The medium-sized channels, which were nonspecific cation channels, as judged from their reversal potential around 0 mV, were found in the majority of the patches. Different populations with a conductance in the range of 30–70 pS but different current-voltage relations, pharmacology and kinetics were recorded. The open times ranged from rapid flickering to dwell times of many seconds.

One class of medium-sized channels activated without drug application in many inside-out-, but also in some cell-attached patches, suggesting a calcium-dependence. Once activated, these channels did not inactivate in salines with reduced Ca^{2+} concentration (10^{-4}–10^{-7} mol l^{-1}), however (N=11). These channels were always observed in at least 3 copies per patch. Individual transitions between open- and closed states could take up to 100 ms (Fig. 2), while immediately before or after these slow transitions, very sharp transitions were observed (N=6 openings and 3 closings in different recordings). This suggests the presence of several subconductance levels that are too small to resolve. Spontaneous or excision-dependent activation of this channel type always involved multiple copies in rapid succession, as shown in Fig. 2, which prevented the analysis of the I-V relation during a single recording. Summarizing the observations of all recordings done in this study (Fig. 9A), the channels of 30–70 pS single-unit conductance reverse around 0 mV. Their I-V relation is presumably linear, but inwardly rectifying channels were also observed with Cs solution in the pipette and sTTX in the bath (Fig. 7). The inward currents conducted by this channel type were much more transient and noisy than the outward currents, suggesting a limited permeability to Cs^+ (Fig. 5). At membrane potentials more negative than -40 mV, no more unitary currents, but only current fluctuations could be observed (Fig. 9A). This property and the presence of multiple channel copies prevented a quantitative analysis of these channels. Protein
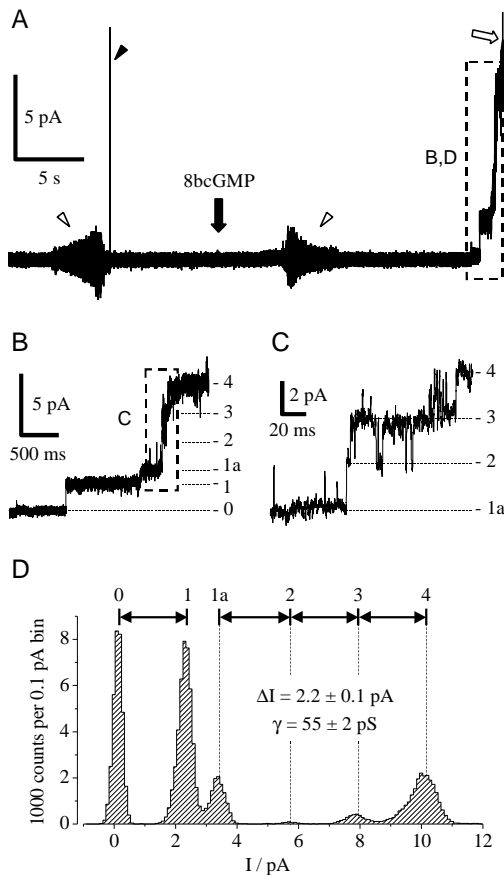
Fig. 3: At least 4 copies of a medium-sized ion channel activated after puff application of 8 bromo cyclic GMP (8bcGMP). (A) Several nl of a 10 mmol l^{-1} 8bcGMP solution were applied to an inside-out patch in sTTX at a membrane potential of +40 mV. The high-frequency artifacts (open arrowheads) indicate, when the application pipette was moved into and out of the bath. The large, transient artifact (filled arrowhead) occurred when the pipette first touched the surface of the bath. About 20 s after drug application several copies of a channel activated in rapid sequence (indicated section shown at an enlarged time scale in B). About 2 s after the first observed channel activity, a current of >100 pA developed (open arrow; truncated), in which no single-channel currents could be resolved. (C) Enlarged view of the section indicated in B. Individual channel openings and closings can be seen. (D) Amplitude histogram of the section shown in B. The differences in the current levels (ΔI) were 2.2±0.1 pA, corresponding to a single-unit conductance (γ) of 55±2 pS (means ± SD). A smaller channel with a conductance of about 28 pS caused the transition from current level 1 to 1a. Current levels in B–D correspond to each other. Data were lowpass-filtered at 2 kHz.

kinase C activation by the application of phorbol ester (TPA) appeared to enhance the activation of this channel class (Fig. 9A).

In 2 of 7 experiments, medium-sized channels that had activated spontaneously or after patch excision were blocked by 10 mmol l^{-1}, but not by 1 mmol l^{-1} Zn^{2+} applied to the cytoplasmic face, and were insensitive to 20 mmol l^{-1} TEA (Fig. 6). While

Zn^{2+} is known as a chloride channel blocker that also affects other channels at concentrations as high as 10 mmol l^{-1}, TEA blocks K$^+$- and a number of other cation channels. Spontaneous or excision-dependent activation of medium-sized channels was also observed with 10 mmol l^{-1} Zn^{2+} in the pipette solution (N=25 of 31 experiments), indicating that only a subpopulation of these channels is zinc-
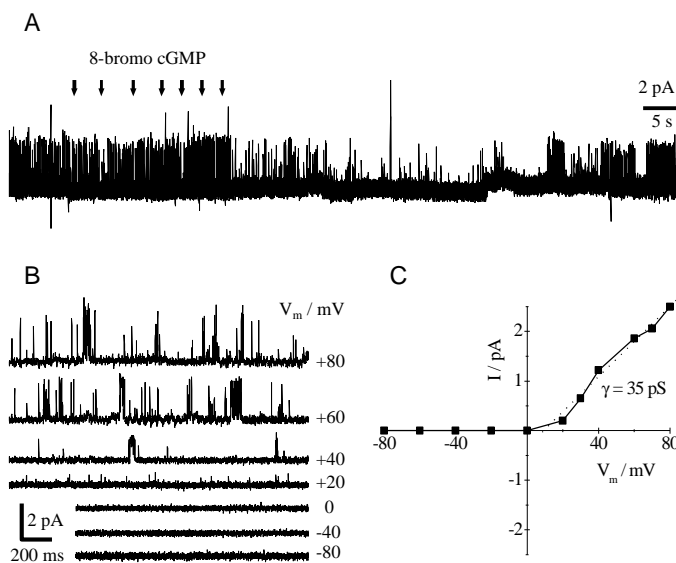
Fig. 4: An outwardly rectifying channel was transiently inactivated by 8-bromo cGMP. (A) The application of several pulses of 8-bromo cGMP (arrows) to an inside-out patch at a membrane potential of +80 mV inactivated a single copy of an active channel. After about 40 s of wash the channel gradually regained its original activity. (B)–(C) Current-voltage relation of the same channel type obtained in another inside-out recording. (B) The patch was held at different potentials for several seconds, and the single-unit conductance was determined by amplitude histograms (not shown). While the channel conducted no inward currents, the slope conductance of the outward currents was about 35 pS (C). Data were lowpass-filtered at 1 kHz.

A

8bcGMP

B

8bcGMP   TEA

10 pA
10 s
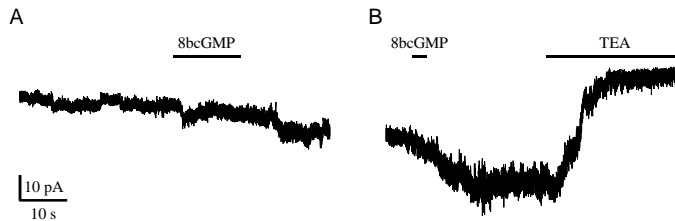
Fig. 5: One type of medium-sized channels was activated by 8-bromo cGMP (8bcGMP) and blocked by tetraethylammonium (TEA). (A) The same channels that conducted steady outward currents at positive potentials (Fig. 7A) exhibited irregular and unsteady currents at a membrane potential of -40 mV. During the initial 25 s, an amplitude histogram (not shown) revealed current levels of about 2.8 pA, corresponding to a single-unit conductance of 70 pS. After the application of 9 pulses of 10 mmol l^{-1} 8bcGMP (several nl per pulse) during the indicated interval, the current slightly increased. Single-channel activity could not be detected anymore. (B) About 35 s after the end of trace A, 6 more pulses of 8bcGMP were applied, leading to a further increase in the current without detectable current levels. The application of 20 mmol l^{-1} TEA in the bath solution eliminated the current except for a residual that had been present from the beginning of the recording. Data were lowpass-filtered at 2 kHz.

10 mM Zn^{2+}

20 mM TEA

1 mM Zn^{2+}

10 pA
500 ms

10 mM Zn^{2+}
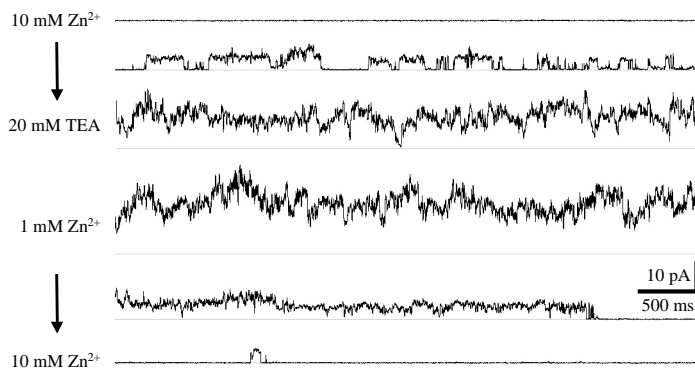
Fig. 6: A subpopulation of the medium-sized channels was sensitive to high concentrations of zinc. About 25 s after an inside-out patch held at V_m = +80 mV was exposed to sTTX/10Zn bath solution, all previously active channels were closed (upper trace). When the zinc was washed out with sTTX/TEA channel activity reappeared (second trace), until after the complete replacement of the bath solution no distinct current levels could be detected anymore (third trace). In a bath solution containing 1 mmol l^{-1} of zinc (fourth trace), channel activity continued to the same amount as in sTTX (not shown) and sTTX/TEA. The even higher average current than in the previous trace is probably due to the fact that the wash out of the higher zinc concentration was still incomplete. Switching back to sTTX/10Zn blocked the channel activity again (bottom two traces). Note that distinct current levels were only observed during the wash out and wash in of the sTTX/10Zn solution, as indicated by the arrows on the left. The amplitude histograms of traces 2 and 5 suggested a single-unit conductance of about 40 pS, but the presence of many substates (not shown). In traces 3 and 4 no distinct current levels could be detected.
The dotted lines indicate the zero-current levels. Traces were separated by about 1 min each, except for traces 5 and 6, which are consecutive. Data were lowpass-filtered at 2 kHz.

sensitive. In other recordings, the currents through medium-sized channels were reduced by TEA (N=3; Fig. 5), indicating that another subpopulation is sensitive to this blocker.

Large channels

In addition to the small and the medium-sized channels, large channels of more than 70 pS were observed. Like most of the medium-sized channels, they typically activated without any drug application or other obvious change in the conditions. Frequently the activation was correlated to the activation of medium-sized channels, giving the impression of a coupling mechanism. Single-unit conductances of up to 550 pS were observed (Fig. 8), in one recording even 1.7 nS (not shown), but the transitions between the conductance states again suggest the presence of multiple substates. In most observations, the single-unit conductance of the large channels was below 250 pS, but distinct conductance classes could not be detected (Fig. 9).

Once activated, the large channels were almost unaffected by replacing all cations in the bath solution with N-methyl-D-glucamine (NMDG), a very large cation impermeant to most cation channels. This suggests that the large channels are chloride- or nonspecific anion channels. The tested agents known as chloride channel blockers (6 mmol l^{-1} Ni^{2+}, 10 mmol l^{-1} Zn^{2+}, 1 mmol l^{-1} 4-acetamido-4-thiocyano-stilbene-2,2'-disulfonic acid (SITS), 1 mmol l^{-1} 4,4'-diisothiocyanostilbene-2,2'-disulfonic acid (DIDS), 1 mmol l^{-1} 2-(3-trifluoromethyl-anilino)-nicotinic acid (niflumic acid), 500 µmol l^{-1} anthracene-9-carboxylic acid, 100 µmol l^{-1} picrotoxin) did neither influence the medium-sized, nor the large channels, however.

Effects of protein kinase C activation

After activation of protein kinase C (PKC) with phorbol esters (TPA; N=58), medium-sized channels were observed more frequently (Fig. 9). Typically, however, the detection of single-channel currents was even more difficult after the application of this agent. In most recordings, large currents (up to several tens of nS in aggregate conductance) developed after TPA application, in which no single-channel activity could be discerned. Only the fact that these currents typically developed in the course of several 100 ms and occasionally inactivated later, distinguished them from a broken seal. All agents tested (TEA, Ni^{2+},
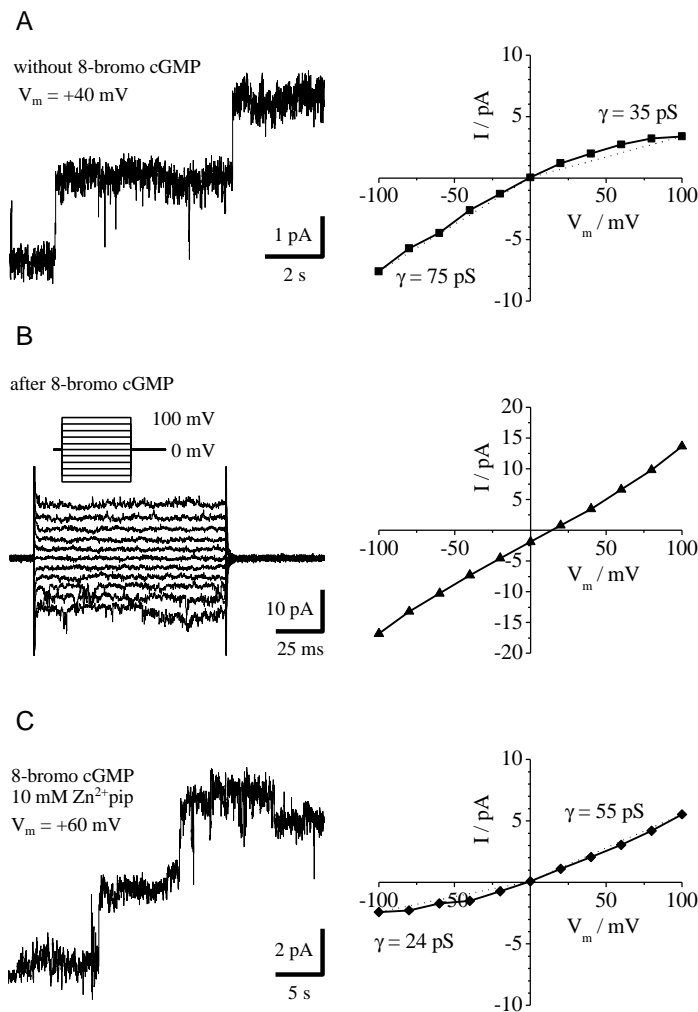
A

without 8-bromo cGMP
$V_m = +40$ mV

1 pA

2 s

$\gamma = 35$ pS

I / pA

V_m / mV

$\gamma = 75$ pS

B

after 8-bromo cGMP

100 mV

0 mV

10 pA

25 ms

I / pA

V_m / mV

C

8-bromo cGMP
10 mM Zn^{2+}pip
$V_m = +60$ mV

2 pA

5 s

$\gamma = 55$ pS

I / pA

V_m / mV

$\gamma = 24$ pS

Fig. 7: Medium-sized channels with different current-voltage (I-V) relations. (A) A medium-sized channel with dwell times of many seconds was active after patch excision. Immediately after the trace shown, a voltage step protocol was applied. Afterwards, the current amplitude was the same as before, and another channel copy of the same conductance activated. Thus, a single-channel I-V curve was computed basing on the observed single-channel current of 1.85 pA at +40 mV. The channel is an inward rectifier with chord conductances of 35 pS at positive and 75 pS at negative potentials, respectively. (B) After puff application of 8-bromo cGMP, a relatively steady current of about +7 pA at +60 mV was observed before and after the step protocol shown. The I-V relation was linear, with a reversal potential of about +15 mV. The total slope conductance of about 150 pS suggests that the current was conducted by 3 channel copies. (C) In a different recording, two copies of a medium-sized channel activated shortly before puff application of 8-bromo cGMP, probably due to the cyclic nucleotide leaking out of the application pipette. A single-channel I-V relation could be determined in the same way as in A, suggesting a linear, zero-crossing current of 55 pS conductance. The inward currents were most likely reduced by 10 mmol l^{-1} Zn^{2+} included in the extracellular solution. Data were lowpass-filtered at 200 Hz in A and C and at 2 kHz in B.

Zn^{2+}, SITS, DIDS, niflumic acid, anthracene-9-carboxylic acid, picrotoxin) influenced this current to only a marginal extent or not at all. Only the large cation NMDG reduced the current by about 10% in 5 of 7 experiments.

Effects of 8-bromo cGMP

The membrane-permeant cGMP analogue 8-bromo cGMP (8bcGMP) was applied at concentrations between 5 µmol l^{-1} and 10 mmol l^{-1} dissolved in sTTX with an application pipette, and at a concentration of 10 or 100 µmol l^{-1} in the bath solution. Since puff application with a pipette cannot be directed immediately to the patch or cell without destroying the seal, the final concentration the preparation faces is unknown. Since a detailed analysis of all application modes and concentrations did not reveal consistent differences (not shown), they were pooled. Of a total of 77 applications, 49 were puff applications with an 8bcGMP concentration of 10 mmol l^{-1}. Concentrations of 100 or 500 µmol l^{-1} were applied in the same way in 15 experiments, 5 times the concentration was 5 µmol l^{-1}. Bath application at a concentration of 100 µmol l^{-1} was performed twice, in 7 applications

the bath solution contained 10 µmol l^{-1} 8bcGMP. All control applications listed in Table 3 were puff applications with sTTX.

The typically delayed action of 8bcGMP (Fig. 3), in addition to the fact that channels or currents frequently activated by patch excision or mechanical intrusion during cell-attached recordings (i.e., by an increase of the Ca^{2+} concentration on the cytoplasmic side), made it hard to determine, whether an observed activation was caused by 8bcGMP. Thus, for the statistics, every activation within 5 min after drug- or control application was scored as being application-dependent.

All single-channel currents observed in this study are summarized in Fig. 9. In the absence of 8bcGMP, the medium-sized channels dominate. After 8bcGMP application, large channels were observed more frequently. Distinct conductance levels that would allow a more detailed classification of the channels could not be detected. In the figure, the conductances observed in all ionic conditions were pooled. However, when the single channels conductances were analyzed for each ionic condition separately (not shown), distinct conductance levels

could not be discerned either. The apparent absence of inward currents in the absence of 8bcGMP (Fig. 9A) is mainly due to the fact that the medium-sized channels frequently exhibited rapid current fluctuations with no detectable unitary currents. The figure comprises only unitary currents, however.

Table 3 summarizes all observations of activation and inactivation of ion channels or currents after 8bcGMP- or control (sTTX) application, and spontaneous or excision-dependent activation. Currents (+) and large currents (++), in which no unitary currents could be detected, activated after 13 and 18 of 77 applications, respectively (17 and 23%). However, both were also observed after 2 of 9 control applications each (22%). In 20 of 82 observations (24%) currents developed without any drug application. The activation of large currents without drug application was observed in 25 of 82 cases (30%).

Activation of medium-sized channels (m) was observed after 15 of 77 applications of 8bcGMP (19%), never after control application, and in 11 of 82 observations (13%) without drug application. Considering only observations in the absence of the PKC activator TPA, medium-sized channels activated three times as frequently after 8bcGMP application (9 of 49 applications = 18%) than without drug application (2 of 36 observations = 6%). Likewise, in the absence of TPA, large channels activated after 4 of 49 applications of 8bcGMP (8%), but only in 1 of 36 observations without drug application (3%). In the presence of TPA, however, the activation of large channels was observed in 15% (7 of 46) of the observations without drug application, but only after 7% (2 of 28) of the applications of 8bcGMP. This suggests that the medium-sized and the large channels are activated by both, cGMP and PKC.

Inactivation of an active channel by 8bcGMP was observed only once (Fig. 4). It is very likely, however, that inactivation occurred more frequently, but was obscured by the activation of other channels. After 4 applications of 8bcGMP and 2 control applications, patches without any channel activity remained silent (no activation). Currents or channels that had been present before were not activated any further, but not inactivated either, after 3–7 applications of 8bcGMP. The same was observed once for each of the currents, medium-sized- and large channels after control application.
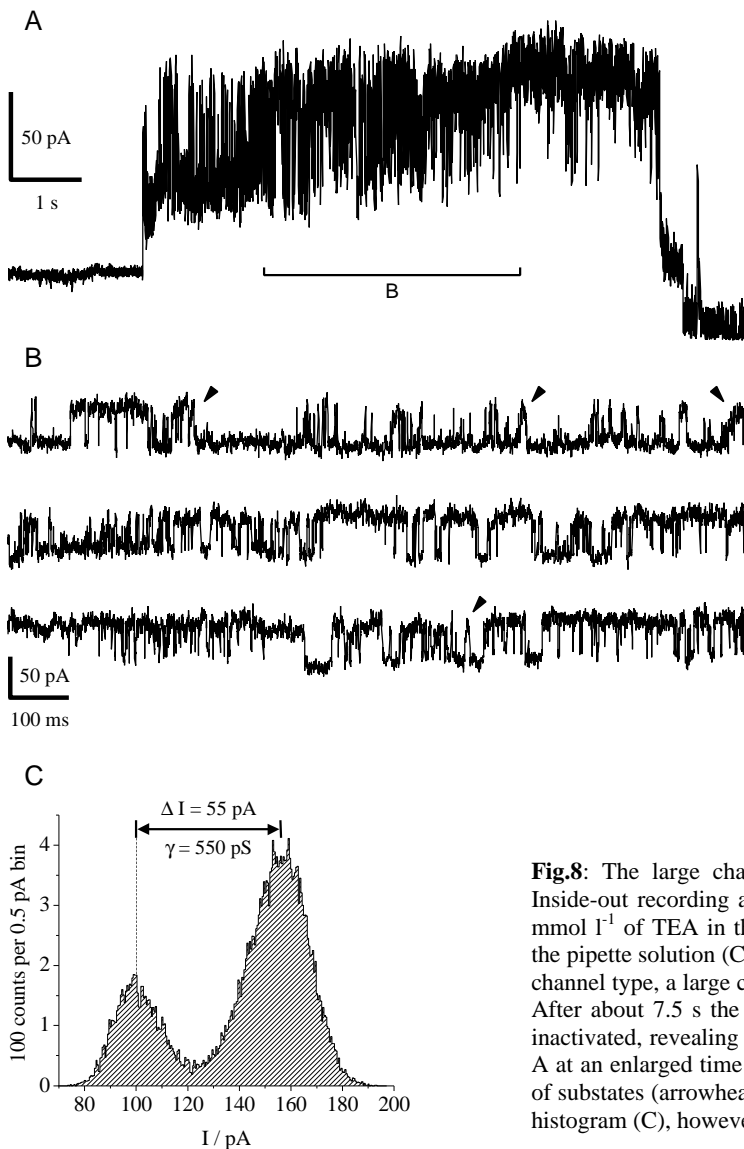
Fig.8: The large channels were not blocked by TEA and Zn^{2+}. Inside-out recording at a membrane potential of +100 mV with 20 mmol l^{-1} of TEA in the bath (sTTX/TEA) and 10 mmol l^{-1} Zn^{2+} in the pipette solution (Cs/10Zn). (A) From the open state of a different channel type, a large channel activated without any drug application. After about 7.5 s the large channel and the initially open channels inactivated, revealing several substates. (B) The section indicated in A at an enlarged time scale. Individual transitions suggest a number of substates (arrowheads), which cannot be resolved in an amplitude histogram (C), however.

Table 3: All observations after drug application.

n observations		no activation	no effect on open channels			activation				in-activation	not evaluable	Σ
			+	m	l	+	++	m	l			
8bcGMP	TPA	2	-	-	-	8	8	6	2	1	1	28
application	no TPA	2	5	3	7	5	10	9	4	-	4	49
Σ 8bcGMP		4	5	3	7	13	18	15	6	1	5	77
control	TPA	-	-	-	-	-	-	-	-	-	-	-
application	no TPA	2	1	1	1	2	2	-	-	-	-	9
Σ control		2	1	1	1	2	2	-	-	-	-	9
without	TPA					15	9	9	7		6	46
application	no TPA					5	16	2	1		12	36
Σ without						20	25	11	8		18	82
Σ total		6	6	4	8	35	45	26	14	1	23	168

Channel activation until 5 min after the application was scored as application-dependent.
8bcGMP: 8-bromo cGMP.
TPA: phorbol ester
+/++: fluctuating currents / large currents without detectable unitary currents
m: medium-sized channels
l: large channels.

A: without 8-bromo cGMP
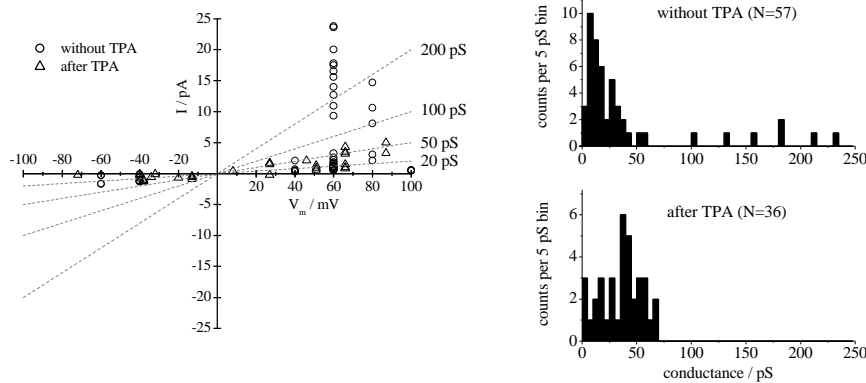
B: after 8-bromo cGMP
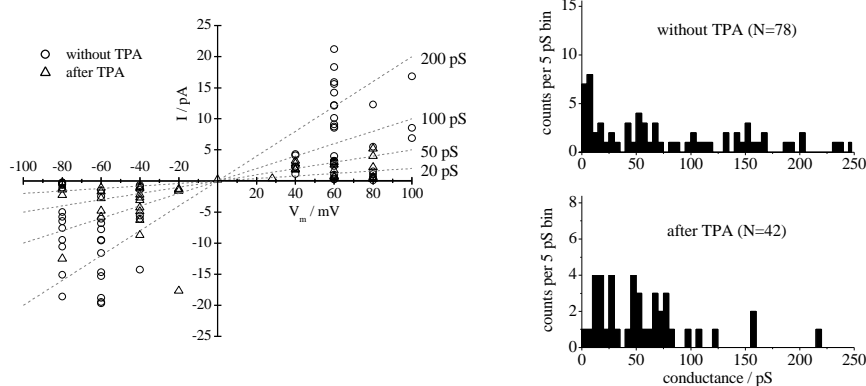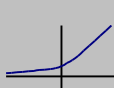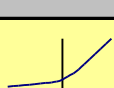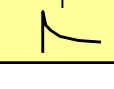
Fig. 9: Single-channel conductances observed with or without the application of phorbol ester (TPA) and 8-bromo cGMP. The figure summarizes all observations of single-channel currents made in the current study. The absence of single-channel observations (as e.g. for larger inward currents in A) does not indicate the absence of channel activity. The inward currents were either fluctuating and unsteady (Fig. 5), or exhibited too many substates or too many active channel types to allow analysis of the single-channel conductances.
(A) In the absence of 8-bromo cGMP and TPA, most observed single channels had a conductance clearly below 50 pS, as shown in the frequency distribution histogram (right, top). After the application of TPA, the conductance of the observed single channels was shifted to the right. (B) After the application of 8-bromo cGMP there was a tendency to large single-unit conductances, both with and without TPA. Inward unitary currents above 50 pS were only observed after the application of 8-bromo cGMP.
Since the number of observations (N) was different in each condition, the Y axes of the histograms are normalized to 0.2 * N.
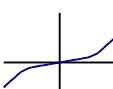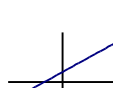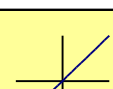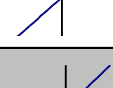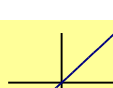
Table 4: Currents and current components in ORNs of Mandcua sexta.

Name	Abbreviation	IV curve	Properties	Activation	Inactivation / Block	No effects
potassium currents						
delayed rectifier	I_K		outwardly rectified IV, delayed activation, TEA block	depol	TEA Cs⁺	Ni^{2+}
cGMP-inactivated outward rectifier	$I_{K (cGMP)}$		outwardly rectified IV, cNMP block	depol	cAMP cGMP ATP	
non-TEA-blockable delayed rectifier	$I_{K (-TEA)}$		outwardly rectified IV, delayed activation, no TEA block	depol	cGMP??	TEA
rapidly inactivating outward rectifier	I_A		not tested	depol	4 AP	
slowly inactivating delayed rectifier	$I_{K i}$		outwardly rectified IV, slow inactivation after depol	cGMP cAMP	TEA (slow, weak)	
calcium-activated outward rectifier	$I_{K (Ca2+)}$		IV flattened in positive V_m	10^{-6} M Ca^{2+}	cGMP	TEA Cs⁺ CTX

Name	Abbreviation	IV curve	Properties	Activation	Inactivation / Block	No effects
nonspecific cation currents						
calcium-dependent	$I_{cat}{}^+{}_{(Ca2+)}$		IV steeper in positive AND negative V_m	10^{-6} M Ca^{2+}	mM Ca^{2+} TEA cGMP?	Ni^{2+}
fast steady, non-inactivating γ (K) > γ (Ca^{2+})	$I_{cat}{}^+{}_s$		clearly negative reversal potential		TEA cGMP?	cAMP
late, large, long-lasting	I_{LL}		slow activation after depol, inactivation after hyperpol	long large depol, Ca^{2+}??	Ni^{2+}? Ca^{2+}?	TEA (partly)
fast	$I_{cat}{}^+{}_?$		linear IV, TEA block	Ca^{2+}	TEA cAMP? cGMP?	
PKC-dependent	$I_{cat}{}^+{}_{(PKC)}$		not tested	PKC	TEA	
unknown						
non-specific cat- or anion	$I_?$		linear IV, no TEA block	cNMP?? Ca^{2+}?		TEA, SITS, (DIDS), 9AC, PTX, Zn^{2+} niflumic acid
inward rectifier	I_{ir}		IV steeper in negative V_m	?	?	

Currents and properties newly described in this study are highlighted in yellow. The currents that were not tested in this study, (I_A and $I_{cat}{}^+{}_{(PKC)}$) are grayed. The currents were scored present or absent according to the current-voltage (I-V) relation and/or the criteria given in the Properties column.

IV: current-voltage relation, cNMP: cyclic nucleotides, depol: depolarization, V_m: membrane potential, hyperpol: hyperpolarization, PKC: protein kinase C, CTX: charybdotoxin, SITS: 4-acetamido-4-thiocyanostilbene-2,2'-disulfonic acid, DIDS: 4,4'-diisothiocyanostilbene-2,2'-disulfonic acid, 9AC: anthracene-9-carboxylic acid, PTX: picrotoxin.

Perforated patch clamp recordings

Current types

In a total of 20 perforated patch clamp recordings, 223 voltage step protocols were applied. Eleven types of currents or current components were distinguished by their current-voltage (I-V) relation, their time course, or their pharmacology (Table 4). The table, in addition, contains two currents, I_A and I_{cat}^+ (PKC), which were not observed in these experiments. Other experiments (Zufall et al., 1991b, M. Stengl unpublished, Hörbrand, 1996, single-channel recordings in this study) suggest their presence, however, so they were included in the table for completeness.

The presence or absence of a current type was scored on a range from -1 to +2 for each voltage step protocol. Definite absence was scored as -1, the unambiguous presence was scored as +1, and very large or predominant currents were scored as +2. Currents that could not be scored present or absent, because they were defined as drug-dependent or would have been obscured by a large current, were scored as 0. Observations, in which a statement about the presence or absence of an individual current was possible (i.e., a score ≠0 was assigned), are referred to as **defined observation**. Frequency indices for each current type were computed by averaging the scores of individual observations (Fig. 10). As in the single-channel recordings, in the course of an experiment there was a tendency to the activation of large currents that could not or only infrequently be reversed by the application of agents known as ion channel blockers.

Potassium currents

Potassium currents, as characterized by their outwardly rectified I-V relation, were typically observed in the beginning of a recording. Six types of K+ currents were distinguished.

- The delayed rectifier current I_K (Fig. 11) is voltage-activated, exhibiting a delayed onset with the full current developing at time constants of about 2–5 ms and a strict outward rectifica-


Fig. 10: (A–B) The presence or absence of a current or current component was scored in the range of -1 to +2 during each voltage step protocol. For currents that were characterized by slow components kinetics (I_{Ki} and I_{LL}), observations before or after the step protocols were analyzed. The frequency indices for individual conditions were computed by averaging the scores. Some of the currents have a higher frequency index in the presence of the blockers TEA (20 mmol l⁻¹) or Ni²⁺ (6 mmol l⁻¹). This is due to the fact that these currents typically activated in the course of the recording, or even in the presence of the blockers, but were not inactivated by the blockers. Therefore, both a frequency index that remains unaltered and an increased frequency index indicate the insensitivity to a blocker. A higher frequency index does not indicate an activation, however. (A) The frequency indices computed from all observations. Since many of the currents could only be scored present or absent under specific conditions (e.g. $I_{K\ (-TEA)}$ could only be detected when TEA was applied to a preparation with active I_K), many zero-scores may contribute to the frequency indices. (B)) The frequency indices computed from only defined observations. The sample sizes (N) , that are variable in these conditions, are given below the figure.

Data are means of the scores ± S.E.M. See Table 4 for the abbreviations of the currents. ★: p<0.05, ★★: p<0.01, Student's t test (blocker versus saline).
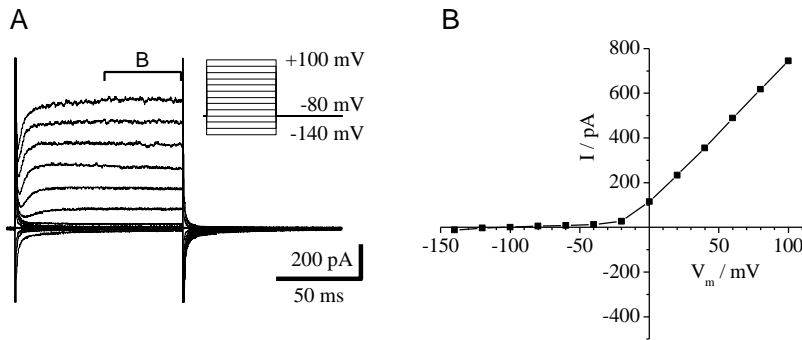
Fig. 11: The delayed rectifier current I_K was frequently observed in the beginning of the recordings. (A) A voltage step protocol applied to a perforated patch elicited outwardly rectified currents that developed to a plateau with a time constant of about 5 ms. The step protocol is shown in the insert: From a holding potential of -80 mV the potential was first stepped to -140 mV for 100 ms, then back to the holding potential for another 100 ms. In each successive sweep, the potential during the step was incremented by +20 mV up to a final value of +100 mV. The current responses to 5 of these standard step protocols were averaged to yield the mean current response. Capacitive transients are truncated for clarity. (B) Current-voltage (I-V) plot of the mean current response in the plateau phase, as indicated in A.

tion. This current is further characterized by its sensitivity to TEA and Cs^+, but is insensitive to millimolar Ni^{2+}. This current was observed in 31 of 155 step protocols with a defined observation. The average frequency index was -0.42±0.06 (mean ± S.E.M.) when all observations were considered, -0.52±0.08 (N=134) under the same conditions, but considering only defined observations (Fig. 10). This current is defined as TEA-sensitive. However, its frequency index remains unchanged (-0.36±0.08) when all 44 step protocols applied in the presence of this blocker are taken into account. Only considering the defined observations (Fig. 10B), the frequency index matches the expectations (-1.00±0.00, N=19), illustrating that the average frequency index may severely be influenced by many zero-scores. Therefore, only the defined observations are further referred to here.

- The cGMP-sensitive potassium current (I_K (cGMP)) differs from I_K only in its sensitivity to the cyclic nucleotides cGMP and, to a lesser extent, to cAMP (Zufall et al., 1991b; Stengl et al., 1992). The channels

underlying this current are most likely a subpopulation of those underlying I_K. Since this current can only be recognized when cNMPs are applied to a recording with active I_K, or when I_K activates after washing out the cNMPs (as shown in Fig. 12), it was only observed in one recording, in 3 of 155 defined observations. The frequency index in sTTX bath solution was -0.96±0.03 (N=134). In the presence of TEA, this current was never present (frequency index -1.00±0.00) in each of 17 defined observations.

- The TEA-insensitive potassium current (I_K (-TEA)), in contrast, had a frequency index of -0.79±0.14 in the presence of TEA (N=19). In the absence of any blockers, the frequency index was -0.98±0.02 (N=112). Similarly to I_K (cGMP), I_K (-TEA) very likely contributes to the total I_K and can only be recognized under rare conditions. So it was only observed in one recording in 3 of 133
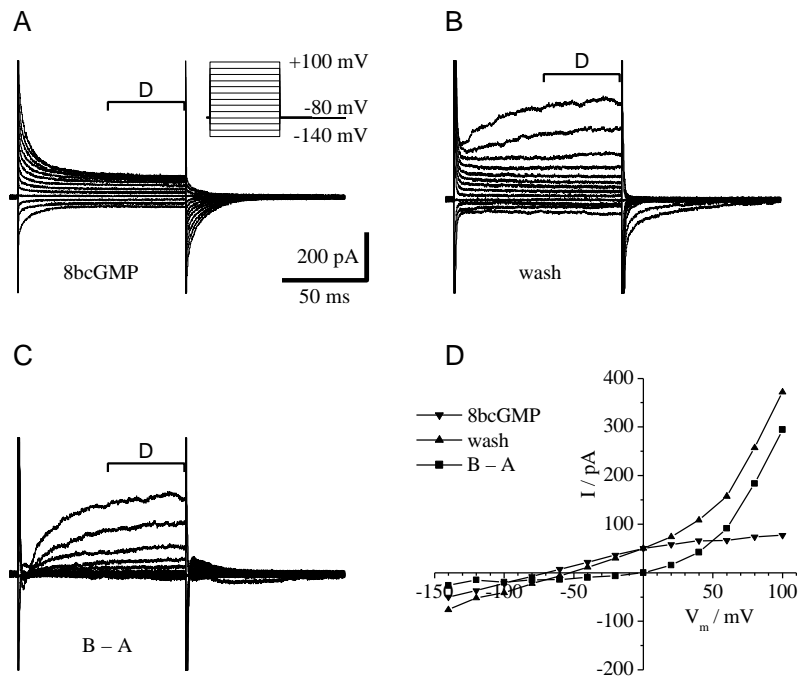

Fig. 12: The cGMP-sensitive potassium current I_K (cGMP) was observed when 8-bromo-cGMP (8bcGMP) was washed out during a recording. (A) In the presence of about 100 μmol l^{-1} 8bcGMP, a linear current response with a reversal potential of -70 mV was observed. The voltage step protocol shown in the insert is the same as in Fig. 11. (B) After about 5 min at an elevated flow rate of the bath perfusion, delayed, outwardly rectified currents had developed. (C) The difference between the currents shown in A and B reveals the delayed rectifier currents. (D) The I-V relations of the indicated portions of the protocols in A–C. The difference current (solid squares) shows slight contaminations of an inward current. Voltage step protocols and scaling are identical in A–C.

defined observations (Fig. 13).

- The slowly inactivating K$^+$ current (I_{Ki}) is characterized by a slow inactivation when the membrane potential is stepped from negative to positive values (Fig. 14). It was not observed during, but after the step protocols. This current probably also contributes to the total I_K. The TEA block of this current was slow and incomplete. Being present in 40 of 176 defined observations, the frequency index of I_{Ki} was -0.37±0.09 in the absence (N=134) and -0.81±0.10 in the presence of TEA (N=32).

- The calcium-activated potassium current ($I_{K (Ca^{2+})}$), characterized by a plateau at positive potentials in its outwardly rectifying I-V curve (Fig. 15), is activated by Ca^{2+} concentrations above 10^{-6} mol l^{-1} and insensitive to TEA, Cs$^+$ and charybdotoxin (Zufall et al., 1991b). This current was observed in 41 of 165 cases, the frequency indices were -0.51±0.08 (N=135) and -0.21±0.21 (N=22) in the absence and presence of TEA, respectively, indicating that it is TEA-insensitive.

- The rapidly inactivating K$^+$ current (I_A) (Zufall et al., 1991b) was not observed in the current study.

Fig. 13: Not all classes of delayed rectifier potassium currents were TEA-sensitive. (A) Delayed rectifier currents recorded in normal saline. (B) After about 2 min in bath solution containing 20 mmol l^{-1} TEA, only a minor fraction of the delayed rectifier currents was abolished. (C) The I-V plot of the indicated sections reveals slight contaminations with linear currents that are more obvious in TEA. Voltage step protocols and scaling are identical in A and B.

Nonspecific cation currents

- The calcium-dependent cation current ($I_{cat^+ (Ca^{2+})}$) is characterized by a zero-crossing I-V curve (Zufall et al., 1991a; Stengl, 1993) that becomes steeper at more positive and negative membrane potentials (Fig. 16). It has a bell-shaped calcium dependence, being activated at Ca^{2+} concentrations above 10^{-6} mol l^{-1} and inactivated in the millimolar range. It is sensitive to TEA, but not to Ni^{2+}. This current was present in 36 of 193 defined observations, its frequency index was -0.46±0.08 (N=142) in sTTX, and -0.89±0.08 in sTTX/TEA (N=37).

Fig. 14: The slowly inactivating potassium current I_{Ki}. (A) After voltage steps from negative holding potentials to more positive potentials, a slowly inactivating outwardly rectified current was observed. The inactivation typically had a time constant of 1.2–2 s. Whenever this current was observed, it was associated with current noise that increased with increasingly positive potentials, but did not decrase with the inactivation. (B) Shortly before the bath perfusion was switched to sTTX/TEA, I_{Ki} was recorded after stepping the membrane potential from -50 mV to 0 mV (left panel). About 1 min after exchanging the bath solution for sTTX/TEA, the current was almost completely blocked. The residual slowly inactivating component was still observed after another 2 min in TEA. When the blocker was washed out, I_{Ki} fully recovered (not shown). The transients at the voltage steps are due to switching artifacts.

Fig. 15: The calcium-activated potassium current $I_{K\ (Ca^{2+})}$ was characterized by a plateau in the I-V relation at positive potentials. (A) In the beginning of a recording, only a delayed rectifier I_K current was present. (B) Presumably because mechanical drift had brought Ca^{2+} into the cell, about 2 min later a larger current had activated, which did not increase any further at potentials of $\geq +80$ mV. (C) The differential current represents an outward rectifier with a small inward component. The overshoot at current onset (arrowhead) suggests that the current present in A had partly inactivated. One minute later, the delayed current onset had disappeared completely (not shown). (D) The I-V curves of the sections indicated in A–C. It remains open, whether the reduction of the current at $V_m=100$ mV is a property of $I_{K\ (Ca^{2+})}$ or caused by the inactivation of I_K. Likewise, the inward currents at potentials more negative than -60 mV might be caused by different channels. Voltage step protocols and scaling are identical in A–C.
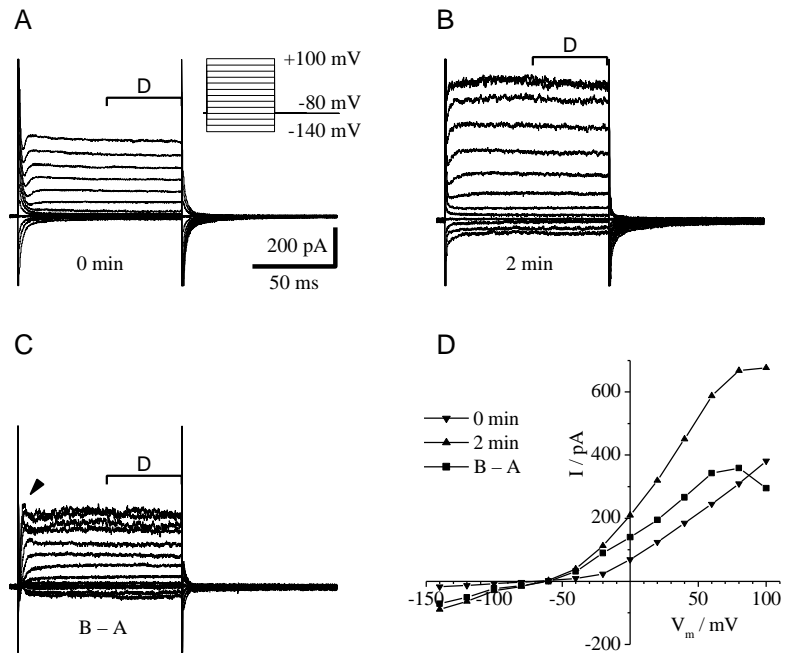
- The fast, steady, non-inactivating cation current ($I_{cat}^+{}_s$) exhibits a linear I-V relation with a reversal potential probably more negative than about -70 mV, suggesting a higher permeability of the channels for K^+ than for Ca^{2+}. The activator of this current, which is presumably composed of several components, is currently unknown. Since $I_{cat}^+{}_s$ was typically rather small, it was scored present, whenever the reversal potential was more negative than about -5 mV. While it was known that this current is TEA-sensitive, this study provided weak evidence for an inactivation by cGMP, but not cAMP. Negative reversal potentials were present in 99 of 179 defined observations. The frequency indices were $+0.50\pm0.09$ in the absence (N=131) and -0.66 ± 0.13 in the presence of TEA (N=35).

- A current with a linear, zero-crossing I-V curve, but very characteristic kinetics was

Fig. 16: (A–B) The calcium-dependent nonspecific cation current $I_{cat}^+{}_{(Ca^{2+})}$ is characterized by a curved I-V relation. The I-V curve of this current is relatively flat around the reversal potential, getting steeper at large positive and negative potentials. The negative reversal potential is presumably caused by a contamination with $I_{cat}^+{}_s$ (Fig. 17). A different current, I_{LL} (Fig. 18), is most probably responsible for the prominent tail currents and the slow drifts at very positive and negative potentials.
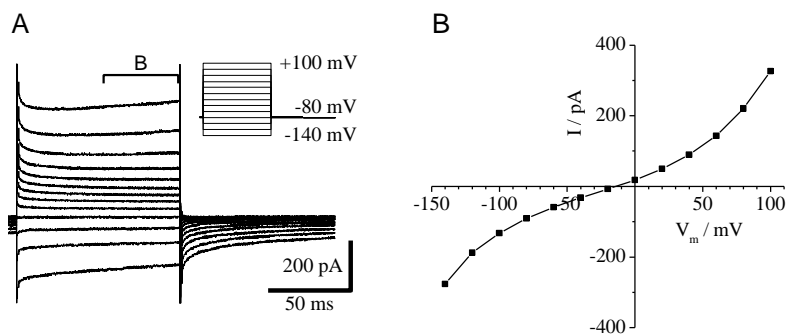

Fig. 17: (A–B) The fast, steady, non-inactivating cation current $I_{cat}^+{}_s$ exhibits a very negative reversal potential, which is caused by its higher conductivity for K^+ than for Ca^{2+}. This current was typically relatively small. In the recording shown here, it is only superimposed by a small component of the Ca^{2+}-dependent cation current $I_{cat}^+{}_{(Ca^{2+})}$ causing the slightly curved I-V relation. This suggests a reversal potential even more negative than -70 mV. In most recordings, this current was observed together with other, zero-crossing currents that shifted the reversal potential to more positive values.
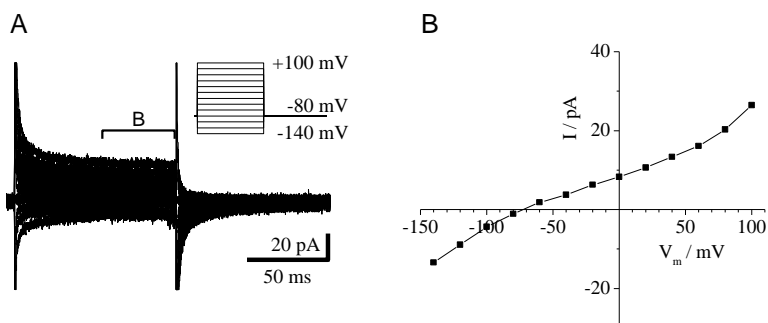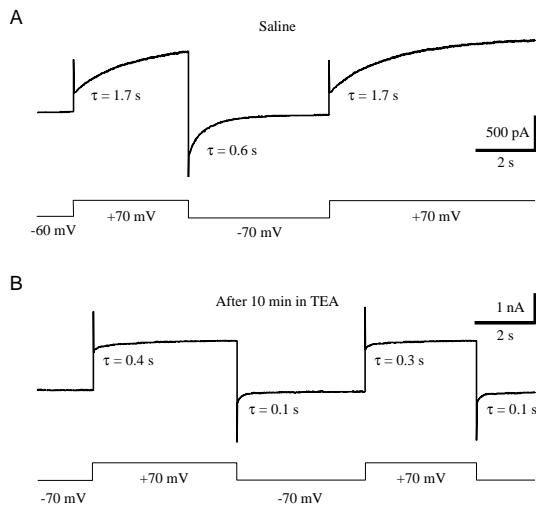
Fig. 18: The late, large, long-lasting cation current I_{LL} was recognized by its slow activation and inactivation. (A) When the membrane potential was switched to depolarizing values, in some recordings a large current developed at a time constant (τ) of up to several seconds. After switching back to hyperpolarizing potentials, the current inactivated at a time constant of typically about $1/3^{rd}$ the time constant after depolarization. In voltage step protocols this current caused characteristic tail currents (Fig. 16). I_{LL} was typically observed after the membrane potential was held at potentials more positive than +50 mV for many seconds, suggesting a Ca^{2+} dependence. (B) Prolonged exposure to TEA reduced, but failed to completely block I_{LL}. After about 10 min in sTTX/TEA bath solution, the time constants were shortened. The trace originates from a different recording, in which the current before application of the blocker had similarly slow kinetics as in A.

typically observed many minutes after the beginning of the recording and, once activated,

was very persisting. It was therefore termed late, large, long-lasting current and abbreviated I_{LL}. This current was characterized by a slow activation after depolarization and a slow inactivation after hyperpolarization (Fig. 18). The current response to a voltage step protocol had a characteristic shape and prominent tail currents (Fig. 16). These characteristics were present in 86 of 181 defined observations. This current frequently activated after long depolarization to +50 mV or more and might therefore be Ca^{2+}-activated. The slow kinetics of I_{LL} apparently required potentials more positive than about +30 mV and more negative than about -20 mV to develop. In one experiment, voltage step protocols with hyperpolarizing steps of 5 s and depolarizing steps of 10 s duration were applied (not shown). They did not reveal any correlation between the kinetics and the potential value, once +30 or -20 mV were exceeded, respectively. The frequency indices of +0.02±0.10 in the absence (N=134) and +0.55±0.24 in the presence of TEA (N=33) suggest that I_{LL} is not TEA-sensitive (Fig. 10). The observation of the current on a slow time scale on the strip charts, however, indicate that TEA incompletely, or extremely slowly reduces this current. After prolonged exposure to TEA, the kinetics of the activation and inactivation were slowed down (Fig. 18B). Likewise, the strip chart records suggest a block by millimolar Ni^{2+}, that remains incomplete, however, and therefore does not influence the frequency index.

- Little is known about a nonspecific cation current that was typically observed earlier in
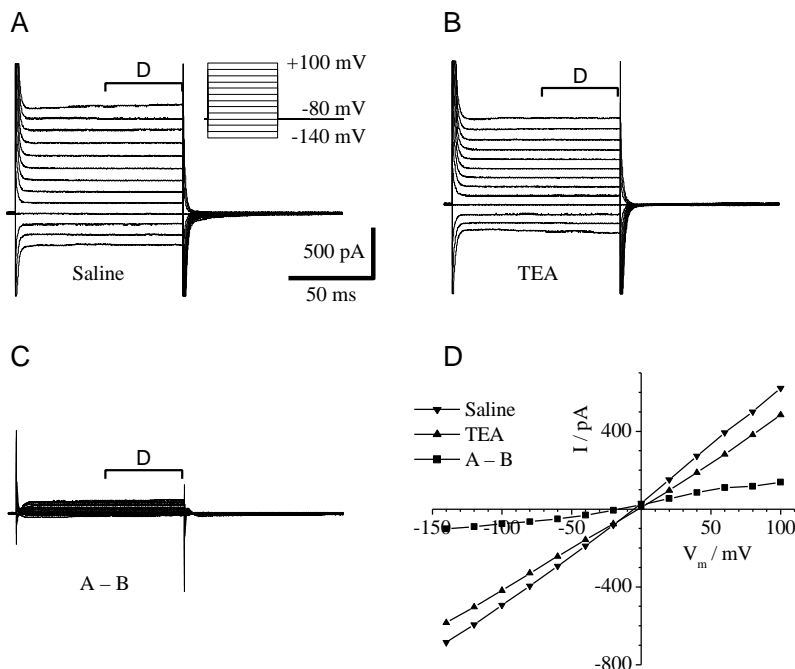

Fig. 19: The fast cation current ($I_{cat}^+{}_?$) was recognized by its sensitivity to TEA. (A) The current response to a voltage step protocol applied in saline was linear and zero-crossing. (B) About 2 min later, after the application of 20 mmol l^{-1} TEA, a fraction of the current was blocked. (C–D) The differential current reveals $I_{cat}^+{}_?$, the TEA-sensitive, linear, zero-crossing current fraction. The negative reversal potential is due to a conribution of $I_{cat}^+{}_s$ (Fig. 17). Voltage step protocols and scaling are identical in A–C.
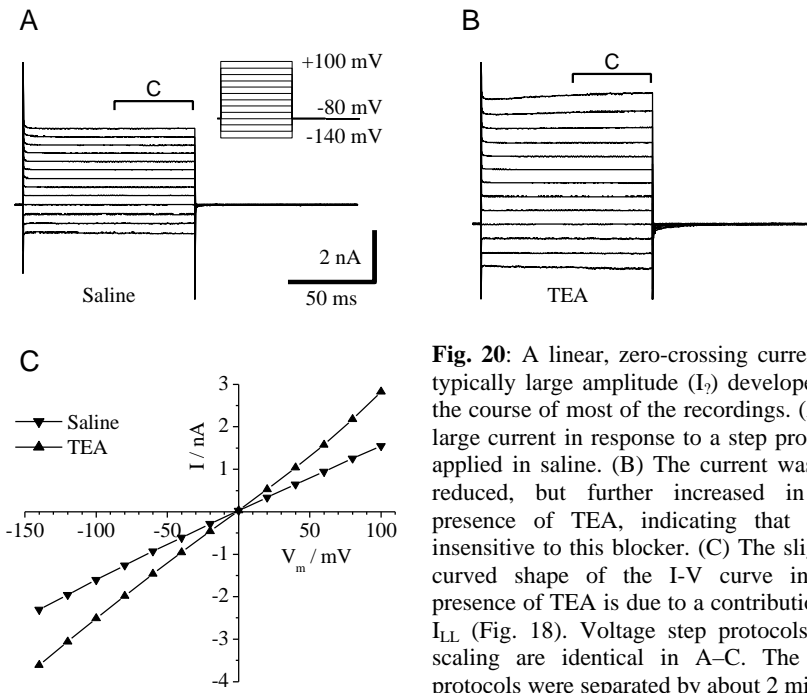
Fig. 20: A linear, zero-crossing current of typically large amplitude ($I_?$) developed in the course of most of the recordings. (A) A large current in response to a step protocol applied in saline. (B) The current was not reduced, but further increased in the presence of TEA, indicating that it is insensitive to this blocker. (C) The slightly curved shape of the I-V curve in the presence of TEA is due to a contribution of I_{LL} (Fig. 18). Voltage step protocols and scaling are identical in A–C. The step protocols were separated by about 2 min.

the experiments than I_{LL} and $I_?$ (see below) and did not exhibit the characteristic kinetics of I_{LL}. We termed it fast cation current ($I_{cat}^+{}_?$). It is activated by Ca^{2+} and blocked by TEA. It was present in 7 of 25 defined observations and yielded frequency indices of -0.43 ± 0.20 (N=21) in the absence and -1.00 ± 0.00 (N=3) in the presence of TEA. Since this current has a linear I-V relation, it was hard to distinguish from $I_?$, which is not TEA-blockable, however (see below). Therefore, $I_{cat}^+{}_?$ was only scored present, when a linear, zero-crossing current disappeared in correlation with switching the bath solution to sTTX/TEA (Fig. 19).

- The protein kinase C-activated cation current ($I_{cat}^+{}_{(PKC)}$), as described by Stengl (Stengl, 1993), was not specifically tested for in the perforated patch clamp experiments, since no PKC activators were applied. It is not unlikely, however, that $I_{cat}^+{}_?$ or another of the cation currents described here is identical to $I_{cat}^+{}_{(PKC)}$.

Currents of unknown origin
- A current of so far unknown origin was present in the majority of the experiments (122 of 143 defined observations). In contrast to I_{LL}, it did not

exhibit any slow kinetics. It differed from $I_{cat}^+{}_?$ by its insensitivity to TEA (Fig. 20). Since we were unable to determine, whether this typically rather large current is carried by cations or anions, we termed it $I_?$. The frequency index of $+0.82\pm0.09$ (N=114) was even higher in the presence of TEA ($+1.43\pm0.11$; N=21).

- An inwardly rectified current (I_{ir}) was present in 51 of 195 defined observations. It was characterized by an I-V curve with a reversal potential near 0 mV or slightly negative that was steeper at negative membrane potential (Fig. 21). Since $I_{K(Ca^{2+})}$ also produced a depression of the I-V curve at positive potentials, it remains unknown, whether the I-V curve is flat or increasing in this region. Blockers of I_{ir} are currently unknown. This current had frequency indices of -0.58 ± 0.07 in the absence (N=144) and -0.10 ± 0.17 in the presence of TEA (N=39), clearly indicating that this current is not TEA-sensitive. It does not appear to be Ni^{2+}-sensitive either (Fig. 10).

Influence of cyclic nucleotides
When 8-bromo-cAMP (8bcAMP; N=13) and 8-bromo-cGMP (8bcGMP; N=13), membrane-permeant derivatives of the cyclic nucleotides cAMP and cGMP, were applied to the bath (10 mmol l^{-1} in 10 µl sTTX, resulting in a final concentration of about 100 µmol l^{-1} in a bath volume of 1 ml), in most experiments no immediate effect was evident.
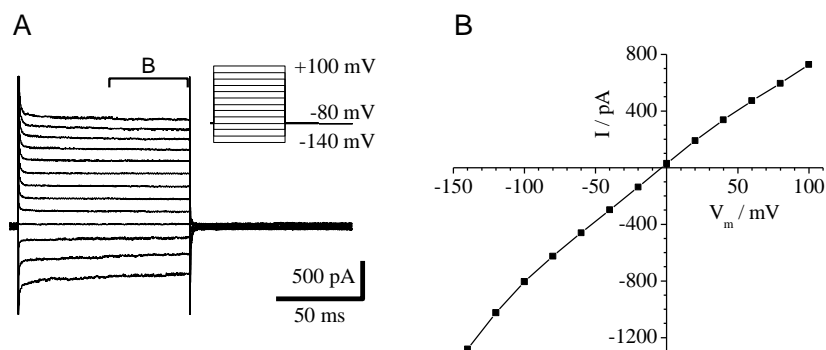

Fig. 21: (A–B) In response to some voltage step protocols an inwardly rectified current component (I_{ir}) was observed. The decisive criterion for the presence of I_{ir} is the inward rectification at negative potentials. An inward rectification only at positive potentials could have also been caused by $I_{K(Ca^{2+})}$ (Fig. 15).
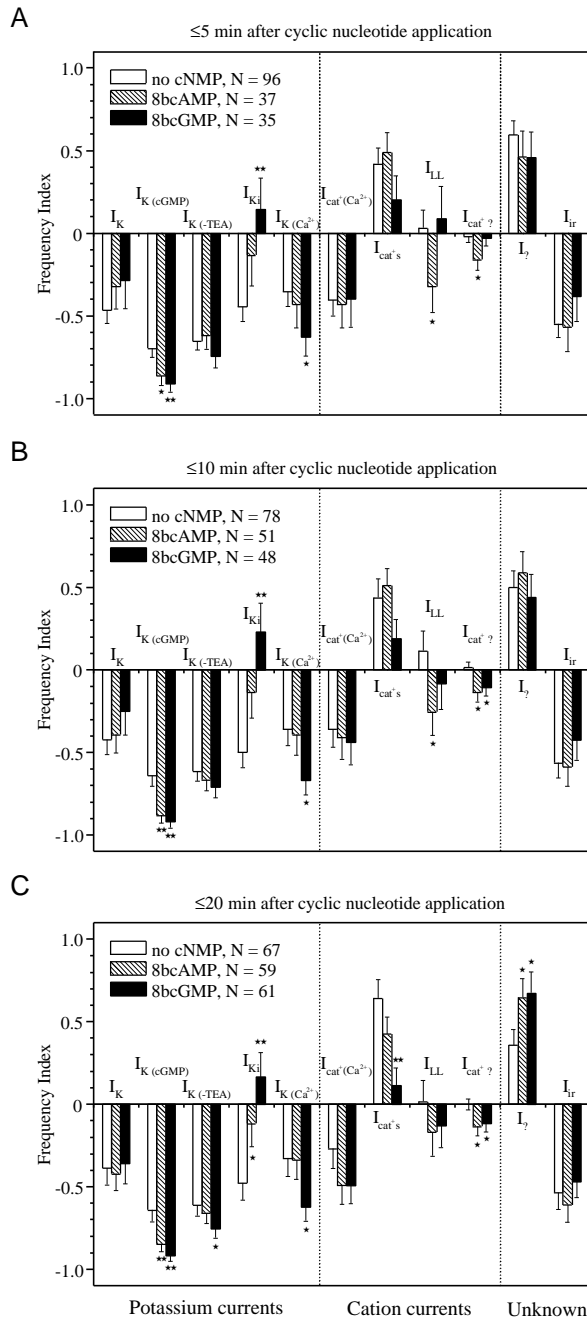
Fig. 22: Various currents were influenced by cyclic nucleotides. (A–C) The presence or absence of a current or current component was scored in the range of -1 to +2 during or around each voltage step protocol. The frequency indices for individual conditions were computed by averaging the scores. The frequency indices were compared including all step protocols that were applied until 5 (A), 10 (B), and 20 (C) min after drug application.

Data are means ± S.E.M. See Table 4 for the abbreviations of the currents. cNMP: cyclic nucleotide, 8bcAMP: 8-bromo cAMP, 8bcGMP: 8-bromo cGMP, ★: p<0.05, ★★: p<0.01, Student's t test (drug application versus no cNMP).

interval after which a voltage step protocol was considered being in the presence of the agents was restricted to 5, 10, 15 (not shown) or 20 min after the application (Fig. 22).

When considering the observations until 5 min after drug application, 6 currents were significantly influenced by cyclic nucleotides (Student's t-test vs. no application): I_{Ki} was activated by 8bcGMP, while $I_{K\,(cGMP)}$ and $I_{K\,(Ca^{2+})}$ were inactivated by this agent. $I_{K\,(cGMP)}$, I_{LL} and $I_{cat\,?}^{+}$ were inactivated by 8bcAMP (Fig. 22A). Except for the reduction in the frequency index of I_{LL} by 8bcAMP, these effects remained significant until 20 min after the application (Fig. 22C), suggesting that they were only slowly or not at all reversible. When the observations until 10 min after the application were considered, $I_{cat\,?}^{+}$, that had not been affected after 5 min, was inactivated by 8bcGMP, too (Fig. 22B). This effect also appears to be only slowly reversible, if at all. Considering all observations until 20 min after drug application, in addition to the previous results, I_{Ki} was also significantly activated by 8bcAMP, but less effectively than by 8bcGMP, $I_{cat\,s}^{+}$ and $I_{K\,(-TEA)}$ were inactivated by 8bcGMP, and $I_{?}$ was activated by both cyclic nucleotides. The latter is especially surprising, since $I_{?}$ was rather inactivated than activated by the cyclic nucleotides when only observations until 5 min after drug application were considered. We assume that this apparent effect is caused by the fact that $I_{?}$ was observed in the end of most experiments, when typically one or both cyclic nucleotides had already been applied. Therefore, the evidence for a delayed activation of this current is weak. The fact that the activation of I_{Ki} by 8bcAMP is only statistically significant after 20 min does most

Therefore, the frequency indices for each current were compared in the absence and presence of the cyclic nucleotides. Since the single-channel recordings suggest a delayed action of the cyclic nucleotides, at least on some of the ion channels, the

likely not indicate a delayed activation, however. This effect is consistently observed at all times, and the lack of statistical significance is probably just a matter of sample sizes. So we assume a strong activation of this current by cGMP and a weaker

activation by cAMP. The same presumably applies to the inactivation of $I_{K\,(-TEA)}$ by 8bcGMP.

Discussion

Ion channels and currents in cultured olfactory receptor neurons (ORNs) of the hawkmoth *Manduca sexta* were investigated using two different patch clamp techniques. Single-channel currents were recorded in cell-attached- and inside-out recordings. Whole-cell currents were recorded using the perforated patch technique, which does not deplete the cells of higher molecular messengers, in contrast to classical whole-cell recordings (Gómez-Puyou and Gómez-Lojero, 1977; Rae et al., 1991; Walz, 1995). In single-channel recordings, three classes of ion channels were observed, two of which are presumably activated by 8-bromo cGMP. Due to the abundance and large variety of ion channels, they could not be further characterized, however. The perforated patch experiments revealed 3 new currents and thus contributed to the knowledge of ion currents in *M. sexta* ORNs.

Single-channel recordings

With the voltage-dependent Na^+-and K^+ channels blocked by TTX in the bath and Cs^+ in the pipette, the single-channel recordings revealed a large variety of ion channels. According to their single-unit conductance, they were grouped in three classes, termed small, medium-sized, and large channels.

Small channels

Small channels of 2–20 pS single-unit conductance were not observed frequently. In the 3 recordings, in which they were not superimposed by larger channels, they exhibited very long dwell times of many seconds (Fig. 2). The channel conducted inward currents at a membrane potential of +27 mV in this inside-out recording, suggesting that it was a Ca^{2+} channel. The inositol-trisposphate-(IP$_3$)-dependent Ca^{2+} currents in *Manduca sexta* ORNs, as described by Stengl (Stengl, 1994), are transient and Ca^{2+}-sensitive. The IP$_3$-dependent Ca^{2+} channels would therefore probably be inactive in an inside-out recording with millimolar Ca^{2+} in the bath solution, as described here. Furthermore, the transience of the IP$_3$-dependent current would be incompatible with open times of many seconds. A statement about this, however, requires a more detailed analysis of these channels than was possible in this study. Too frequently, the small channels were obscured by larger channels. They could typically only be detected by the presence of conductance shifts in amplitude histograms, such as the step between levels 1 and 1a in Fig. 3, which do not allow a founded analysis of the I-V relation and behavior.

Thus, the identity of the small channels remains elusive.

Medium-sized channels and currents without unitary conductance levels

The group of medium-sized channels comprises several different channel types. One type is characterized by its behavior at hyperpolarizing potentials. While at depolarizing potentials unitary outward currents can be discerned (Fig. 7A), inward currents at hyperpolarizing potential show rapid fluctuations and no more unitary currents (Fig. 5). An IP$_3$-activated channel with very similar behavior was described in rat ORNs (Lischka et al., 1999). However, more than one channel type with this behavior appeared to be present in the majority of the patches. Relatively stable, TEA-sensitive inward currents, as shown in Fig. 5, were observed less frequently than rapid flickering that resembled a breaking seal, as can be seen in the voltage step protocol in Fig. 7B. A breaking seal, however, can typically not be stabilized, but is rather destroyed completely by applying more positive potentials. These channels were nonspecific cation channels, as judged from their reversal potential around 0 mV. They appeared to be PKC-activated since they were more frequently observed after application of TPA (Fig. 9). Thus, part of the observed medium-sized channels might be identical to PKC-activated nonspecific cation channels and -currents found in *Antheraea polyphemus* (Zufall and Hatt, 1991) and *M. sexta* (Stengl, 1993).

The statistics reveal the activation of medium-sized channels by 8bcGMP (Fig. 9, Table 3). This activation does not appear to be direct, or it requires co-factors that are washed away in cell-free patches, as indicated by comparatively long delay times between 8bcGMP application and activation (Figs. 3, 5). The frequently observed activation of many ion channels and classes in rapid sequence, after 8bcGMP application, but also excision-activated (i.e., activated by a rise of the intracellular Ca^{2+} concentration), suggests the presence of transducisomes in *M. sexta* ORNs. These aggregates of proteins, that have been found in insect- (Paulsen et al., 2000) and vertebrate photoreceptors (Körschen et al., 1999), putatively serve in keeping the distances for second messengers short, in this way increasing the effectiveness of the transduction cascade and reducing its latency (Burack and Shaw, 2000; Hille, 2001). The assumption of transducisomes might explain, why the application of an agent might remain ineffective for periods of up to minutes, but then activate many different ion channels almost synchronously, as shown in Fig. 3. We assume that a co-factor required for the activation was absent in inside-out patches, but once a single molecule happened to bind to its receptor, the entire cascade was triggered. A possible candidate that is required early in the transduction cascade (reviewed by Stengl et al., 1998) is GTP

(Stengl, 1993). In part of the single-channel recordings, 1 mmol l^{-1} ATP was added to the bath with out any evident and consistent effect. The effects of GTP remain to be investigated, however.

In the presence of the PKC activator TPA, the activation of medium-sized and large channels, but typically of currents without distinctive unitary currents, was observed more frequently without application of 8bcGMP than in the presence of this agent (Table 3). This suggests that PKC-dependent nonspecific cation channels (Zufall and Hatt, 1991; Stengl, 1993) are also present in the presumptive transducisomes. Our findings of activation of channels or currents, that can not readily be distinguished from each other, by both, 8bcGMP and TPA, are furthermore consistent with the finding of a nonspecific cation channel that was activated by cGMP and TPA in the silkmoth *Antheraea polyphemus* (Zufall and Hatt, 1991). The single-channel conductance of this so-called AC_1 channel was 56 pS in that study, which is somewhat higher than the majority of the single channels we observed after TPA application (Fig. 9A). The AC_1 channels furthermore were less effectively activated by 8bcGMP than by native cGMP. This might explain, why a noticeable activation by 8bcGMP was only observed in the absence of TPA (Table 3).

Inactivation of an ion channel was only observed after 1 of 77 applications of 8bcGMP (Fig. 4). It appears likely, however, that 8bcGMP inactivation occurred more frequently, but was obscured by the activation of other channels or currents. This channel exhibited strict outward rectification and a slope conductance of 35 pS, thus resembling the cyclic nucleotide-sensitive K^+ channel described by Zufall et al. (Zufall et al., 1991b). The transient, flickering openings of this channel and the fact that it was only observed twice may be due to the presence of Cs^+ in the pipette, which blocks most K^+ currents.

Large channels and large currents without unitary conductance levels

In most recordings, large channels (Fig. 8) or currents of up to several tens of nS in aggregate conductance, in which no single-channel levels could be discerned, activated sooner or later. In part, this activation was observed after 8bcGMP application, in part it occurred without drug application, presumably Ca^{2+}-dependently, in part it occurred after TPA application. When single-channel conductances could be determined, they ranged up to several hundreds of pS, suggesting chloride- or nonspecific anion channels (Hille, 2001). This assumption is further supported by the fact that only a minor fraction of the large currents was blocked by the large cation NMDG, which is virtually impermeant to most cation channels. All agents tested (TEA, Ni^{2+}, Zn^{2+}, SITS, DIDS, niflumic acid, anthracene-9-carboxylic acid, picrotoxin) did not significantly reduce the large

currents, making a further characterization on the single-channel level impossible.

Most medium-sized, but also the large channels exhibited subconductance states that could not be resolved (Figs. 2, 5, 6, 8), and thus the single-channel conductance could only be determined in the minority of the recordings. Together with the large currents, this made the interpretation of the single-channel results in terms of cGMP effects difficult. A further characterization of the ion channels in ORNs of *Manduca sexta* on the single-channel level requires cloning and heterologous expression of individual channel types. First results of screening antennal cDNA in collaboration with Alan Nighorn (Tucson, Arizona, USA) have revealed the presence of two types of cyclic nucleotide-gated channels (A. Nighorn, personal communication).

Perforated patch clamp recordings

The whole-cell currents in ORNs of *M. sexta* were divided into 13 current types of three groups, potassium currents, nonspecific cation currents, and currents of unknown origin (Table 4). Part of the currents or current components were known and more or less exhaustively characterized before. Other currents, such as the slowly inactivating K^+ current I_{Ki} and the late, long-lasting current I_{LL}, are first described in this study. To others, which were known, but not completely characterized, this study contributed knowledge of the pharmacology. Two currents, I_A and $I_{cat}^+{}_{(PKC)}$, were not investigated in the perforated patch recordings. The rapidly inactivating potassium current I_A was characterized in detail by Zufall et al. (Zufall et al., 1991b). The protein kinase C-dependent cation current $I_{cat}^+{}_{(PKC)}$ (Zufall and Hatt, 1991; Stengl, 1993) was observed after PKC activation by phorbol esters in the single-channel recordings. No PKC activators were applied in the perforated patch clamp experiments, however. Nevertheless, it is not unlikely that one of the other cation currents investigated is identical to $I_{cat}^+{}_{(PKC)}$, most probably $I_{cat}^+{}_?$. In general, the division of the currents into individual current types does not exclude that the same ion channels underlie more than one current type. As for example, presumably all K^+ currents except $I_K^+{}_{(Ca^{2+})}$ contribute to the total outward rectifier current I_K.

Potassium channels

Potassium currents, as characterized by their outwardly rectified I-V relation, were typically observed in the beginning of a recording. Six types of K^+ currents were distinguished.

- The delayed rectifier current I_K (Fig. 11), to which probably all delayed rectifier currents contribute, was only observed in the beginning of the recordings, but later disappeared or was

obscured by larger currents. It was defined as being TEA-sensitive, but insensitive to Ni^{2+}, which is known as Ca^{2+} channel blocker. When only the defined observations were taken into account (Fig. 10B), this current appeared to be blocked by Ni^{2+}, however. Although this result is statistically significant, it is merely caused by the fact that Ni^{2+} was typically used late in the recordings, when no more I_K was present. In no recording was Ni^{2+} directly applied to an outward rectifier current. TEA, however, was applied while these currents were present, and extinguished them in each of 4 experiments. This further illustrates that, with this non-standard analysis method, not only the results of the statistics, but also momentary observations must be taken into account. Regarding the apparent Ni^{2+} block, the same applies to all K^+ currents.

- The cGMP-sensitive potassium current ($I_{K (cGMP)}$) can only be recognized when 8bcGMP is applied to a recording with active I_K, or when I_K activates after washing out the 8bcGMP. The sample shown in Fig. 12 is the only occasion when this current was clearly observed. Like in the single-channel recordings, inactivation is likely to have occurred more frequently, but to have been obscured by the activation of other currents. A direct TEA block of this current has not been observed, so what was written about the apparent Ni^{2+} block in the previous paragraph also applies to TEA for $I_{K (cGMP)}$, although both effects are statistically significant.

- The TEA-insensitive potassium current ($I_{K (-TEA)}$) can only be seen under very specific conditions, too. In only one recording a fraction of the delayed rectifier current remained after the application of TEA (Fig. 13). On this background, the inactivation by cGMP, that is suggested by the statistics, requires further testing.

- The slowly inactivating K^+ current (I_{Ki}), as characterized by a slow inactivation when the membrane potential was stepped from negative holding potential to more positive values (Fig. 14), has not been described in moth olfactory receptor neurons before. It was activated by 8bcGMP and, to a weaker extent, by 8bcAMP (Fig. 22). The cyclic nucleotide-gated channels described in *Antheraea polyphemus* (Zufall and Hatt, 1991) and Heliothis virescens (Krieger et al., 1999) have a linear I-V relation, and therefore do not very likely underlie I_{Ki}. Slow inactivation is known from the *Shab* and *Shal* potassium channel families (Hille, 2001), but has also been described for some *Shaker* channels (K_V 1.3: Bowlby et al., 1997; Fadool et al., 1997), as well as for *ether-á-go-go* (EAG) channels (Stansfeld et al., 1996; Bauer and Schwarz, 2001). EAG channels, in turn, are

structurally related to *Shaker*, but also to the cyclic nucleotide-gated cation (CNG) channels. The properties of these channels appear to be determined by their subunit composition (Chen et al., 2000). In *Drosophila* there is evidence that EAG channels conduct K^+ outward as well as Ca^{2+} inward currents under the control of cAMP and voltage (Brüggemann et al., 1993). Cation channels with a sequence homology to CNG channels were cloned in the moth *Heliothis virescens* (Krieger et al., 1999). These channels are activated by cAMP, but also by cGMP (J. Krieger, personal communication). A gene with considerable sequence homology to CNG channels has recently also been cloned in *M. sexta* (J. Witten, personal communication). We therefore assume that EAG- or EAG-like channels underlie the slowly inactivating K^+ current I_{Ki}. Ion channels encoded in an EAG-related gene (erg) contribute to the maintenance of the resting potential (Bauer and Schwarz, 2001). Therefore, the activation of this current by cGMP might underlie the accelerated decline of sensillar potentials in the adapted state (Chapter 2). Since no other type of delayed rectifier currents was activated by 8bcGMP, the activation of I_{Ki} might also be responsible for the prolonged repolarizing phase of spontaneous action potentials that was observed after 8bcGMP injection during tip recordings (Chapter 3). Basing on the assumption that the adaptation of the action potential response (Chapter 2) is mediated by an influence on the delayed rectifiers rather than on the voltage gated sodium channels, this would, in turn, suggest that the adaptation of the action potential response and the accelerated decline of the sensillar potential, which originally appeared to be caused by distinct mechanisms, are actually caused by the same, cGMP-dependent activation of the channels underlying I_{Ki}.

- The calcium-activated potassium current ($I_{K (Ca^{2+})}$), characterized by a plateau at positive potentials in its outwardly rectifying I-V curve (Fig. 15), could not be blocked by TEA (Fig. 10A). However, it was observed significantly less frequently after application of 8bcGMP, but not 8bcAMP (Fig. 22). This sensitivity to cyclic GMP has not been described before.

- The rapidly inactivating K^+ current (I_A) (Zufall et al., 1991b) was not observed in the current study.

Nonspecific cation currents

- The calcium-dependent cation current ($I_{cat^+ (Ca^{2+})}$) is characterized by a zero-crossing I-V curve that becomes steeper at more positive and negative membrane potentials (Fig. 16; Stengl, 1993). A sensitivity to cyclic GMP, as

described by Zufall et al. (Zufall et al., 1991a), was not found, however (Fig. 22). Together with the nonlinear I-V relation of $I_{cat}^+{}_{(Ca^{2+})}$, in contrast to that channel, this suggests that the channel described by Zufall et al. does not underlie this current.

- The negative reversal potential that characterizes the fast, steady, non-inactivating cation current ($I_{cat}^+{}_s$) was consistently less frequently observed after the application of 8bcGMP (Fig. 22). This effect is more pronounced (and becomes only statistically significant), if all observations until 20 min after the application are considered. An effect of 8bcAMP was not observed, however. This contradicts the assumption that the cyclic nucleotide-sensitive delayed rectifier channel (Zufall et al., 1991b) might contribute to the negative reversal potential, since this channel was shown to be more sensitive to cAMP than cGMP. It was blocked by TEA, but a direct effect of Ni^{2+} was not observed. So the lack of observations in the presence of Ni^{2+} does not indicate a block (see above).

- The late, large, long-lasting current (I_{LL}) has not been described before. It is presumably a nonspecific cation current, but might turn out to be a chloride- or anion current. I_{LL} was characterized by a slow activation after depolarization and a slow inactivation after hyperpolarization (Fig. 18). Thus, the I-V relation of the activated current is linear and zero-crossing when obtained by brief voltage steps, such as in a step protocol. When taken after a prolonged period, however, this current appears as an outward rectifier. It was observed less frequently after application of 8bcAMP, but not 8bcGMP, but this effect was transient and was only statistically significant for the first 10 min after the application (Fig. 22). Like for I_{Ki}, the slow kinetics suggest that this current might be a member of the *Shab*, *Shal* or *Shaker* or of the EAG or EAG-related channels. Like I_{LL}, EAG channels are controlled by cAMP and by voltage (Brüggemann et al., 1993). Thus, I_{LL} might also contribute to the stabilization of the resting potential (Bauer and Schwarz, 2001; Hille, 2001)

- The fast cation current ($I_{cat}^+{}_?$) resembled I_{LL} in its sensitivity to 8bcAMP, but was also observed less frequently 10 min after the application of 8bcGMP. It was typically observed earlier in the experiments than I_{LL} and could only rarely be discerned by its sensitivity to TEA from the large $I_?$ currents that occurred later (Fig. 19). Slow gating of this current was not observed. The sensitivity to 8bcGMP contradicts the assumption that the PKC-dependent cation channels found in *Antheraea polyphemus* underlie $I_{cat}^+{}_?$. Due to its TEA sensitivity it might be identical to the PKC-

dependent cation current in *M. sexta*, however (Stengl, 1993). PKC activators were not applied in the current study, but an activation by increase of the intracellular Ca^{2+} concentration does not appear unlikely.

Currents of unknown origin

- A large, linear, zero-crossing current of so far unknown origin developed in the majority of the experiments, reminiscent of the large channels and currents observed in the single-channel recordings. It was not blocked by TEA or Ni^{2+}, nor was it influenced by the cyclic nucleotides. The apparent activation by the blockers (Fig. 10) and both cyclic nucleotides when considering the observations until 20 min after application (Fig. 22C) is due to the fact that the current was typically present late in the experiments (cf. above). We assume that the large channels observed in the single-channel recording underlie $I_?$, and therefore do not expect that it is inactivated by any of the blockers tested there. We did not attempt to find out, whether $I_?$ is a cation- or anion current in this series of experiments.

- An inwardly rectified current (I_{ir}) was observed in some of the experiments. No effects of the tested blockers and the cyclic nucleotides were detected, however. Different types of inwardly rectified currents have been described in *M. sexta*, but since I_{ir} could not be specifically influenced in the current study, its identity remains elusive.

Correlation to cGMP effects observed in tip recordings

In tip recordings of trichoid sensilla in intact animals, the repolarization phase of spontaneous action potentials was prolonged, but reduced in amplitude, while the peak-to-peak amplitude of the action potentials increased after injection of 8bcGMP (Chapter 3, Fig. 1). This suggests an effect of cGMP on delayed rectifier channels and linear, zero-crossing channels, respectively. The prolongation of the repolarizing phase suggests a slower decline of delayed rectifier currents, which is consistent with the cGMP-dependent activation of I_{Ki}. The reduced amplitude of the negative phase indicates the inactivation of a more rapidly declining delayed rectifier current, which might be represented by either $I_{K(cGMP)}$ or $I_{K(Ca^{2+})}$. The increase of the peak-to-peak action potential amplitude, which occurred at a different time scale, suggests an increase of the resistance of the ORNs, presumably caused by inactivation of a linear, zero-crossing current. Only one of the currents fulfills this criterion: $I_{cat}^+{}_?$. Since the TEA-sensitive portion typically made up only a minor fraction of linear, zero-crossing currents (Fig. 19), it is very likely that

other effects contribute to the observed resistance increase, however.

Conclusion

Similarly to the single-channel recordings, the perforated patch recordings revealed a large variety of different ion currents or current components. The large conductance of the channels and currents observed in both approaches suggests the presence of chloride- or nonspecific anion channels that serve in stabilizing the resting potential. This would be consistent with the observation that these currents developed in the course of the experiments. Prolonged duration of a patch clamp experiment is frequently associated with poor control of the intracellular Ca^{2+} concentration, by mechanical disturbance in cell-attached recordings, and by the influence of Ca^{2+}-permeable channels in perforated patch recordings. Due to the limited Ca^{2+} permeability of amphotericin B, the precise and timely control of intracellular Ca^{2+} is hard to achieve with Ca^{2+} chelators. Although the Ca^{2+} concentration in the pipette solution was adjusted to 10^{-7} mol l^{-1} with BAPTA in most of the perforated patch experiments, we were apparently unable to control the intracellular Ca^{2+} concentration. The influence of Ca^{2+} brought into the cell by Ca^{2+}-permeable channels might have triggered cascades that are only triggered by strong stimulation in the intact sensillum. In the current study, this led to the development of compound currents, of which individual components were hard to isolate. The single-channel recordings suggest that the activation of the large channels and currents is not reversible by reducing the Ca^{2+} concentration later. Thus, further experiments using bath solutions with reduced Ca^{2+} concentration from the beginning of the recording might be a way to better discern and characterize individual currents.

References

Bauer, C. K. and Schwarz, J. R. (2001). Physiology of EAG K$^+$ channels. *J. Membr. Biol.* **182**(1), 1-15.

Boekhoff, I., Seifert, E., Göggerle, S., Lindemann, M., Krüger, B. W. and Breer, H. (1993). Pheromone-induced second-messenger signaling in insect antennae. *Insect Biochem. Mol. Biol.* **23**(7), 757-762.

Bowlby, M. R., Fadool, D. A., Holmes, T. C. and Levitan, I. B. (1997). Modulation of the Kv1.3 potassium channel by receptor tyrosine kinases. *J. Gen. Physiol.* **110**(5), 601-610.

Brüggemann, A., Pardo, L. A., Stühmer, W. and Pongs, O. (1993). Ether-a-go-go encodes a voltage-gated channel permeable to K$^+$ and Ca^{2+} and modulated by cAMP. *Nature* **365**(6445), 445-448.

Burack, W. R. and Shaw, A. S. (2000). Signal transduction: hanging on a scaffold . *Curr. Opin. Cell Biol.* **12**(2), 211-216.

Chen, M. L., Hoshi, T. and Wu, C. F. (2000). Sh and eag K$^+$ channel subunit interaction in frog oocytes depends on level and time of expression. *Biophys. J.* **79**(3), 1358-1368.

Eide, P. E., Caldwell, J. M. and Marks, E. P. (1975). Establishment of two cell lines from embryonic tissue of the tobacco hornworm, *Manduca sexta* (L.). *In Vitro* **11**, 395-399.

Fadool, D. A., Holmes, T. C., Berman, K., Dagan, D. and Levitan, I. B. (1997). Tyrosine phosphorylation modulates current amplitude and kinetics of a neuronal voltage-gated potassium channel. *J. Neurophysiol.* **78**(3), 1563-1573.

Gómez-Puyou, A. and Gómez-Lojero, C. (1977). The use of ionophores and channel formers in the study of the function of biological membranes. *Curr. Top. Bioenerget.* **6**, 221-257.

Hamill, O. P., Marty, A., Neher, E., Sakmann, B. and Sigworth, F. J. (1981). Improved patch-clamp techniques for high-resolution current recording from cells and cell-free membrane patches. *Pflügers Arch.* **391**, 85-100.

Hille, B. (2001). Ion Channels of Excitable Mebranes, Third Edition. Sunderland, Massachchusetts: Sinauer Associates.

Hörbrand, T. (1996). Mechanismen der olfaktorischen Adaptation bei *Manduca sexta* auf Ionenkanalebene. Master Thesis, Universität Regensburg.

Körschen, H. G., Beyermann, M., Müller, F., Heck, M., Vantler, M., Koch, K. W., Kellner, R., Wolfrum, U., Bode, C., Hofmann, K. P. and Kaupp, U. B. (1999). Interaction of glutamic-acid-rich proteins with the cGMP signalling pathway in rod photoreceptors. *Nature* **400**(6746), 761-766.

Krieger, J., Strobel, J., Vogl, A., Hanke, W. and Breer, H. (1999). Identification of a cyclic nucleotide- and voltage-gated ion channel from insect antennae. *Insect Biochem. Mol. Biol.* **29** , 255-267.

Lischka, F. W., Zviman, M. M., Teeter, J. H. and Restrepo, D. (1999). Characterization of inositol-1,4,5-trisphosphate-gated channels in the plasma membrane of rat olfactory neurons. *Biophys. J.* **76**(3), 1410-1422.

Paulsen, R., Bahner, M. and Huber, A. (2000). The PDZ assembled "transducisome" of microvillar photoreceptors: the TRP/TRPL problem. *Pflügers Arch.* **439**(3 Suppl), R181-R183.

Rae, J., Cooper, K., Gates, P. and Watsky, M. (1991). Low access resistance perforated patch recordings using amphotericin B. *J. Neurosci. Methods* **37**(1), 15-26.

Redkozubov, A. (2000). Guanosine 3',5'-cyclic monophosphate reduces the response of the Moth's olfactory receptor neuron to pheromone. *Chem. Senses* **25**, 381-385.

Stansfeld, C. E., Röper, J., Ludwig, J., Weseloh, R. M., Marsh, S. J., Brown, D. A. and Pongs, O. (1996). Elevation of intracellular calcium by muscarinic receptor

activation induces a block of voltage-activated rat ether-a-go-go channels in a stably transfected cell line. *Proc. Natl. Acad. Sci. U. S. A.* **93**(18), 9910-9914.

Stengl, M. (1993). Intracellular-messenger-mediated cation channels in cultured olfactory receptor neurons. *J. Exp. Biol.* **178**, 125-147.

Stengl, M. (1994). Inositol-trisphosphate-dependent calcium currents precede cation currents in insect olfactory receptor neurons in vitro. *J. Comp. Physiol. A* **174**, 187-194.

Stengl, M. and Hildebrand, J. G. (1990). Insect olfactory neurons *in vitro*: morphological and immunocyto-chemical characterization of male-specific antennal receptor cells from developing antennae of male *Manduca sexta. J. Neurosci.* **10**(3), 837-847.

Stengl, M., Zufall, F., Hatt, H. and Hildebrand, J. G. (1992). Olfactory receptor neurons from antennae of developing male *Manduca sexta* respond to components of the species-specific sex pheromone *in vitro. J. Neurosci.* **12**(7), 2523-2531.

Stengl, M., Ziegelberger, G., Boekhoff, I. and Krieger, J. (1998). Perireceptor events and transduction mechanisms in insect olfaction. In *Insect Olfaction* (ed. B. S. Hansson), pp. 49-66. Berlin, New York, Heidelberg: Springer.

Stengl, M., Zintl, R., de Vente, J. and Nighorn, A. (2001). Localization of cGMP immunoreactivity and of soluble guanylyl cyclase in antennal sensilla of the hawkmoth *Manduca sexta. Cell Tissue Res.* **304**, 409-421.

Walz, W. (1995). Perforated patch-clamp technique. In *Patch-Clamp Applications and Protocols* (ed. A. Boulton), pp. 155-171. Totowa, NJ: Humana Press.

Ziegelberger, G., van den Berg, M. J., Kaissling, K.-E., Klumpp, S. and Schultz, J. E. (1990). Cyclic GMP levels and guanylate cyclase activity in pheromone-sensitive antennae of the silkmoths *Antheraea polyphemus* and *Bombyx mori. J. Neurosci.* **10**(4), 1217-1225.

Zufall, F. and Hatt, H. (1991). Dual activation of a sex pheromone-dependent ion channel from insect olfactory dendrites by protein kinase C activators and cyclic GMP. *Proc. Natl. Acad. Sci. U. S. A.* **88**, 8520-8524.

Zufall, F., Hatt, H. and Keil, T. A. (1991a). A calcium-activated nonspecific cation channel from ofactory receptor neurones of the silkmoth *Antheraea polyphemus. J. Exp. Biol.* **161**, 455-468.

Zufall, F., Stengl, M., Franke, C., Hildebrand, J. G. and Hatt, H. (1991b). Ionic currents of cultured olfactory receptor neurons from antennae of male *Manduca sexta. J. Neurosci.* **11**(4), 956-965.

Acknowledgements

Danksagung

Ich danke Frau HD Dr. Monika Stengl für die Betreuung meiner Doktorarbeit. Sie hat mir sehr selbstständiges Arbeiten ermöglicht und stets ausreichend Mittel für die sorgfältige Durchführung der Experimente zur Verfügung gestellt. Darüber hinaus hat sie meine Teilnahme an mehreren internationalen Konferenzen gefördert und mir so die Möglichkeit gegeben, Kontakte und Freundschaften zu Forschern und Labors auf der ganzen Welt zu knüpfen.

Ebenso danke ich dem Zweitgutachter, Herrn Prof. Dr. Roland Brandl, und den anderen Mitgliedern der Prüfungskommission, Frau Prof. Dr. Renate Renkawitz-Pohl und Herrn Prof. Dr. Uwe Homberg, für ihren Beitrag zum erfolgreichen Abschluss meiner Promotion.

Mein besonders herzlicher Dank gilt Herrn Prof. Dr. Kai Hansen. Er hat weit mehr für mich getan als „nur das eine Kabel abgeschnitten." Von ihm und nach seinem Vorbild habe ich gelernt, was Elektrophysiologie meiner Meinung nach sein sollte: Stets den Methoden kritisch gegenüberstehen, sich klarmachen, wie jede einzelne Komponente eines Messstandes das Signal verändert oder beeinflussen könnte, und immer „mal eben überschlagen", ob das Ergebnis überhaupt im plausiblen Bereich liegt. Ich hoffe, eines Tages, so wie er, stets die passende Formel parat zu haben.

Viele der Ergebnisse die hier gezeigt werden stammen aus Ableitungen, die von Karin Fischer, Steffi Krannich und Christian Flecke durchgeführt und ausgewertet wurden. Vielen Dank für die sorgfältige Arbeit, das Engagement und das Feedback zu XtraCell.

Unter den vielen Leuten, denen ich dafür danken möchte, dass sie mir Zugang zu ihren Messständen und Einblick in ihre Methoden gewährt haben, ragen besonders Dr. Blanka Pophof und Prof. Dr. Karl-Ernst Kaissling heraus. Unser heutiger *tip recording*-Stand hat ihre Messstände in Seewiesen zum Vorbild. Vielen Dank auch an Dr. Tom Christensen für das Bombykal, das er uns für die Stimulationsversuche zur Verfügung gestellt hat.

Die Liste derjenigen Kollegen, denen ich für fruchtbare Diskussionen und methodische Tipps danken möchte ist zu lang, um sie hier wiederzugeben. An erster Stelle stehen Ingrid Jakob, Philippe Lucas, Xavier Grosmaitre, Jean-Pierre Rospars, Frederic Marion-Poll, Phil Heyward, Paul Stevenson, Joachim Schachtner, Thomas Reischig, Alexej Redkozubov, Ed Blumenthal und Thomas Kröber.

Die Experimente wären nicht möglich gewesen ohne die Arbeit der Fachbereichswerkstätten in Regensburg und Marburg. Hier möchte ich besonders Horst Schmidt und Günther Stöckl danken. Die Begeisterung und Sorgfalt mit der Horst Schmidt – oft schon bis zum nächsten Tag, und meist noch etwas ausgefeilter als gewünscht – selbst kleine und kleinste Teile angefertigt hat, hat viel zum Gelingen der Arbeiten beigetragen. Günther Stöckl hat durch viele gute Ideen einige Teile der Versuche überhaupt erst ermöglicht.

Mein Dank geht ebenfalls an Axon Instruments, im Besonderen an Dave Gallegos, Cliff Christian, Chris Mathes, Burt Maertz, Greg Richardson, Andrew Olson, Ward Yuhas und Alan Finkel. Sie haben etliche meiner Vorschläge in pCLAMP umgesetzt und dadurch viel dazu beigetragen, Experimente leichter auswertbar oder erst möglich zu machen.

Darüber hinaus möchte ich den zahlreichen Studenten, die in den einzelnen Kapiteln namentlich aufgeführt sind, dafür danken, dass sie sich um die Insektenzucht gekümmert haben – was nicht immer ganz einfach war.

Zu guter letzt Vielen Dank allen in den Arbeitsgruppen in Regensburg und Marburg für die angenehme Atmosphäre, für die Gesellschaft beim Mittagessen und für die eine oder andere gemeinsame Motorradfahrt. Dank an Angela, Bernhard, Björn, Chico, Christian, Eva, Felix, Harm, Jana, Jochen, Julia, Jutta, Karl-Heinz, Karin, Keram, Luci, MartinaK, MartinaM, Matze, Micha, Michael, Monika, Nils, Nina, Norman, Patrick, Rita, Frau Rochelt, Rudi, Sabine, Sandra, Steffi, Stephan, Frau Thies, ThomasH, ThomasR, Uwe, Wolf und Wolfgang.

Fehlt noch jemand? – Tja, so ist das!